CAPACITY OF ECCENTRICALLY LOADED
SLENDER CONCRETE BLOCK WALLS

CAPACITY OF ECCENTRICALLY LOADED SLENDER CONCRETE BLOCK WALLS

By

PIOTR DANIEL SUWALSKI, B.Sc.

A Thesis
Submitted to the School of Graduate Studies
in Partial Fulfillment of the Requirements
for the Degree
Master of Engineering

McMaster University
September 1986

MASTER OF ENGINEERING (1986) McMASTER UNIVERSITY

(Civil Engineering) Hamilton, Ontario

TITLE : Capacity of Eccentrically Loaded Slender Concrete Block Walls

AUTHOR : Piotr Daniel Suwalski, B.Sc. (Technical University of Wroclaw)

SUPERVISOR : Dr. R. G. Drysdale

NUMBER OF PAGES : xx, 304

ABSTRACT

The behavior of concrete block walls subjected to vertical compressive loads with out-of-plane eccentricities was investigated both experimentally and analytically. Particular attention was devoted to the effect of wall slenderness on capacity.

In the experimental study, 14 full scale walls and numerous small specimens were tested to provide complete and reliable data concerning the behavior of concrete block walls and its components. Plain walls and partially grouted reinforced walls were tested in symmetric single curvature under compressive loads with out-of-plane eccentricities. Reinforced walls were tested in pure bending, as well.

Prisms were tested to analyze the behavior of concrete masonry in compression with no slenderness or eccentricity effects. Bond tests were carried out to determine the behavior at interfaces of grout and steel reinforcing bars as well as between mortar and concrete blocks. Material tests were conducted to determine the mechanical properties of the blocks, mortar, grout and steel reinforcement used.

A two-dimensional finite element model for the vertical cross section of block masonry walls was developed. It is capable of modeling local failure modes such as cracking, crushing and debonding. Material properties of the concrete blocks, mortar, grout, and steel bars were treated individually. The large deformation analysis allowed for consideration of the slenderness effect. The model was verified through comparison with experimental results. Fairly good agreement was

obtained.

The material properties of specimens tested during the experimental investigation were the basis of a parametric study. Results of this study were used to investigate the effect of the wall slenderness and the eccentricity of applied loads on the capacity of concrete block walls. They were used to evaluate the current provisions in the Canadian Masonry Code, CAN3-S304-M84. An attempt was made to develop original design equations based on the reduction coefficient approach. The proposed equations for plain and reinforced blockwork were shown to provide more consistent predictions of capacity than current design methods.

ACKNOWLEDGEMENTS

I wish to express my sincere gratitude to Dr. R. G. Drysdale for his supervision and encouragement during the course of this study.

I feel indebted to Dr. F. Mirza for lending his computer routines. Special thanks are due to Jeff Walker for allowing me to utilize his computer program.

Acknowledgment is due to McMaster University for financial support. This research was funded by Operating Grants from the Natural Sciences and Engineering Research Council of Canada. The contribution of the mason's time made available through the Ontario Masonry Contractor's Association and the Ontario Masonry Promotion Fund is appreciated. I would like to thank the Ontario Concrete Block Association for the donation of the blocks.

I would like to thank my friends, Piotr Ostrowski, Ugur Polat and Bill Chow for their valuable suggestions concerning numerical analysis. Finally, a special note of deep appreciation is due to my friends, Krystyna and Piotr Ostrowski for their help and encouragement.

TABLE OF CONTENTS

LIST OF FIGURES:

LIST OF TABLES

CHAPTER 1

INTRODUCTION

1.1 Foreword

Masonry is one of the oldest building materials, but until the last 30 years the design of masonry structures was based on "rules of thumb". To some extent, lack of modern design methods has made masonry less competitive compared with other structural materials. However use of more advanced methods could change that situation. The application of engineered and rationally designed masonry requires the development of rational codes of practice in this area.

In most situations for design of masonry, the code committees have been able to provide relatively safe methods of design. However, some design recommendations have been approved without sufficient verification from experimental results. The design of concrete block walls for axial load and out-of-plane bending is such an example. The experimental data from testing solid brick walls, carried out by the Structural Clay Products Institute[(74)], were used as the basis for the design equation for both brickwork and blockwork in the Canadian code[(55)].

Recent research carried out by Yokel et al[(82)], Fattal and Caettano[(36)], Drysdale et al[(27)], Hatzinikolas et al[(45)], Turkstra[(77)], and others has improved the understanding of the behavior of concrete block walls in out-of-plane bending. Additional efforts have resulted in the introduction of different provisions concerning the design of axially loaded walls in the new Canadian code, CSA Standard CAN3-S304/M84[23]. The proposed Load-Deflection Method based on the moment magnifier method or on the P-delta effect is an attempt to use a method which rationally models the behavior of the eccentrically loaded walls. This code is viewed here as an interim provision prior to introduction of the limit states code, at which time it is hoped that the accuracy of the design methods will be improved and much better documented.

The development of design provisions for walls requires investigation of the full spectrum of parameters affecting capacities. Large numbers of experimental results are required to obtain statistically significant data. Unfortunately, only a few experimental programs have been carried out and these quite often contain results which are incompatible or at least not readily compatible, since different experimental procedures were used. This situation may explain substantial differences between national codes. Certain cases, such as reinforced masonry walls loaded with eccentricity higher than one half of the wall thickness, have not been tested at all, but code recommendations[23] cover this range as well.

It is known that analytical models can be used to generate behavioral information as a substitute for experimental data. However, due to the complex behavior of masonry blockwork, reinforced concrete block walls in particular have not been properly modeled using simple numerical models. In this regard, the finite element method is a very powerful tool which is being used increasingly to solve this type of complicated modeling problem. However for it application, knowledge of material properties and verification of accuracy are prerequisites.

1.2 Objectives and Scope

The general purpose of this investigation was to contribute to the knowledge of the behavior of eccentrically loaded, concrete block walls. It was anticipated that this goal could be accomplished through a combination of an experimental program, including tests on full scale walls, and through development of a finite element model. The latter would be capable of representing the behavior of the masonry walls and thus provide a means of extending the range of the investigation.

It was intended that the experimental data be used for direct comparison of design provisions as well as for verification of the numerical model. The numerical model, once verified using this and other data would be used for a more thorough evaluation of design methods. In addition to the evaluation of existing design methods, it was hoped that insight into the behavior of concrete block walls might lead to suggestions for modifications or alternatives to these design methods.

The investigation concentrated on the axial load capacity of plain and reinforced concrete block walls subject to out-of-plane eccentric loading. Symmetric, single curvature cases were considered. Twelve full scale walls with constant height and width were tested. Only one combination of hollow blocks, mortar and grout, commonly used in Ontario, was used. The eccentricities of loads were chosen to cover the common range for different types of walls. The ranges chosen were from nearly concentric to kern eccentricity for plain walls, and from concentric to pure bending for reinforced walls. The height of the walls was chosen to be in the range of most common use, which being sufficiently slender that the influence of this effect on load capacity of the wall would be significant.

1.3 Outline of the Thesis

To help the reader follow the organization of the material in this thesis, the following outline is presented.

Chapter 2 contains a review of selected literature concerning the following:

1.Previous experimental investigations of concrete block walls subject to eccentric out-of-plane loading.

2.Analytical methods used in the modeling of block walls.

3.Design methods which account for the influence of wall slenderness and eccentricity of vertical load.

Chapter 3 contains a description of auxiliary tests and some physical properties of the materials used in the full scale wall tests. The experimental results of 14 full scale concrete block walls are reported in Chapter 4. The finite element model for masonry walls is described in Chapter 5. Some basic derivations and descriptions of elements used as well as the verification of the model are included. In Chapter 6, the numerical results for walls and prisms are presented and compared to the experimental data. Chapter 7 contains the evaluation of existing design methods and design equations based on the results of the current research program are proposed. Finally, in Chapter 8, a brief summary of the results of the experimental and analytical investigation, the final conclusions, as well as recommendation for future research are presented.

CHAPTER 2

LITERATURE REVIEW

2.1 Introduction

The design of load bearing concrete block walls, according to CSA Standard "Masonry Design for Buildings", CAN3-S304/M84[23], is based on the allowable stress design approach or on empirical rules. It also incorporates engineering approaches to design which have the potential to introduce improvements through rational analysis. This step to further remove empirical features from the Engineered Masonry provisions should lead to a much more consistent approach to safety and a more economical design than the previous Engineered or the Conventional Method of masonry design. The current Canadian code may be considered as being in the transitional stage prior to introducing a limit states design code. The limit states design approach will probably be the best solution to the problem of designing masonry. However, the lack of sufficient data concerning the behavior of masonry, the high variability of properties, and inadequate methods of analysis are reasons for inconsistencies in codes of different countries. Therefore, masonry design codes are still far behind the stage reached for the design of concrete or steel structures.

Modern research in masonry started in Europe and North America in the twentieth century. But the traditional approach to masonry remained relatively unchanged until the 1950's, when the Swiss showed the potential of rationally designed masonry structures. Extensive experimental and analytical investigations conducted since then have greatly enriched knowledge of the behavior of masonry.

This chapter contains descriptions of the most important experimental programs and analytical investigations. Also various design approaches and related codes are discussed.

2.2. Previous Experimental Investigations

The experimental program carried out by Richart [67] in 1931, started contemporary research in concrete block masonry. The walls were made of various types of masonry units and were tested in compression under fixed end conditions. In the 1950's an intensive research program on brick masonry was started in Switzerland. However it was not until 1971, when Yokel et al [82] tested a large number of plain and reinforced walls under different eccentricities and lateral loads, that a major North American research program was conducted for concrete block masonry. This experimental program was the basis for the moment magnifier method, proposed by the authors.

The moment magnifier approach was not accepted and masonry codes in North America were based on the Load Reduction Coefficient approach. For brick masonry in the USA, design equations were based on experimental results from test performed on brick walls by the Structural Clay Products Institute [74]. In the USA another coefficient, which will be described later in Section 2.5.1, was accepted for block masonry.

Since then several experimental programs have been carried out on concrete block walls. Interesting tests performed by Read and Clements[64,65,66] concentrated on the capacity of block walls constructed with different types of blocks. Walls were tested under vertical loads. However, fixed end conditions limited the potential use of the results, since the influence of slenderness was negligible. Drysdale et al[27] carried out a limited experimental program on pin-ended plain and reinforced walls under eccentric vertical load and/or lateral load. The experimental results showed that the design equation in the 1975 National Building Code of Canada[55] was not satisfactory for the purpose of designing concrete masonry walls. The inconsistent safety of the design and the significant underestimation of the capacity were suggested as the major disadvantages of this design equation.

Cranston and Roberts[17] carried out tests on plain, eccentrically loaded concrete block walls. However the major emphasis was placed on reinforced concrete masonry walls loaded laterally as simply supported beams. Fatal and Cattaneo[36] tested a large number of brick, concrete block and composite walls under axial (concentric and eccentric) and lateral loads. This study was a continuation of the previous work by Yokel et al[82].

Hatzinikolas et al[44,45] carried out an extensive experimental program on concrete masonry walls. Plain and reinforced walls with different slenderness were tested under pin-ended conditions for different eccentricities. Both single and double curvatures were included. The influence of the amount of vertical reinforcement and the presence of horizontal reinforcement were investigated, as well. Theoretical analysis, based on a classical beam-column approach, was carried out. The proposed design procedure was based on the moment magnifier approach.

Amrhein et al [2] conducted an experimental program to show the potential for very slender reinforced masonry walls. Based on the results obtained, they proposed elimination or a significant increase of the allowable slenderness limits for reinforced masonry walls.

2.3 Analytical Models for Concrete Masonry in Out-of-Plane Bending

The classical methods of analysis of masonry walls in weak axis bending were essentially extensions of the basic differential equation of the beam-column theory. The calculation of the buckling load of an isotropic column under different support and loading conditions was the major objective of these analyses. The methods varied depending on the assumed tensile strength of the material (no tensile strength or limited tensile strength) and on the stress-strain relationship (elastic, elastic-plastic). As reported by Hatzinikolas [44] analytical models of masonry walls in out-of-plane bending were developed by Angervo in 1954 and by Chapman and Statford in 1957. They assumed that a masonry wall was made of a linear elastic isotropic material, with no tensile strength. Many researchers including Yokel [82] and Risager [68] proposed different solutions for the basic differential equation which describes behavior of the ideal elastic column in weak axis bending. A more advanced analysis of masonry walls was performed by Chen and

Atsuta[12]. They assumed an ideal elastic-plastic model for the material.

Various numerical methods can be used to analyze masonry walls loaded as beam-columns. Drysdale et al[27] used a finite strip method to predict the behavior and capacity of plain and reinforced concrete masonry walls. In this method, the height of a wall was divided into a number of small segments and the cross section was divided into strips through the thickness of the wall. Using an incremental, iterative procedure, the balance of the internal and external forces was checked. Material or stability failure could be predicted. A non-linear stress-strain relationship was used to predict the stiffness of the wall. Ojinaga[59] used Newmark's numerical method to analyze masonry walls. In this method the deflected shape of the wall was calculated from the given curvature distribution. Both forementioned methods were fairly successful in predicting the failure loads despite major oversimplifications in the assumptions.

The other popular method used in the modeling of masonry structures is the finite element method. In numerous cases, existing computer packages were used to analyze simple two-dimensional problems. Some numerical models based on this method were developed for the purpose of investigating the behavior of particular types of masonry structures. The detailed review of the finite element method applications in masonry is included in Chapter 5, which contains the description of the proposed finite element model.

2.4 Concepts of Design

Initially all masonry structures were design using simple calculations and "rules of thumb". Research in the area of load bearing masonry structures during the 1960's and 1970's led to the use of more rational, allowable stress design methods. At present, limit states design methods are being developed. In the design process the following limit states have to be considered:

a) ultimate limit states related to capacity;

b) serviceability limit states related to the disruption of the use of the structure due to excessive deflections, local failures, and other problems.

In current masonry research, a major emphasis is on the development of consistently safe methods for predicting ultimate capacities of walls. However, the lack of sufficient experimental data and inadequate analytical models can force the acceptance of unnecessarily conservative provisions for masonry walls.

2.5 Influence of Slenderness and Loading Conditions on the Load Capacity of Walls

Independent of the design philosophy, the influences of slenderness and varying load conditions are the most important effects which have to be considered when designing a masonry wall subjected to axial load and out-of-plane bending. For traditionally thick walls, the slenderness effect was negligible. However, the tendency to use more cost effective, slender walls increased the possibility of buckling failure. High eccentricity of the axial load or lateral loading significantly increases the likelihood of stability failure. The following methods have been used to account for these effects in design:

a) the reduction coefficient method

b) the moment magnifier method

c) the displacement method.

2.5.1 Reduction Coefficient Method

Various reduction coefficients were developed to facilitate the establishment of rational design methods for masonry. Some similarities in all of the reduction coefficient methods are as follows:

1. Eccentric, vertical loads and lateral loads are reduced to a resultant concentric force and a bending moment or to a resultant force applied at a resultant eccentricity. The cross section is designed according to these equivalent loads.

2. The slenderness effect is usually incorporated as a factor which reduces the capacity of the cross section or increases the resultant loads.

3.The reduction coefficients were developed in empirical or semi-empirical ways. Usually they are based on experimental results, as in the case of the design equations developed by SCPI[74]. Sometimes it is not possible to determine, how particular equations for reduction coefficients were developed. The coefficient developed by ACI and used by Amrhein[1] is an example.

Some examples of codes using reduction coefficients are are as follows:

a) Structural Clay Products Institute[74]

The slenderness coefficient (C_s) was computed according to the formula based on results of tests of brick walls:

$$C_s = 1.20-(h/t)*(5.75+(1.5+e_1/e_2)^2)/300 \leqslant 1.0$$

where:

e_1=smaller virtual eccentricity at lateral supports

e_2=larger virtual eccentricity at lateral supports

h=effective height

t=effective thickness

The eccentricity coefficient (C_e) was calculated according to the following formulae:

$$C_e=1.3/(1+6e/t)+(e/t-1/20)*(1-e_1/e_2)/2 \quad \text{for } t/20 \leqslant e \leqslant t/6$$

and

$$C_e=1.95*(1/2-e/t)+(e/t-1/20)*(1-e_1/e_2)/2 \text{ for } t/6 \leqslant e \leqslant t/3.$$

The wall capacity was calculated as the capacity of a short axially loaded wall multiplied by C_s and C_e.

b) ACI Comittee 531, as reported by Amrhein[1]

The reduction factor R was calculated as:

$$R = 1- (h/40t)^3$$

The capacity of a wall due to vertical load was equal to the capacity of short, axially loaded wall multiplied by the reduction factor. The unity equation was used to design walls loaded under combined compressive axial load and bending moment.

c) CSA Standard CAN3-S304/M84[23]

The slenderness and eccentricity coefficients established by SCPI[74] were used. For walls with eccentricities larger than t/3 both axial force and moment were divided by the slenderness coefficient and the unity equation was used.

d) Australian Standard(24)

The reduction factor, K, which depended on slenderness ratio, eccentricity of load, ratios of end eccentricities is as follows:

$$K=0.5(1+e_1/e_2)[(1-2.083e_1/t_w)-(0.0245-0.0365e_1/t_w)(H/T-8)]$$
$$+0.5(1-0.6e_1/t_w)(1-e_1/e_2)[1-0.0225(H/T-8)]$$

where,

e_1 = largest eccentricity

e_2 = smallest eccentricityg,

t_w = actual thickness of wall

H = effective height with actual height, length and support conditions taken into consideration

T = design (effective) thickness.

The reduction factor, K, is used in the design equation where stability failure controls capacity. Other design equations which consider the strain gradient effect were established for cases where the material failure controls the capacity of the wall.

e) New Zealand Standard(25)

The same reduction factor, R, from the ACI Standard(1) is used.

f) British Standards Institution "Code of Practice for Structural Use of Masonry"(25)

The capacity reduction factor,b, allowing for the effects of slenderness and eccentricity is used:

$b=1.1(1-2e_m/t)$

where,

e_m = larger of e_x eccentricity calculated at the top of wall,

and $e_t = 0.6\, e_{x2} + e_a$

$e_a = t\,((h_{ef}/t)^2/2400 - 0.015)$

h_{ef} = effective height

t = wall thickness

g) CIB Recommendations(42)

The slenderness reduction factor, d, allowing for the slenderness of the wall and resultant eccentricity of the load is used.

d = function of ($e/t, p\, l_e / t_{ef}$ [(a))

where,

e = virtual eccentricity (from applied loads and accidental eccentricity)g,

t = actual thickness of the wall

t_{ef} = effective thickness of the wall

l_e = clear height

a = coefficient depending on loads and type of material

p = coefficient depending on supports and width of the wall.

2.5.2 Moment Magnifier Method

The moment magnifier method allows for the influence of slenderness in the design of the cross section. It assumes that the design moment, calculated as an applied vertical force multiplied by initial eccentricity, should be increased to include the effect of secondary bending. The magnification factor was derived directly from the solution for deflection of a symmetric, elastic beam-column. According to Chen and Atsuta[13], the magnification factor can be closely approximated by the simple expression :

$1/(1-P/P_E)$, where $P_E = \pi^2 EI/(h^2)$.

This expression is applicable for both simply supported beam-columns loaded symmetrically by eccentric compressive forces or by concentric force and lateral loading, provided that the ratio of P/P_E is not large. For example, for P/P_E less than 0.6, the error of the approximate solution for a beam-column with uniform lateral loading is less than 2 % compared to the exact solution. In order to cover the cases of unsymmetric loading, a reduction factor C_m is used. Different boundary conditions can be included through assuming wall height, h, equal to the effective height of the wall. The value of EI used to calculate the critical force, P_E , should include changes in cross section resulting from cracking. More precise calculation of the effective stiffness is possible if the moment curvature relationships are known.

The approach described above is used for the design of steel and reinforced concrete beam-columns. Yokel and Dikkers[83] suggested the same approach for the design of masonry walls. They proposed the following equation to calculate the design moment:

$$M = M_o \; (C_m /(1-P/P_{cr}))$$

where M_o = maximum moment imposed by external forces (eccentric vertical load and/or lateral load) and

$$C_m = 0.6 + 0.4 \; M_1/M_2 \geqslant 0.4$$

M_1 = smaller end moment acting on the wall;

M_2 = larger end moment;

M_1 and M_2 have opposite signs for double curvature bending,

$P_{cr} = \pi^2 EI/(kh)^2$ = critical load where the coefficient, k, account for the end conditions. The stiffness, EI, was calculated in the following ways:

$EI = E_i I_n/3.5$ for plain masonry,

$EI = E_i I_n/2.5$ for reinforced masonry,

where, E_i = initial, tangential modulus of elasticity for masonry

and I_n = moment of inertia of the uncracked net section.

For laterally and vertically loaded brick walls they proposed :

$EI = E_i I_n (0.2 + P/P_o) \leqslant 0.7 E_i I_n$

where, $P_o = f'_m * A_m$;

f'_m = characteristic compressive strength of masonry;

A_m = mortared area.

After studing the various shapes of stress-strain relationships, the triangular stress block based on a compressive strength of $a*f'_m$ = 1.6 f'_m was assumed for analysis.

Hatzinikolas et al (44) proposed a modification of the above method. The major difference was in the method of calculating stiffness. Starting from Yokel's solution of the differential equation for a solid plain wall with no tensile strength or a reinforced wall loaded on eccentricity not greater than t/3, they calculated the effective moment of inertia as :

$I = 8 (0.5 - e_t/t) * I_o$

For a reinforced masonry wall loaded with an eccentricity greater than t/3, they suggested that the following expression be used:

$$I = I_o \,(0.5 - e/t) \geqslant 0.1\, I_o \quad (23)$$

CSA Standard CAN3-S304-M84 contains a design method developed by Turkstra and Ojinaga[60],[61]. The following equations for the calculation of effective moments of inertia are used:

For plain masonry:

$I_{eff} = (I_1 + I_2)/4$ for $0 \leqslant e_1/e_2 \leqslant 1$,

I_{eff} = the lesser of $(I_1 + I_0)$ and $(I_2 + I_0)$ for $-1 \leqslant e_1/e_2 \leqslant 0$;

For reinforced masonry:

$I_{eff} = (I_1 + 2I_{cr} + I_2)/4$ for $0 \leqslant e_1/e_2 \leqslant 1$

I_{eff} = the lesser of $(I_1 + 2I_{cr} + I_0)/4$ and $(I_2 + 2I_{cr} + I_0)/4$ for $-1 \leqslant e_1/e_2 \leqslant 0$;

where,

I_1, I_2 = moments of inertia of the end sections (cracked or uncracked corresponding to end eccentricities e_1 and e_2,

I_0 = moment of inertia of the uncracked section

I_{cr} =moment of inertia of the cracked transformed section.

This method is shown in Fig.2.1, redrawn from reference[60]. The proposed method of calculation of effective moment of inertia can be summarized as taking the average stiffness from different cross sections of the wall.

2.5.3 Displacement Method

The displacement method is a method which takes secondary moments into consideration. It was proposed by Turkstra et al[77], and extended by Fenton[37]. The proposed method requires an iterative procedure in

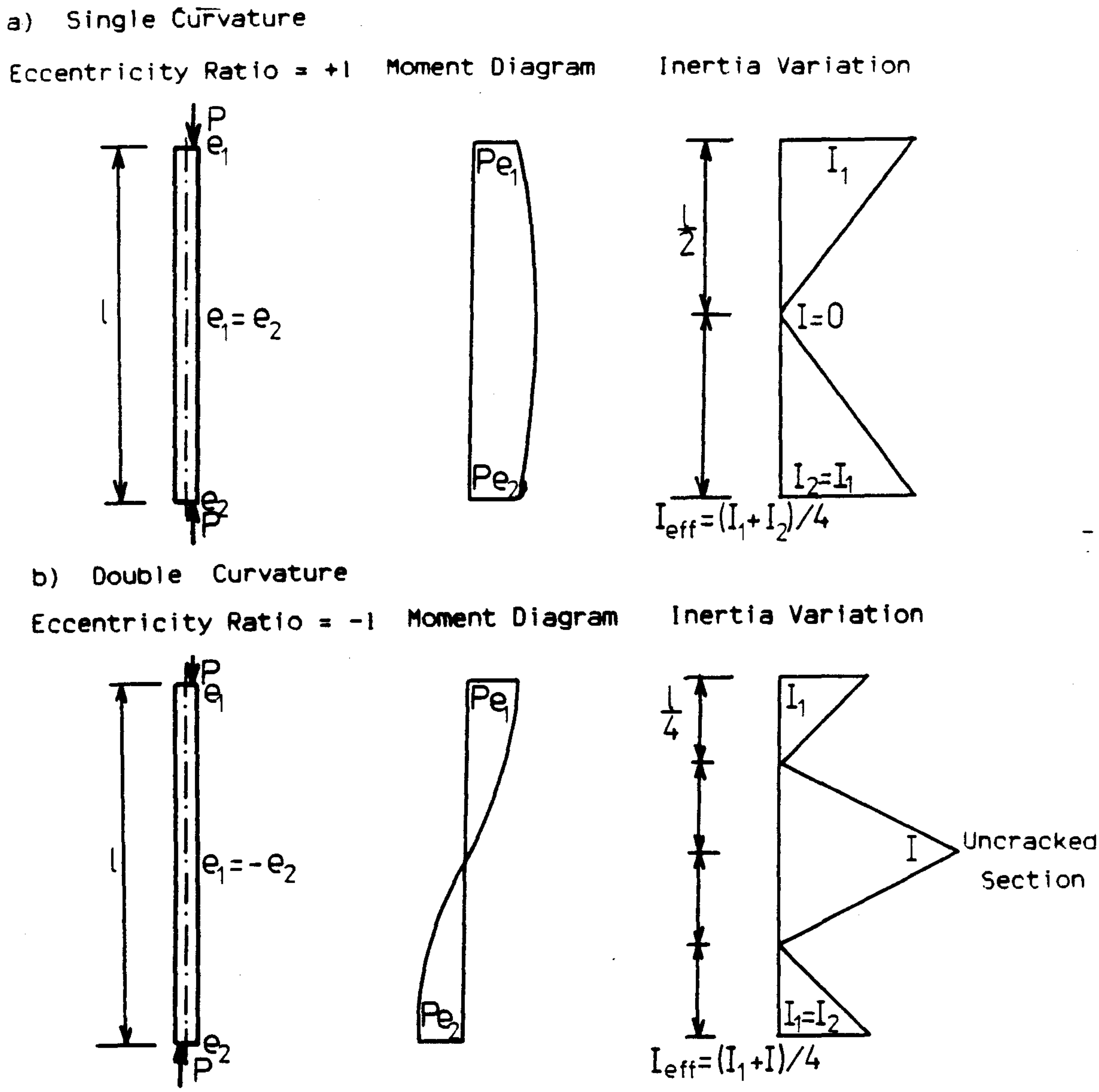

Fig.2.1 Reasoning Behind the Effective Inertia Assumption: (redrawn from Ojinaga and Turkstra[60]).

design. The initial load is assumed and the effective moment of inertia is calculated as was described in Section 2.5.2. and Fig.2.1. Then the displacement at midheight is calculated and the additional moment equal to the force multiplied by the displacement product is added to the initial moment and the capacity of the cross-section is checked. It was suggested by Fenton[37] that, up to a slenderness h/t=25, the added deflection due to secondary moments could be ignored . Nevertheless, he proposed a more accurate method which involves iterating until the residual displacement results in a change in capacity less than some arbitrary value.

2.6 Summary

In this chapter, the literature review was organized into three groups related to specific aspects of this study. They were:

1) Previous experimental studies, investigating behavior of concrete block walls, subjected to axial compressive load and out-of-plane bending moment.

2) Analytical models of concrete block walls.

3) Methods of design for concrete block walls.

The literature review concerning finite element modeling is included in Chapter 5.

CHAPTER 3

MATERIAL PROPERTIES

3.1 Introduction

Masonry is an orthotropic material composed of different elements, with greatly varying properties and interactions which are difficult to assess. For a better understanding of the behavior of structural elements, it is important to learn about the material properties of each material and then the interactions between them, in conditions where the number of variables are limited and where variables can be separated and controlled. Therefore, tests were performed to provide information which would help interpret the results of the full scale wall tests reported in Chapter 4. They also provide the necessary material properties for the analytical study reported in Chapter 6.

Auxiliary tests were done on concrete blocks, mortar, grout and steel reinforcing bars. As well compression tests of two and four block high prisms were performed. Flexural bond tests were carried out to investigate bond between blocks and mortar and pull-out tests were performed to assess bond behavior of the steel reinforcing bar-grout interface .

3.2 Individual Materials

Concrete masonry is a unique building material which is composed of concrete blocks, mortar, grout and reinforcement. Knowledge of the structural properties of each is required for understanding the behavior of the masonry structure as a whole. The major difficulties in assessing the material properties are high variability, dependence on the geometry of the specimens, and test conditions. Therefore, different tests were performed for each material in conditions which closely resembled those of actual masonry structures (as represented by by the test program).

It is the objective of this section to report on the investigation and documentation of the physical and mechanical properties of the materials used in the experimental program. All of these materials were commercially available and were similar to those commonly used in local construction.

3.2.1 Concrete Blocks

Concrete blocks are the most important component of concrete masonry structures. Therefore a series of different tests were performed to obtain information concerning compressive strength, tensile strength, stress-strain relationships, and Poisson's ratio. Only a summary of these results are provided in the following sections.

The reported data are the results of a joint effort with A.Essawy[34] and E.Gazzola[38]. A more detailed description and the full listing of the test results can be found in [38]. The results are summarized in Table 3.1.

3.2.1.1 Physical Properties

Bubble cured, concrete masonry units were used throughout the

Table 3.1 Compressive and Tensile Strength of Concrete Masonry Units

TEST SERIES	TYPE OF TEST	DESCRIPTION		NUMBER OF TESTS	AVERAGE FAILURE STRESS (MPa)	COV (%)	AREA OF APPLIED STRESS	SECANT MODULUS OF ELASTICITY* (MPa)	POISSON'S RATIO**
C1	comp	full hollow block full capping	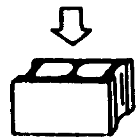	10	22.8	5.4	minimum net area		
C2	comp	half splitter block full capping	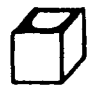	10	22.1	8.7	minimum net area	18.2×10^{3}	0.33
C3	comp	half splitter block face shell capping		10	26.8	4.4	min face shell area	15.5×10^{3}	0.30
C4	comp	4 glued faceshells full capping		10	18.5	6.1	measured area	19.6×10^{3}	0.34
C5	comp	full hollow block head joint capping tested endwise		10	18.7	13.6	average faceshell area	15.6×10^{3}	0.19
T1	splitting tens	half splitter block load face shells	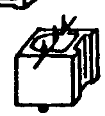	10	1.60	11.4	avg face shell area		
T2	splitting tens	half splitter block load across webs	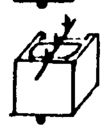	10	1.30	18.1	average web area		
T3	flexural tens	full hollow block tested out-of-plane	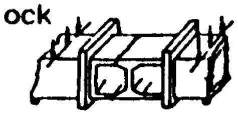	7	2.41	7.1	minimum faceshell area	$EI=1.82\times10^{12}$	

* determined at half the failure stress from only 5 specimens.
** determined from only 5 specimens for compressive strains up to $1000\mu\epsilon$.

experimental program. Two shapes of units were typical: the standard stretcher 190 mm unit having 2 cores with frogged ends, and the 190 mm kerfed or breaker unit, cut into halves. The dimensions of these units are shown in Fig.3.1. The minimum net cross-sectional area of the standard block was found to be 37,800 mm^2, using straight line approximation of the actual section. This resulted in a net to gross area ratio of 0.51.

Although there is no recognized test for the initial rate of absorption (IRA) of blocks, tests were done according to the requirements for clay bricks in ASTM Standard C-67[(6)]. An IRA of 2.97 kg/m^2/ min.) (57.4 g/min./30 $in.^2$), with a coefficient of variation of 28.6% was found based on 10 specimens. The average density of the unit, based on weighting 10 dry blocks, was 2.12 g/cm^3 (132 lb/ft^3), with a coefficient of variation of 8.2%.

3.2.1.2 Compressive Characteristics of Blocks

The compressive strength of the block is affected by the type of capping material, geometry of the specimen and orientation of loading, as well as by moisture conditions and age . Hard capping, using gypsum-cement (hydrostone), was used for all of the tests. This type of capping was chosen since better transfer of load could be guaranteed and a shorter time of hardening was required compared to mortar capping. However, the resulting higher end platen restraint does increase the apparent compressive strength.

Since it was decided that no single type of test adequately

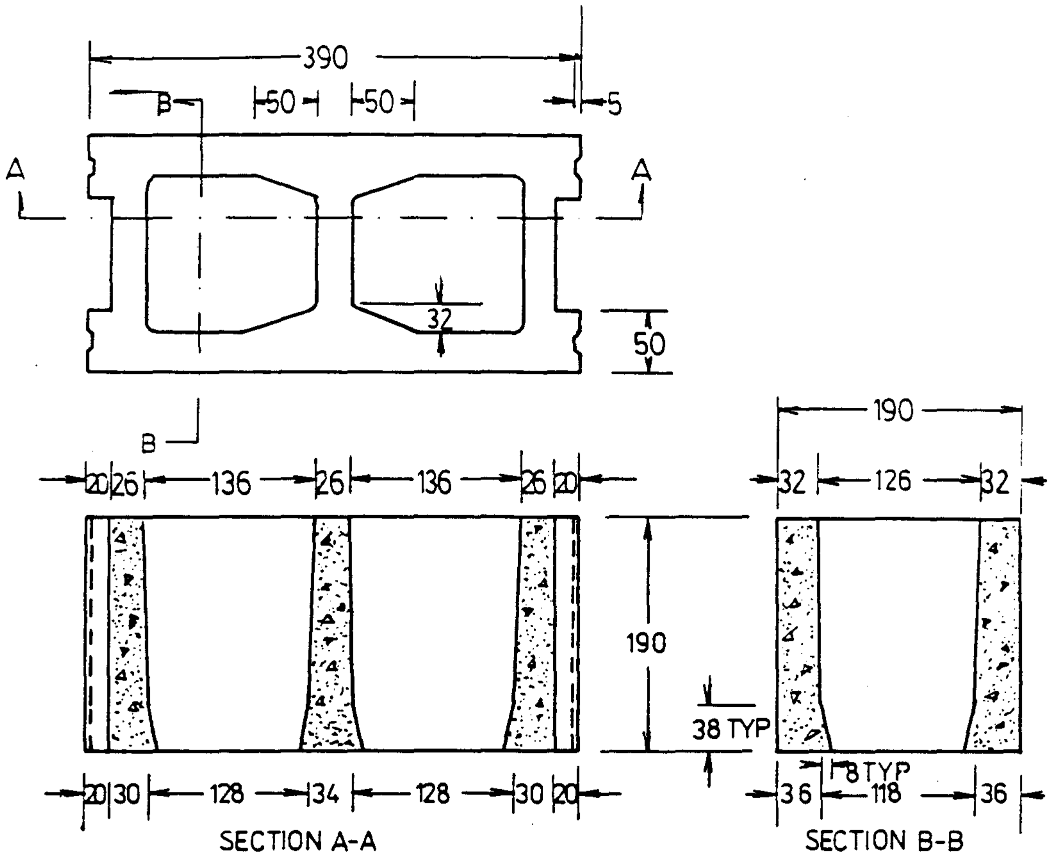

a) Standard Unit

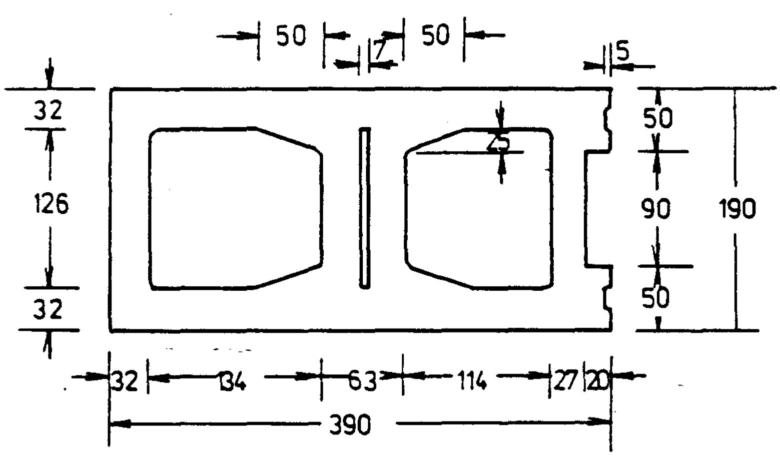

b) Kerfed or Breaker Unit

Fig.3.1 Typical Concrete Masonry Units.

described the compressive characteristics of blocks, the following five series of tests were investigated:

Test Series C1: Tests were done on fully capped, full size units, loaded flatwise as recommended in ASTM Standard C-140 [7] to measure compressive strength of blocks. However, the low aspect ratio causes a significant influence of end platen restraint. Therefore, this test series was performed mainly as a quality control test. No strain measurements were taken.

Test Series C2: Hamid [40] reported that tests of fully capped, half blocks, loaded flatwise were recommended by the National Bureau of Standards. The advantages of this test were: higher aspect ratio, nearly constant cross-sectional area (except for tapering) and the possibility of using standard testing machines with relatively thin capping plates on top of specimens.

Test Series C3: Face shell capped half blocks, loaded flatwise, were tested in conditions similar to the way blocks transfer compression in walls. Data obtained from this test series were thought to be of some possible use in discussion of design procedures. The minimum cross-sectional area, equal to the area of the face shells, was defined by the mortar bedded area. But using this data to obtain mechanical properties is not recommended, since non-uniform distribution of load caused development of the high transverse tensile stresses in the webs. This could significantly change the mode of failure. Besides, the assumption of the minimum cross-sectional area equal to the face shell area was not consistent with failure occurring at the midheight of the block.

Test Series C4: Fully capped specimens made of 4 face shells cut from standard blocks and glued together, using high strenght industrial glue, Sikadur 31, were loaded endwise. Having removed the particular influence of block geometry because of the higher aspect ratio and constant cross-section, this type of specimen could give results, which were thought to best indicate the properties of the material. Complicated preparations were the major disadvantage. The influence of gaps (between the glued face shells) on the strength of specimens was difficult to estimate.

Test Series C5: Tests of face shell capped, full size units, loaded endwise were performed to represent the strength of blocks in the direction parallel to the bed joint. They could not be used to assess structural properties, since the assumed minimum area was valid only for a small part of the block. Besides, the dominating shear type mode of failure did not allow for a proper interpretation of the compressive strength of the material in a uniaxial state of stress.

Test results are summarized in Table 3.1. Fig.3.2 contains all of the stress-strain relationships for the previously mentioned tests. The compressive strength varied from 18.5 MPa for Test Series C4 to 22.8 MPa for Series C1.

Initially, test results for the glued specimens, Series C4, were thought to be the best to assess the properties of the concrete blocks. It was observed that the regression lines for Test Series C2 and C4 initially followed the same curvature up to a strain equal to 0.001. At higher strains, the stiffness of the glued specimens decreased

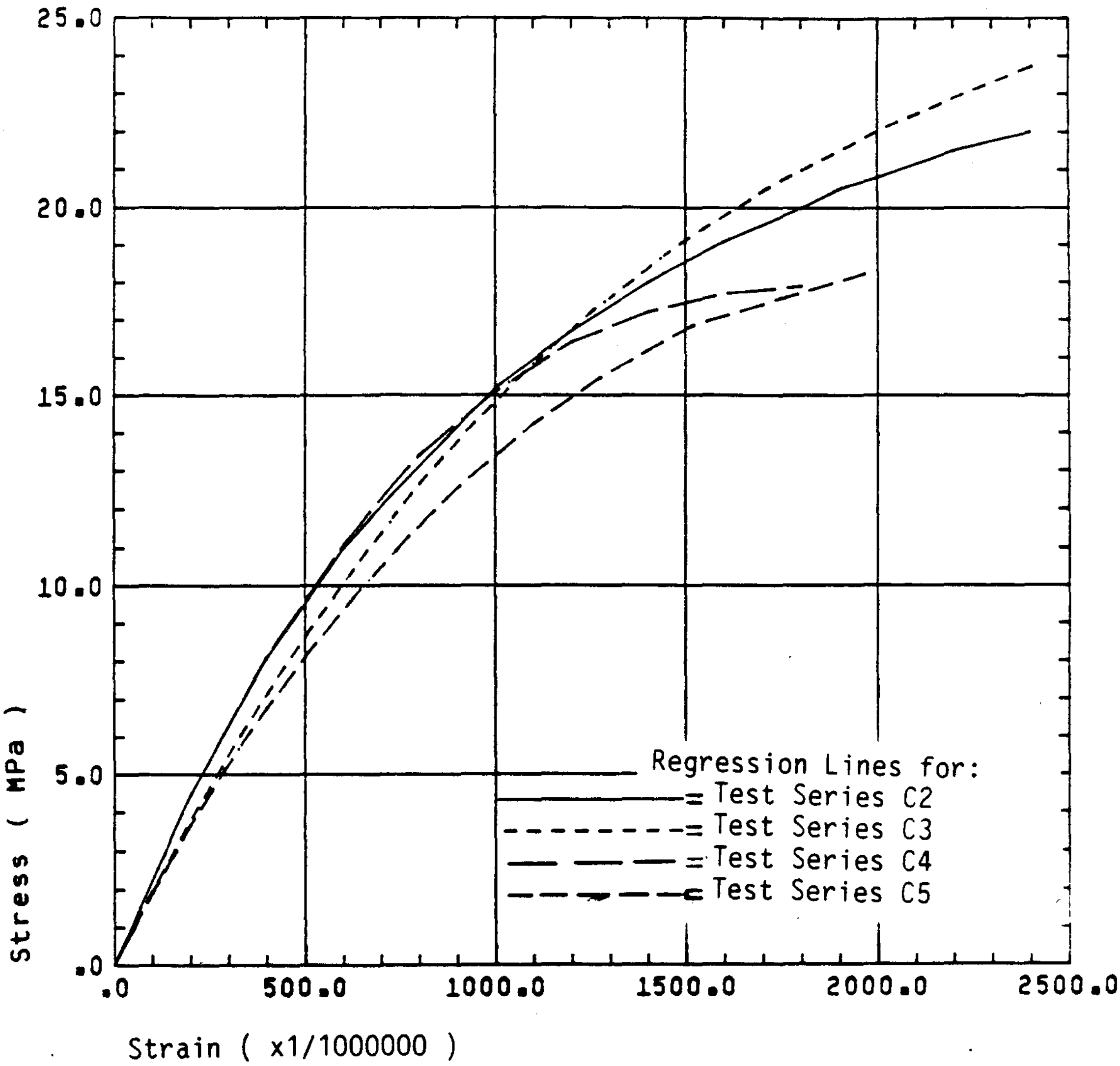

Fig.3.2 Regression Stress-Strain Relationships for Block Tests.

significantly. It was thought that this lower stiffness might have been caused by the lack of continuity or gaps between the spot glued face shells. Therefore, the results from testing fully capped half blocks, loaded endwise (Test Series C2) were finally chosen as the most representative for material properties of blocks in compression.

It was noticed that the values of secant modulus of elasticity obtained from experimental results (19700 MPa for Test Series C4 and 18200 MPa for Test Series C2, were reasonably close to the theoretical value calculated using the empirical formula for concrete[79] $E_c=1350 w^{1.5}\sqrt{(f'_c)}$ ($E_c=33w^{1.5}\sqrt{(f'_c)}$ in Imperial units), equal to 19600 MPa.

3.2.1.3 Tensile Characteristics of Blocks

There is no universally accepted method of measuring the tensile strength of concrete blocks. However, the two major techniques used were splitting tension and flexural tension. As was shown by Hamid[40], tensile strength is affected by the strain gradient. Therefore, the methods were chosen to be representative of stress conditions existing in masonry walls. The splitting tension test was chosen as a measurement of direct tension, whereas bending tests would more adequately represent flexural tension conditions.

Blocks were tested in splitting with line loads applied perpendicular to face shells (Test Series T1), or to webs (Test Series T2). The average strength for 10 specimens was 1.6 MPa for face shells and 1.3 MPa for webs, with a coefficient of variation of 11.4% and 18.0%, respectively. The modulus of rupture of block tested in out-of-plane bending (Test Series T3) was 2.4 MPa as an average of 7 tests, with a coefficient of variation of 7.1%.

The ACI Code, as it was reported in Wang and Salomon[79], used the following empirical equation for split-cylinder tensile strength: $f_{ct} = .473\sqrt{(f'_c)}$ ($f_{ct} = 5.7\sqrt{(f'_c)}$ in Imperial units). In this case, assuming $f'_c = 22.1$ MPa (Test Series C2), it yielded $f_{ct} = 2.2$ MPa which is nearly 10% of f'_c. Lower test values could arise from the inaccuracy or variability of the test. However, it is thought that the lower value is more likely due to the fact that the concrete material in blocks varies and that the manufacturing process may also cause microcracking or other forms of tensile weakening.

3.2.2 Mortar

Type S mortar was used throughout the experimental program. The mortar was mixed in accordance with CSA Standard A179/M76[21]. Normal Portland Cement (type 10, CSA Standard A5/M83[18], type S lime (CSA Standard A82.43/50[19]) and sieved sand were proportioned by weight with 1 part cement, 0.21 part lime and 4.24 parts sand (proportions by volume were 1:1/2:4). The sieve analysis of sand, as shown in Table 3.2, met requirements of CSA Standard A82.56/M76[20]. The finenesses for 3 samples were 2.17, 2.22 and 2.45, where two samples came from one batch of sand and the last value was obtained for different batch of sand. The water content was established by the mason's requirements for suitable workability. It provided mortar with an initial flow ranging from 105% to 120%, with an average of 117%. Mortar was mixed manually in 43.5 kg batches. From each batch three 51 mm (2 in.) cubes were cast

Table 3.2 Sieve Analysis of Mortar Sand

Sieve Size	Percentage Passing Specimen # 1	Specimen # 2	Specimen # 3
#8	99.9	100.0	100.0
#16	82.6	89.0	90.1
#30	44.9	52.5	54.0
#50	19.1	24.7	26.0
#100	8.5	11.8	12.3

Table 3.3 Sieve Analysis of Grout Sand

Sieve Size	Percentage Passing
#4	98.7
#8	88.3
#16	73.9
#30	39.7
#50	17.5
#100	7.2

in non-absorbent molds.

Various tests were performed to evaluate mechanical properties of the mortar in conditions representative of circumstances existing in actual walls. The compressive strength, the modulus of elasticity and the Poisson's ratio were investigated. Two different types of mortar specimens were tested. Also strains were measured over mortar bed joints during the tests of plain prisms.

It was expected that there would be a significant difference between mortar in bed joints and in cubes. Therefore, tests for the density and the volume of voids were performed. Calculated values were based on results of weight measurments of mortar specimens in air and water with completly filled voids. The density of the mortar in cubes was 1.89 g/ cm^3 (118 lb/ft^3) and the volume of voids was 22.5% of total volume. For mortar taken from the bed joints these values were 2.04 g/cm^3 (127 lb/ft^3) and 15.9%, accordingly. In both cases the given values are the average results for 3 samples.

The 78 air cured mortar cubes were tested in compression at the age of 11 months. The average compressive strength was 20.8 MPa, with a coefficient of variation of 12.7%. For 10 cubes lateral and vertical strains were recorded. No conclusive results were obtained due to high variability. The analysis of the data obtained from the strains measurements over bed joints was similarly inconsistent. The modulus of elasticity, obtained from the analysis of the experimental results, ranged from 9500 MPa to 22300 MPa.

Due to lack of conclusive results, tests for the modulus of rupture of mortar was used to evaluate the modulus of elasticity of mortar. A schematic view of the test set-up is shown in Fig.3.3. The seven specimens were cut from mortar bed joints from previously tested walls. They were formed in the shape of prismatic beams about 190 mm long, with a cross section of about 30 mm by 11 mm. Each beam was loaded at two points. Deflections at midspan were measured using an induction deflectometer with a resolution of 0.001 mm. The load was applied through a steel ring load cell with four electric resistance strain gauges connected as a full bridge. The load cell was calibrated up to 200 N, with an accuracy of about 1%. Readings from both the deflectometer and the load cell were recorded on an oscilloscope. The load was applied very slowly up to failure, with each test taking about 5 minutes. After each test, results were plotted using a plotter connected to the oscilloscope. Relationships were approximated by straight lines which was a justified simplification, since linear behavior dominated with mortar becoming plastic only close to failure. The modulus of elasticity obtained in this way was 16690 MPa, calculated as an average of six tests. The coefficient of variation was 12.3%. The modulus of rupture obtained from these experiments was 5.4 MPa, with a coefficient of variation of 24.4%.

It is known that the physical properties of mortar are influenced by the proportions of the components, the geometry of specimens, the curing conditions and the method of testing. This was shown by Hamid[40], and the experiments described above. The commonly used air cured cubes can be used only for quality control, since they are not truly representative of the actual mortar in masonry structures. The

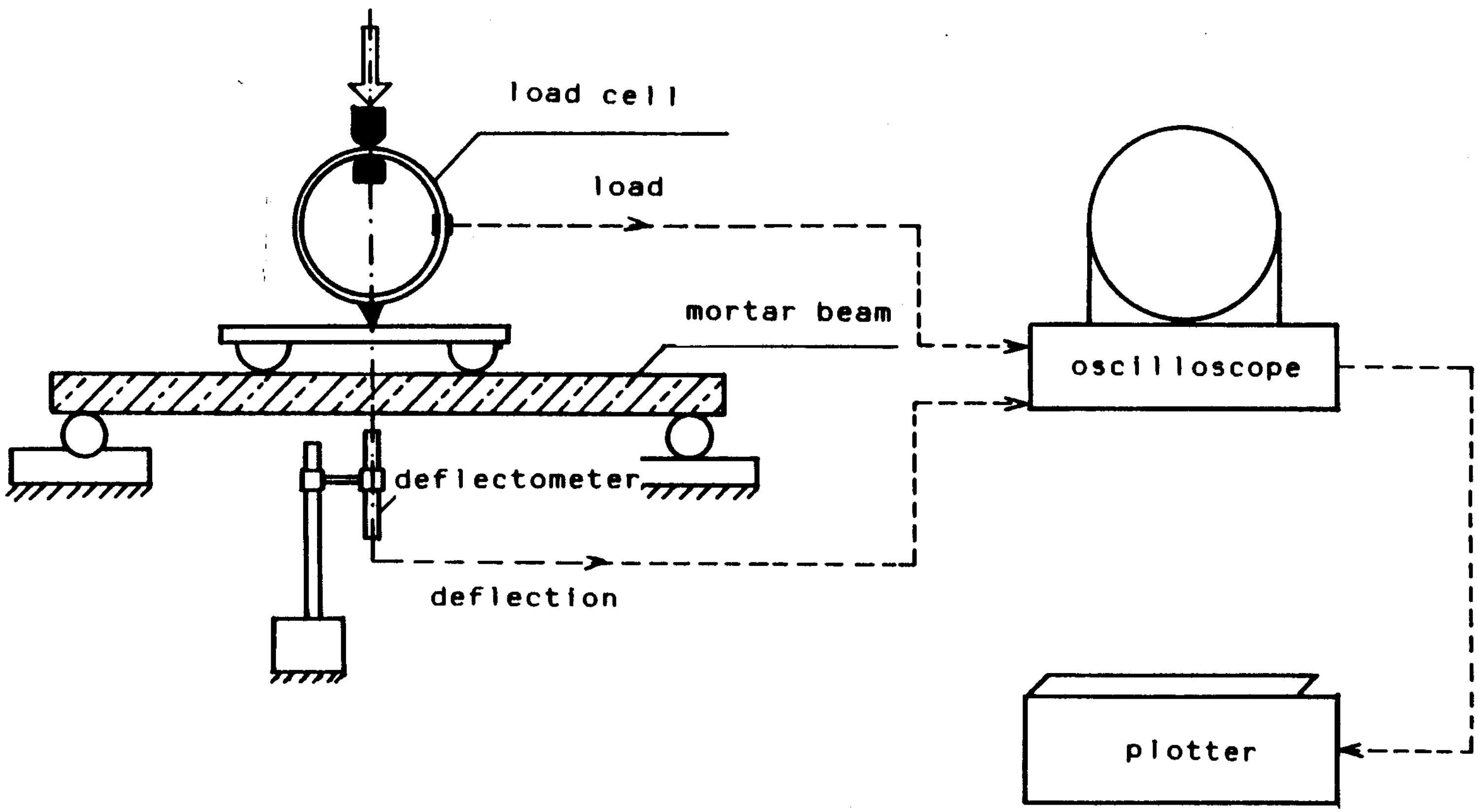

Fig.3.3 Schematic View of Test Set-Up for Mortar Beams.

absorption of water from mortar by masonry units seemed to be the most important factor, as shown by Hamid[40]. Higher compaction of mortar in bed joints than in cubes was likely the second most important factor and might also be related to moisture absorption. As indicated by the porosity of 15.9% voids in bed joints compared to 22.6 voids in cubes, the mortar was altered by being placed between blocks. Nevertheless, since there were not any better methods available, the tests performed were used to evaluate the properties of mortar to be used later in the numerical analysis. The assumed value of the modulus of elasticity, based on the modulus of rupture test, was inside the range obtained from mortar cube tests and from strain measurements over bed joints in prisms. This was deemed to be representative of the modulus of elasticity of mortar.

The assumed compressive strength, equal to the average strength of mortar cubes, was believed to represent the lower bound of the actual strength of mortar. Since the failure of walls is not usually caused by failure of mortar in compression, the influence on the accuracy of the analysis should not be significant. Similarly, the influence of error in the estimation of the modulus of elasticity of mortar on the numerically predicted deflections of walls would not be significant since mortar bed joints represented only about 5% of the total height of a typical wall.

3.2.3 Grout

Fine grout was used throughout this test program. It contained Portland Cement ,lime and sand in the following proportions:

1.0:0.1:3.33 by volume; or 1.0:0.044:3.55 by weight. The gradation of the concrete sand used in the mixes is shown in Table 3.3. It met the specification of ASTM Standard C404/70[8]. The water-cement ratio was established to give a slump of about 280 mm. Grout was vibrated using a 30 mm diameter poker type vibrator. The density of grout was found to be 2.07 g/cm^3 (129 lb/ft^3), with 12.0% voids. The two types of control specimens used were air cured 152 mm diameter by 304 mm high cylinders and block molded 75 mm by 75 mm by 150 mm prisms, cast with an absorbent paper towel as a separator.

For each of ten batches of grout, one cylinder and one prism were prepared. Grout specimens were stored in the laboratory. At the age of 8 months, they were tested in uniaxial compression or in splitting tension.

Uniaxial compression test: For five grout cylinders tested under axial load, vertical strains were measured using the "Demec" strain indicator with a 200 mm gauge length. The average strength was 30.0 MPa, with a coefficient of variation of 3.5%. The stress-strain results for all the tests are shown in Fig.3.4, where each point represents an average of three readings. From a regression analysis, the following fourth degree polynomial was obtained:

$$s = 20361\,e - 306511\,e^2 - 5.16*10^8\,e^3 + 1.15*10^{11}\,e^4 ,$$

where s is in MPa and e is strain. The secant modulus of elasticity, calculated for one half of the compressive strength, was 17410 MPa.

The five grout prisms tested in uniaxial compression had vertical strains measured using the "Huggenberger" mechanical strain indicator, with a 100 mm gauge length. The average compressive strength was 35.3

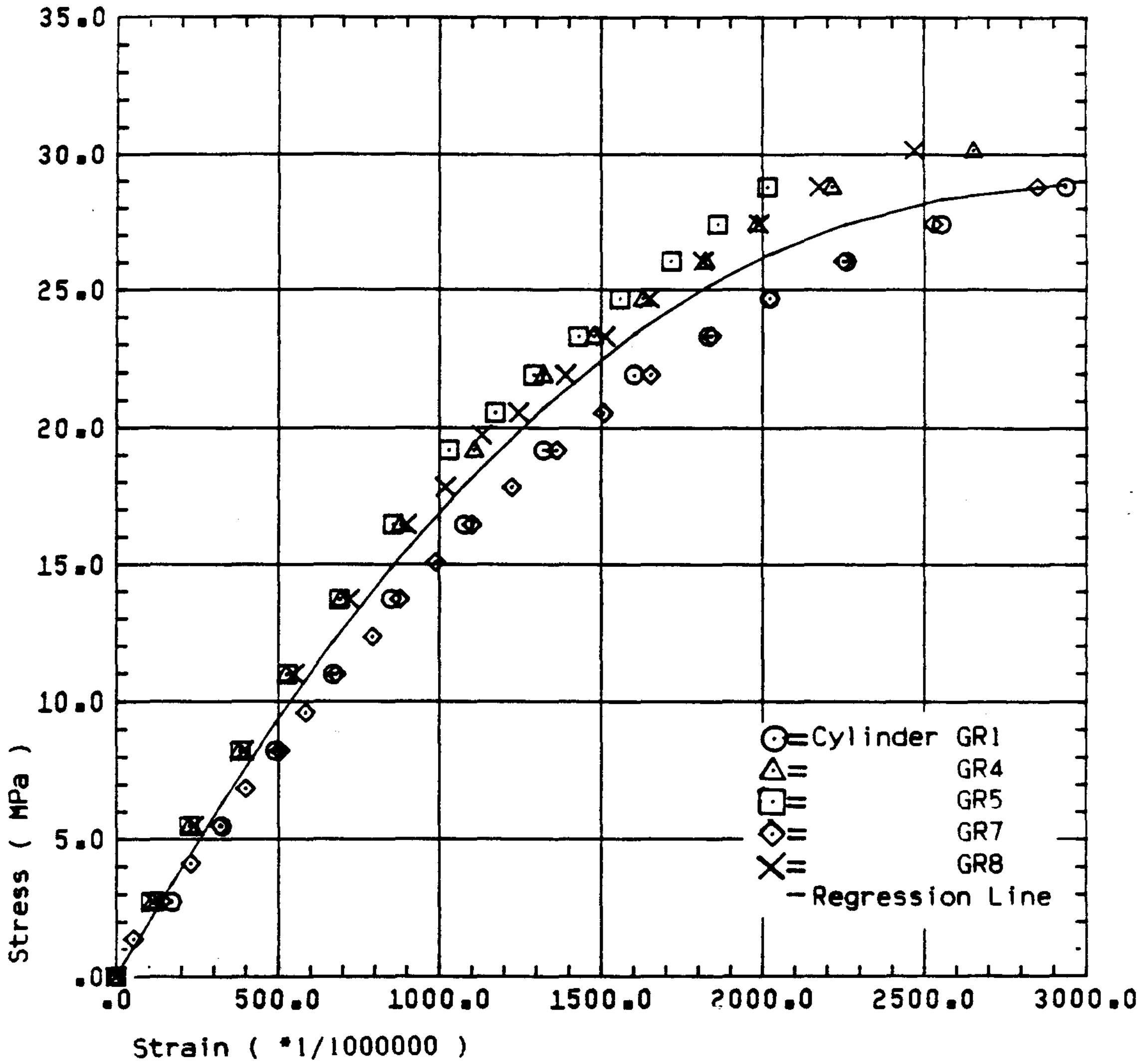

Fig.3.4 Stress-Strain Results for Grout Cylinders.

MPa with a coefficient of variation of 7.3%. The stress-strain relationships for all specimens are shown in Fig.3.5, with each point representing an average of two readings. From a regression analysis, the following fifth degree polynomial was obtained:

$$s = 24144\, e - 2400923\, e^{2} - 5.22*10^{8}\, e^{3} - 4.27*10^{10}\, e^{5}$$

where, s is in MPa and e is strain. The secant modulus of elasticity, calculated for one half of the average compressive strength, was 21840 MPa.

<u>Splitting tension</u>: The four cylinders tested in splitting tension were loaded through 16 mm diameter bars. Plywood strips (20 mm wide and 6 mm thick) were placed between the bars and the surface of the cylinders to prevent local stress concentrations. All the specimens failed in splitting due to transverse tensile stresses. The splitting tensile strength of the grout was calculated using the relationship: $f'_{ct} = 2P / \pi Dh$, where P is the applied force, and D and h are the diameter and height of the cylinder, respectively. The average tensile strength was 2.9 MPa with a coefficient of variation of 3.2%.

The five grout prisms were tested in a similar way and the average tensile strength was 2.9 MPa with a coefficient of variation of 21.4%.

3.2.4 Steel Bars

The vertical reinforcement used was 15M bars. Tension tests of three specimens resulted in an average yield stress of 462 MPa, with a coefficient of variation of 2.3% and an average modulus of elasticity of 203000 MPa based on a bar of 2.00 cm^{2}.

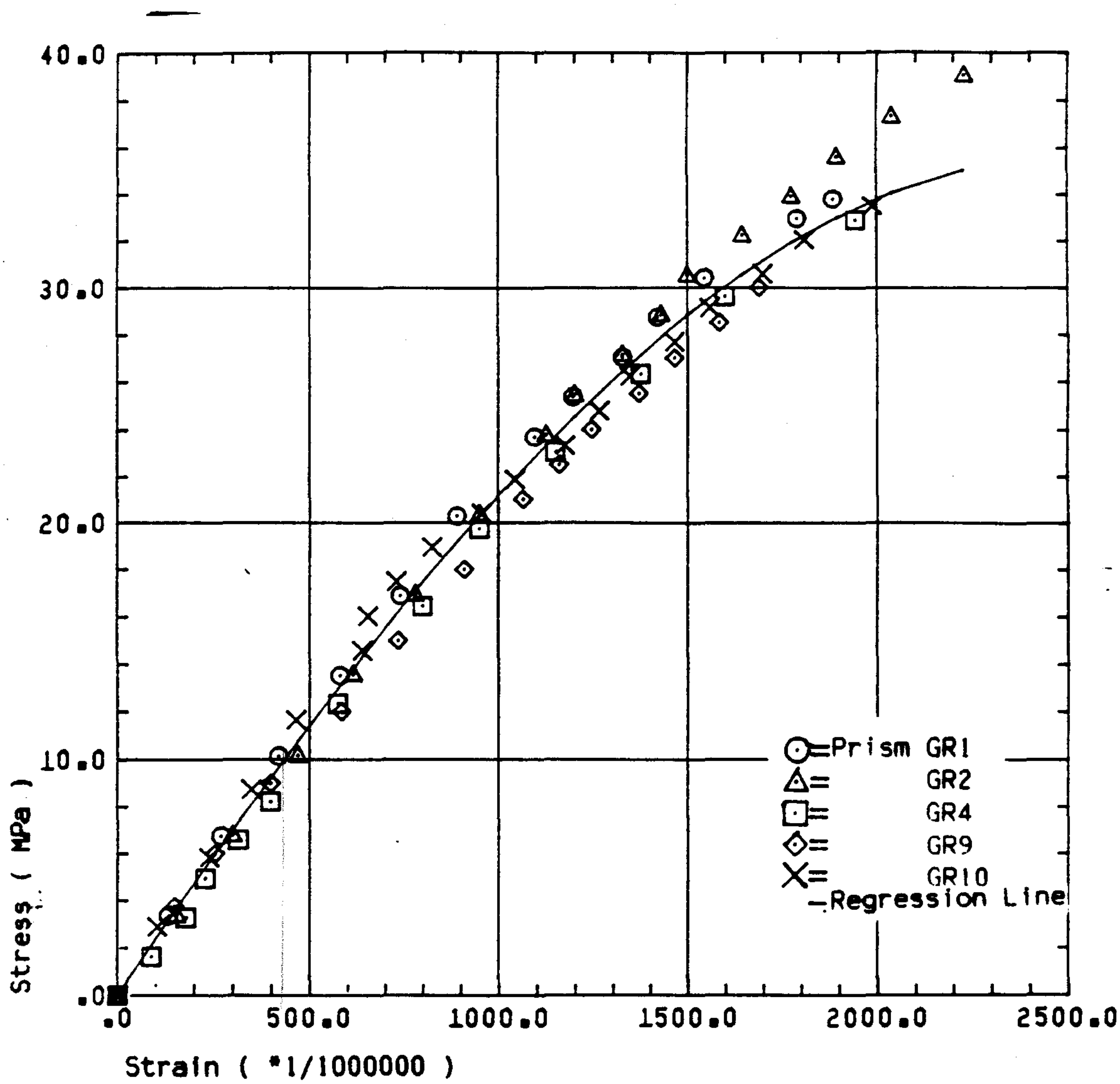

Fig.3.5 Stress-Strain Results for Grout Prisms.

3.3 Tests of Concentrically Loaded Block Prisms

3.3.1 General

According to CSA Standard CAN3-S304/M84[23], Clause 5.3, the compressive strength of masonry can be determined by testing prisms two or more blocks high. For this investigation two and four block high prisms were tested. The four block high prisms were chosen as the standard to avoid the influence of end platen restraint. Experimental results[10,51,81], and finite element analysis,[15], indicate that the behavior of four block high prisms are representative for the performance of masonry walls for conditions not influenced by slenderness or strain gradient. Prisms were tested essentially in conformance with CSA Standard A369.1/M84[22], with the exception of using pin-pin end conditions instead of the suggested pin-fixed condition. In addition, fibreboard was not used as capping, but hard gypsum plaster was used.

3.3.2 Fabrication and Preparation of Prism for Testing

The prisms were made by an experienced mason at the same time as the test walls were fabricated. The eleven 2 block high prisms were build in stack pattern and the eleven 4 block high prisms were fabricated in running bond. Three 4 blocks high prisms, prepared for grouting, were built with full mortar bed joints, the remaining prisms had face shell bedding. All mortar joints were tooled with a cylindrical jointer. The prisms were stored in the laboratory and were air cured under the same conditions as the slender walls. A schematic view of the test set-up is shown in Fig.3.6. A 2500 kN Riehle testing machine was used to load the prisms. Load was transferred from the spherical seated loading head through a 25 mm by 51 mm rectangular bar to a 76 mm thick top capping plate. The bottom capping plate was seating on a cylindrical bearing consisting of two plates with grooves and a 38 mm diameter bar. The capping plates were bonded to the ends of prisms using approximately 3 mm thick layers of gypsum-cement. All the ungrouted prisms were capped along the face shells. This was facilitated by the use of cardboard to prevent the capping from spreading over the webs of the blocks.

During testing, strains were recorded at each load increment using the "Demec" mechanical strain indicator or electric strain transducers. A sketch of the location of the mechanical gauge points and strain transducers is shown in Fig.3.7.

3.3.3 Test Results for 2 Block High, Ungrouted Prisms

There is no universally accepted approach concerning the assumption of the active cross section of masonry structures made of hollow units. The gross area is not representative since areas of cores and webs not covered with mortar are not excluded. On the other hand, the assumption of the minimum face shell thickness, as a basis for calculation of the mortared area, is not precise, since it does not consider overlapping of parts of blocks, irregularity of the shape of cores and penetration of mortar. However, the influence of the assumed cross sectional area for design purpose is minimized as long as the same area is used to analyze the results of tests of prisms and to

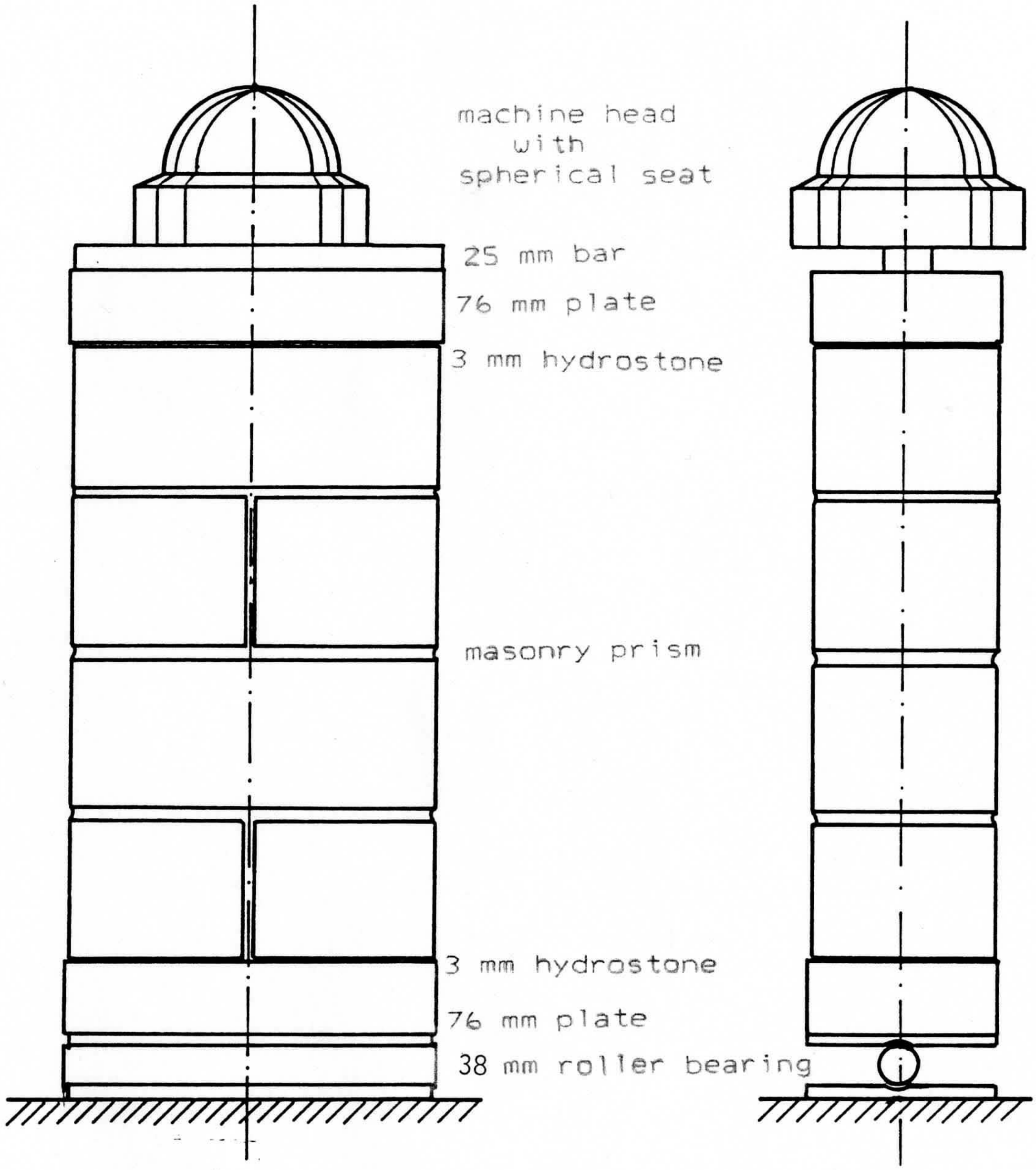

Fig.3.6 Schematic View of Test Set-Up for Prisms.

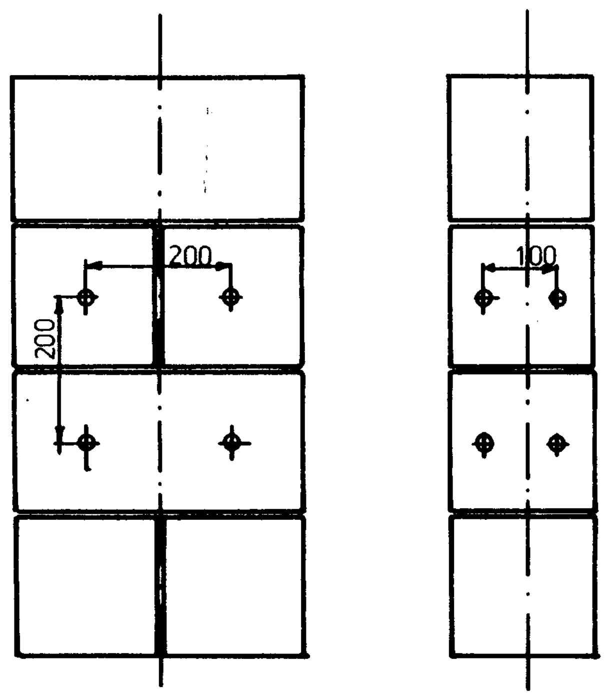

a) Set No.1

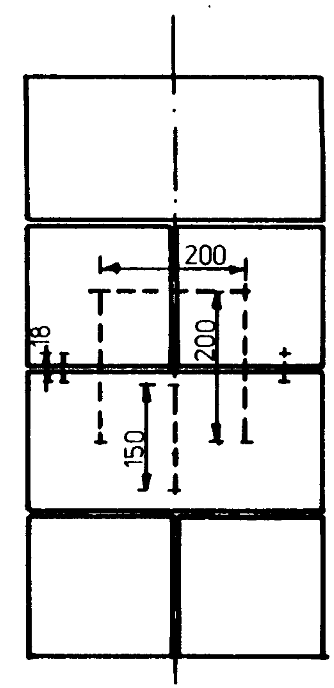

b) Set No.2

Fig.3.7 Locations of Strain Measuring Points.

design a wall. This of course requires that the same materials and workmanship are used.

The precise evaluation of mortar bedded area is crucial for the theoretical analysis of masonry, which takes the actual geometry into account. Careful comparison of the solid areas of the top and bottom surfaces of the concrete blocks used in the present program, suggested that the maximum mortar bedded area was equivalent to the area of two 40 mm wide mortar strips. The verification using the actual specimens supported this assumption. This area was used in the analysis of all test results and in the finite element model. It meant that the effective area of mortar was about 25% more than the minimum area resulting from the minimum face shell thickness of 32 mm. Similar effective areas of mortar in bed joints were assumed by Hatzinikolas et al[44], as well as by Drysdale and Wong[32].

Two block high ungrouted prisms were tested in two sets. The first set consisted of three prisms. The mean failure load was 654.3 kN, with a coefficient of variation of 7.5%. Assuming the mortar bedded area, as it was described above , the mean strength was 21.0 MPa. The stress-strain relationships for all three prisms are shown in Fig.3.8. Each data point represents an average of four readings. Strains were measured over bed joint using a 200 mm gauge length. The regression line for this data was:

$$s = 19275\ e - 2738473\ e^{2} - 1.95*10^{9}\ e^{3} + 5.13*10^{11}\ e^{4}$$

with the secant modulus of elasticity at half the strength equal to 16950 MPa. A conical failure, similar to that for fully capped, full size units, predominated. These results seemed to suggest that a higher

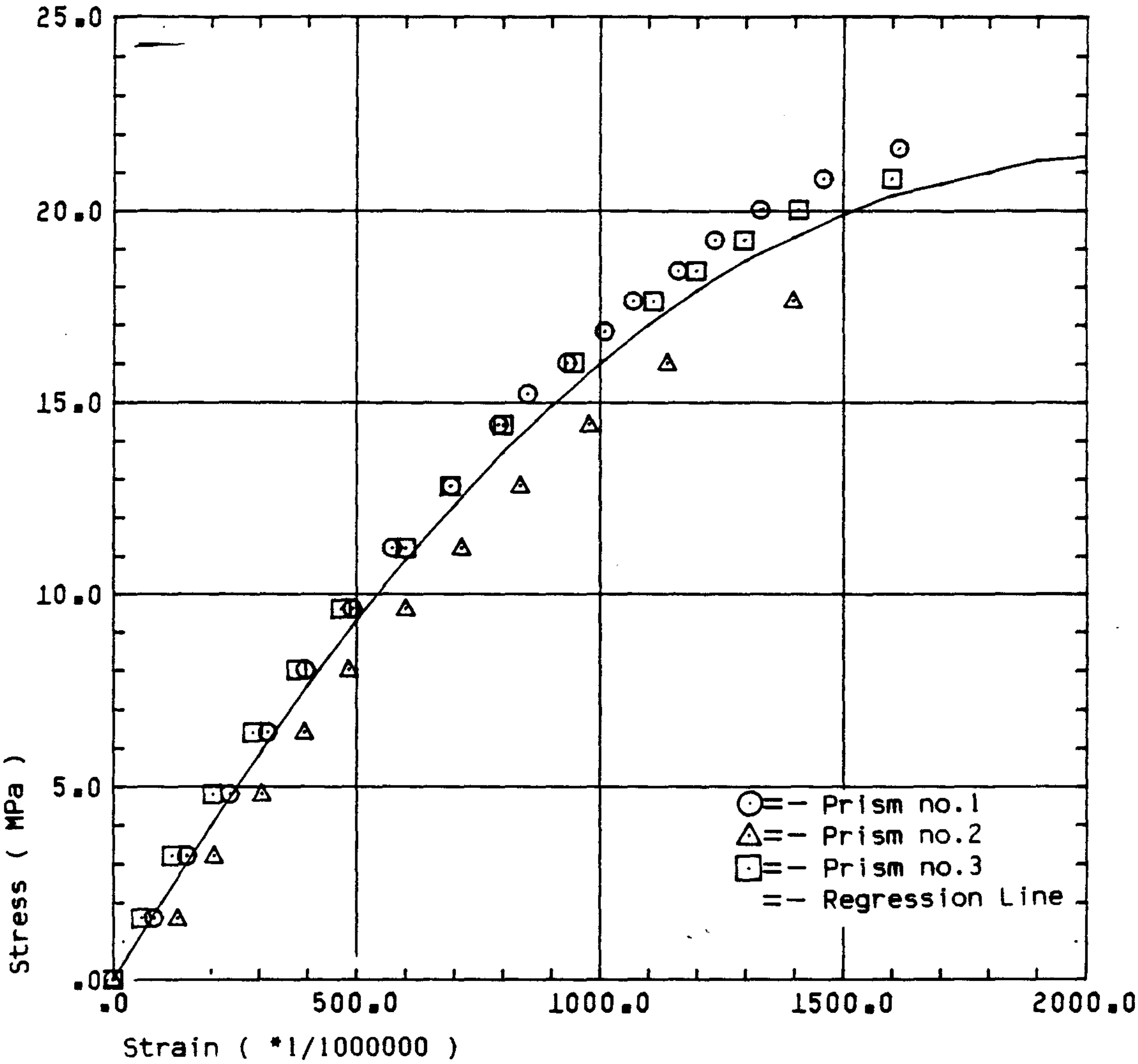

Fig.3.8 Stress-Strain Results for 2 Block High Plain Prisms (Data Set No. 1).

penetration of mortar than had been assumed may have occurred.

Therefore, in the second set of 2 block prisms, webs were checked and wet mortar was removed from the central narrow parts of the webs up to the wider parts forming the pear shape of the cores. The mean failure load for five specimens was 533.2 kN, with a coefficient of variation of 7.8%. Assuming the same area as for the first set, the average strength was 17.1 MPa. For 3 prisms, strains were recorded using electrical strain transducers. Strains were measured over bed joints using a 200 mm gauge length. For the stress-strain results shown in Fig. 3.9, each point represents the average of four readings. The following fourth degree polynomial was obtained from a regression analysis:

$$s = 24761\,e - 19120960\,e^{2} + 1.99 * 10^{11}\,e^{3} - 9.58 * 10^{12}\,e^{4}$$

with the secant modulus of elasticity at half of the strength equal to 20530 MPa. In addition , strains were measured within the block height using a 150 mm gauge length and over mortar bed joints using a 17 mm gauge length. Failure was always initiated by vertical splitting of the webs and followed by the buckling of the face shells at the higher load levels.

3.3.4 Test Results for 4 Block High Ungrouted Prisms

Prisms were tested in two sets. The first set consisted of three specimens. The mean failure load was 608.3 kN, with a coefficient of variation of 7.6%. Assuming a mortar bedded area equal to the equivalent area of two 40 mm wide strips, the average strength was 19.5 MPa. During loading, strains were measured over the middle bed joint using 200 mm

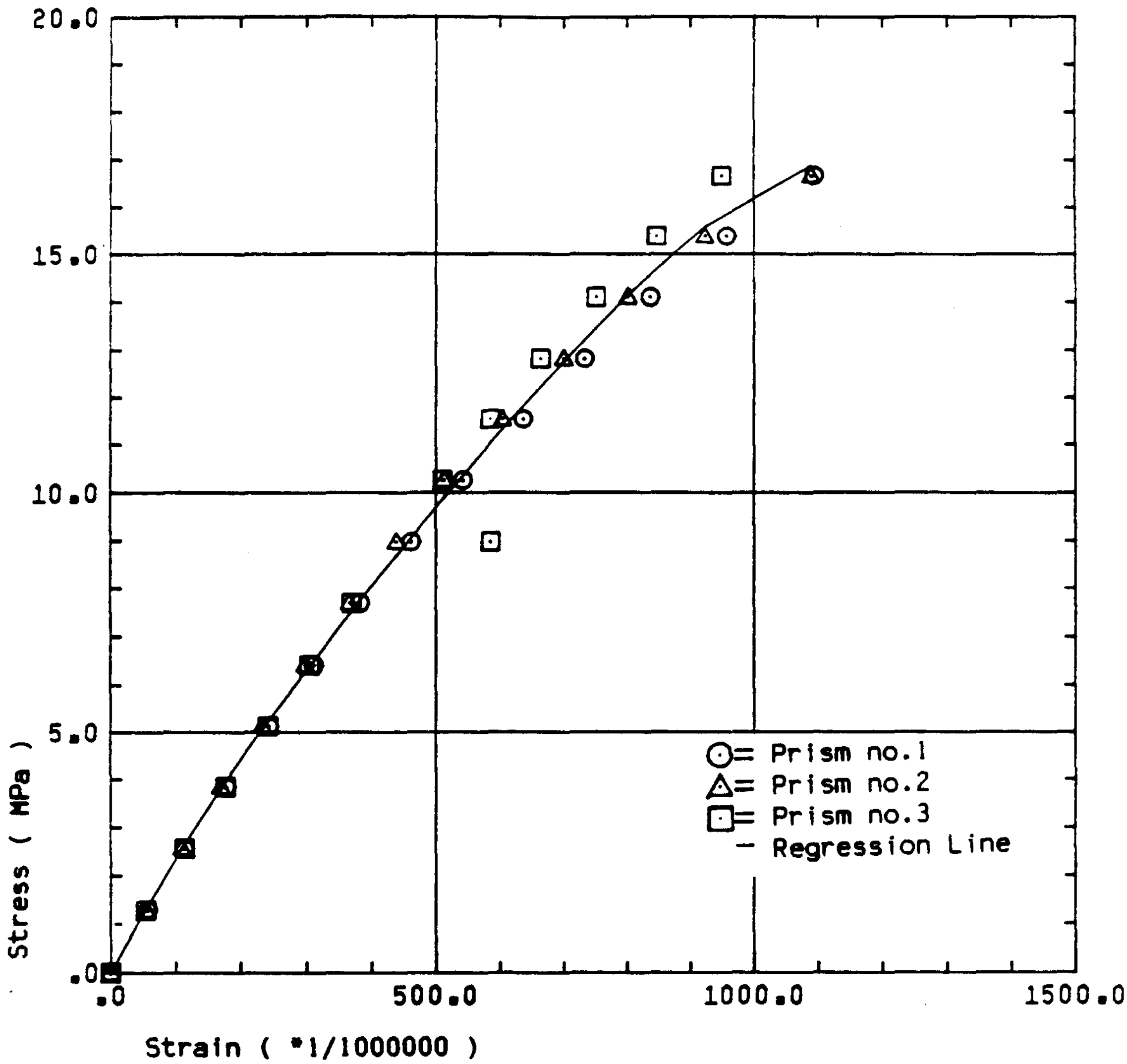

Fig.3.9 Stress-Strain Results for 2 Block High Plain Prisms (Data Set No. 2).

gauge lengths. The stress-strain relationships, obtained as a result of these tests are shown in Fig.3.10. Each point represents the average of four readings. The regression line for this set of data was:

$$s = 22713\ e - 5297930\ e^{2} - 6.47*10^{11}\ e^{4}$$

with the secant modulus of elasticity at half of the strength equal to 20060 MPa. Prisms failed in a conical failure mode with visible separation of the outside webs at the two midheight blocks. The typical failure mode is shown in the photograph in Fig.3.11(a). Inspection of the prisms after failure showed that the penetration of mortar was higher than assumed. Nevertheless, these prisms could not be classified as fully bedded since the webs are not aligned in prisms built in running bond.

To avoid this problem, prisms in the second set were checked for mortar laying on webs and excess mortar was carefully removed. The mean failure load for five specimens was 550.2 kN, with a coefficient of variation of 2.8%. Assuming the same mortar bedded area as for the previous set, the average prism strength was 17.6 MPa. Strains were recorded for two prisms using electric strain transducers. Strains were also measured over bed joint using a 200 mm gauge length. Stress-strain results are shown in Fig.3.12, where each point represents the average of four readings. The regression line was:

$$s = 24416\ e - 9890601\ e^{2} + 2.37*10^{9}\ e^{3} - 9.27*10^{11}\ e^{4}$$

with the secant modulus of elasticity at half of the strength equal to 20530 MPa. All the prisms failed due to splitting of webs with buckling of the face shells following. The typical failure mode is shown in Fig.3.11(b).

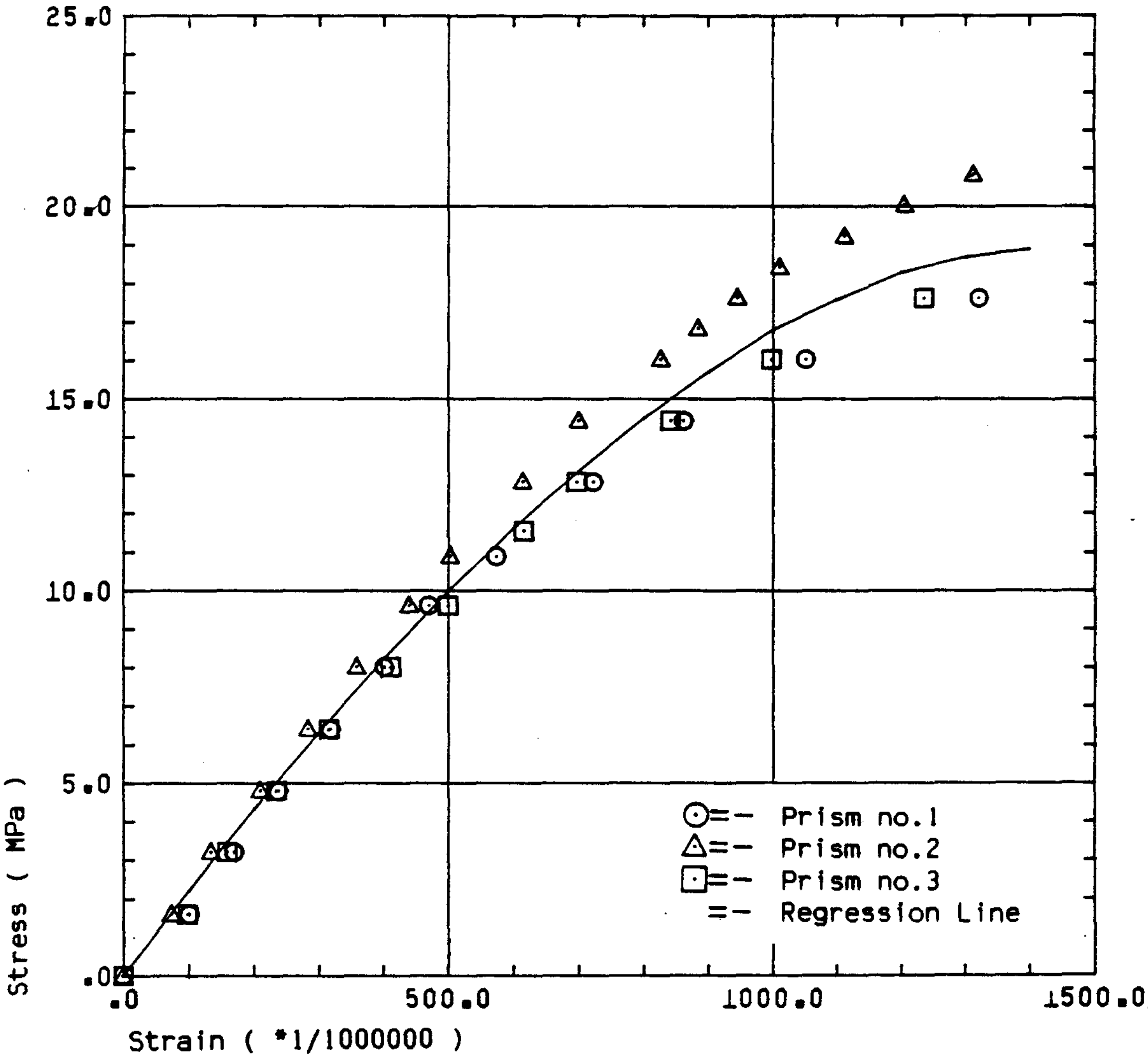

Fig.3.10 Stress-Strain Results for 4 Block High PLain Prisms (Data Set No. 1).

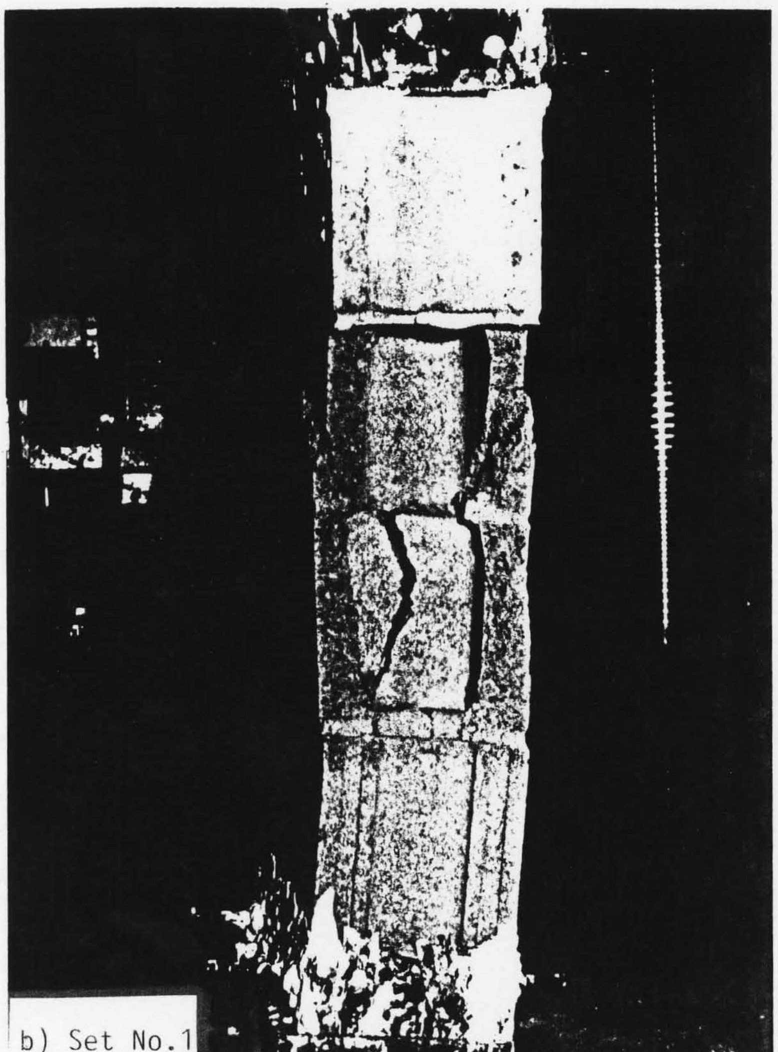

b) Set No.1

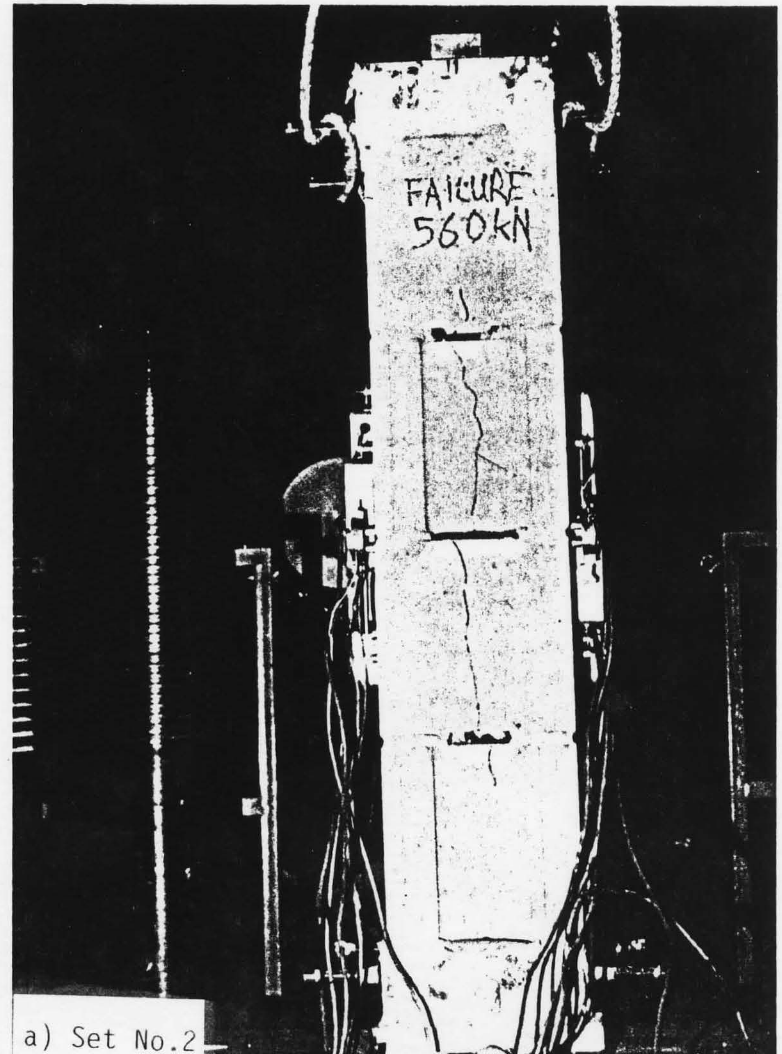

a) Set No.2

Fig.3.11 Typical Failures for 4 Block High Plain Prism.

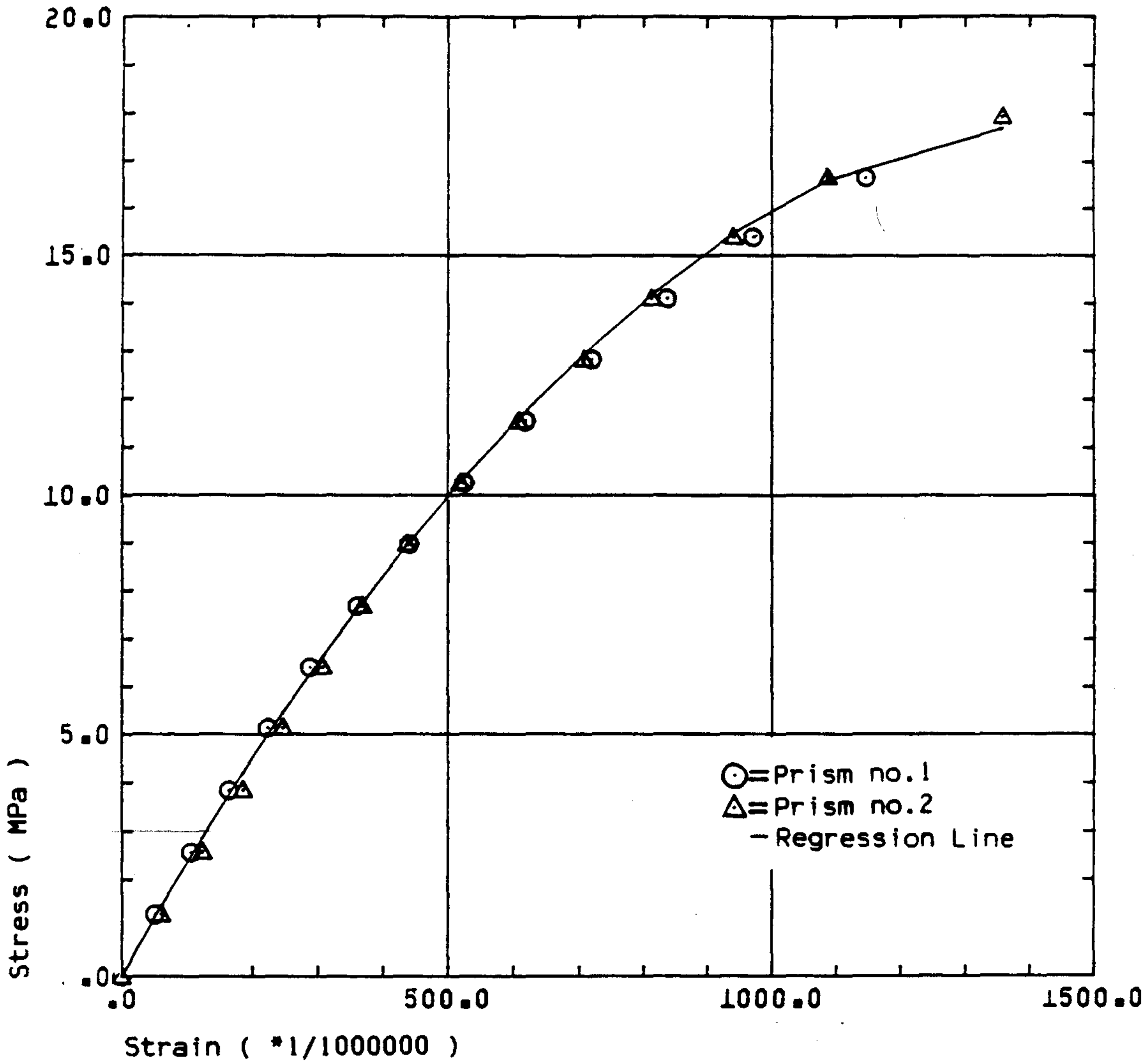

Fig.3.12 Stress-Strain Results for 4 Block High Plain Prisms(Data Set No.2).

3.3.5 Test Results for 4 Block High, Grouted Prisms

Three grouted prisms were tested. The mean failure load was 1006.7 kN, with a coefficient of variation of 14.7%. Assuming an area equal to the gross area of the block, the average strength of these prisms was 13.6 MPa. Strains were measured over joints, using a "Demec" mechanical strain indicator with a 200 mm gauge length. The stress-strain results for all the prisms are shown in Fig.3.13, with each point representing the average of 6 readings. The following equation was obtained from a regression analysis:

$$s = 17260\,e - 6744199\,e^{2} + 1.57*10^{9}\,e^{3} - 5.20*10^{11}\,e^{4}$$

The secant modulus of elasticity calculated for half of the mean strength was 14360 MPa. The prisms failed due to crushing of the blocks followed by crushing of the grout. The failure usually was observed to initiate by vertical cracks in the outside webs. Then cracks developed through the face shells, causing separation of the webs from the face shells. This was followed by spalling of the face shells of the two middle blocks. A typical view of a grouted prism after failure is shown in Fig.3.14.

3.3.6 Summary of Test Results for Prisms

The prism test results are summarized in Table 3.4. They indicate that the precise description of prisms was required for proper evaluation of the results. The strength of a prism may be affected by factors related to fabrication, such as the geometry of blocks, type of

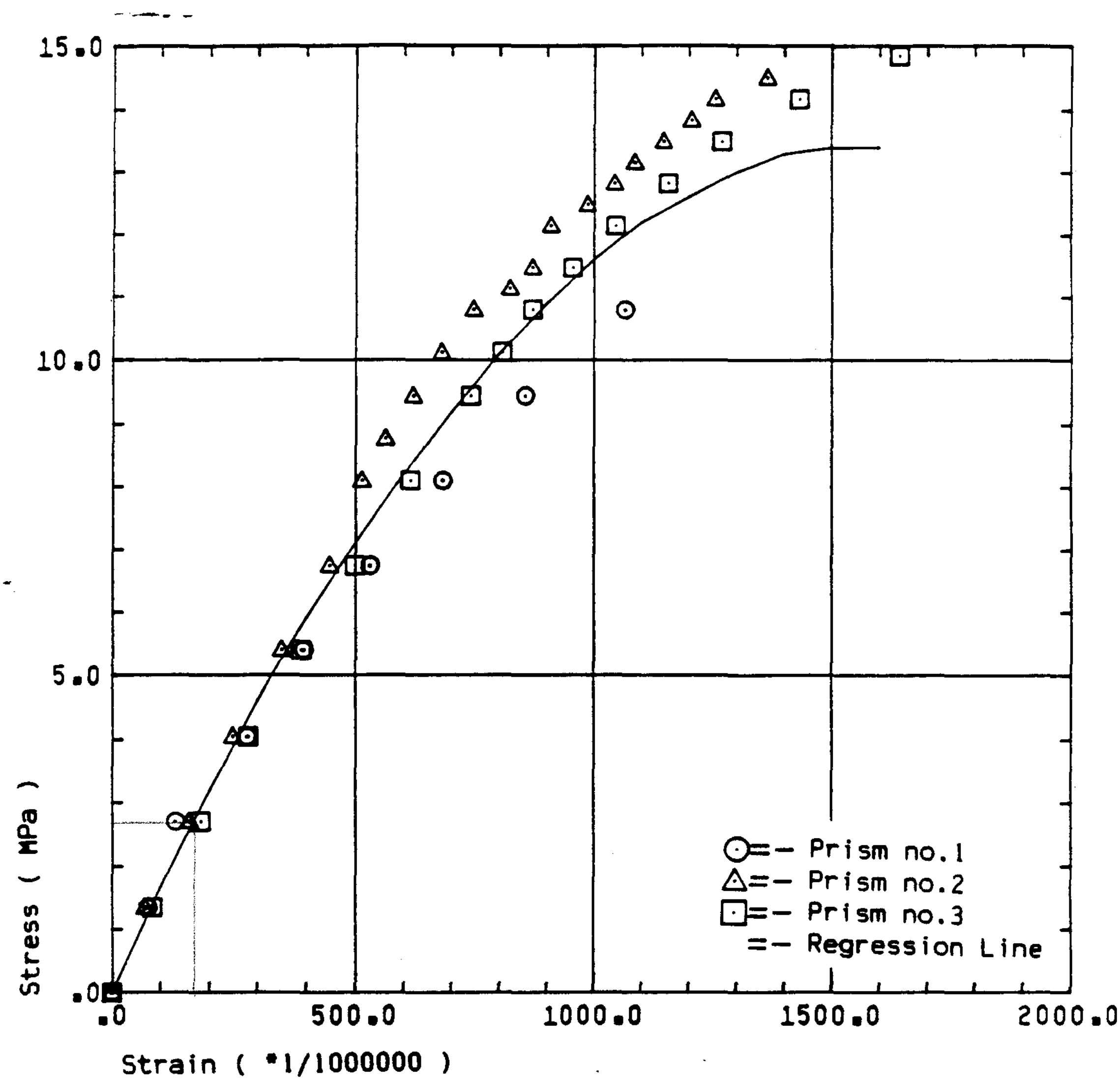

Fig.3.13 Stress-Strain Results for 4 Block High Grouted Prism.

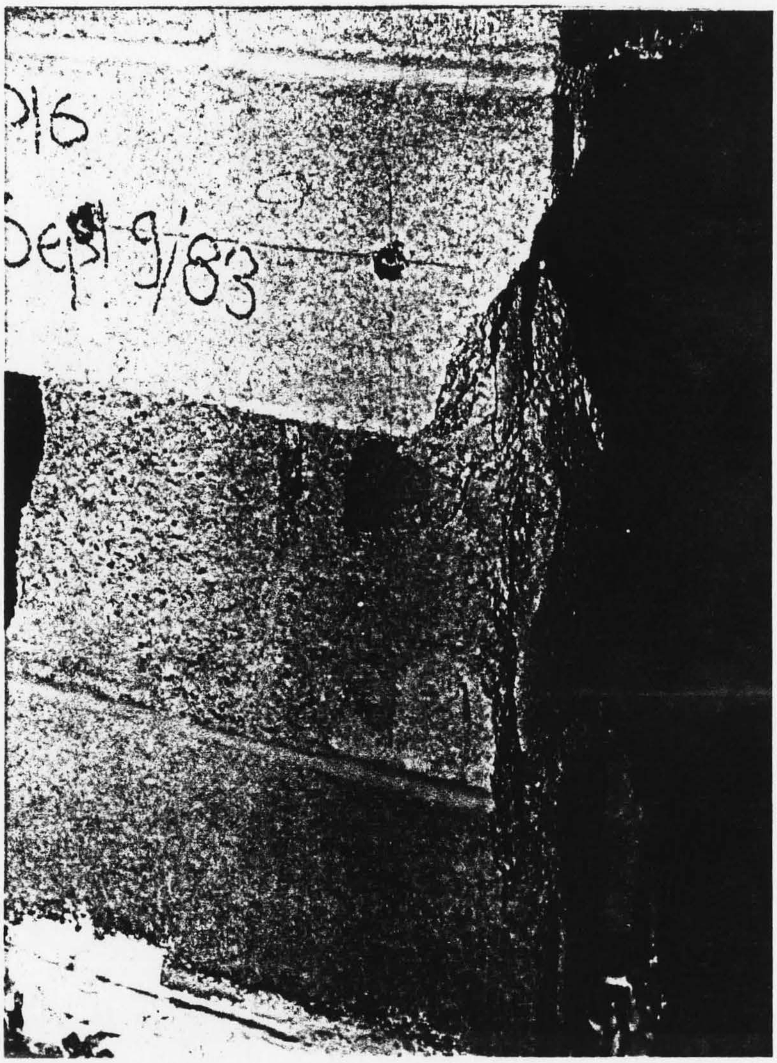

Fig.3.14 Typical Failure for a 4 Block High Grouted Prism

Table 3.4 Summary of Test Results for Prisms

Type of Prism	Set of Data	Number of Specimens	Mean Failure Load	Mean Stress at Failure *	Coeff. of Variation	Sectant Modulus of Elasticity **	Initial Modulus of Elasticity	Notes
			[kN]	[MPa]	[%]	[MPa]	[MPa]	
2 bl. plain	1	3	654	21.0	7.5	16950	19280	High mortar penetration
4 bl. plain	1	3	608	19.5	7.6	20060	22710	High mortar penetration
2 bl. plain	2	5	533	17.1	7.8	19400	24760	Face shell bedded
4 bl. plain	2	5	550	17.6	8.3	20530	24420	Face shell bedded
4 bl. grout.	1	3	1007	13.6	14.7	14360	17260	Fully bedded

*
Based on the mortar bedded area equal to 390 x 80 mm for plain prisms and based on the gross cross sectional area equal to 390 x 190 mm for grouted prisms.

**
Sectant Modulus of Elasticity calculated at the half of Mean Sress at Failure.

bed joints (full or face shell bedding) and actual penetration of mortar. As well, it can be influenced by loading conditions, such as type of end supports, stiffness of loading plates, type of capping and method of capping (full or face shell capping). The tests on prisms carried out by Maurenbrecher (51) showed similar relationships.

The comparison of the regression stress-strain relationships, shown in Fig.3.15, indicated fairly consistent behavior of ungrouted prisms in the elastic range. The differences in the strengths of different sets of prisms may have resulted from the different failure modes. In general, the first sets of 2 and 4 block high prisms, for which the higher penetration of mortar was suspected, showed higher strength than prisms where webs were not covered with mortar. The results obtained from the second sets of ungrouted prisms were accepted as representative for the masonry tested, since the failure mode was the same as for the plain walls, loaded with small eccentricity. In both cases, vertical cracks in the webs initiated the final failure.

Comparing the results for plain and grouted prisms, it can be seen that despite higher failure loads for grouted prisms, the stiffness and strength based on gross area was lower than for plain prisms with values based on mortar bedded area. It indicated that grouted masonry was not equivalent to solid, even if the strength of the grout was much higher than the strength of the blocks.

3.4 Tests for Bond between Blocks and Mortar

3.4.1 General

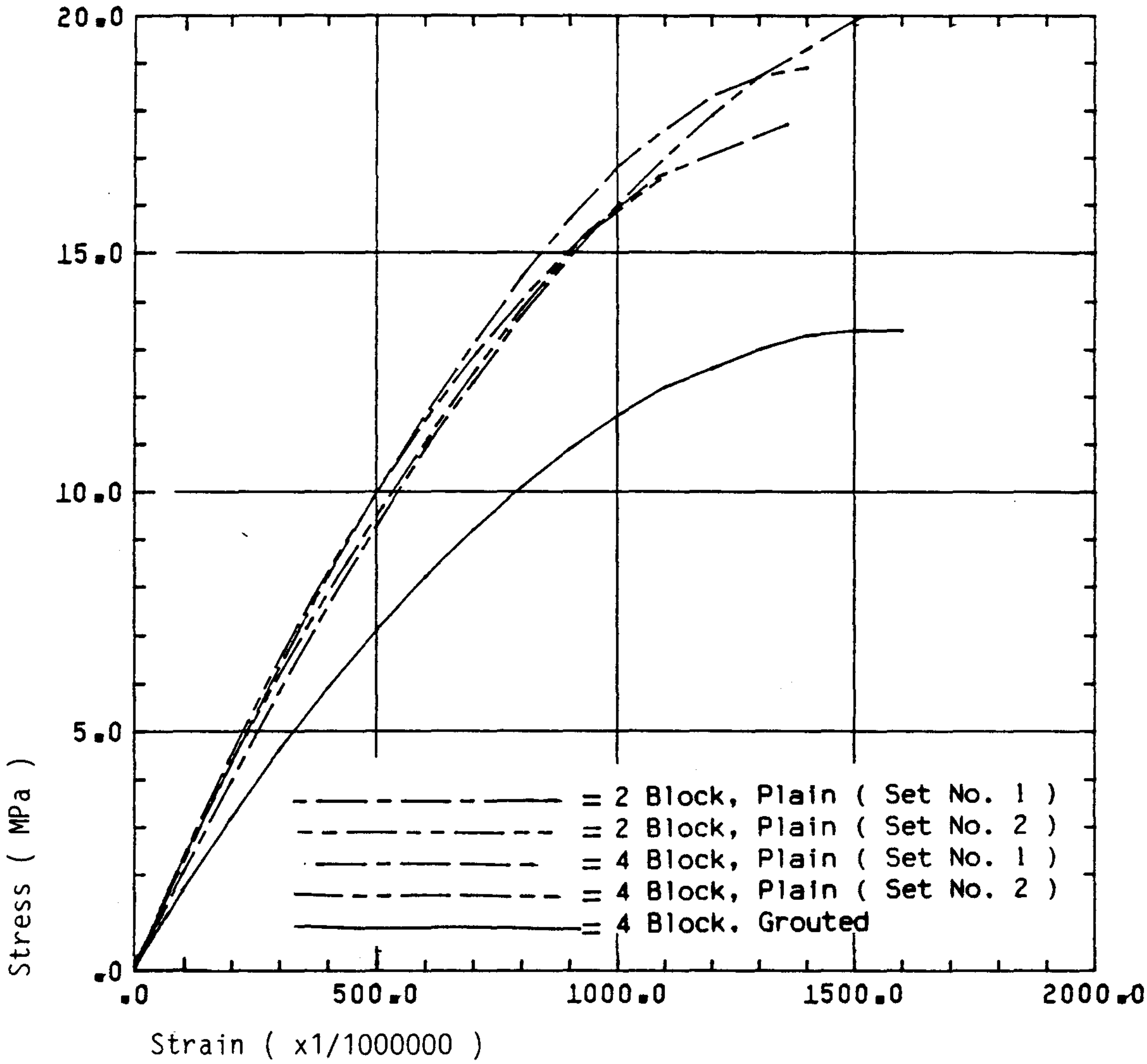

Fig.3.15 Regression Stress-Strain Relationships for Prisms.

The tensile strength of ungrouted concrete block masonry in the direction normal to the bed joints is controlled by the bond between the mortar and the masonry unit. Drysdale et al[28] showed that the strength of the individual materials was not directly related to the strength of the interface between them. Other factors, such as initial rate of absorption of units, water retentivity of mortar, and surface characteristics seem to be more important.

In the case of grouted concrete block masonry, the tensile strength of the grout affected the moment capacity as reported by Drysdale and Hamid[33]. Reinforcement does not significantly affect the initial cracking moment. However, it can be a controlling factor for the ultimate capacity in out-of-plane bending normal to the bed joints.

In the following section, the tests performed to obtained the bond strength of concrete block masonry are described.

3.4.2 Fabrication and Testing Procedure

Five 5 block high prisms were built in stack pattern. All joints were tooled using a cylindrical jointer. The materials used during fabrication were the same as for the other specimens. The bond prisms were cured in the laboratory. They were tested at an age of 12 months, using the bond wrench technique used by Hughes and Zsembery[47]. Load was applied by a 450 kN hydraulic jack and was controlled using a 100 kN load cell, calibrated with an accuracy of 3 N. The test set-up is shown in Fig.3.16.

3.4.3 Test Results

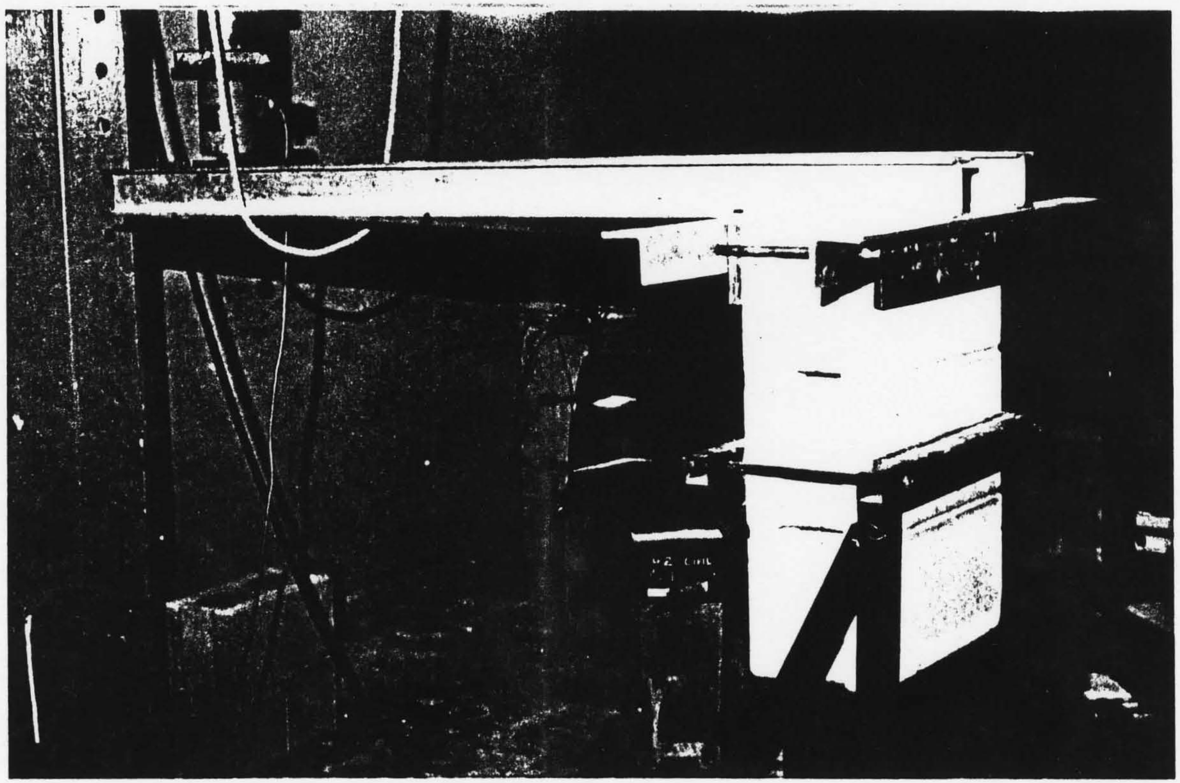

Fig.3.16 Test Set-Up for Mortar-Block Bond Test.

The mean failure bending moment from 17 tests was 680 Nm, with a coefficient of variation of 26.2%. Assuming the net mortar bedded area equal to the area of two 40 mm wide strip of mortar, as was assumed for the other specimens, the bond strength was 0.36 MPa at the extreme fibers of the mortar. Arbitrarily taking into account only the minimum 32 mm thickness of the face shells the calculated bond strength was 0.41 MPa. All calculations were performed assuming linear elastic behavior. Similar values for hollow block masonry were reported by Drysdale and Hamid[33], who tested 2 block wide by 8 block long specimens as beams loaded at two points.

3.5 Tests of Bond between Steel Bars and Grout Poured into Blocks.

3.5.1 General

Bond behavior of the steel-concrete interface has been extensively investigated by many researchers. Development of the finite element models for reinforced concrete requires a well defined bond stress-slip relationship, such as obtained by Mirza and Houde[54]. Only a few investigations have been conducted for bond in grouted masonry, and these were mainly concerning brick masonry. Some conclusions concerning grout bond to reinforcing steel were reported by Isberner[48]. However, no relationship was derived.

The purpose of the tests reported here, was to obtain information concerning behavior of the reinforcement in conditions representative of reinforced concrete masonry walls.

3.5.2 Fabrication and Testing Procedure

Twelve specimens were prepared to test bond strength by the direct pull-out method. Specimens were 1, 2, and 3 blocks high. Reinforcing bars were grouted into block prisms made of half blocks cut from breaker units. A stiff flat bar was welded to a portruding part of the embedded bar in the direction perpendicular to the direction of the bar to allow for a measurement of slip. All materials used, including the 15M bars, were the same as those used in construction of the slender reinforced walls. Specimens were air cured in the same conditions as the prisms and walls. The pull-out specimens were tested at an age of 11 months.

A 600 kN Tinius-Olsen universal testing machine was used for the tests of the specimens rested on the fixed head of the testing machine and were supported on two 16 mm thick steel plates laying along the face shells of the block. The gap left between plates allowed for a free movement of the transverse bar welded to the embedded bar. The movement of the transverse bar, equal to the slip of the embedded bar, was measured using dial gauges.

The following procedure was used to limit bending of the bar during loading. First the embedded bar was fixed in the pulling head. Then the specimen was lowered and the existing gap between the surface of the specimen and the supporting plates was filled with gypsum-cement. In this way, the vertical alignment of the bar and the direction of the applied force were secured. Three dial gauges with an accuracy of 0.0025 mm were used to measure displacement of the loaded and free ends of the embedded bar. A photograph of the test set-up is shown in Fig.3.17.

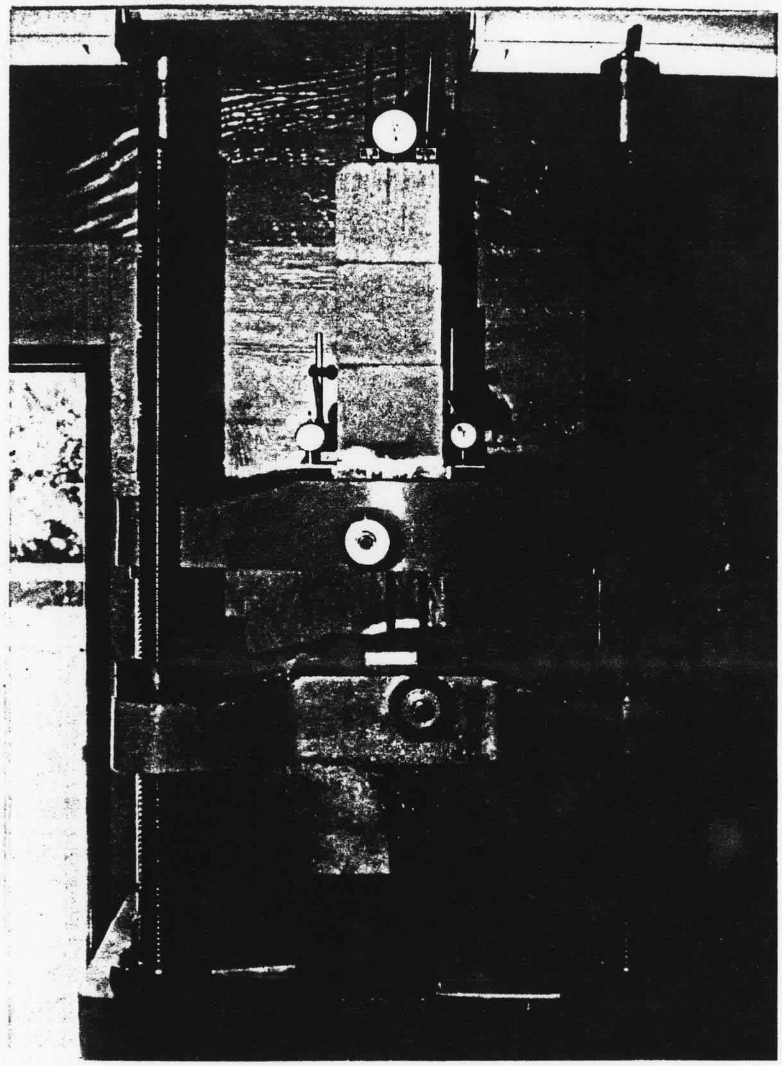

Fig.3.17 Test Set-Up for Reinforcing Bar-Grout-Block Test.

3.5.3 Test Results

Testing started with the 3 block high specimens. In all cases the embedded bar yielded. No displacements at the free end of the bars were recorded. Except for a small cone of grout at the loaded end, no separation between the block and the grout was observed. The force-slip results for three 3 block high specimens are shown in Fig.3.18.

Two block high specimens failed in a similar way, excluding specimen no 7, which failed in pull-out. Again no separation of the block and grout was visible. The force-slip results for the four, 2 block high specimens are shown in Fig.3.19. Results for both the loaded and the free ends of the bars are shown.

One block high specimens failed in three different failure modes. Specimens 8 and 9 failed due to pull-out of the bars. Specimen 10 failed due to complete separation of the grout and the block with vertical cracks in the block. In the case of Specimen 11, the steel bar yielded. Separation of blocks and grout was visible in all cases. The force-slip results for these four specimens are shown in Fig.3.20.

3.5.4 Discussion of the Test Results

Since the direct derivation of a bond stress-slip relationship was impossible, the following simple procedure was used:

1.It was assumed that bond along the embedded bar was not damaged until failure.

2.Linear distribution of bond stresses along the bar was assumed.

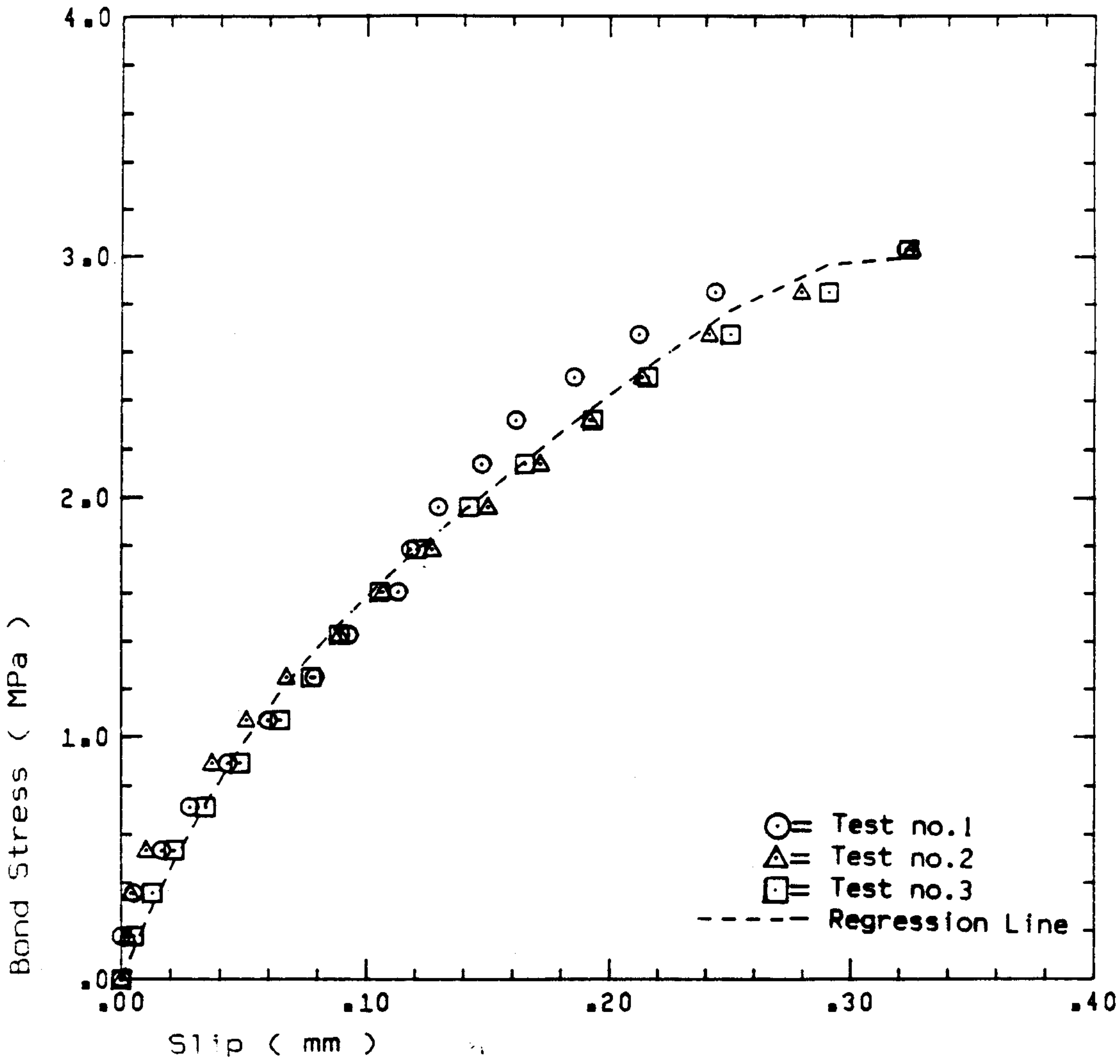

Fig.3.18 Bond Stress-Slip Results for 15M Bar Grouted in 3 Block High Prisms.

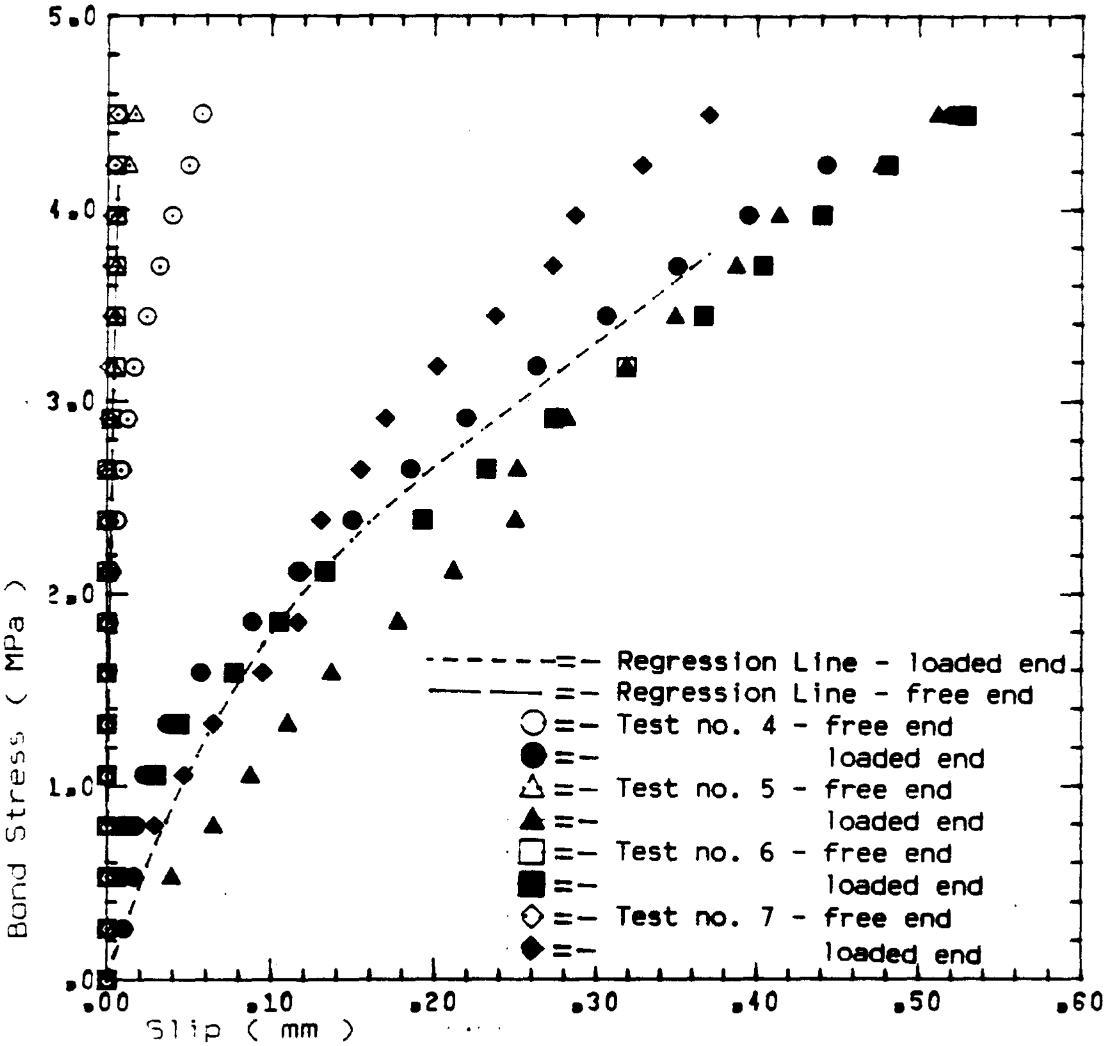

Fig.3.19 Bond Stress-Slip Results for 15M Bar Grouted in 2 Block High Prisms.

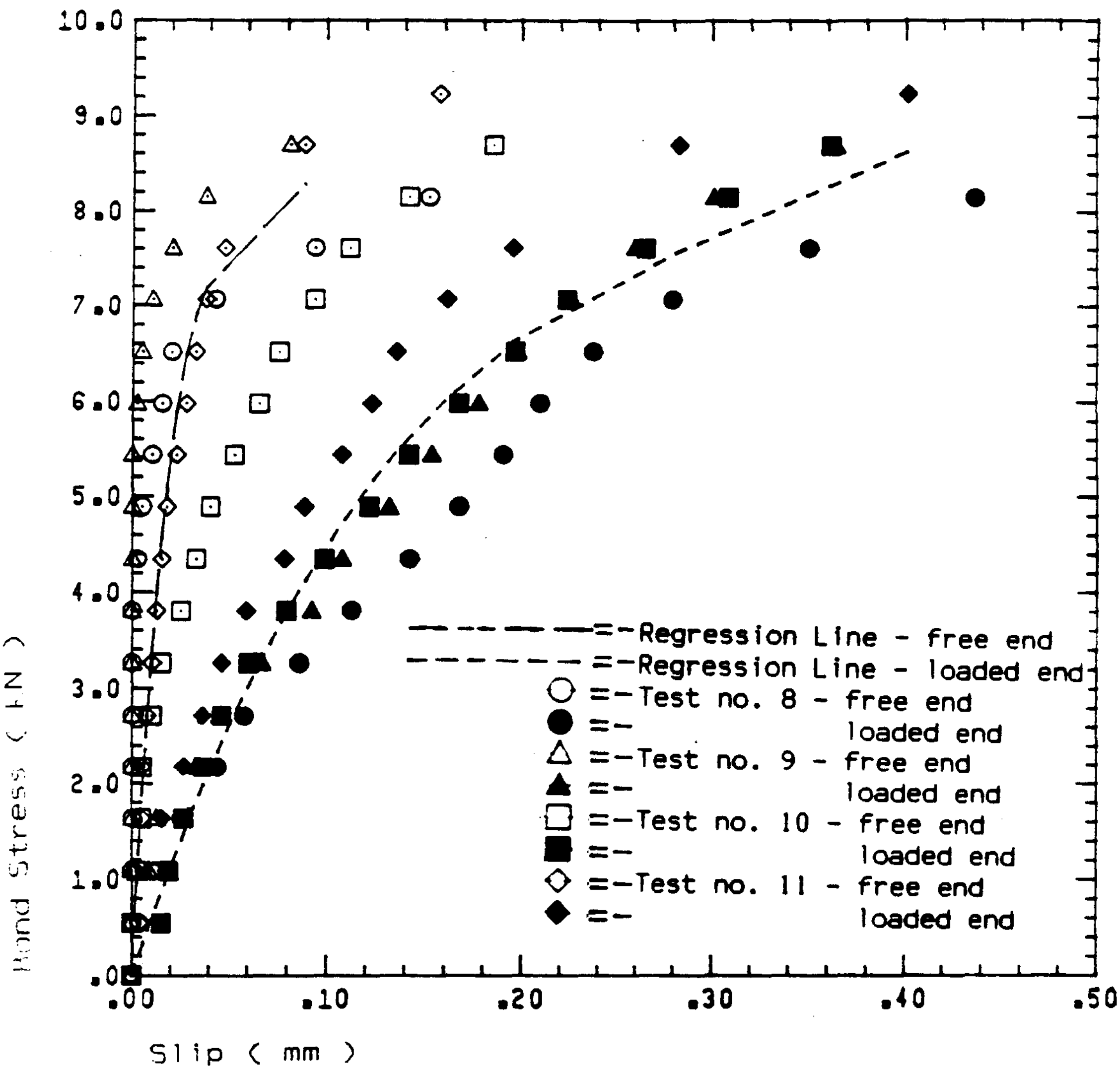

Fig.3.20 Bond Stress-Slip Results for 15M Bar Grouted in 1 Block High Prisms.

3. The following equation was used to calculate the equivalent stiffness of bond:

$$P = \pi D l_d K (d_{loaded} + d_{free})/2$$

where, D = diameter of the embedded bar in mm;

l_d = embedment length in mm;

d_{loaded} = slip of the loaded end of bar in mm;

d_{free} = slip of the free end of bar in mm;

K = equivalent stiffness in MPa/mm;

P = pulling force applied to the bar in N.

The values of K, calculated as described above, are shown in Fig.3.21. Since the assumption required that both ends of the bars slipped, only the results for the 1 block high specimens (specimens 8,9,10,11) were used. There was a recognizable relationship between the value of the applied force, P, and the recorded slip, d, represented by the calculated stiffness, K. The average slip, $d = (d_{loaded} + d_{free})/2$ was chosen as the representative slip at a particular load. Then the following relationship between stiffness, K, and average slip, d, was obtained from a regression analysis:

$$K = 205 - 2419\,d + 11184\,d^2 - 74039\,d^4$$

Stiffness, K, represents the slope of the bond stress-slip curve. Therefore, it was possible to derive a function describing the bond stress, u_{bs}:

$$K = d\,u_{bs} / d\,d, \text{ thus } u_{bs} = \int K\,dd$$

$$u_{bs} = 205\,d - 12095\,d^2 + 3728\,d^3 - 18510\,d^5 + C$$

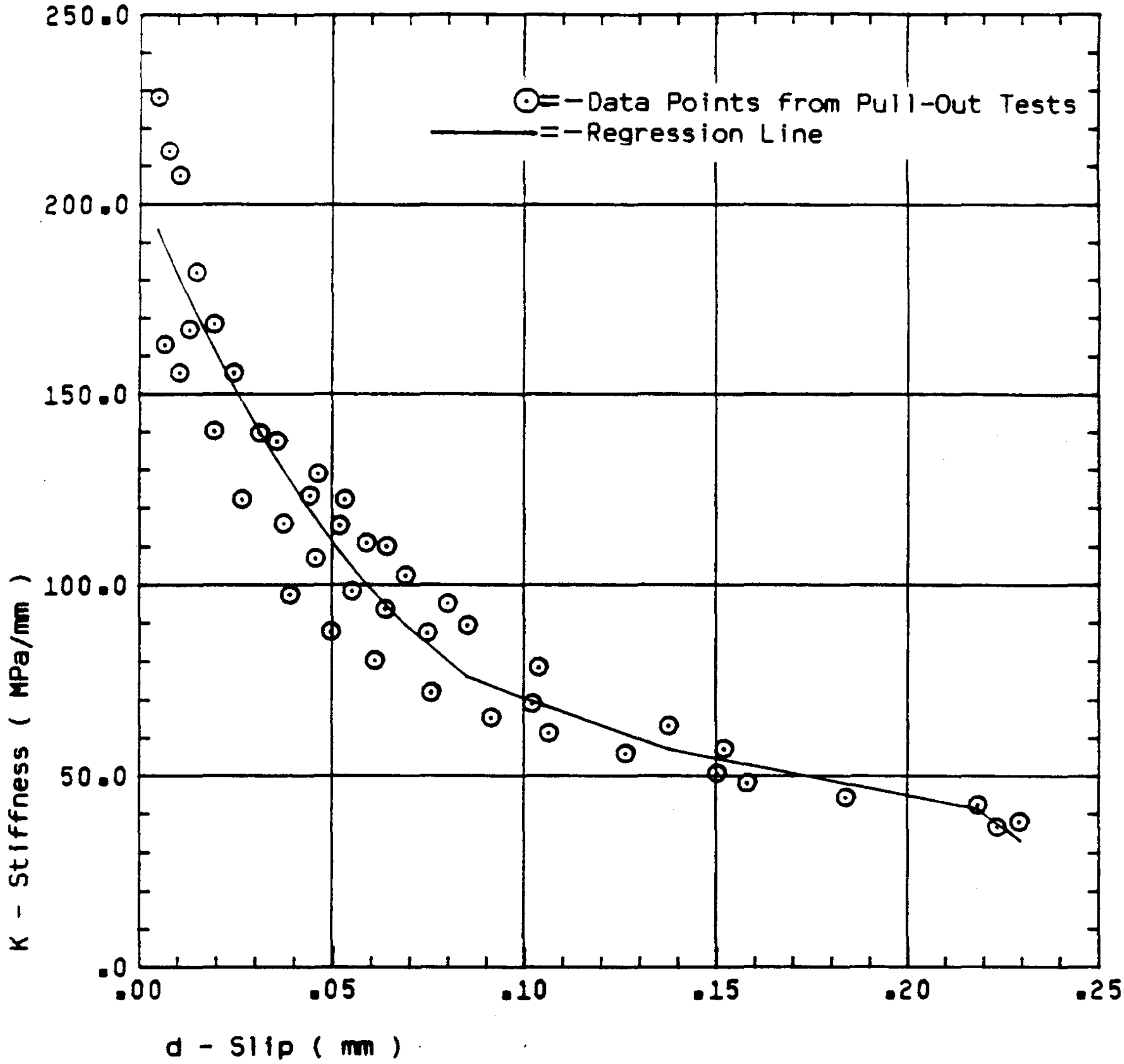

Fig.3.21 Bond Stiffness-Slip Relationship for Pull-Out Test.

The value of C is zero since the bond stress is equal to zero for no slip. In Fig.3.22 the relationships obtained were compared to the relationship derived by Mirza and Houde [54].

From the analysis of the failure modes of different specimens the following conclusions were obtained:

1) The embedment length of bars should be more than the height of 1 block.

2) Two blocks were enough to develop the yielding stress in a 15M bar.

3) Debonding between block and the grout core is possible therefore a single block cannot provide proper embedment . However, in a wall the tapered but continuous shape of the grout core should prevent such behavior.

3.6 Summary

In this chapter, the mechanical properties of the concrete blocks, mortar, grout and reinforcing bars used in the fabrication of the test specimens were discussed. In addition, the results of tests of masonry assemblages were reported. Two and four block high prisms were tested in axial compression. Also bond specimens were used to investigate the bond phenomena between blocks and mortar and between reinforcing bars and grout in blocks.

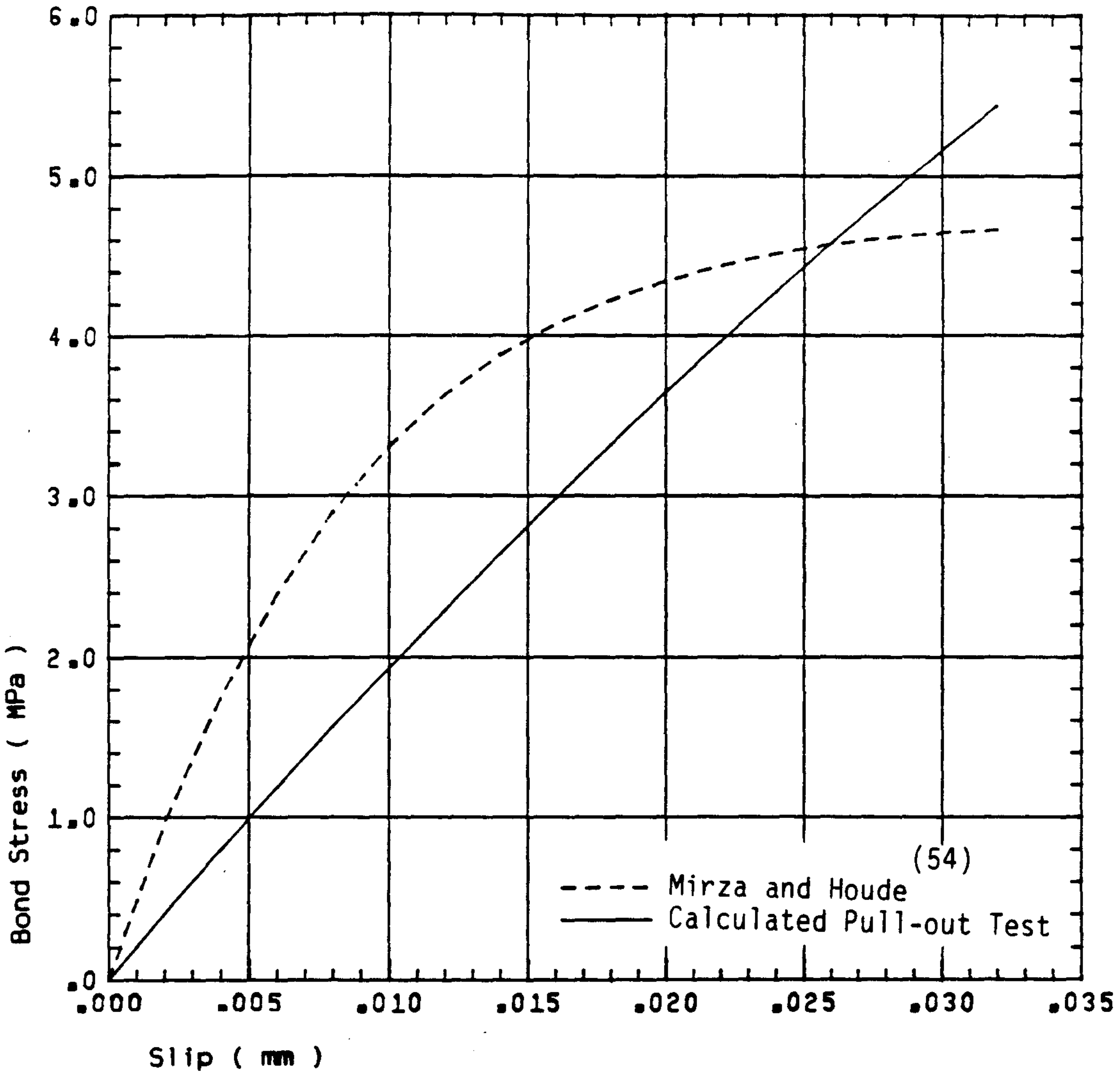

Fig.3.22 Comparison of Bond Stress-Slip Relationships.

CHAPTER 4

TESTS OF SLENDER WALLS

4.1. Introduction and Description of Test Specimens

This chapter contains the test results from 14 full scale wall tests constructed of the same materials as those described in Chapter 3. The main aim of this experimental program was to provide well defined data which could be used to verify a numerical model. In addition, it provided direct experience and insight into the factors affecting behavior of concrete block walls.

The wall testing program consisted only of walls made using hollow concrete blocks. As mentioned previously, properties of the single types of block, mortar, and grout and the resulting masonry assemblages were presented in Chapter 3. Six walls were built without any reinforcement and were not grouted. Another six were reinforced vertically with one 15M bar in each of the two outside cores, which were then filled with grout. All the walls were tested under eccentric vertical axial load. Load was applied by a hydraulic loading system and distributed through a stiff steel beam. Both ends were pin-ended to allow for free rotation. Eccentricity of the load was constant at both ends with the accuracy within 5 mm of the intended eccentricity. The actual eccentricity could be measured within an average accuracy of 1mm. Undamaged parts of two reinforced walls were tested in pure bending. A more detailed description of the test set-up and testing procedures are provided in Section 4.2 and Sections 4.3.2 and 4.4.2, respectively.

Several factors were taken into account in choosing the geometry of the walls, boundary conditions and methods of loading. The height was chosen to be in the range where a significant effect of slenderness on the capacity of walls would be expected. Also, walls with a similar slenderness ratio had been tested by Hatzinikolas et al[44,45], who carried out an extensive experimental program. The possibility of using a single test set-up and therefore simplifying the testing process was taken into account, as well.

The length of walls was chosen to have a uniform layers of 2 full blocks and one half block in each course. Such walls were stiff enough to be built and moved without any special devices. Moreover the limiting capacity of the loading equipment and the need to produce uniformity of the applied load along the length of wall were taken into consideration.

The pin-ended conditions at both ends of the walls were adopted to achieve well defined boundary conditions. Together with equal eccentricity of load at both ends, these conditions allowed use of symmetry about the midheight of wall (neglecting the self-weight of the wall). The symmetry was important since it reduced the size of numerical problem, saving computation time and memory. Furthermore, symmetry would tend to limit the failure region to the mid-height of the wall, thus measurements could to concentrate in that area. Also failure of the extremities was thought to be best avoided because of difficulty in interpreting the influence of the load transfer equipment. The eccentricities of the vertical loads were chosen to cover the practical range of use for each kind of wall. For the plain walls this meant a range from nearly concentric up to one third of wall thickness whereas in the case of the reinforced walls, the range of eccentricity was from one sixth of wall thickness to pure bending.

4.2. Equipment and Instrumentation

4.2.1 Test Set-Up for Walls Tested in Compression and in Out-of-Plane Bending.

A schematic view of the test set-up is shown in Fig.4.1. It consisted of:

1.A steel frame consisting of two steel columns (W360x162) and two steel channels (C380x50); connected together by six M24 bolts at each joint.

2.Two 51mm thick steel plates used for distribution of load to the steel channels.

3.A hydraulic jack with load capacity of 1800 kN.

4.A load cell with 2000 kN capacity.

5.A spherical seat consisting of two 152x152x51 mm plates and a 38mm ball.

6.A loading beam made of a W360x45 (strengthen by stiffeners) with a 38mm round bar welded along the bottom flange.

7.Two pairs of steel plates where in each pair one plate was 38mm thick with 13mm deep grove and three sets of holes and the other was 19mm (later increased to 38mm) thick with one set of holes with internal thread.

8.A 38 mm bar welded to a 13 mm thick plate bedded on the surface of

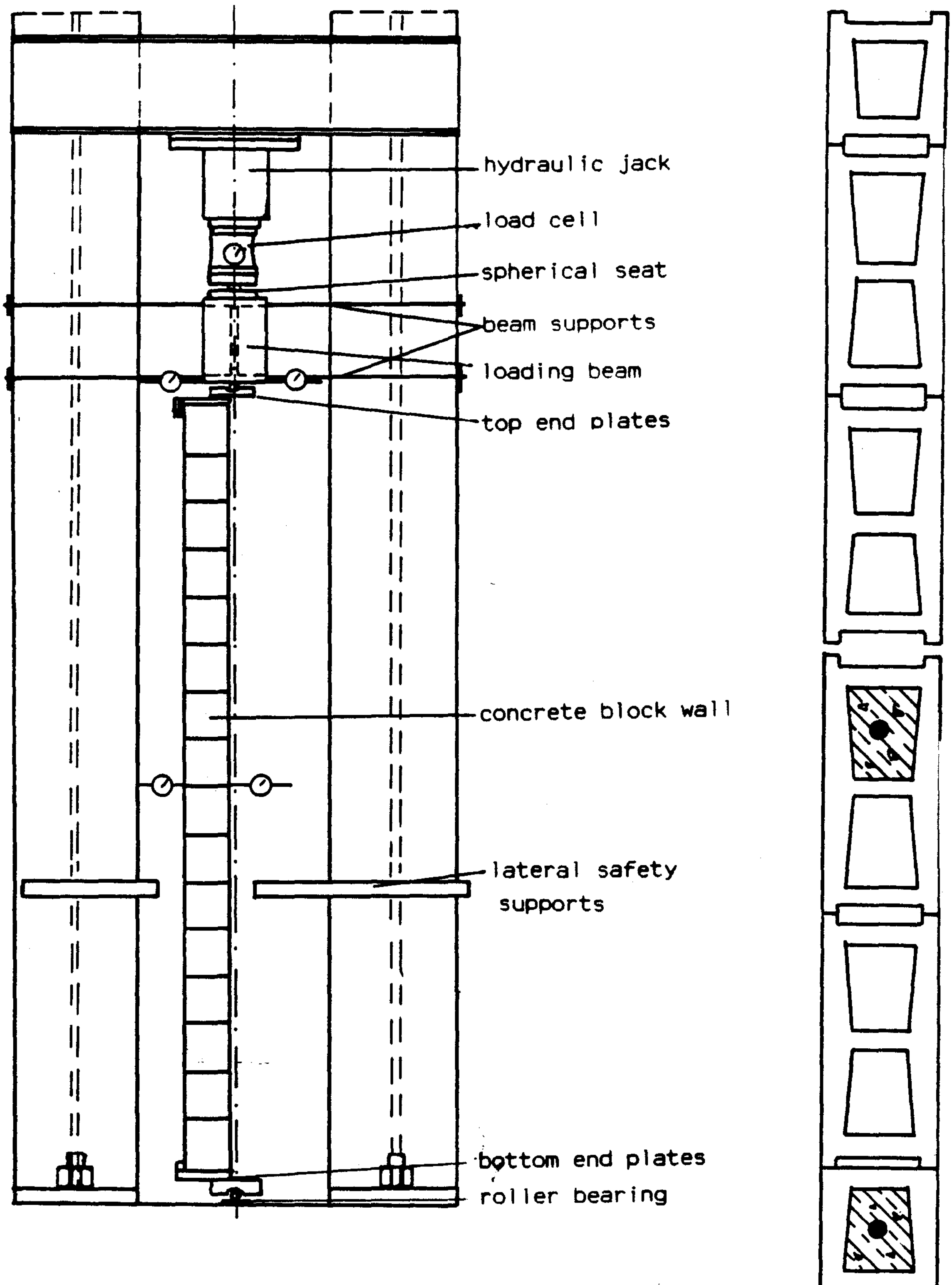

Fig.4.1 Schematic View of the Test Set-Up for Walls Loaded under Vertical Eccentric Load.

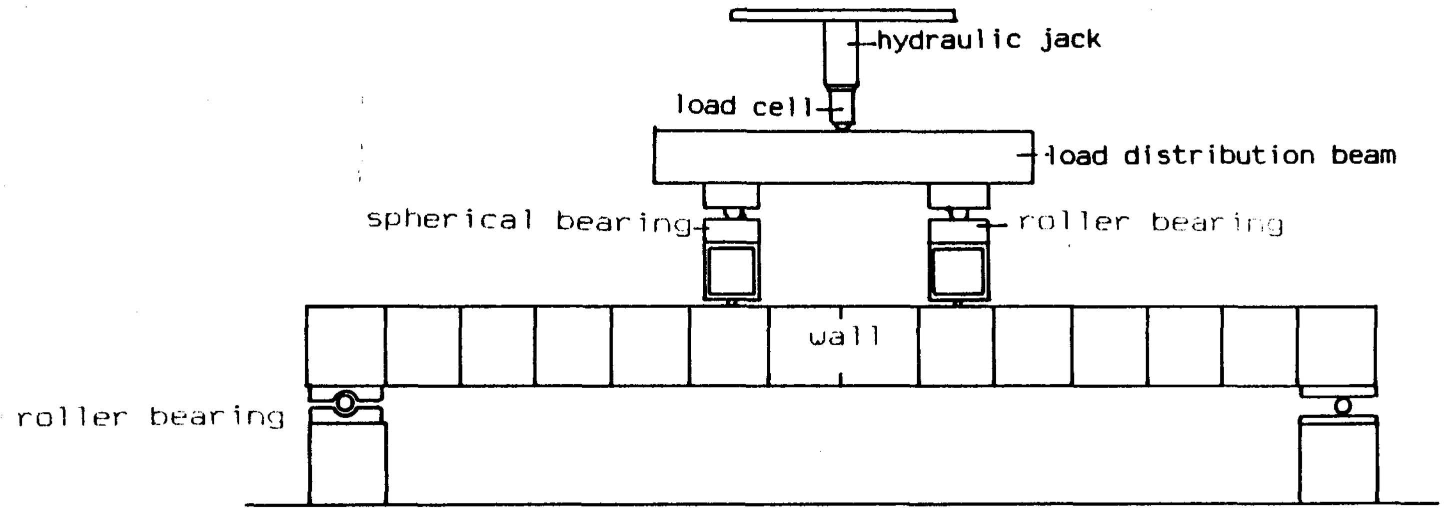

Fig.4.2 Schematic View of the Test Set-Up for Walls Tested in Pure Bending.

floor with a thin layer of hydrostone.

4.2.2. Test Set-Up for Walls Tested in Pure Bending

A schematic view of the test set-up is shown in Fig.4.2. It consisted of:

1.A steel column made from a W360x162 section.

2.Two steel C380x50 channels connected as a cantilever to the column at the one end by four M24 bolts .

3.A 51mm thick plate with a slide device allowing for adjusting the position of hydraulic jack attached to it.

4.A hydraulic jack with 450 kN capacity.

5.A load cell with 220 kN capacity.

6.A top loading beam made using a 100x100 hollow section.

7.Spherical and cylindrical bearings.

8.Two hollow sections with 25 mm wide by 6mm thick bars welded to the bottom side.

9.Two supports, each being made of two 38mm thick plates and 38 mm diameter bar.

4.2.3 Instrumentation

During each test, force, strains and displacements were measured. A load cell connected to a Beam Digital Strain Indicator was used to indicate applied load. The load cells were calibrated before each test using a 2500 kN Riehle Test Machine. The strains were measured using "Demec" and "Huggenberger" mechanical strain indicators or, for some prisms and walls in pure bending, electric strain transducers were used. The mechanical measuring instruments have a theoretical accuracy of 0.00001 mm/mm. The "Demec" strain indicator had a 200 mm gauge length and the "Huggenberger" strain indicator used a 100 mm gauge length. The electrical strain transducers gave measurements over 150 mm or 200 mm gauge lengths.

Since "Demec" and "Huggenberger" mechanical strain indicators are widely used, no description is provided. The strain transducers is a measuring instrument build by H.Wong and described in his thesis [38]. The most important element is a steel ring with attached electrical strain gauges. Transducers were calibrated using the "Demec" mechanical strain indicator. The main advantage of this instrument is the possibility of connecting it to the computer data acquisition system. Displacements were taken using dial gauges having an accuracy of 0.0025 mm.

The typical gauge locations are shown in Fig.4.1. The layouts of the strain gauge points are provided in Fig.4.3a and Fig.4.3b. All the vertically loaded walls were positioned along the East-West direction in such way that the south face of each wall was in compression and north face was in tension or in lesser compression.

4.3 PLain Concrete Block Walls

4.3.1 Fabrication and Preparation of the Plain Walls for Testing

Six walls, each composed of 16 two and half blocks courses, were constructed in running bond with mortar applied only on the face shells of the blocks. The walls were fabricated by an experienced mason. In all

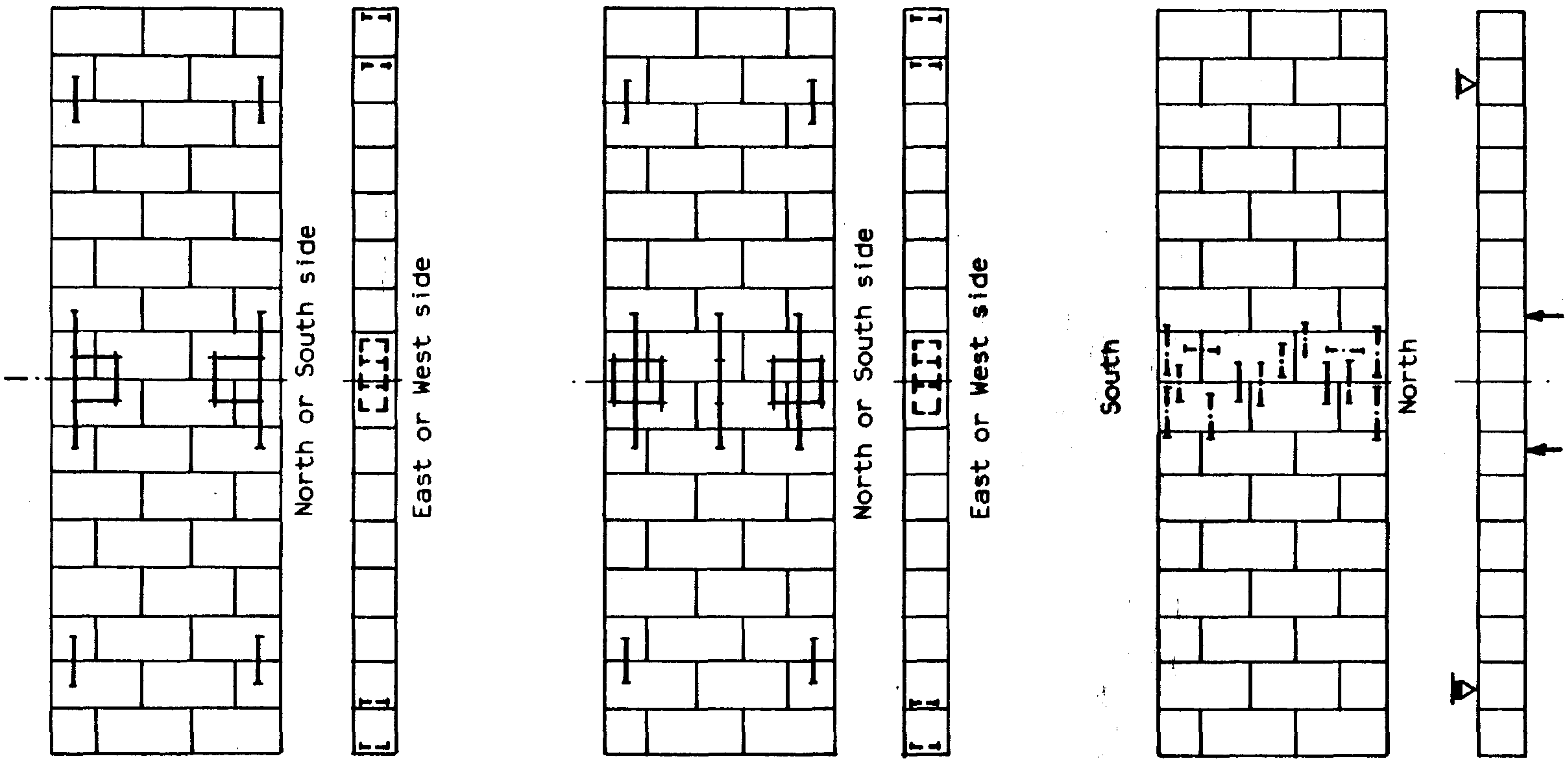

Demec
Huggenberger
Strain Transducer

a) Vertical Loading, Arrangement No.1

b) Vertical loading, Arrangement No.2

c) Pure Bending

Fig.4.3 The Layout of the Strain Gauges for the Full Scale Walls.

the walls, the first course was laid directly on a polyethylene sheet placed on the concrete floor. The mason kept one face in alignment using a horizontal string and level. Mortar joints were compacted using a cylindrical jointer. The thickness of mortar joints was 10 mm.

Walls were stored and tested in the laboratory where temperature is controlled at 20 deg C ± 2 deg C and humidity is not controlled (the average relative humidity was approximately 50% over the period of the test program). Specimens were tested at an age between five and eight months. A sketch of the schematic cross section of these walls is shown in Fig.4.1.

The preparation of walls for testing was starting with mounting points for the mechanical strain indicators. The layout of the strain gauge points is shown in Fig.4.3. The points were made of hard brass in the shape of 6 mm disks with a hole in the center drilled using a #60 drill. They were glued to the surface of the wall using hot sealing wax. Later, the pairs of end plates were prepared to set the desired eccentricity. It was obtained by bolting together two plates with bolts going through the proper set of holes in the plate with a grove. Three sets of holes in the plate with the grove allowed placement to obtain the eccentricities of 0, t/20, t/6, t/3, 23t/60, and t/2, where t is the 190 mm thickness of wall. Accuracy of placement was accomplished by carefully aligning the edge of the first plate with the face of the wall before bolting on the groved plate. Other eccentricities could be accommodated by shifting the position of the plate which was bearing directly on the end of wall.

One pair of the plates was fixed on top of the wall using a thin layer of hydrostone for bond. Next, the wall was moved by crane and put on the other set of plates already laying on the round bar, positioned on the floor of the laboratory. Hydrostone was again used to fasten the plates to the bottom surface of the wall. Temporary lateral supports were used to keep the wall in a vertical position. Then the loading beam was positioned on the top of the wall with the round bar welded to the beam laying in the grove of the top end plate.

During testing, the loading beam was kept in position by four (later eight) threaded rods which together with small channels formed loops around the steel columns of the testing frame. A spherical seat was put on the top of the loading beam to transfer load from the load cell which was placed between this seat and the bottom surface of the piston of the hydraulic jack. After the piston was moved down so that there was no gap between the loading cell and the piston, the whole arrangements was checked for vertical alignment and adjusted if any inaccuracy was observed. The schematic view of the test set-up is in Fig.4.1.

4.3.2 Test Procedure for Plain Walls

The initial readings were taken for strain and deflections. Then a small load was applied to keep the wall in a vertical position, so that the temporary lateral supports could be removed. At this stage vertical alignment was checked and adjusted in case of any inaccuracy. Then the initial shape of wall was measured using a reference line and an engineering scale. Measured values represented distance from the compression face of the wall to a thin string connecting the centers of the end bearings. Reading were taken at the midheight of each course at both ends of the wall. In this way, the actual initial eccentricity was measured as well. The nominal eccentricity, the actual eccentricity calculated as average eccentricity at mid-height of wall, and the deviation from the nominal eccentricity along height of each wall were shown in Fig.4.4.

Load was applied slowly and maintained at a constant level while readings were being taken. After each load increment, the alignment of the loading beam was checked and adjusted (if necessary), and any movement were recorded. It was intended to take readings at ten load increments to obtain smooth curves. In one case the wall failed earlier than had been expected and only seven readings were recorded. During other tests the number of reading varied from 11 to 22, with an average of 14 readings per test. Close to failure load, especially when explosive failure was expected, the dial gauges were removed from the midheight region of the wall. It was assumed that the wall had failed after a sudden drop in force was registered by the load cell and when it was not possible to return to the previous level of load. This happened either after explosive failure, when a significant part of the cross section was damaged or when buckling occurred. A more detailed description of the test results is provided in Section 4.3.3.

4.3.3 Test Results for the Plain Walls

Some of the information about materials and testing procedure are

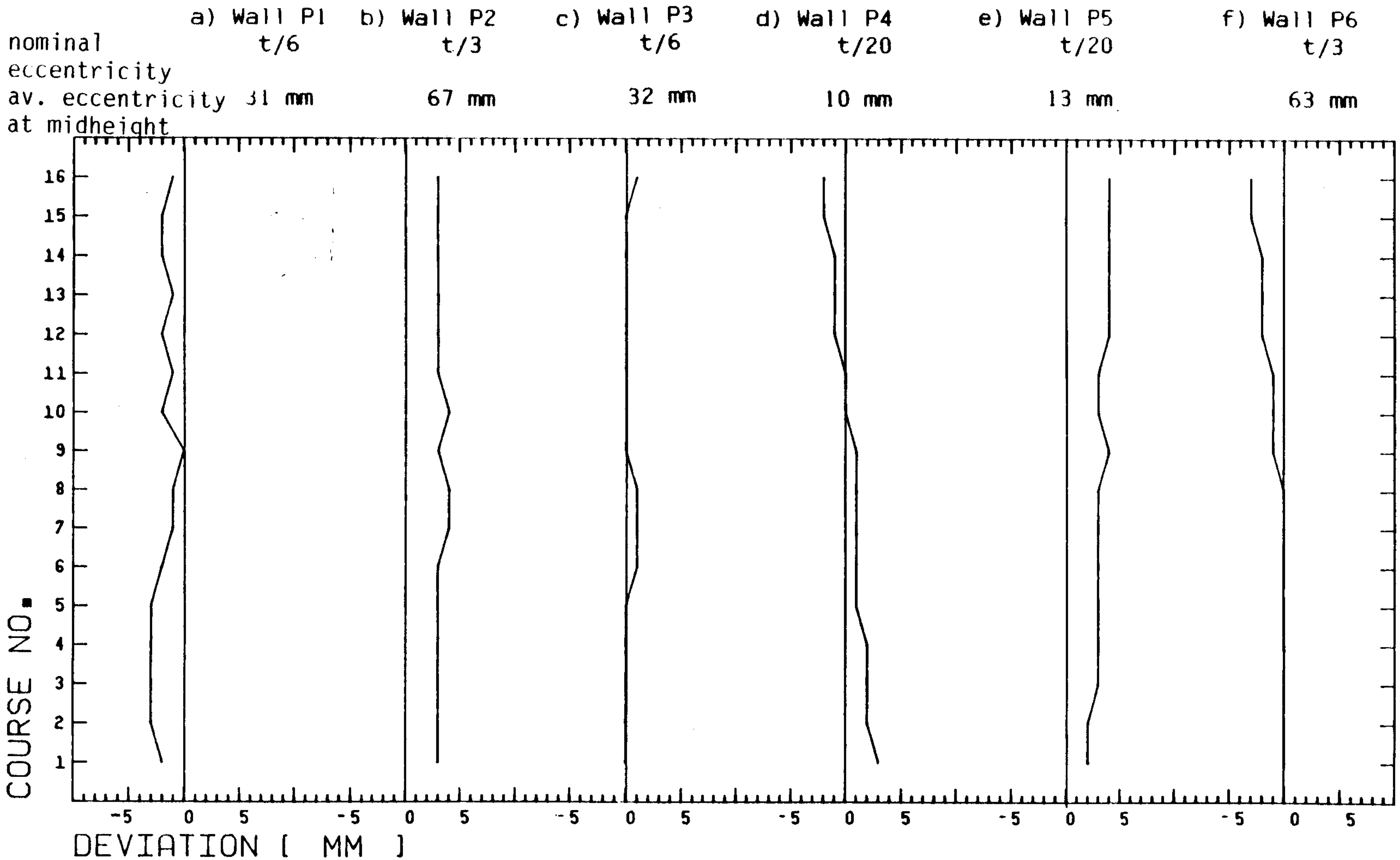

Fig.4.4 Measured Deviation of Eccentricities for Plain Walls.

summarized in Table 4.1. The test results are shown in Table 4.2. Results of the tests on the materials used in fabrication of the walls were described in details in Chapter 3.

The load-lateral displacement and load-moment relationships are shown later in Section 4.5.1.

4.3.3.1 Failure Mode for Wall P1

For Wall P1, the nominal eccentricity was t/6 and the measured deviation of eccentricity along the height is shown in Fig.4.4a. The wall failed due to the splitting of the webs in the blocks at the five bottom courses. The first visible cracks occurred in the second course from the bottom on both sides of the wall at a load of 300 kN. Cracks propagated with increasing load. It seemed that failure of wall P1 may have been somewhat premature, since the wall had been unloaded during the test and reloaded to failure. This cycling of load may have weakened it. In addition the thickness of the end plates was only 19 mm for this test but was increased to 38 mm for subsequent tests. The stiffness of these end plates could influence the capacity of the wall by causing premature splitting at the end regions of wall. Fig. 4.5 is a photograph of wall P1 after the failure. The load-strain relationships at the midheight of the wall is shown in Fig.4.7.

4.3.3.2 Failure Mode for Wall P2

The nominal eccentricity for wall P2 was t/3 and the measured deviation of eccentricity along the wall is shown in Fig.4.4b. This wall failed in buckling with all bed joints cracking on the tensile side of

Table 4.1 Data for Full Scale Walls

Wall Number	Age (months)	Average Compressive Strength of Mortar* (MPa)	Reinforcement	Load Increments
P1	5	22.4	---	19x50kN
P2	5.5	22.4	---	8x50kN, 4x25kN
P3	6.5	22.4	---	7x100kN, 6x50kN
P4	6.5	18.3	---	11x100kN
P5	7	18.3	---	12x100kN
P6	8	22.4	---	9x50kN, 11x25kN
R1	9	20.8	2x15M	5x100kN, 2x50kN
R2	10	19.7	2x15M	5x25kN, 10x10kN
R3	10.5	21.4	2x15M	7x50kN, 7x25kN
R4	11	21.4	2x15M	5x25kN, 11x10kN
R5	11.5	20.8	2x15M	7x100kN, 4x50kN
R6	11.5	19.7	2x15M	11x10kN, 11x5kN
S1	12	21.4	2x15M	8x5kN
S2	12	21.4	2x15M	17x2kN

* Based on Mortar Cube Tests for batches used during fabrication of each wall.

Table 4.2 Test Results for Full Scale Walls

Type of Loading	Type of Wall	Wall Number	Nominal Eccentricity e/t*	Actual Eccentricity at Mid-height	Failure Load	Maximum Lateral Defl.	Maximum Bending Moment	Failure Mode
				mm	kN	mm	kNm	
vertical	plain	P1	1/6	31	892	6.1	33.3	splitting
eccen-		P2	1/3	67	502	8.3	37.7	buckling
tric		P3	1/6	32	1055	7.5	42.0	splitting
load		P4	1/20	10	1060	3.5	14.3	apparatus failure
		P5	1/20	13	1180	4.8	20.7	splitting
		P6	1/3	63	750	13.7	57.3	crushing
	rein	R1	1/3	61	594	13.3	44.0	buckling
	forced	R2	1/2	102	216	46.9	32.2	buckling crushing
		R3	1/3	65	521	18.0	43.2	buckling
		R4	1/2	96	231	50.1	33.7	buckling
		R5	1/6	34	1000	11.2	45.2	crushing
		R6	3/4	142	140	45.2	26.2	buckling
bending		S1	B	B	---	----	15.2	crushing
moment		S2	B	B	---	----	17.0	crushing

*

t=190 - wall thickness;

e - eccenetricity of load.

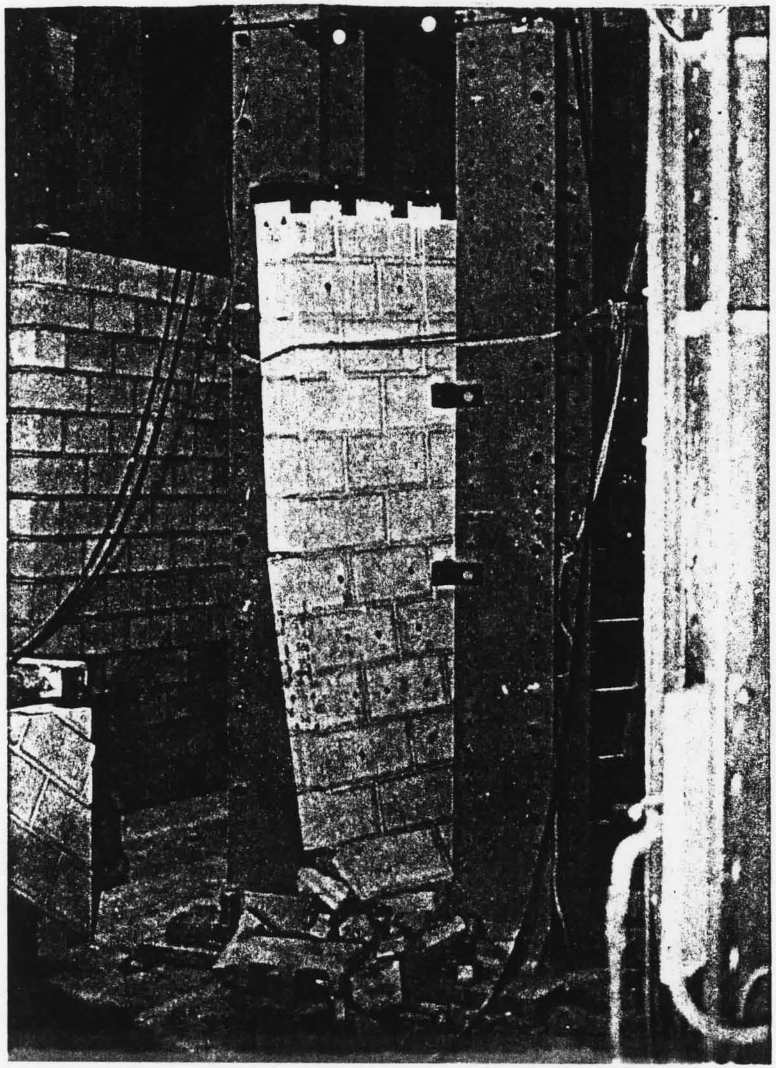

Fig.4.5 View of the Wall Pl after Failure.

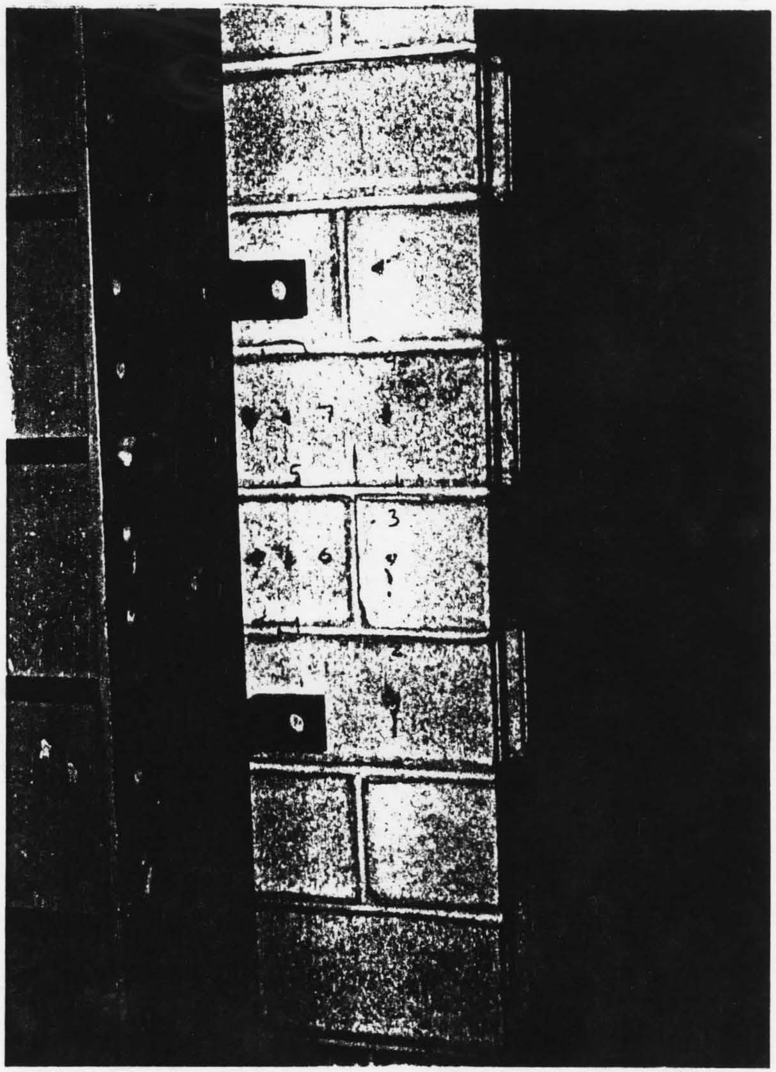

Fig.4.6 Tensile Side of Wall P2 after Failure.

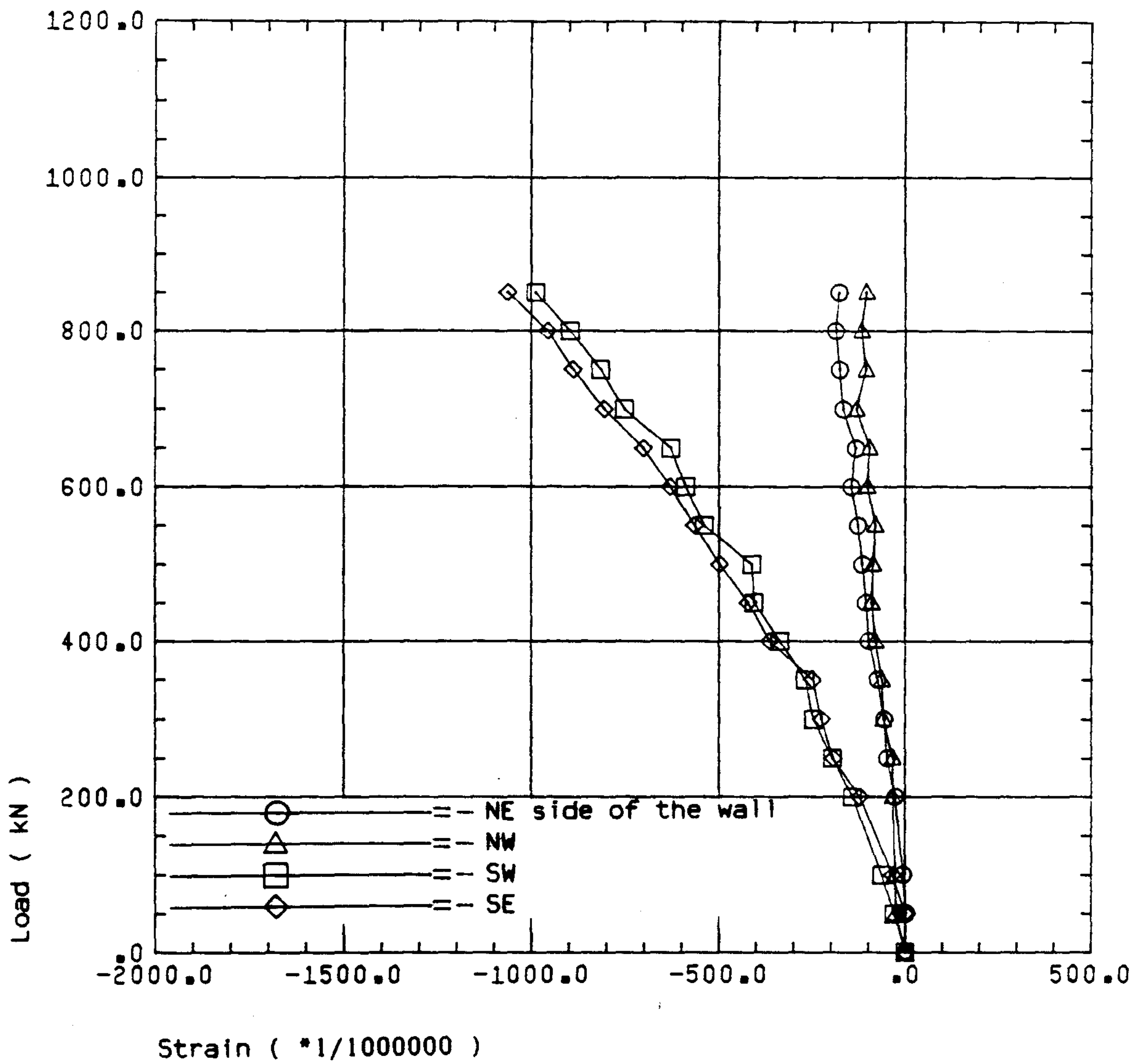

failure load: 892 kN
eccentricities:
nominal 32 mm
actual 31 mm

Fig.4.7 Load-Strain Results at Midheight of Wall P1.

the wall. The first crack was recorded at the first joint above midheight at a load 150 kN. The highest strain recorded on the compressive side was 990×10^{-6}, which was far below the maximum compressive strain for concrete masonry. In the photograph in Fig.4.6, the cracks on the tensile side of wall P2 are indicated with lines from felt marker pens. The load-strain relationships are shown in Fig.4.8.

4.3.3.3 Failure Mode for Wall P3

For Wall P2, the nominal eccentricity was t/6 and the measured deviation along the height of wall is shown in Fig.4.4c. The wall failed due to splitting of the webs in the blocks at the four bottom courses. The first crack occurred at the bottom at a load of 200 kN and at the top of the wall at 600 kN. Cracks propagated with increasing load. The second crack in the web parallel to the first one had a marked effect on behavior and coincided with a significant increase in the rate of deflection. It is thought that this cracking affected the failure. Some small cracks occurred in the webs at the midheight of the wall but their influence was not thought to be significant since they did not propagated through the whole height of the web. The recorded strains showed that the midheight parts of the webs were still in compression in the lateral direction. A view of Wall P3 after failure is shown in the photograph in Fig.4.9. The load-strain results at the midheight region of the wall are shown in Fig.4.11

4.3.3.4 Failure Mode for Wall P4

The nominal eccentricity was t/20 for Wall P4 and the measured

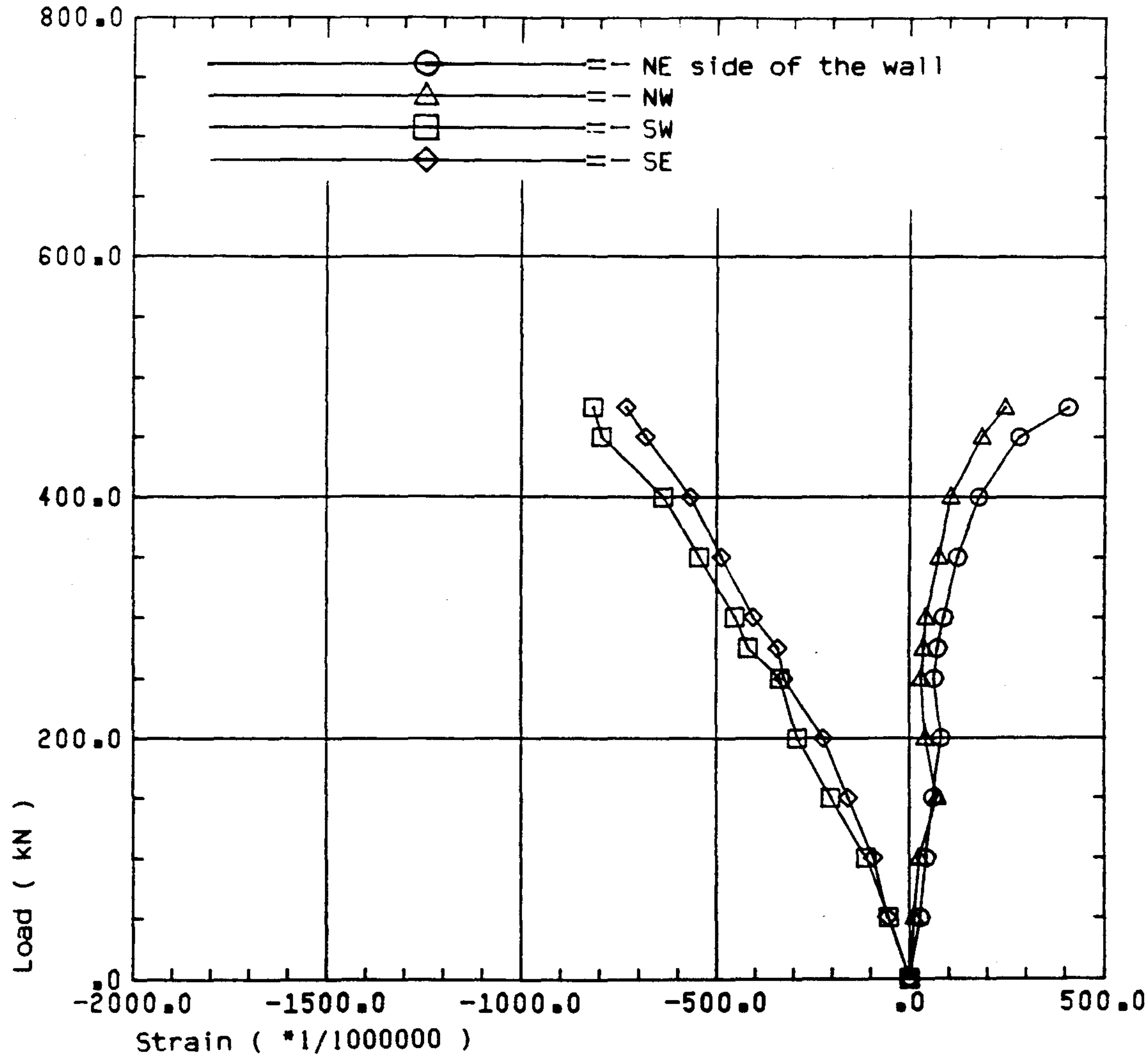

failure load : 502 kN
eccentricities:
nominal 63 mm
actual 67 mm

Fig.4.8 Load-Strain Results at Midheight of Wall P2.

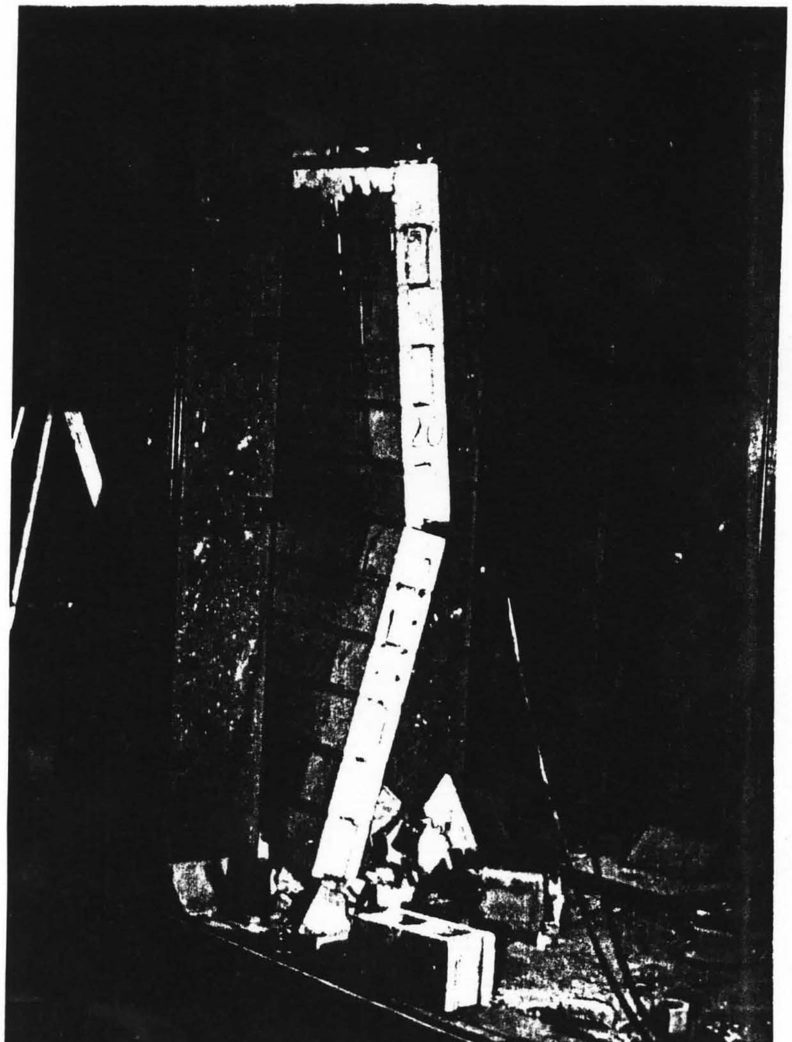

Fig.4.9 View of the Wall P3 after Failure.

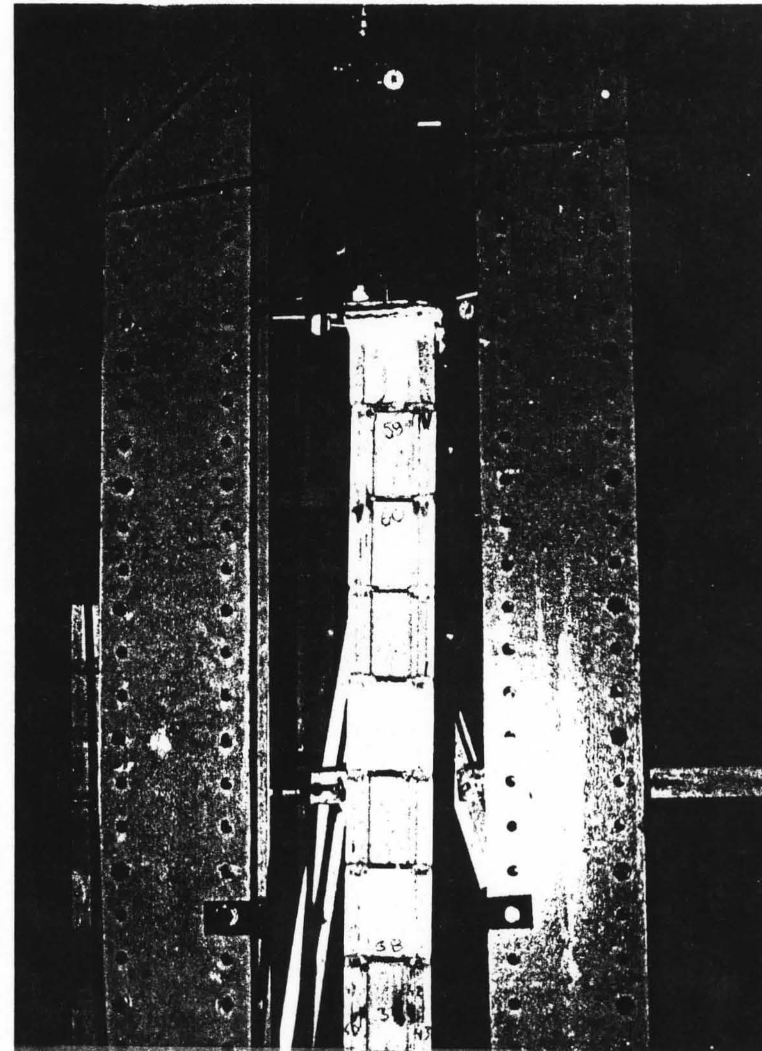

Fig.4.10 View of the Top Part of tHe Wall P4

with Buckled Loading Beam.

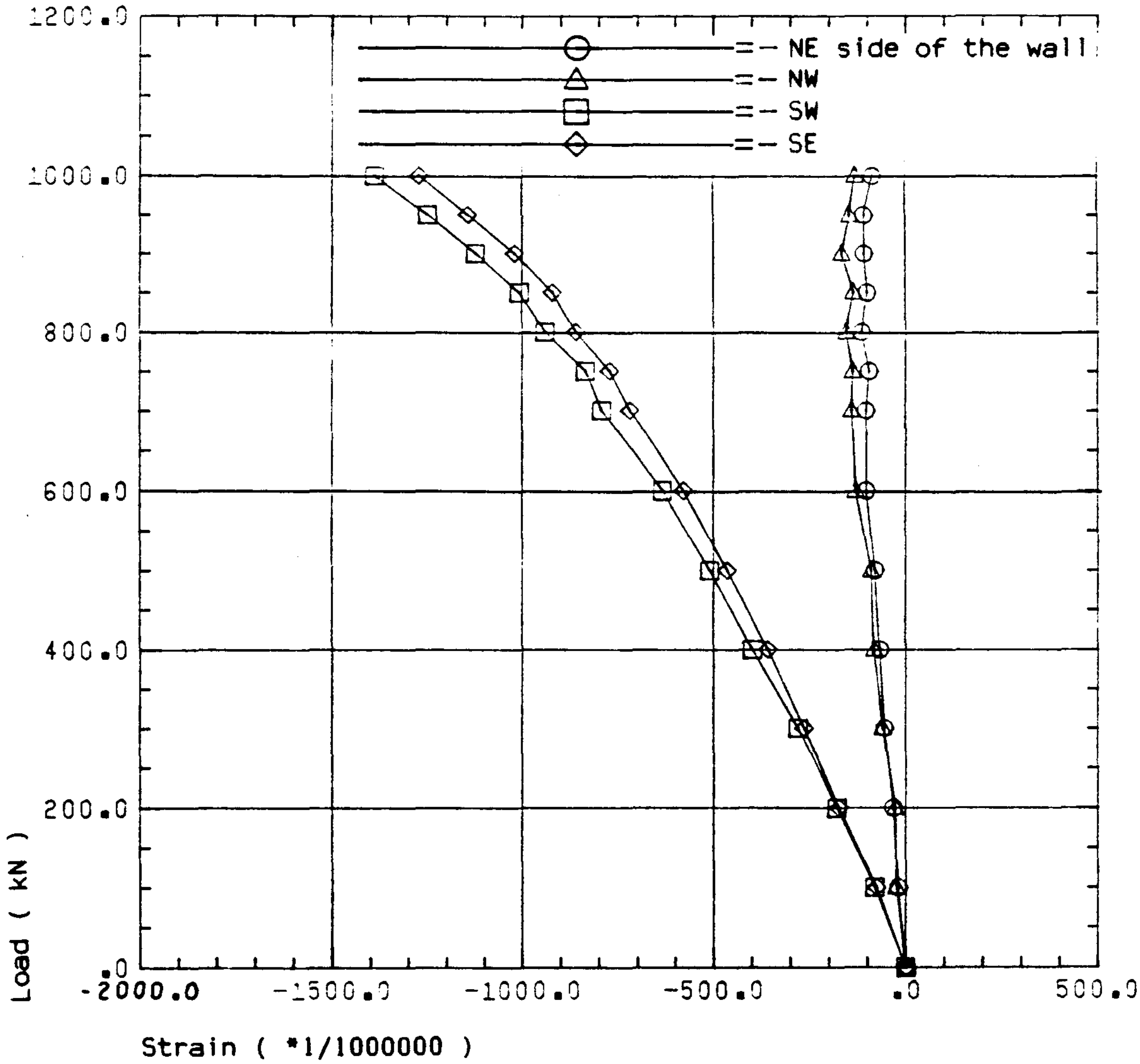

failure load: 1055 kN
eccentricities:
nominal 32 mm
actual 32 mm

Fig.4.11 Load-Strain Results at Midheight of Wall P3.

deviation along the height of the wall is shown in Fig.4.4d. The wall failed prematurely due to sudden buckling of the loading beam. The resulting damages to the wall did not allowed for retesting. Additional stabilizing bars were constructed to prevent re-occurrence of this problem in the future. The first visible cracks occurred at the bottom of the wall at a load of 200 kN. There was a significant change in the tensile strains recorded in webs at the midheight. Rapid increase could suggest the existence of minor invisible cracks. This behavior could result in the splitting failure in that region. The photograph in Fig.4.10 shows the top part of Wall P4 with the buckled loading beam on the top of it. The recorded load-strain relationships for the both faces at the midheight region of the wall are shown in Fig.4.12.

4.3.3.5. Failure Mode for Wall P5

For Wall P5, the nominal eccentricity was t/20 and the actual eccentricity was recorded and shown in Fig.4.4e in the form of deviation from the nominal eccentricity along the height of the wall.

Wall P5 failed due to splitting of the webs, which occurred in the bottom ten courses. The remaining six top courses had cracked webs as well. Cracking of the webs started at the bottom of the wall at a load of 200 kN and at about 700 kN small cracks developed in the webs at the midheight region. It seemed that the sudden connection of the propagating cracks resulted in an explosive failure. The photograph in Fig.4.13 shows the remains of Wall P5 after failure. The load-strain relationships recorded at the midheight region of the wall are shown in

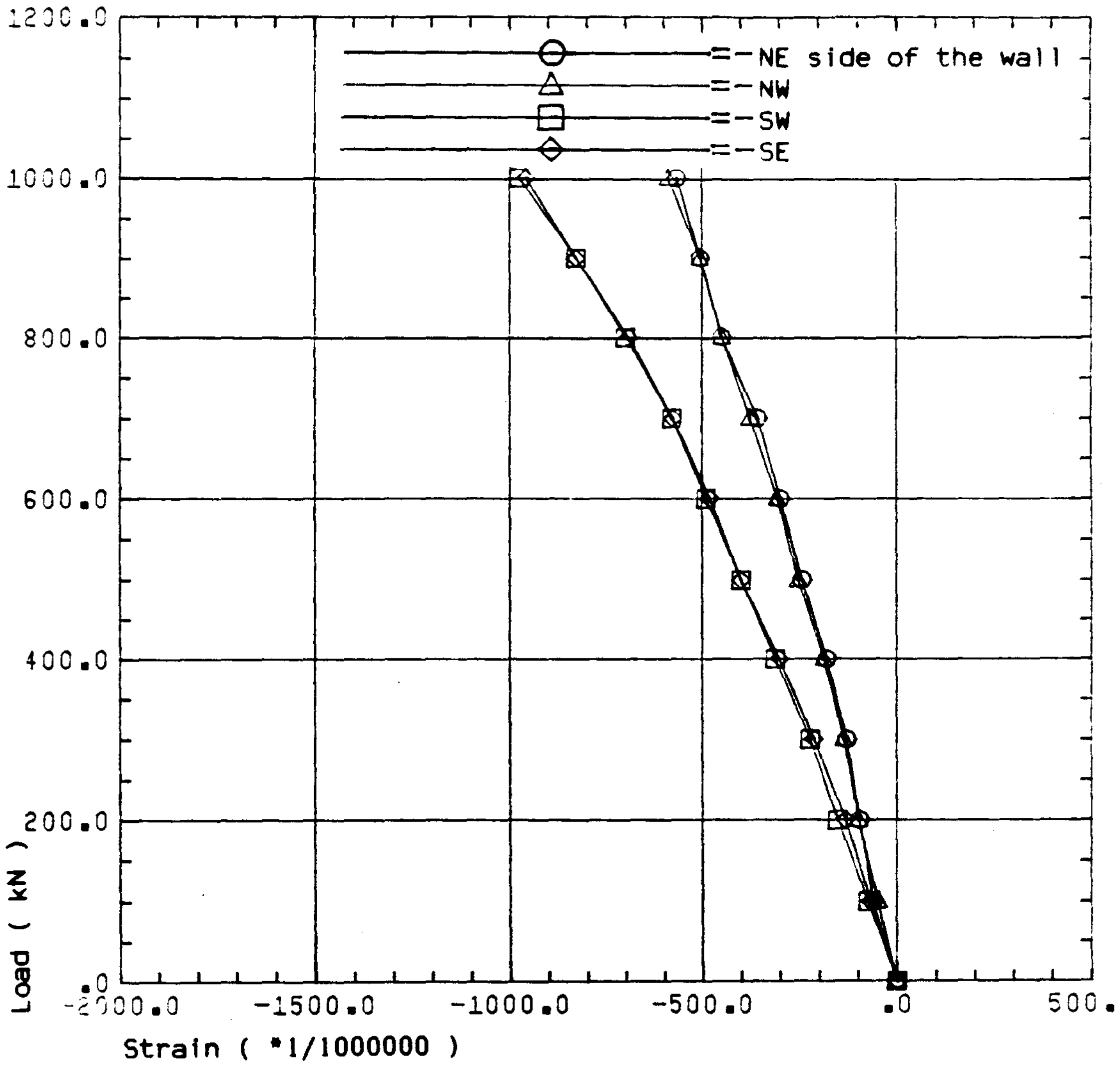

failure load: 1060 kN
eccentricities:
nominal 9.5 mm
actual 10 mm

Fig.4.12 Load-Strain Results at Midheight of Wall P4.

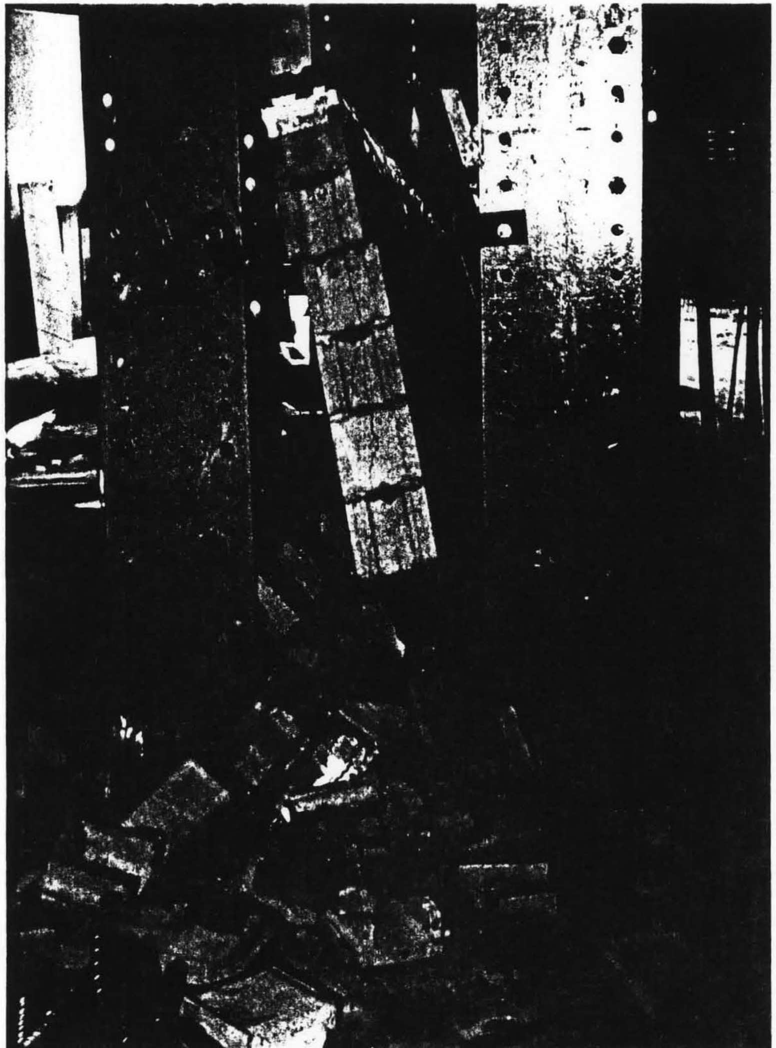

Fig.4.13 View of the Wall P5 after Failure.

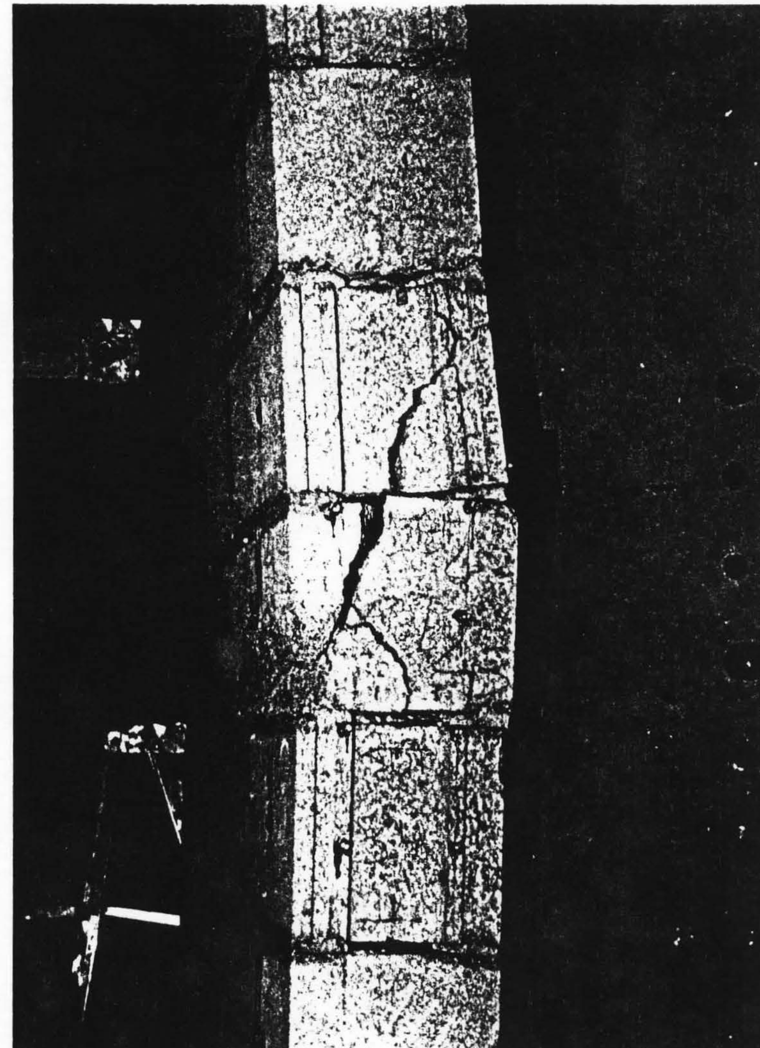

Fig.4.14 Midheight Region of the Wall P6

after Failure.

Fig.4.15.

4.3.3.6 Failure Mode for Wall P6

The nominal eccentricity was t/3 for Wall P6 and the actual eccentricity along the height of the wall is shown in Fig.4.4f, as a deviation from that nominal value.

The wall seems to have failed when the stresses at the compressive side of the wall reached the compressive strength of the blocks. Spalling of the face shells along the mortar bed joint is quite visible in the photograph in Fig.4.14 which shows the midheight region of the wall after failure. The maximum compressive strain recorded over the midheight joint was 1670×10^{-6}. The load-strain relationships at the midheight of the wall are shown in Fig.4.16.

4.4 Reinforced Concrete Block Walls

4.4.1 Fabrication and Preparation of Reinforced Walls for Testing

Six walls composed of 16 courses of two and half block were constructed in running bond with mortar applied on face shells and on the webs surrounding the outside cores. The dikes created by the mortar on the webs prevented spreading of grout to other cores. The walls were fabricated by an experienced mason. In all walls, the first course was laid directly on a polyethylene sheet placed on the laboratory floor. After the first ten courses were constructed, a 15M bar was put in each of the two outside cores of the wall. A 38 mm diameter by 12 mm thick disk was welded on the bottom end of each bar and two 350 mm long 10M bars were welded to each disk to improve anchorage of these bars. After

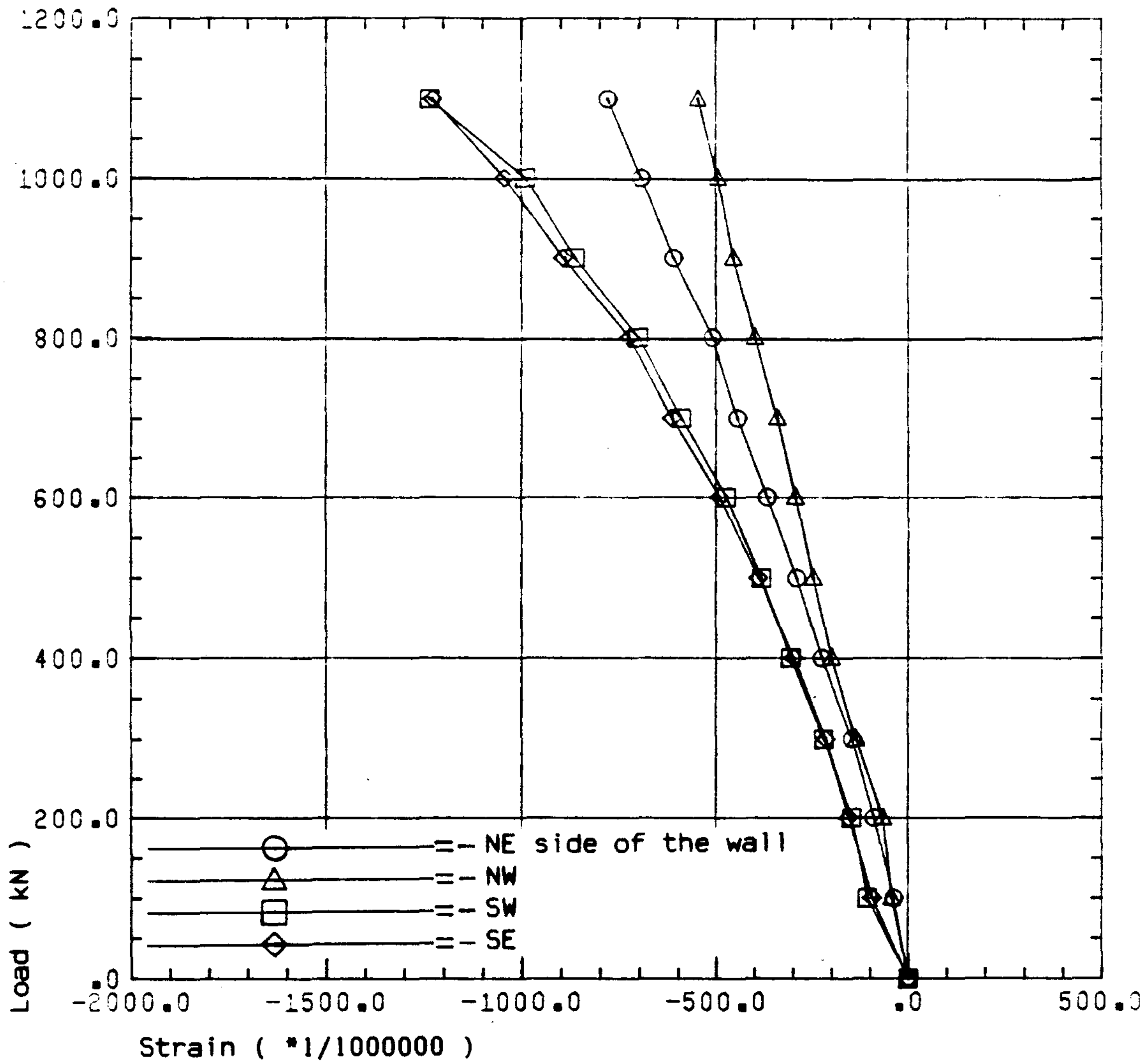

failure load: 1180 kN
eccentricities:
nominal 9.5 mm
actual 13 mm

Fig.4.15 Load-Strain Results at the Midheight of Wall P5

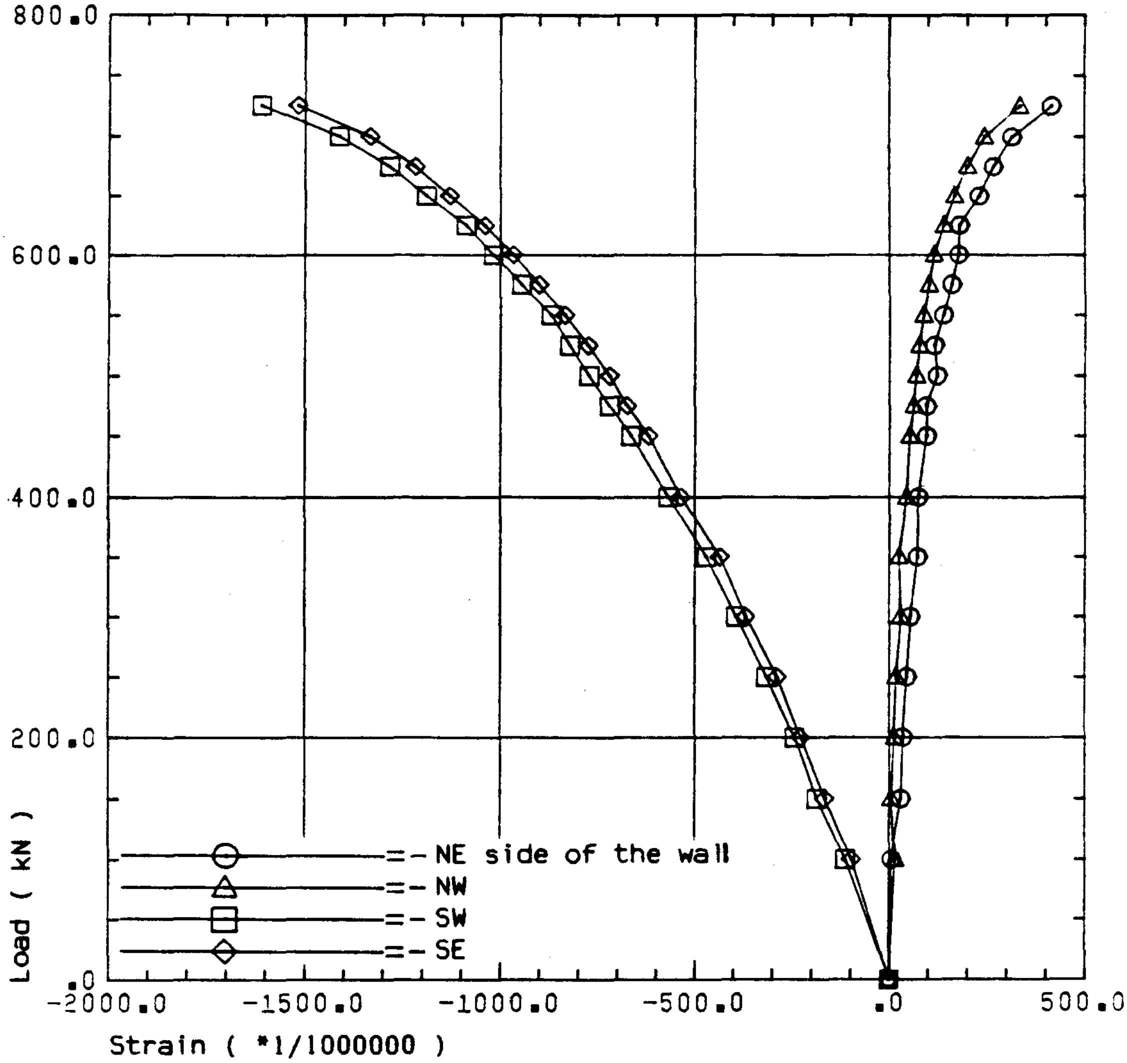

failure load: 750 kN
eccentricities:
nominal 62 mm
actual 63 mm

Fig.4.16 Load-Strain Results at Midheight of Wall P6 four days the outside cores were filled with grout up to the midheight level of the tenth course. Specially cut openings on the tensile side of the bottom course facilitated positioning and securing of the reinforcing bars in the center of the cores. It also provided a check on the filling of the cores. In the next stage, the remaining six courses were laid and after four days the outside cores were filled to the top of wall. Before the grout had time to set, discs and 10M bars arrangement similar to those used at the bottom were added at the top of each grouted core. The main 15M reinforcing bars extended above the top surface of the wall. Walls were stored and tested in the laboratory were the temperature was 20 deg C±2 deg C and the average relative humidity was approximately 50%. They were tested at an age of 8 to 12 months.

Preparations of a wall for testing started with gluing strain points on the wall surface using hot sealing wax. Then 100 mm lengths of 15M bars were welded to bottom ends of the reinforcing bars. Holes were drilled in the 38 mm thick end plates large enough to let the reinforcing bars go through and leave room for an internal weld. These plates were bedded on the ends of wall using thin layers of hydrostone which would assure uniform bearing. Later two 25 mm diameter threaded bars with plates at the ends were used to prestress wall. The prestress was needed to keep the end plates in position and to strengthen the wall, since it had to be turned and positioned on its side to allow for welding the reinforcing bars to the end plates. After welding, the projecting parts of the reinforcing bars were cut off and welds were ground flat. The plates with groves were bolted to the already fixed end plates and the whole specimen was ready to be placed in the test set-up. As described previously, the side of the wall where high compression was expected was placed facing South and the other side of the wall where tensile stresses or lower compressive stresses were expected was placed facing North. The remaining preparations were the same as were described in Section 4.3.1.

Specimens used for testing of reinforced walls in pure bending were cut from walls which had failed in buckling with no material damages except for cracking along the bed joints on the tension side. Preparation of specimen for testing started with gluing strain transducers to wall surface in the constant moment region. Then the specimen was positioned on supports where thin layers of hydrostone between the support plates and the surface of the specimen assured uniform loading. The loading beams were put on top of the specimen. A schematic view of the test set-up is shown in Fig.4.2. It is similar to the set-up used by Gazzola[38].

4.4.2 Test Procedure for Reinforced Walls

The test procedure for the reinforced walls under vertical eccentric loading was the same as described for plain walls in Section 4.3.2.

The test procedure for the reinforced walls in pure bending was significantly different since a different test set-up and instrumentation were used. At the beginning of each test, initial strain and deflection readings were taken. Load was applied and increased in equal intervals up to failure. Since strain transducers were connected to a computer data recording system, all the strain readings were taken at very nearly the same time after each load increment. Displacements were of secondary importance since the tensile side had been previously cracked. After testing each specimen was cut along the failure plane and the exact positions of the reinforcing bars were recorded.

4.4.3 Test Results for the Reinforced Walls

In this section, the test results for the reinforced walls are described. The load-lateral displacement and the load-moment relationships for all six walls are shown later in Section 4.5.2.

4.4.3.1 Failure Mode for Wall R1

The nominal eccentricity was t/3 for Wall R1 and the deviation from it along the height of the wall is shown in Fig.4.17a.

The wall failed in buckling with all the bed joints cracked on the tensile side. The first crack occurred at a load of 300 kN at the first mortar joint above midheight of the wall. The highest strain of 1090×10^{-6} registered on the compression side was far less than the maximum strain expected for concrete masonry. The deformed shape of wall R1 is shown in the photograph in Fig.4.18. The load-strain results, recorded at the midheight region of the wall, are shown in Fig.4.20.

4.4.3.2 Failure Mode for Wall R2

For Wall R2, the nominal eccentricity was t/2, actual eccentricity along the height of the wall was recorded and shown in

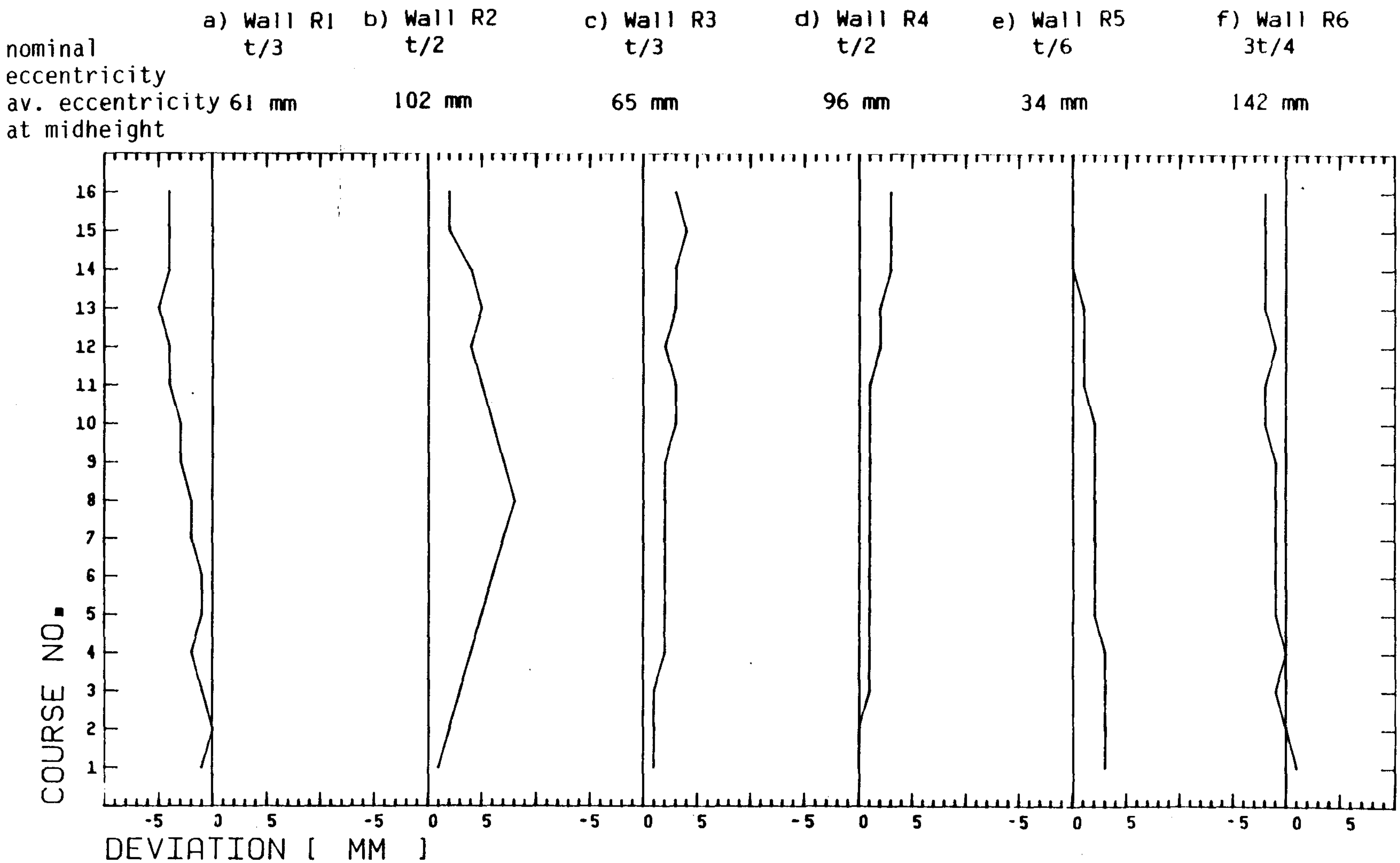

Fig.4.17 Measured Deviation of Eccentricities for Reinforced Walls.

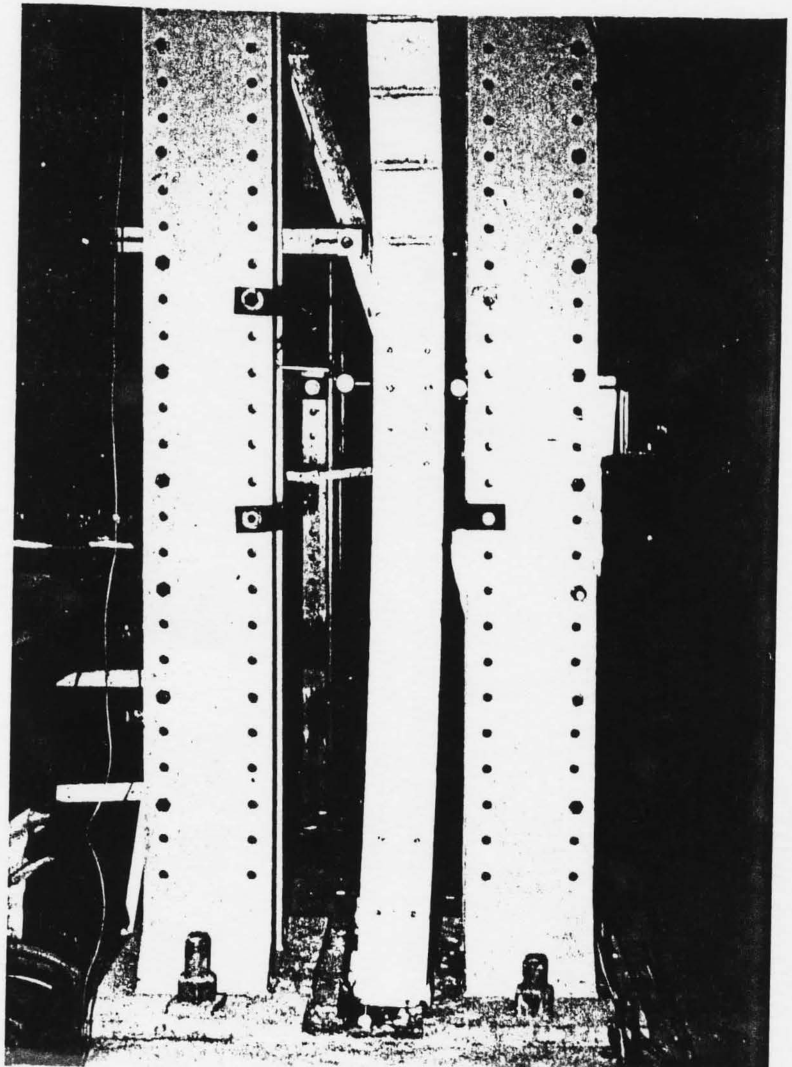

Fig.4.18 View of the Wall R1 after Failure.

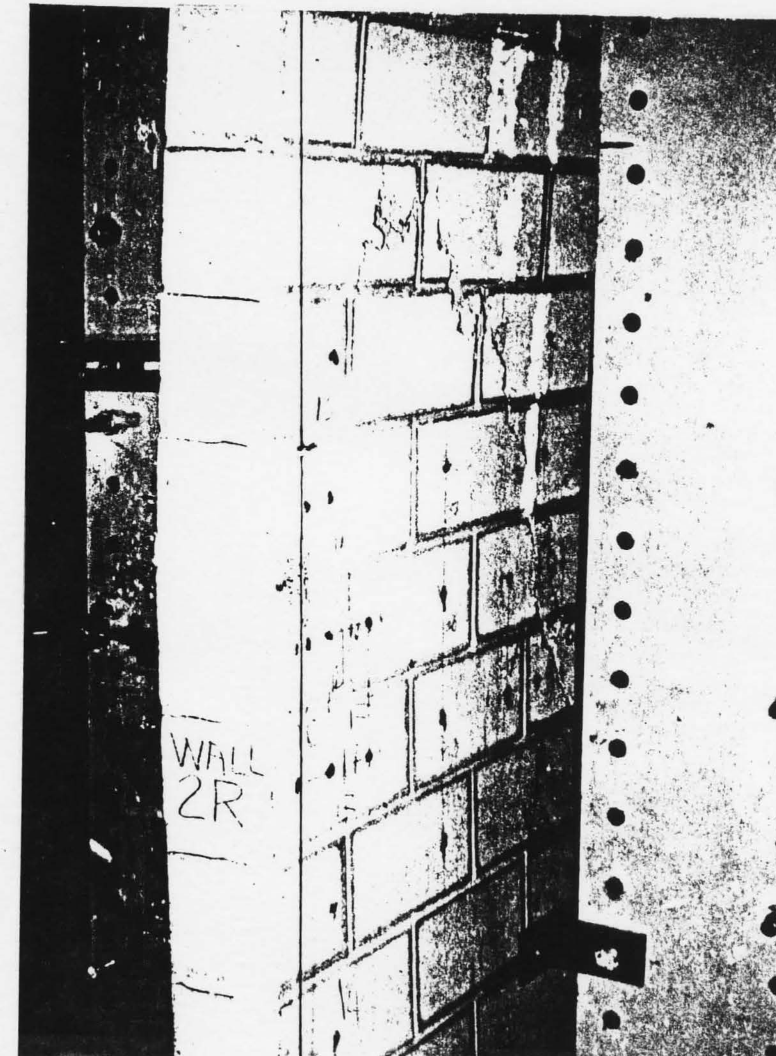

Fig.4.19 Midheight Region of the Wal R2

after Failure.

Fig.4.17b as a deviation from that nominal value.

The wall seemed to fail in buckling with all the mortar bed joints cracked on the tensile side of the wall. However, the recorded high strains on the compressive side of the wall indicate possibility of compression failure as confirmed by crushing of the material which can be seen in Fig.4.19. The load-strain relationships at the midheight are shown in Fig.4.21.

4.4.3.3 Failure Mode for Wall R3

The nominal eccentricity was t/3 for Wall R3 and the actual eccentricity is shown in Fig.4.17c in form of the deviation from that nominal eccentricity along the height of the wall.

The wall failed in buckling. All of the bed joints on the tensile side of the wall were cracked. The first crack was recorded at a load of 300 kN at the first joint above the midheight. The highest strain recorded on the compressive side of the wall was 1130×10^{-6}, which was below the maximum strain for compression failure of concrete masonry. The load-strain relationships for the midheight region of the tested wall are shown in Fig.4.22.

4.4.3.4 Failure Mode for Wall R4

For Wall R4, the nominal eccentricity was t/2 and the measured deviation along the height of the wall is shown in Fig.4.17d.

The wall failed in buckling. All the bed joints were cracked on the tensile side of the wall. The first crack was observed at a load of 75 kN at the first joint below the midheight of the wall. The maximum strain recorded on the compression side of the wall was 1980×10^{-6} but no

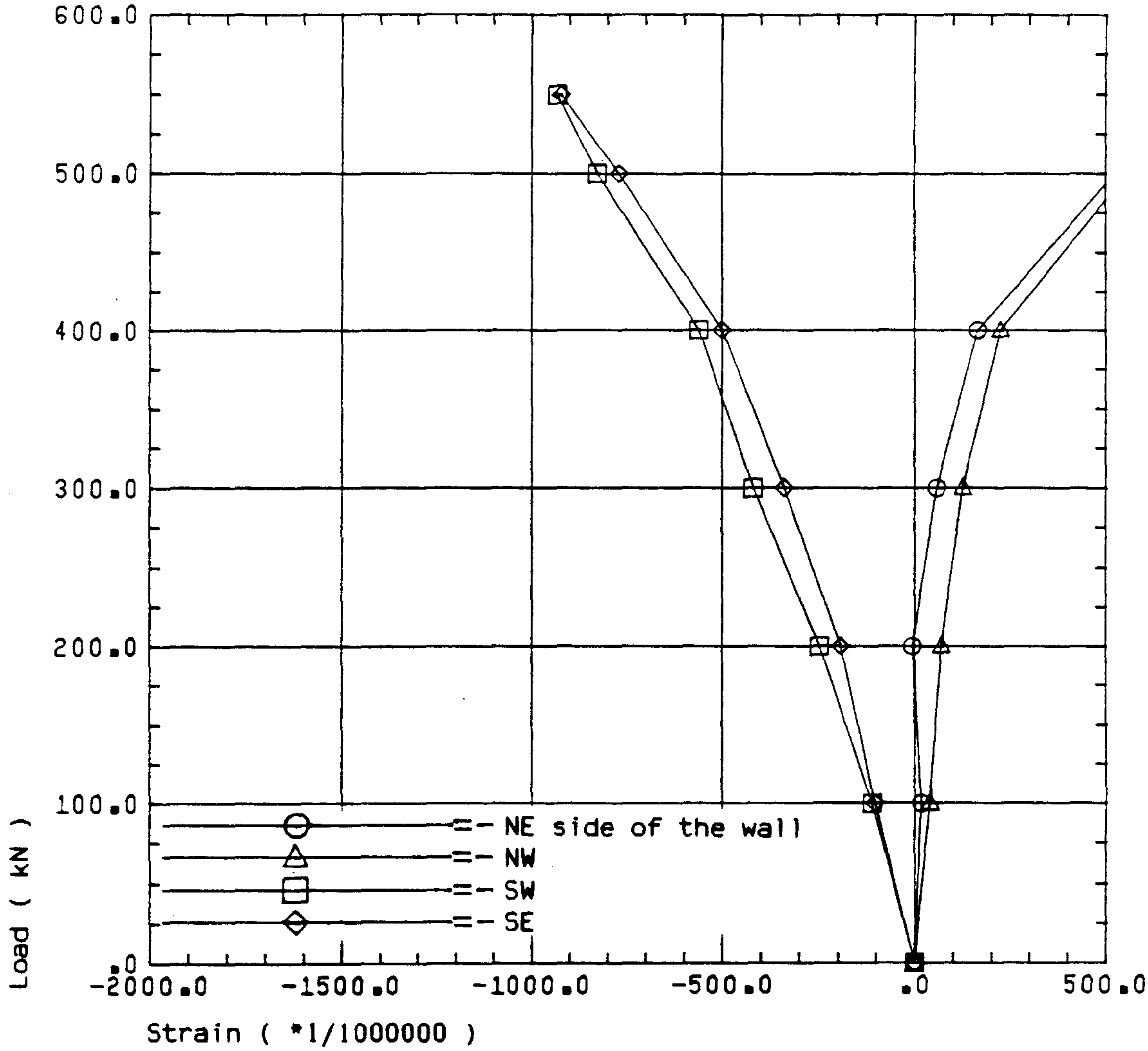

failure load: 594 kN
eccentricities:
nominal 62 mm
actual 61 mm

Fig.4.20 Load-Strain Results at the Midheight of Wall R1.

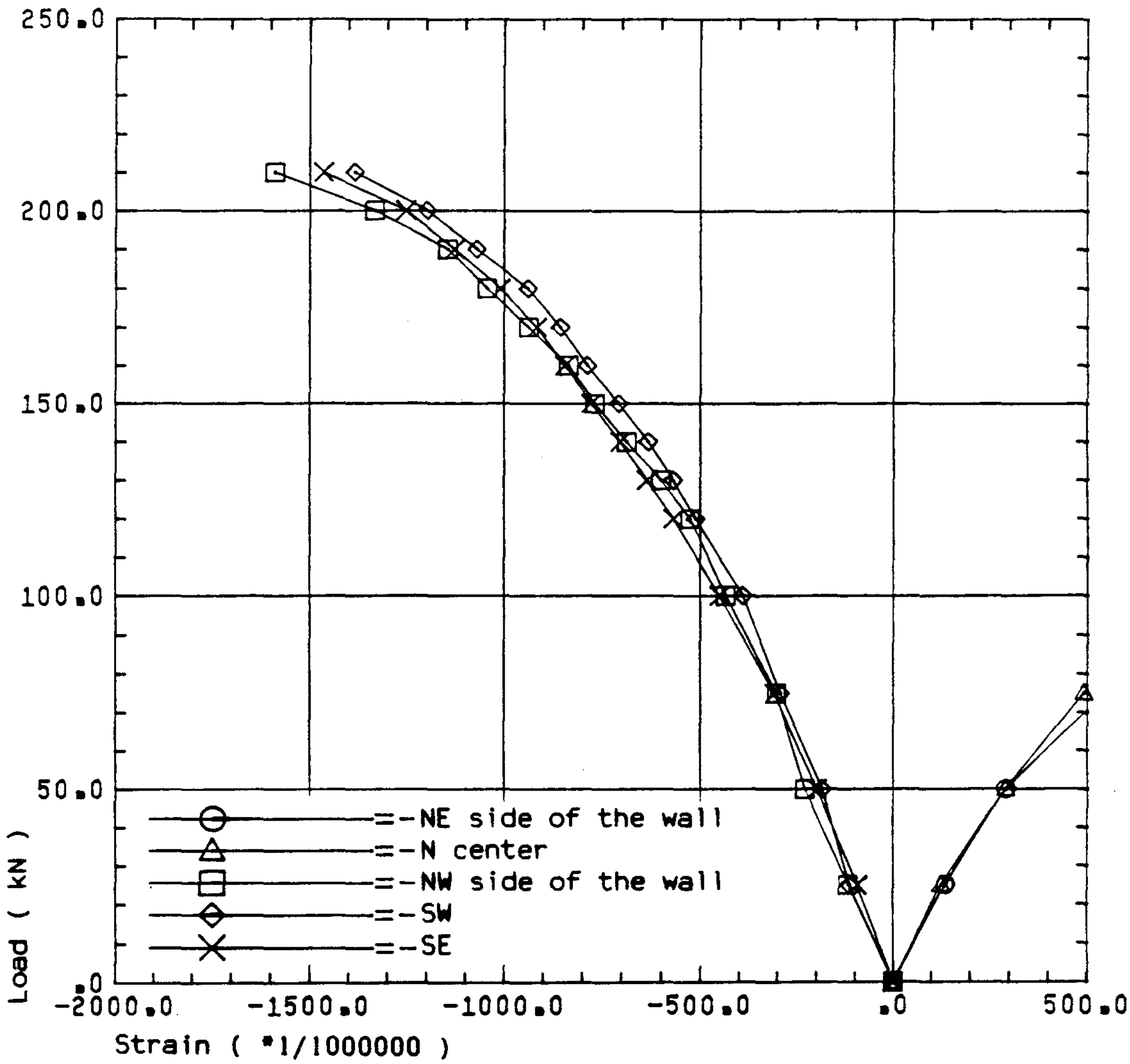

failure load 216 kN
eccentricities:
nominal 95 mm
actual 102 mm

Fig.4.21 Load-Strain Results at the Midheight of Wall R2.

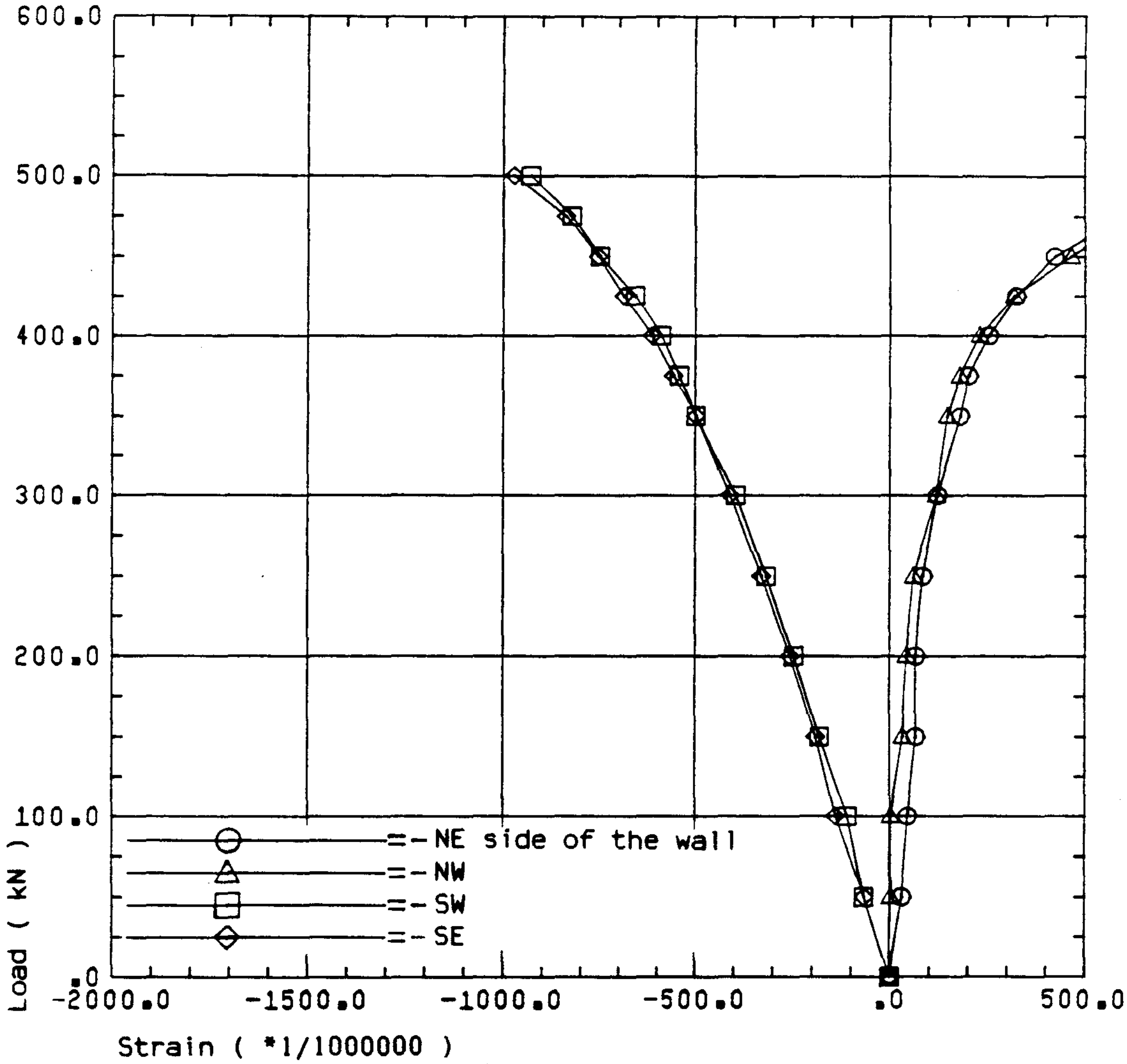

failure load: 521 kN
eccentricities:
nominal 62 mm
actual 65 mm

Fig.4.22 Load-Strain Results at the Midheight of Wall R3.

signs of crushing were observed. The photograph in Fig.4.23 shows a view of the midheight region with cracks visible in the mortar joints between the webs of the blocks. The load-strain relationships are shown in Fig.4.25.

4.4.3.5 Failure Mode for Wall R5

The nominal eccentricity for Wall R5 was t/6 and the actual eccentricity is shown in Fig.4.17e as the deviation along the height of the wall. The wall failed due to crushing and spalling of the face shells of the blocks in which the cores had been filled with grout. Failure occurred at the place where the grout from the two different pours joined. This construction joint may have influenced the capacity of the wall. As can be seen in Fig.4.24., significant separation of the grouted columns from the rest of the wall occurred. This separation started at a load of 600 kN when a sudden increase occurred in the lateral tensile strains measured on the sides of the wall. At the load of 700 kN, the crack was visible. The load-strain relationships for the midheight region of the wall are shown in Fig.4.26.

4.4.3.6 Failure Mode for Wall R6

For Wall R6, the nominal eccentricity was 3t/4 and the actual eccentricity was measured and is shown Fig.4.17(f) in the form of measured deviation from the nominal eccentricity along the height of the wall.

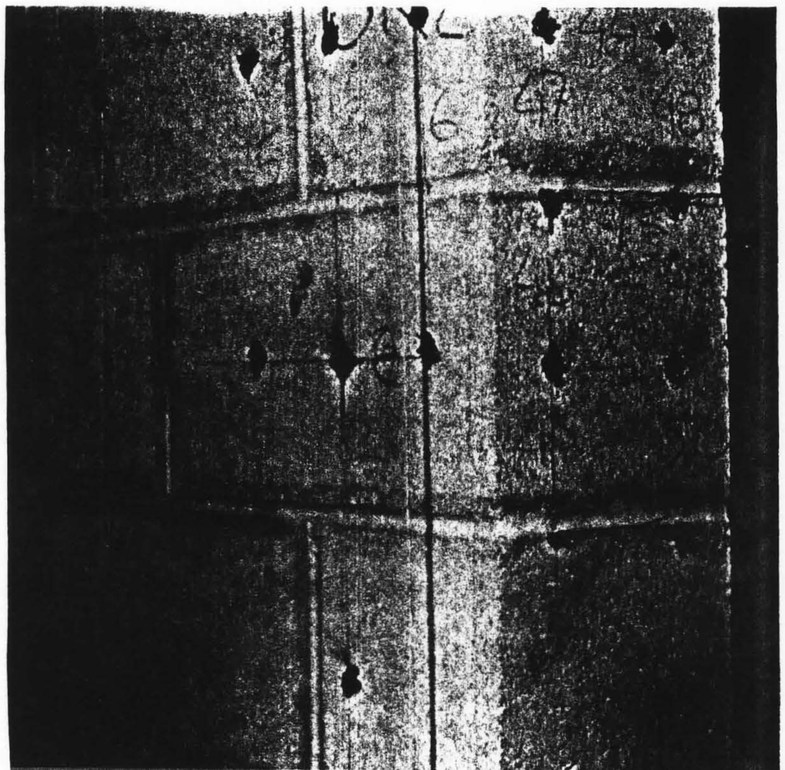

Fig.4.23 View of the Midheight Region of Wall R4 after Failure.

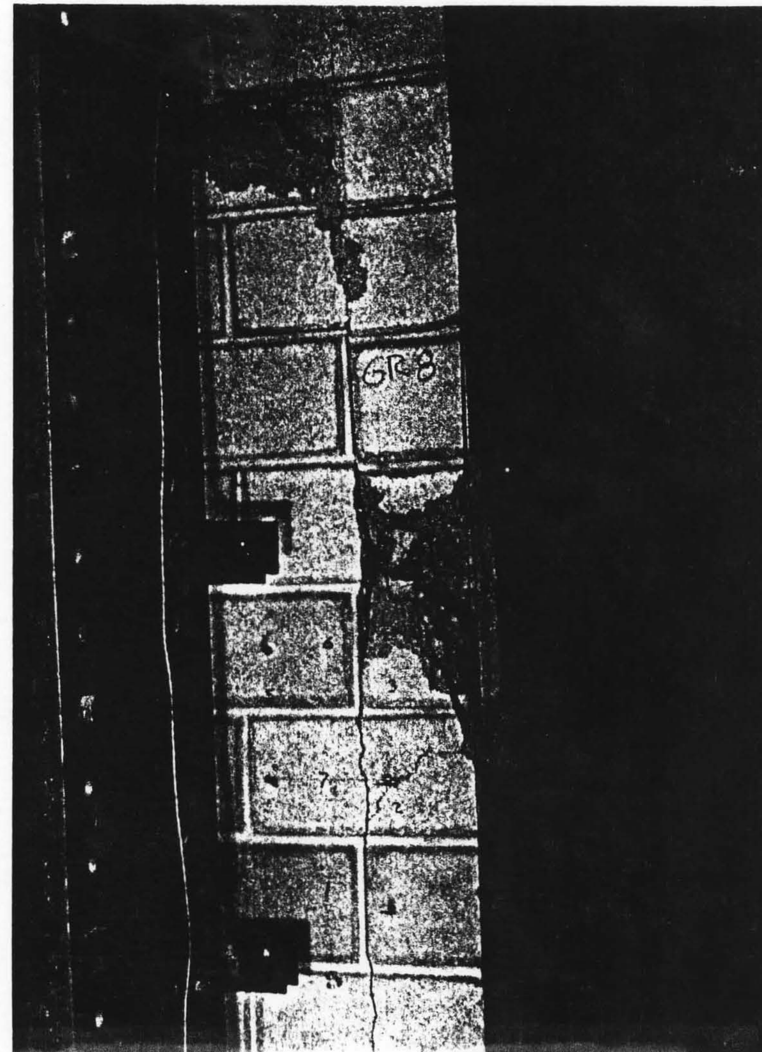

Fig.4.24 View of the Compression Side of the Wall R5 after Failure.

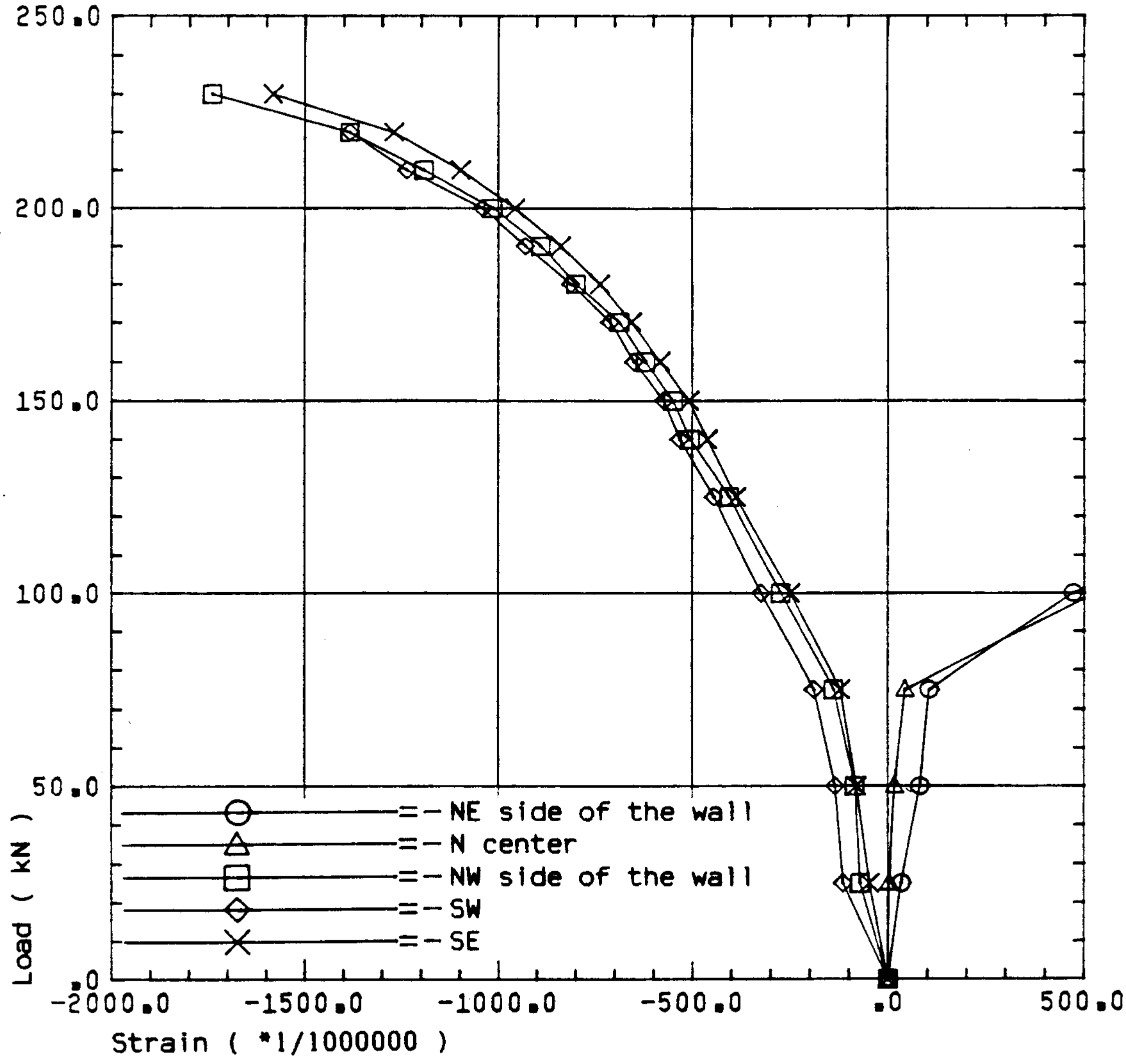

failure load: 231 kN
eccentricities:
nominal 95 mm
actual 96 mm

Fig.4.25 Load-Strain Results at the Midheight of Wall R4.

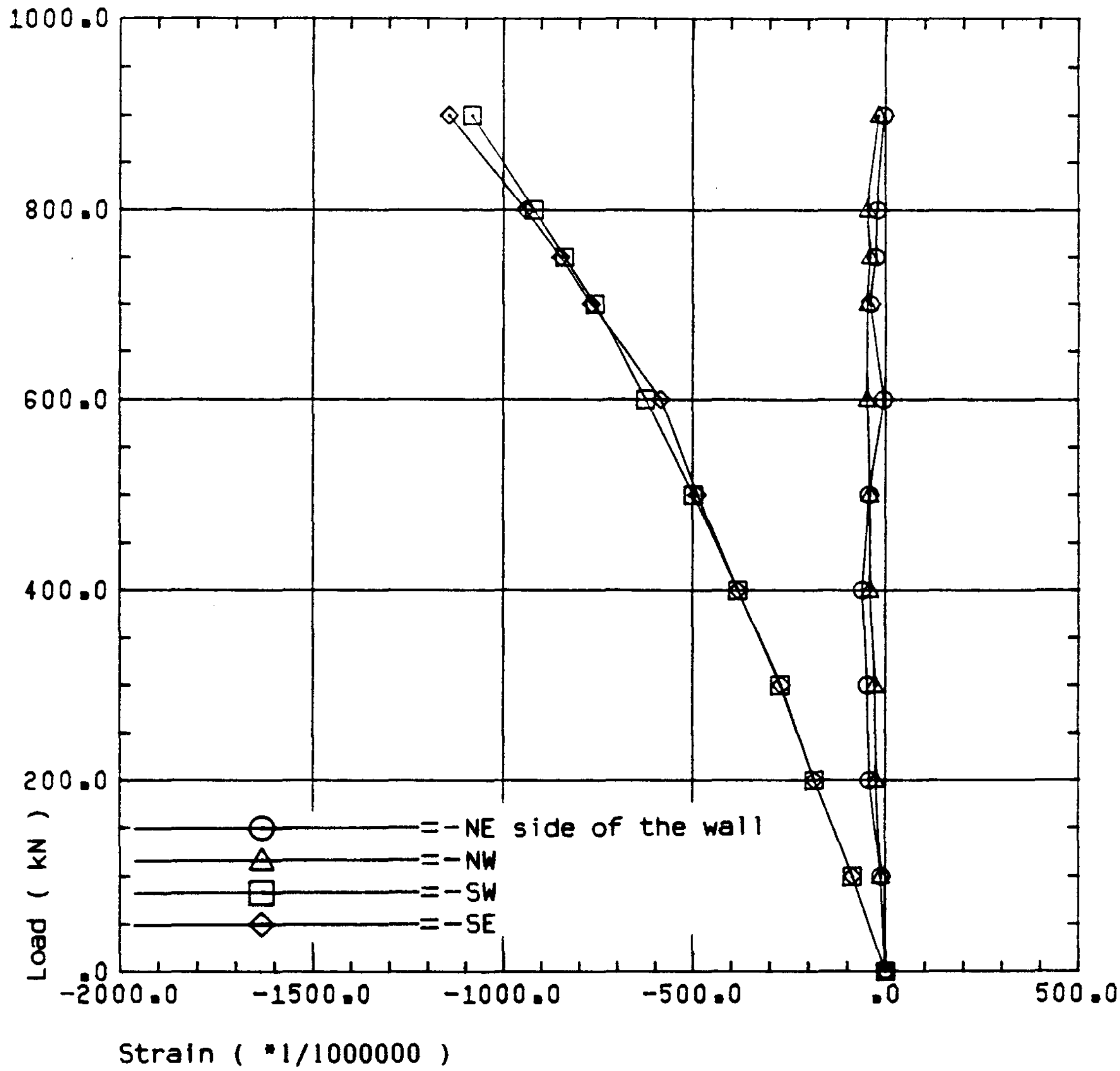

failure load: 1000 kN
eccentricities:
nominal 32 mm
actual 34 mm

Fig.4.26 Load-Strain Results at the Midheight of Wall R5.

The wall failed in buckling. All the bed joints were cracked on the tensile side of the wall. The first crack occurred after the first load increment at a load of 10 kN. The photograph in Fig.4.27 shows the deformed shape of the wall after failure. The highest recorded compressive strain was 790×10^{-6}. The load-strain relationships for the midheight region are shown in Fig.4.29.

4.4.3.7 Failure Mode for Wall S1

Wall S1 was tested in pure bending and failed due to crushing of the face shells of the blocks in the constant moment region. The maximum compressive strains recorded was 2766×10^{-6}. A view of the compressive side of the wall after failure is shown in Fig.4.28. The moment-strain data are shown in Fig.4.30.

4.4.3.8 Failure mode for Wall S2

Wall S2 was tested in bending. It failed when the face shells on the compressive side of the wall spalled. The maximum compressive strain recorded was 3416×10^{-6}. The moment-strain results are shown in Fig.4.31.

4.5 Discussion of the Test Results

A description of the walls tested was given in tabulated form in Table 4.1 and the test results were summarized in Table 4.2. The load-midheight deflection results are shown in Fig.4.32 for plain walls and in Fig.4.33, for reinforced walls. The load-moment interaction diagrams

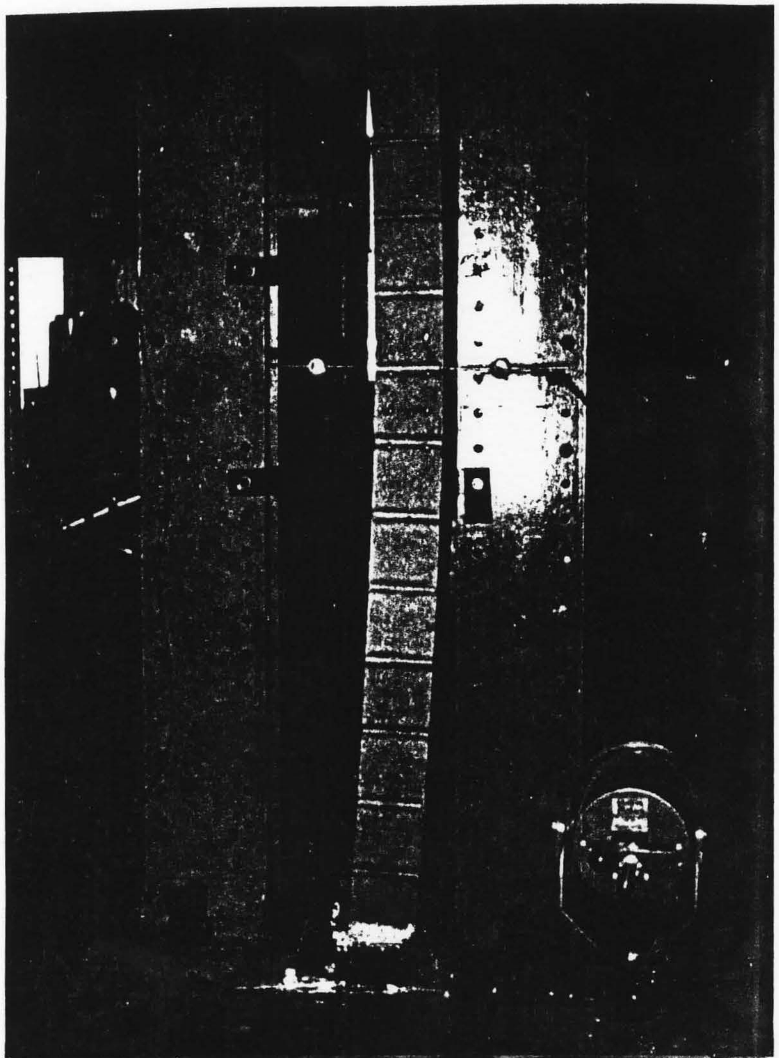

Fig.4.27 View of the Wall R6 after Failure.

Fig.4.28 View of the Constant Moment Region of Wall S1 after Failure.

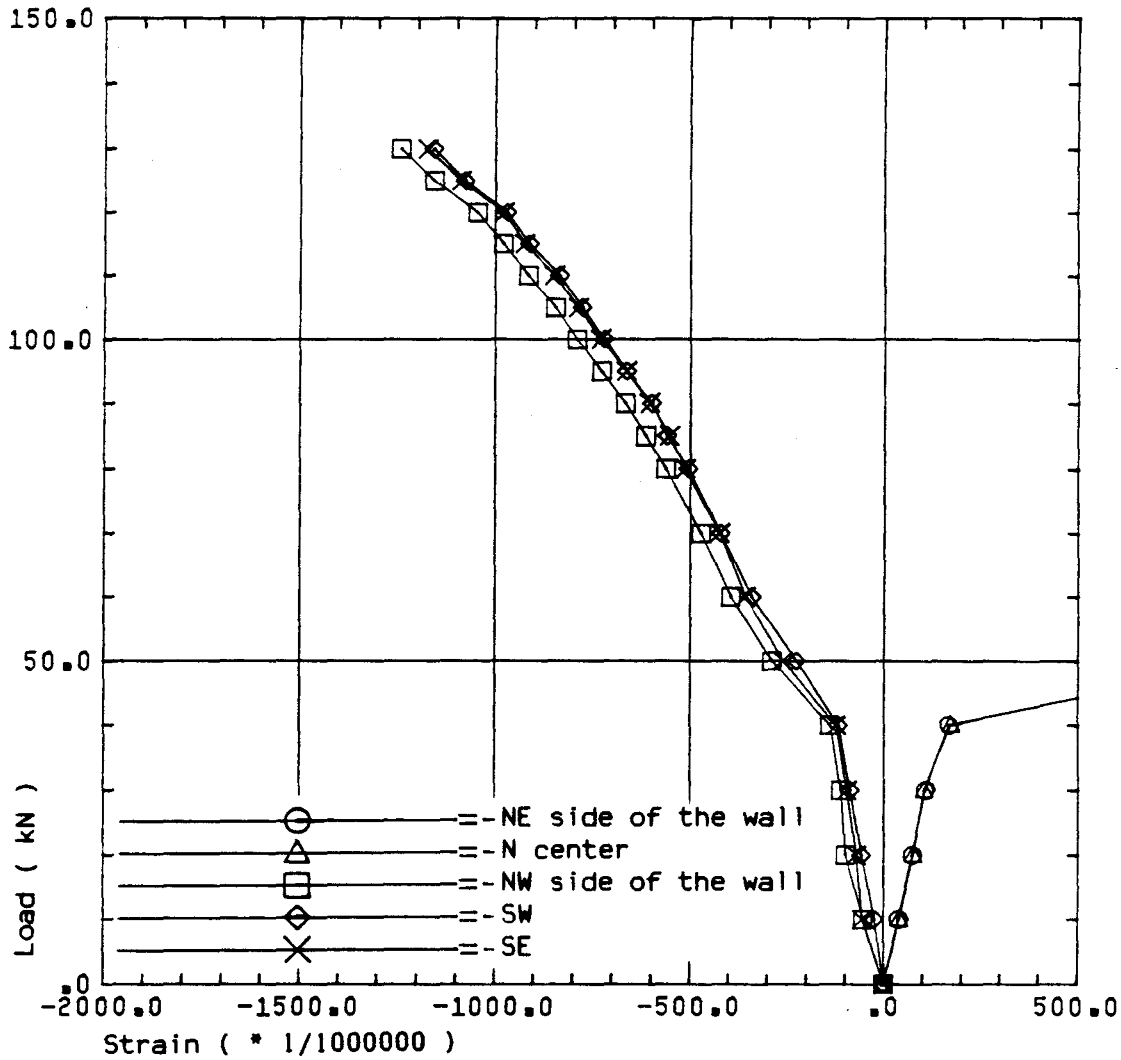

failure load: 140 kN
ecccentricities:
nominal 143 mm
actual 142 mm

Fig.4.29 Load-Strain Results at the Midheight of Wall R6.

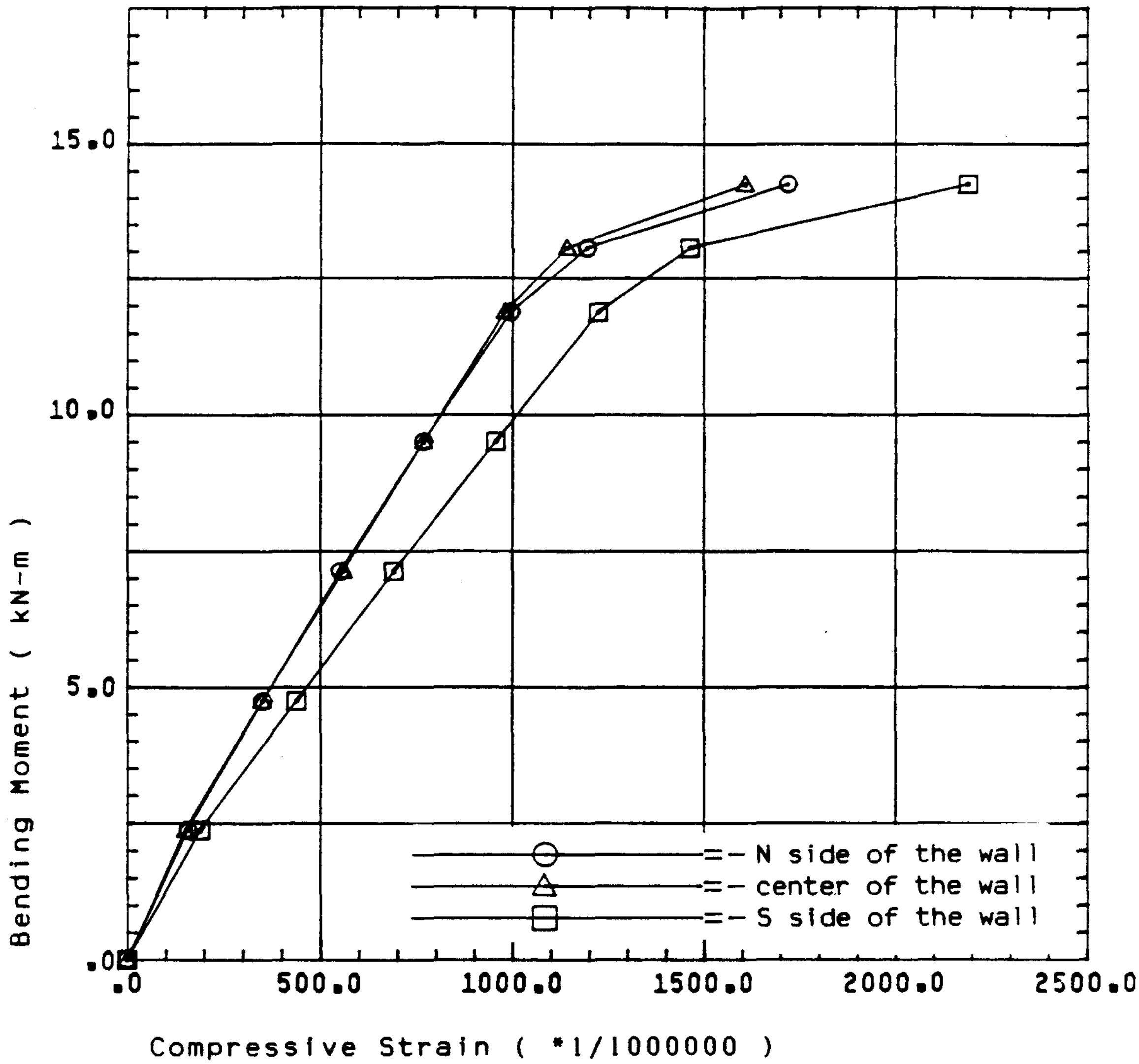

failure moment: 15.2 kNm

Fig.4.30 Moment-Strain Results at the Midspan of Wall S1.

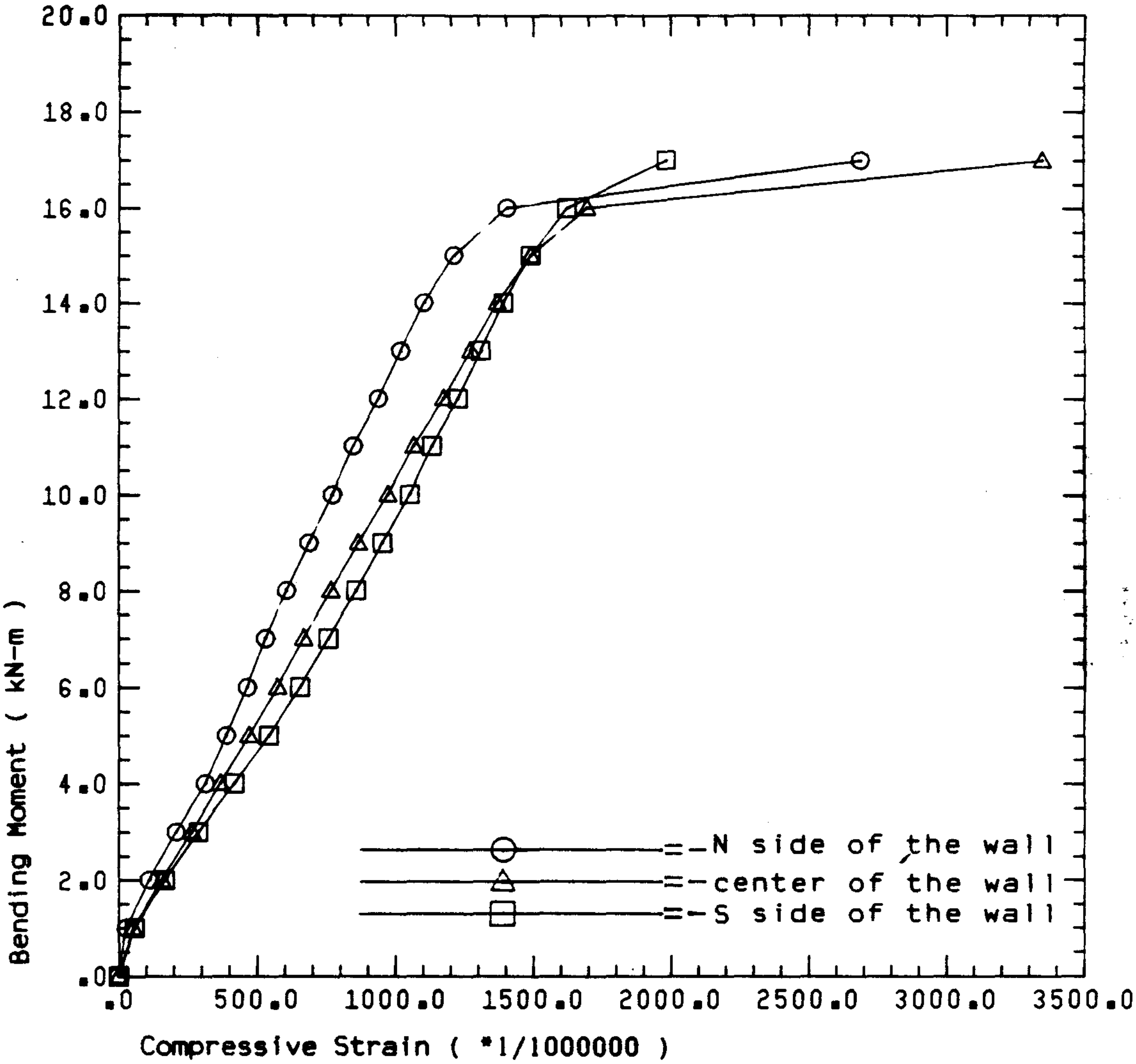

failure moment: 17 kNm

Fig.4.31 Moment-Strain Results at the Midspan of Wall S2.

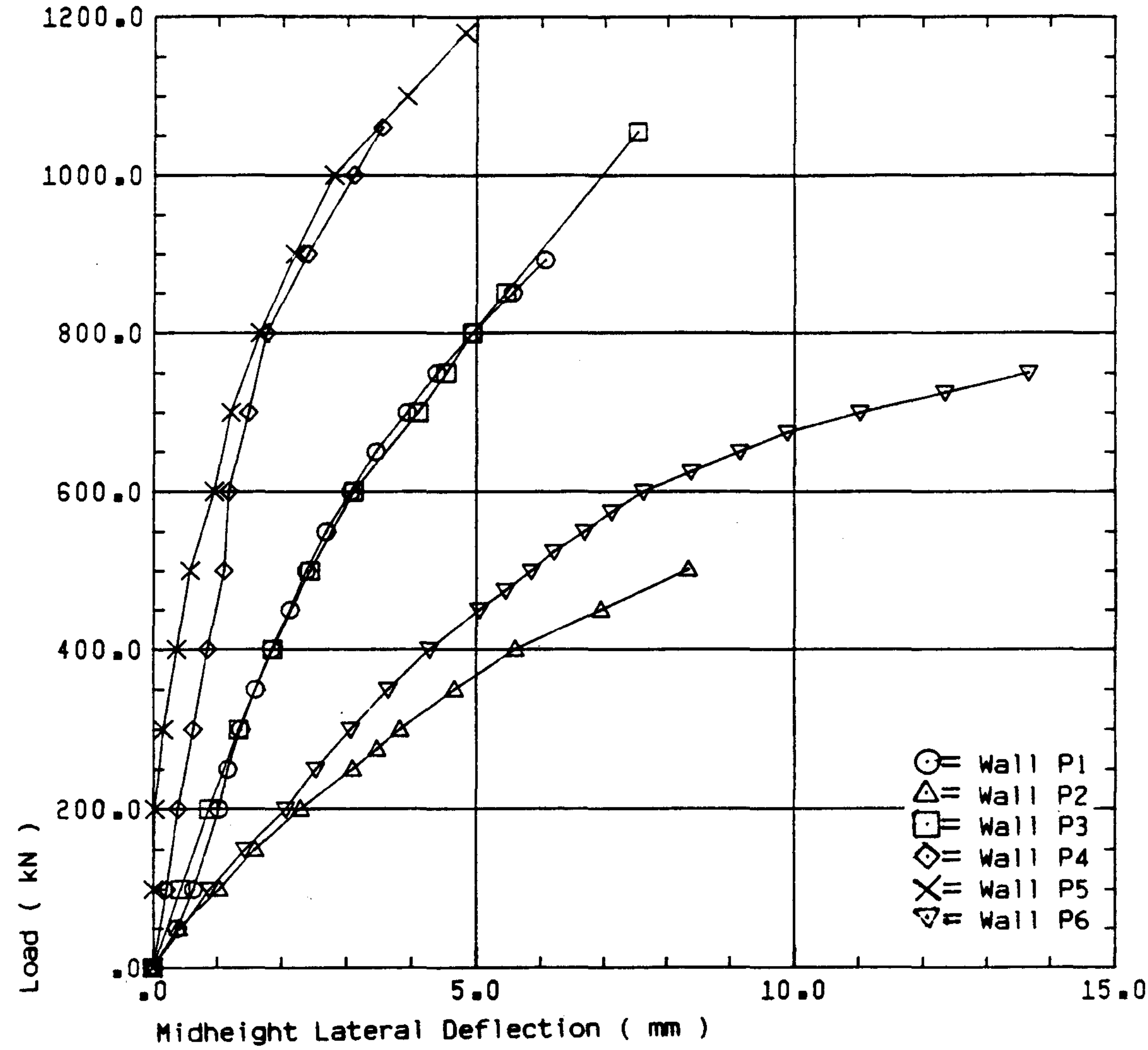

Fig.4.32 Load-Midheight Deflection Results for Plain Walls.

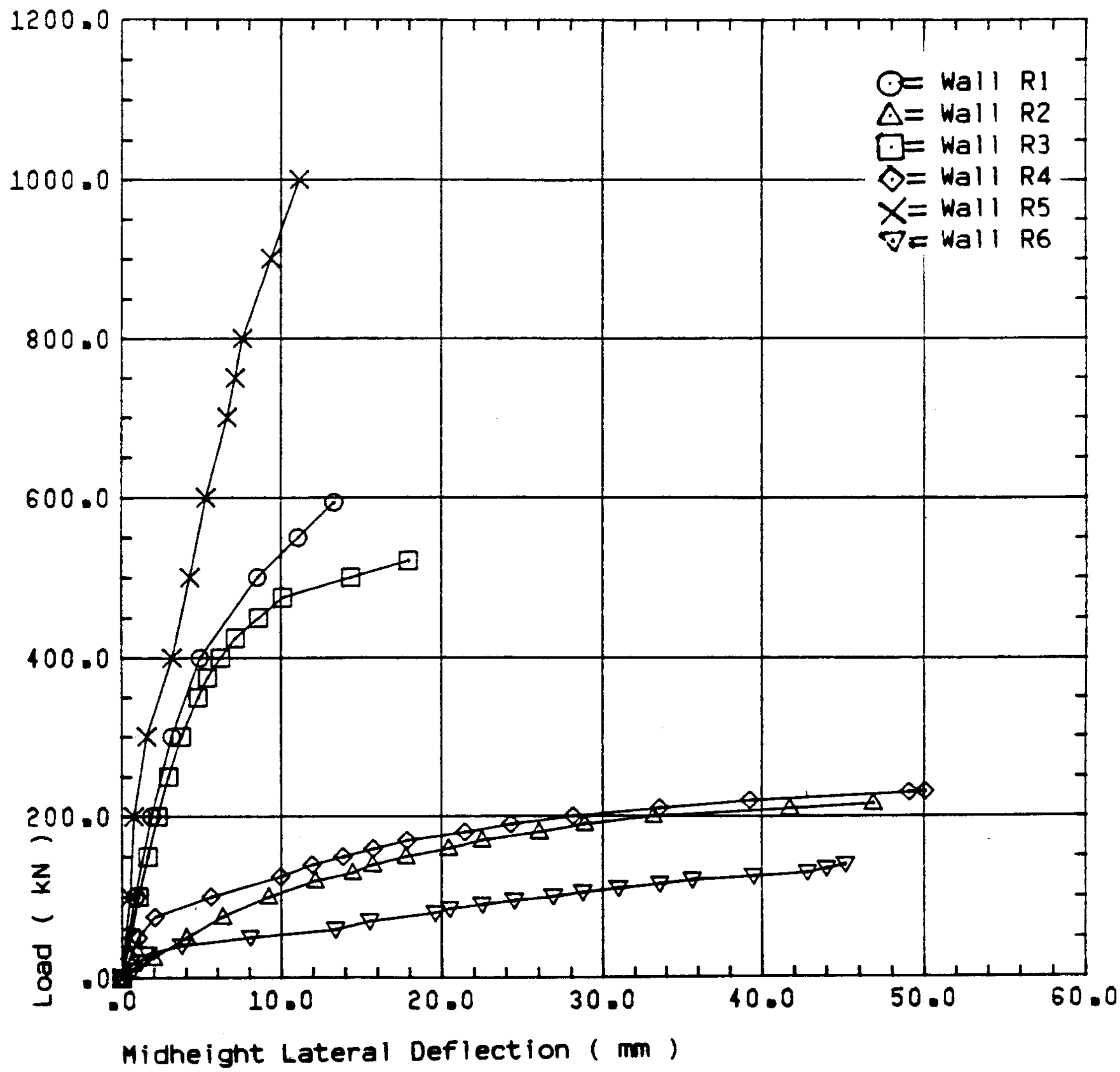

Fig.4.33 Load-Midheight Deflection Results for Reinforced Walls.

for plain and reinforced walls were drawn in Fig.4.34 and Fig.4.35, respectively.

4.5.1 Plain Walls

Specimens P1, P3, P4 and P5, for which the nominal eccentricity was less than or equal to 1/6 of the wall thickness (the actual eccentricity was equal to or less than 32 mm), failed due to splitting of the webs of blocks. The same kind of failure was reported by Hatzinikolas et al[44], Fattal and Caetano[36] and Read and Clements[65].

Specimens P2 and P6, for which the nominal initial eccentricity was 1/3 of the wall thickness had slightly varying actual eccentricities of 67 mm and 63 mm, respectively. They failed in different modes of failure. Wall P2 failed due to buckling and no material failure was observed. The testing procedure permitted control of lateral deflection. Therefore the wall was not damaged after reaching the failure load. Wall P6 failed due to the crushing of the face shells of blocks on the compressive side of the wall.

The failure mode obtained for Wall P2 was different, than the mode observed by Hatzinikolas et al[44] for that kind of loading condition. The calculated kern distance was equal to 61 mm, assuming the effective mortar bedded area equal to 40 mm. The effective mortar bedded area was discussed in Chapter 3 where the minimum face shell thickness of 32 mm was increased by 25% due to active mortar penetration. The eccentricity of 63 mm for wall P6 was higher than the kern distance. However, the

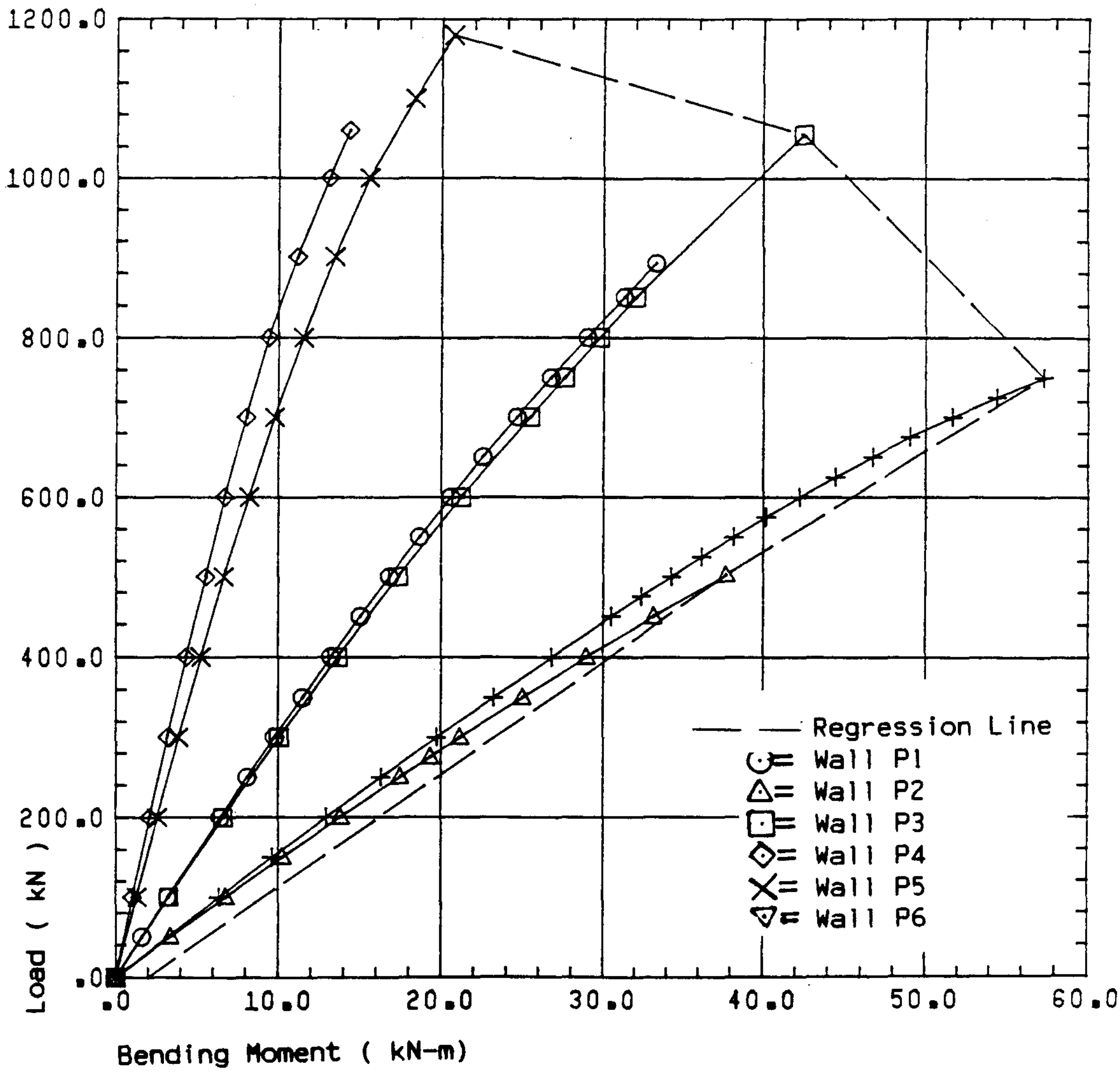

Fig.4.34 Interaction Diagram for Plain Walls Drawn from Experimental Data.

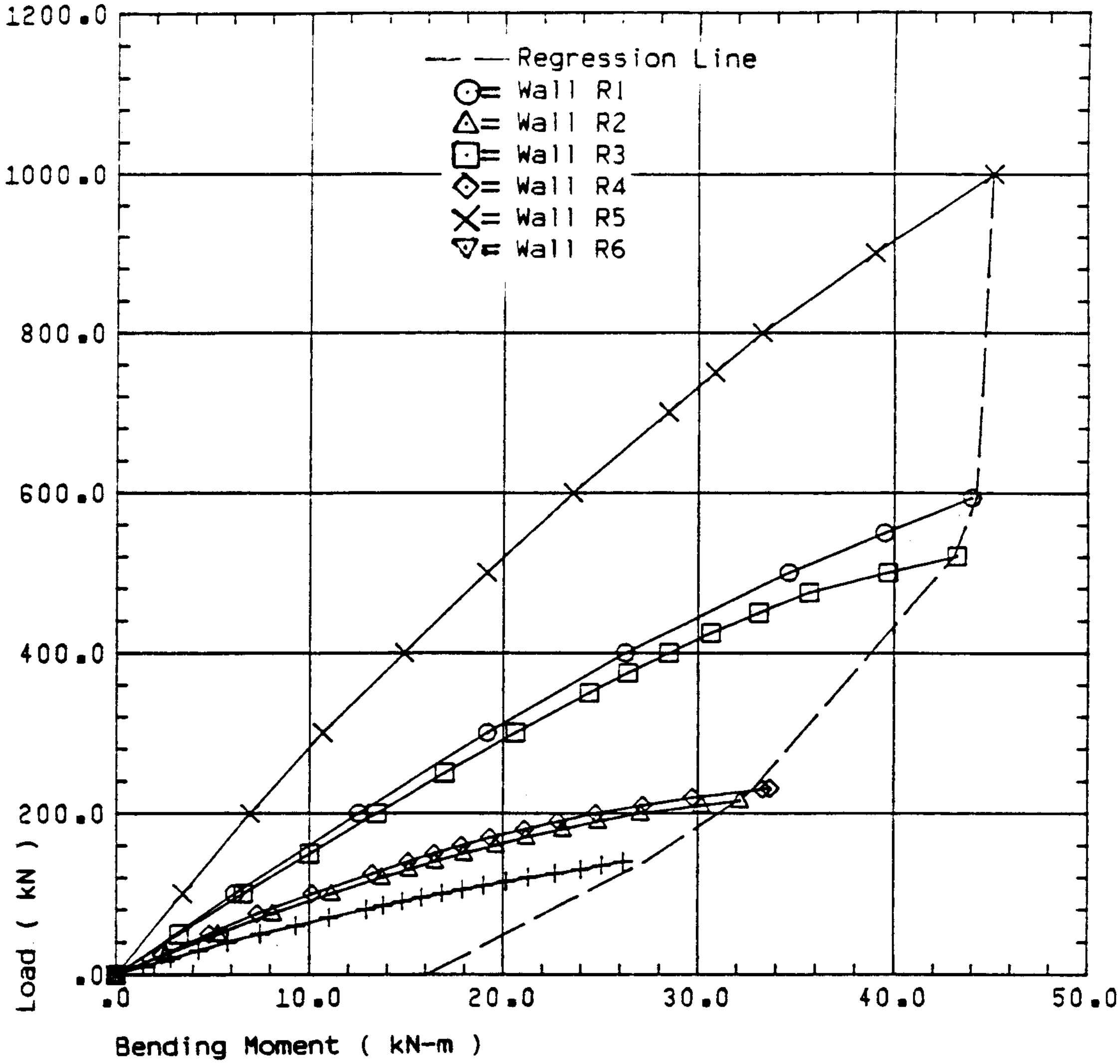

Fig.4.35 Interaction Diagram for Reinforced Walls.

existing bond between blocks and mortar could prevent debonding along bed joints. Therefore, development of high compressive strains in face shells, resulting in crushing failure, was possible. For wall P2, the higher eccentricity of load, equal to 67 mm, was found. Therefore, tensile stresses were higher and debonding occurred followed by instability failure. In such a sensitive region of transition between cracked and uncracked masonry the influence of slenderness may be even more significant.

4.5.2 Reinforced Walls

Wall R5, for which the nominal eccentricity was 1/6 of the wall thickness and the actual eccentricity was 34 mm, failed due to crushing of the high compression side of the wall. At failure significant separation of the grouted columns from the rest of the wall occurred . Similar failure descriptions for that kind of wall were reported by Hatzinikolas et al[44].

All of the remaining walls failed in buckling. Nominal eccentricities ranged from 1/3 to 3/4 of the wall thickness and the actual eccentricities ranged from 61 mm to 142 mm. The failure modes were different than reported by Hatzinikolas et al[44] for similar walls. Since, the calculated kern distance for the reinforced walls was 44 mm, all the walls had one side of the wall in tension. It resulted in the visible cracks along the mortar joints on the tension side of the walls. For the depth of mortar , tensile strength was controlled by the bond strength which was in the range of 0.3 to 0.4 MPa. The tensile strength of the grout was about 2.9 MPa. However, since the area of grout was small, the benefit of tensile stresses in the grout to produce internal resisting moment was small compared to the moment capacity of the reinforced section. It was observed that cracks propagated beyond half of the wall thickness. When significant tensile stresses developed in the reinforcing bars positioned at the middle of wall no further propagation of cracks was observed. Since all bed joints were usually cracked on the tensile side of the wall, it could be assumed that the actual slendernesses for such walls increased from about 18 for the uncracked wall to more than double for the cracked walls. This could explain why walls failed in buckling. In addition, the movable lateral supports, used to limit deflection during testing, held the wall in place after the buckling load was reached. Therefore, no secondary failures occurred to confuse the true failure mode.

4.6 Summary

In this chapter, tests of full scale walls were reported. Fabrication methods, test procedures and results were presented. For each wall, failure mode, load-strain results, load-lateral deflection and load-moment results were shown. Discussion of the results for plain and reinforced walls was included.

CHAPTER 5

FINITE ELEMENT MODEL FOR MASONRY WALLS

5.1 Introduction

This chapter contains the description of the proposed finite element model for masonry walls subjected to axial compressive load with out-of-plane eccentricity. The numerical procedure is described and elements of verification are included.

The realistic modeling of all the components of masonry walls and their interfaces was the major goal in the development of the present model. In addition to a concrete masonry wall being made of concrete blocks, mortar, grout and reinforcement, the bond existing between materials greatly influences the behavior of the structure. A complicating factor is that the constitutive equations for the component materials and for bond relationships are nonlinear[4,14,54,85]. In addition, there are other phenomena such as local cracking and crushing of concrete, debonding, and stability failure which are important for proper modeling of masonry structures.

5.2. Application of the Finite Element Method in the Analysis of Masonry Walls.

The applications of the Finite Element Method in masonry closely followed advances in finite element modeling of reinforced concrete. An extensive summary of the research on finite element applications in reinforced concrete is given in "State-of-the-Art Report on Finite

Element Analysis of Reinforced Concrete"[85].

The first attempts towards modeling of the masonry walls were based on the linear elastic analysis of an isotropic material such as in Smith and Rahman[72], and Stafford Smith and Carter[73]. Application of the developments in modeling of nonlinear behavior of reinforced concrete[56,57] made it possible to advance the analysis of masonry structures in a similar manner. Still, there have been relatively few applications of the finite element method to masonry walls .

Brooks et al[11] investigated the influence of debonding between bricks and mortar on the behavior of a masonry prism. Double nodes along the tensile part of interface between the block and the mortar was used.

Page[62] analyzed brick walls subjected to in-plane loading using rectangular plane stress elements with isotropic elastic properties. The mortar was modeled using the nonlinear joint elements.

An interesting application of the finite element method to masonry was shown by Araya and Hegemier[4,5]. Their analysis incorporated material nonlinearity, cracking, crushing, tension stiffening effects, and modeling of the bond between concrete blocks and mortar. Ideal bond between grout and reinforcement was assumed and, for simplicity, a stacking pattern of blocks was used in place of running bond. They used their model for the analysis of a shear wall and a three-block shear prism.

Anand and Young[3] analyzed a composite wall in out-of-plane bending. They developed a composite element capable of predicting the interlaminar shearing stresses between the brick and the block wythes.

5.3 Nonlinear Analysis of Masonry Walls.

In the this section the theoretical basis of the finite element model are described.

Both material and geometric nonlinearities are considered. The material nonlinearity relates to local cracking, crushing and debonding. However, the materials were actually assumed to be linear, elastic-ideal brittle. Large deformations, local material failures and nonlinear bond stress-slip relationship for steel reinforcement required use of incremental solution procedures.

The geometric nonlinearities due to large displacements were not severe. The maximum lateral deflection measured for eccentrically loaded walls was less than half of the wall thickness. Strains and stresses were referred to the undeformed configuration.

5.3.1 General Derivation of the Stiffness Matrix

The finite element method is a generalized approach for solving the continuum mechanics problems. In structural mechanics, the displacement finite element method is most frequently used [84]. The formulation can be derived from the virtual work principle. For nonlinear problems, this formulation facilitates an incremental solution procedure.

The equilibrium equation for a body based on the virtual work principle is written in the following manner:

$$(C ((w))) = \int_V [B]^T (s) dV + (f) = (0) \tag{5.1}$$

where, (C ((w))) represents the sum of internal and external forces. The variation of Eq.(5.1) with respect to variation of deformation vector d(w) is as following:

$$d(C) = \int_V d[\overline{B}]T (s)dV + \int_V [\overline{B}]T d(s)dV + d(f) \tag{5.2}$$

The component matrices are derived below, where the local displacement vector within the element is described in terms of the nodal displacement degrees of freedom:

$$(u) = [N](w) \tag{5.3}$$

where, (u) = displacement vector;

[N] = shape functions matrix;

(w) = nodal displacement vector.

The strain vector is a function of displacements:

$$(e)=[L](u) \tag{5.4}$$

where, (e) = strain matrix;

[L] = linear differential operator.

Substituting Eq.(5.3) into Eq.(5.4) the following equation can be written as:

$$(e) = [L][N](w) = [B](w) \tag{5.5}$$

where, (e), strains are expressed in terms of the nodal displacements. If the geometric nonlinearities are considered, the incremental strains are related to the incremental displacements in the following manner:

$$d(e) = [\overline{B}] d(w) \tag{5.6}$$

where,

$$[\overline{B}] = [B] + [B_L ((w))] \tag{5.7}$$

Matrix [B] is constant and matrix [B_L ((w))] is a linear function of the displacements.

The stress vector can be written in terms of the strains:

$$(s) = [\overline{D}](e) \tag{5.8}$$

where, $[\overline{D}]$ is the elastic constitutive matrix, incorporating the effects of local element failures such as cracking or crushing, as will be formulated later.

The variational form of Eq.(5.8) is written as following:

$$d(s) = [\overline{D}] \, d(e) \tag{5.9}$$

Substitution of Eq.(5.6) into Eq.(5.9) yields:

$$d(s) = [\overline{D}][\overline{B}] \, d(w) \tag{5.10}$$

From Eq.(5.7):

$$d[\overline{B}] = d[B] + d[B_L((w))] = d[B_L] \tag{5.11}$$

Substitution of Eqs (5.10) and (5.11) into Eq.(5.2) yields:

$$d(C) = \int_V d[B_L]^T(s)dV + \int_V [\overline{B}]^T[\overline{D}][\overline{B}] \, d(w)dV \tag{5.12}$$

which can also be written as:

$$d(C) = \int_V d[B_L]^T(s)dV + [\overline{K}]d(w) \tag{5.13}$$

The stiffness matrix $[\overline{K}]$ consists of two components:

$$[\overline{K}] = \int_V [\overline{B}]^T[\overline{D}][\overline{B}]dV = [K_0] + [K_L] \tag{5.14}$$

where, the small displacement matrix is given by:

$$[K_0] = \int_V [B]^T [\overline{D}][B]dV \tag{5.15}$$

and the large displacement stiffness matrix is given by:

$$[KL] = \int ([B]^T [\overline{D}][BL] + [BL]^T [\overline{D}][BL] + [B_L][\overline{D}][B])dV \tag{5.16}$$

The first term of Eq.(5.13) can be written as:

$$\int_V d[B_L]^T(s)dV = [K_s]\,d(w) \qquad (5.17)$$

where, $[K_s]$ is called the initial stress stiffness matrix. Therefore, the equilibrum equation for a single element can be written in the following form:

$$d(C) = ([K_s] + [K_0] + [K_L])d(w) = [K_T]d(w) \qquad (5.18)$$

The closed form total tangential stiffness matrix $[K_T]$, for the constant stress, triangular element used in the current finite element model, was derived by Mirza[53].

5.3.2 Modeling of Concrete

The concrete blocks, the mortar and the grout were modeled using the constant stress triangular elements with material properties and thicknesses varying according to the type of material. Therefore, as is shown in Fig.5.1, separate elements were used to model masonry block face shells, mortar bed joints, webs and grout, grout or air voids and the steel loading plates. The material properties and geometry were assumed based on the actual properties of concrete masonry specimens. Linear elastic-brittle stress-strain relationships were used for all materials.

The local material failure criterion, common for all materials, is described in detail in Section 5.4.2. The smeared cracking approach, developed by Rashid and reported in "State-of-Art Report on Finite Analysis of Reinforced Concrete"[85], was used to model the cracked concrete. It was assumed that an element was cracked, when the value of principal stersses exceeded the effective stresses predicted by the

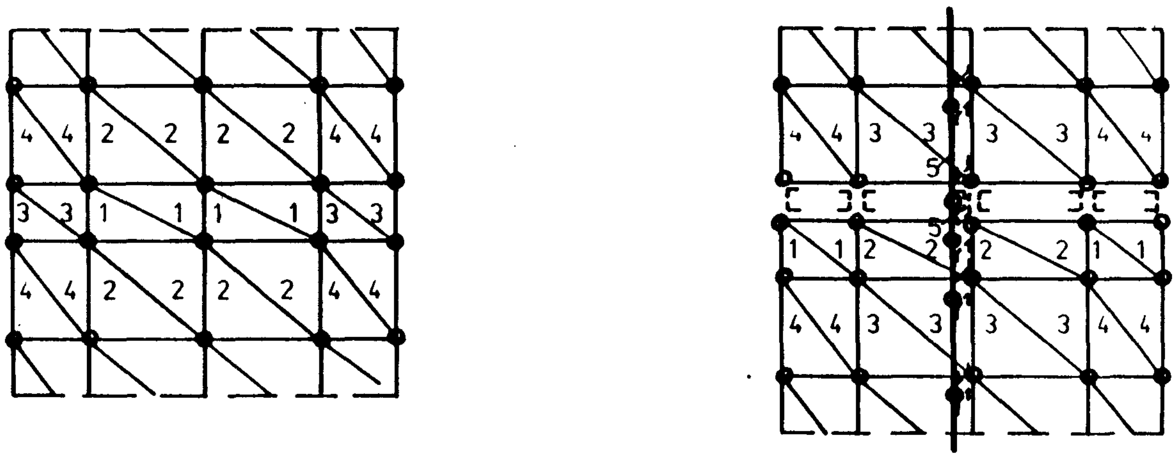

1 - air void
2 - block webs
3 - mortar
4 - block face shells

a) Plain Concrete Block Wall

bond element

1 - mortar
2 - grout
3 - block webs + grout
4 - block face shells
5 - steel reinforcing bar

b) Reinforced Concrete Block Wall

Fig.5.1 Division of Wall Cross Section into Elements According to Geometric and Material Properties.

failure criterion. The direction of cracking was taken as normal to the direction of the higher principal tensile stress. It was assumed that the cracked element had no stiffness in the direction normal to the direction of the crack and the total stress in that direction was reduced to zero. Therefore, the constitutive equation for the j-th element using the incremental formulation can be written in the form of Eq.(5.9):

$$(\Delta s)_j = [\bar{D}]_j (\Delta e)_j$$

where, the elastic constitutive matrix is given by either of the following three cases:

a) for plane stress analysis and uncracked elements:

$$[\bar{D}]j = \frac{E}{1-n2} \begin{bmatrix} 1 & n & 0 \\ n & 1 & 0 \\ 0 & 0 & (1-n)/2 \end{bmatrix} \qquad (5.19)$$

b) for plane strain analysis and uncracked elements:

$$[\bar{D}]j = \frac{E(1-n)}{(1+n)(1-2n)} \begin{bmatrix} 1 & n/(1-n) & 0 \\ n/(1-n) & 1 & 0 \\ 0 & 0 & (1-2n)/(2-2n) \end{bmatrix} \qquad (5.20)$$

$e_{zz} = 0, \; s_{zz} = n\,(s_{xx} + s_{yy})$

c) for cracked elements:

$$[\bar{D}]j = E \begin{bmatrix} 0 & 0 & 0 \\ 0 & 1 & 0 \\ 0 & 0 & 0 \end{bmatrix} \qquad (5.21)$$

An element was assumed to be cracked in a second direction when the tensile stress in the direction parallel to the first crack was higher than the uniaxial tensile strength of the material. In such a case, the stiffness of the element was reduced to nearly zero by dividing the initial stiffness of the element by a large number:

$$[\bar{D}]_j = [\bar{D}]_j \text{ initial} / 1000000 \qquad (5.22)$$

Thus the total stresses in the element were reduced to zero. A similar procedure was used in the case when an element failed in crushing. The stiffness and total stresses for a crushed element were reduced to nearly zero.

The derivation of the stiffness matrix for a concrete element was based on the formulation cited in Section 5.3.1.

5.3.3 Modeling of the Bond Between Mortar and Block

The tensile strength of plain masonry in the direction normal to the bed joint is controlled by the tensile bond strength between the masonry units and the mortar. Therefore, the assumption of ideal bond would increase the tensile strength of plain masonry to the level of the tensile strength of the weaker of two materials ; block or mortar. This would overestimate by 6 to 8 times the experimental bond strength discussed in Section 3.4. In the case of grouted masonry, the tensile strength is influenced by the tensile strength of the grout, but still the bond strength controls the occurrence of the first cracks in out-of-plane bending. There are experimental data concerning tensile bond strength[28]. However, no information is available to estimate the bond stress-relative displacement relationship required in finite element modeling of bond phenomena.

The joint elements developed by Goodman et al[39] were used to model the bond between blocks and mortar. Each 4 node joint element has a finite length and width equal to zero as is shown in Fig.5.2. Without any load applied, bond is represented by the two layers of nodes with the same initial positions. During deformation, separation of nodes

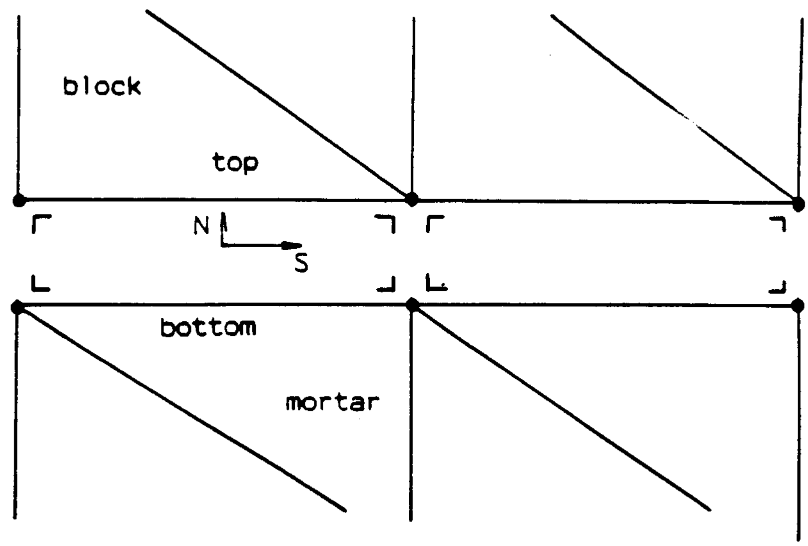

Fig.5.2 Mortar Bond Element.

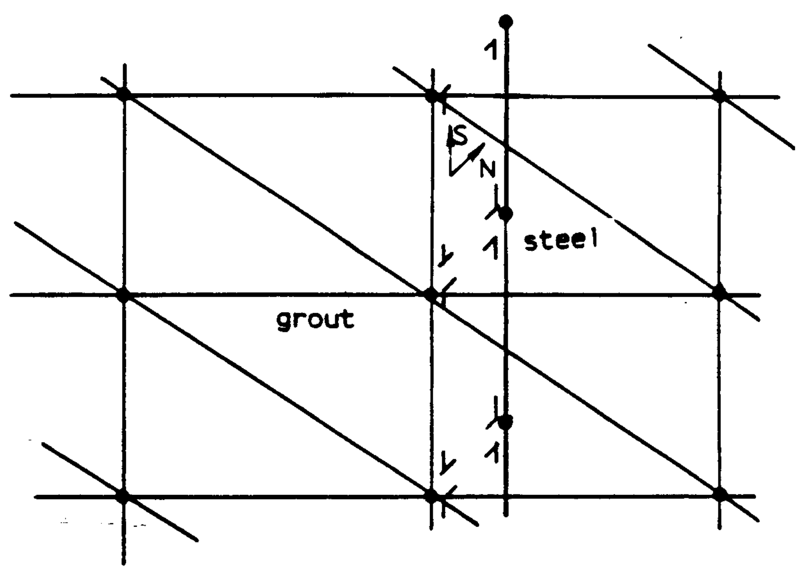

Fig.5.3 Steel Bond Element.

the same initial positions. During deformation, separation of nodes occurs. The resulting forces, representing bond between two materials, are the functions of relative displacements of the nodes:

$$\begin{pmatrix} P_N \\ P_S \end{pmatrix}_j = \begin{bmatrix} k_N & 0 \\ 0 & k_S \end{bmatrix} \begin{pmatrix} w_N^{top} - w_N^{bottom} \\ w_S^{top} - w_S^{bottom} \end{pmatrix}_j$$

or

$$(P)_j^{BM} = [K (s)]_j^{BM} (w_e)_j^{BM} \tag{5.24}$$

where:

P_N, P_S = the normal and tangential force in the center of the element;

k_N, k_S = the stiffness of the element in normal and tangential direction, accordingly;

w_N^{top}, w_N^{bottom} = the normal average displacement of the top and bottom nodes;

w_S^{top}, w_S^{bottom} = the tangential average displacement of the top and bottom nodes;

$(P)_j^{BM}$ = the local internal load for j-th mortar bond element;

$(w_e)_j^{BM}$ = the local, nodal displacement vector;

$[K(s)]_j^{BM}$ = the local stiffness matrix for j-th element;

since,

$$P_N = k_N (w_N^{top} - w_N^{bottom}) = k_N \Delta w_N \tag{5.25}$$

the normal stress in a joint element is:

$$s_N = P_N / A_j = k_N \Delta w_N / A_j \tag{5.26}$$

where, A_j = area of the j-th joint element.

If s_N f_{bond} (tensile bond strength), then the stiffness of the element is reduced to zero. The derivation of the matrix is similar to that published by Goodman et al [39] and therefore it is not reproduced here.

5.3.4 Modeling of Steel Reinforcement

Vertical steel bars grouted in the cores of the blocks are used to reinforce concrete masonry walls. This vertical reinforcement is modeled by bar elements with 2 nodes and 4 degrees of freedom. Only the longitudinal stiffness of a reinforcing bar is considered in the derivation of the stiffness matrix. The effect of curvature between nodes on the change in length of element was neglected. The local stiffness matrix for the bar element is as following:

$$[K]_j^{ST} = \frac{E_{steel}\,A}{l}\begin{bmatrix} 1 & 0 & -1 & 0 \\ 0 & 0 & 0 & 0 \\ -1 & 0 & 1 & 0 \\ 0 & 0 & 0 & 0 \end{bmatrix} \qquad (5.27)$$

where, E_{steel} = modulus of elasticity for steel

A = cross sectional area of the vertical reinforcement

l = length of the bar element

5.3.5 Modeling of the Bond Between Reinforcing Bars and Grout

Goodman Joint Elements [39] are used to model bond between vertical reinforcing bars and grout. The modification proposed by Walker [78] permitted the use of a nonlinear bond stress-slip relationship in the standard joint element .

Similar to the joint elements between blocks and mortar, the joint element is a 4 node element. The 2 nodes in the first layer are common with the steel bar element and the 2 remaining in the second layer are common with the grout constant stress triangular elements as is shown in Fig.5.3. Initially connected nodes separate when load is applied and slip due to imperfect bond occurs. In the numerical model this phenomenon is represented by longitudinal separation of the two layers of nodes. The relative displacement causes the forces between the elements. These forces were found to be nonlinear functions of slip. The relationship can be expressed as local bond stress in terms of slip. An example of such a relationship was reported by Mirza and Houde[54]. The relationship used in the current model was obtained from the bond tests reported in Section 3.5.2. The bond stress-slip relationship obtained is as follows:

$$u_{bs} = 205\,d - 1209.5\,d^2 + 3728\,d^3 - 18510\,d^5 \tag{5.28}$$

where, u_{bs} = local bond stress in MPa;
d = local slip in mm.

The stiffness matrix and the load vector can be derived in the following manner. The relative displacement of the two layers of nodes can be expressed as a function of the tangential displacements of nodes:

$$\begin{pmatrix} \Delta w_S \\ \\ \Delta w_N \end{pmatrix} = \begin{pmatrix} (\ N\ ) \\ \\ (\ 0\ ) \end{pmatrix} (\ w_e\ )_j^{BS} \tag{5.29}$$

Therefore,

$$\Delta w_S = (\ N\ )\ (\ w_e\ )_j^{BS} \tag{5.30}$$

where, (N) = shape function vector,

$$(\ N\ ) = (\ -(1-a)/2,\ 0,\ -(1-a)/2,\ 0,\ (1+a)/2,\ 0,\ (1+a)/2,\ 0),\quad a \in (0,1);$$

(0) = zero vector;

Δw_S = relative displacement of two layers in the longitudinal; direction;

$(w_e)_j^{BS}$ = local, nodal displacement vector for j-th steel bond element.

Since the dowel action of the bars is neglected it is possible to drop the part concerning the normal direction. The elastic stiffness matrix for an element can be derived from the potential energy theorem. Using the notation from Goodman et al[39], the stored potential energy can be written as:

$$D = 0.5 \int_{-L/2}^{L/2} w_i P_i \, dx \tag{5.32}$$

where,

$$P_S = k_S \Delta w_S \tag{5.33}$$

$$k_S = \frac{\partial u_{bs}}{\partial d} \pi D N \tag{5.34}$$

u_{bs} is from Eq.(5.28);

D = diameter of the reinforcing bar in mm ;

N = number of bars in the cross section.

Substituting Eq.(5.32) in Eq.(5.33), the following equation is obtained:

$$D = 0.5 \int_{-L/2}^{L/2} \Delta w_S^T k_S \Delta w_S \, dx \tag{5.35}$$

substituting Eq.(5.30) in Eq.(5.35) the following expression for potential energy can be written:

$$D = 0.5 \int_{-L/2}^{L/2} (w_e)^T (N)^T k_S (N)(w_e) \, dx \tag{5.36}$$

Since $x = (a L) / 2$ (5.37)

where, a is the nondimensional coordinate,

thus, $dx = L/2 \, da$ (5.38)

Substituting Eq.(5.38) into Eq.(5.36):

$$D = 0.5 \int_{-1}^{+1} L/2 \, (w_e)^T (N)^T k_S (N)(w_e) \, da \tag{5.39}$$

Therefore, the final form of the expression for the stored potential energy can be written as follows:

$$D = 0.5 \, (w_e)^T [K]^{BS} (w_e) \tag{5.40}$$

$$\text{where, } [K]^{BS} = L/2 \int_{-1}^{+1} (N)^T k_S (N) \, da \tag{5.41}$$

The element local load vector can be derived in the following manner:

$$(P)^{BS} = [K]^{BS} (w_e)^{BS} \tag{5.42}$$

Substituting Eq.(5.41), Eq.(5.42) it can be written as:

$$(P)^{BS} = L/2 \int_{-1}^{+1} (N)^T k_S (N) \, da \, (w_e) \tag{5.43}$$

The slip, d, can be written as:

$$d = \Delta w_S = (N)(w_e) \tag{5.44}$$

The bond force per unit length is expressed in the following form:

$$T_S = u_{bs} \pi D N \tag{5.45}$$

where, u_{bs}, N, D were defined in Eq.(5.34).

Substituting Eq.(5.45) in Eq.(5.34) ,the stiffness per unit length can be written as:

$$k_S = \partial T_S / \partial d \tag{5.46}$$

Using the relationship from Eq.(5.44), it can be expressed in the following manner:

$$k_S = \partial T_S / \partial (\Delta w_S) \tag{5.47}$$

Also from Eq.(5.44):

$$\partial / \partial (\Delta w_S) = \partial (w_e) / \partial (\Delta w_S) \quad x \quad \partial / \partial (w_e) \tag{5.48}$$

and from Eq.(5.30): $\partial / \partial (\Delta w_S) = (N)^{-1} \partial / \partial (w_e)$
(5.49)

Since, $\int d (w_e) = (w_e)$, (5.50)

substituting Eq.(5.47) in Eq.(5.43) the load vector can be written as:

$$(P)^{BS} = L/2 \int_{-1}^{+1} (N)^T \partial T_S / \partial (\Delta w_S) (N) \partial a (w_e) \tag{5.51}$$

Substituting Eqs.(5.49) and (5.50) in Eq.(5.51), this expression can be written as:

$$(P)^{BS} = L/2 \int_{-1}^{+1} (N)^T T_S (N)^{-1} (N) \partial / \partial (w_e) d(w_e) \partial a \tag{5.52}$$

and final form of the load vector can be written in the following manner:

$$(P)^{BS} = L/2 \int_{-1}^{+1} (N)^T T_S \partial a \tag{5.53}$$

5.4 Numerical Procedure

The approach proposed by Walker[78] was used in the solution procedure. Only the highlights of the method and the modifications introduced are described below. The Newton-Raphson method was used in the incremental solution of nonlinear problem. The incremental procedure was modified by scaling down the load increment if the failure criterion had been exceeded. The geometric nonlinearity and the nonlinear bond stress-slip relationship were included. The major modification resulted from consideration of the different material properties of the components of a concrete masonry wall. Also included was the introduction of a multiaxial failure criterion for concrete and the incorporation of the bond elements between the blocks and the mortar.

5.4.1 General Description of the Numerical Procedure

Letting "n" represent the load increment number and "m" the iteration number, then the iterative procedure was applied as shown in Fig.5.4 and described below:

1. At a particular load level $(f_{n-1})=(f_n^0)$, the displacement vector $(w_{n-1})=(w_n^0)$, the strain vector $(e_{n-1})=(e_n^0)$, the stress vector $(s_{n-1})=(s_n^0)$ and the tangential stiffness matrix $[K_T (w_n^0 , s_n^0)]$ are known. This state can be represented as a point D in Fig.5.4.
2. A load increment (Δf_n^m) is then applied (m=1).
3. After the program has converged for the (n-1) load increment, the

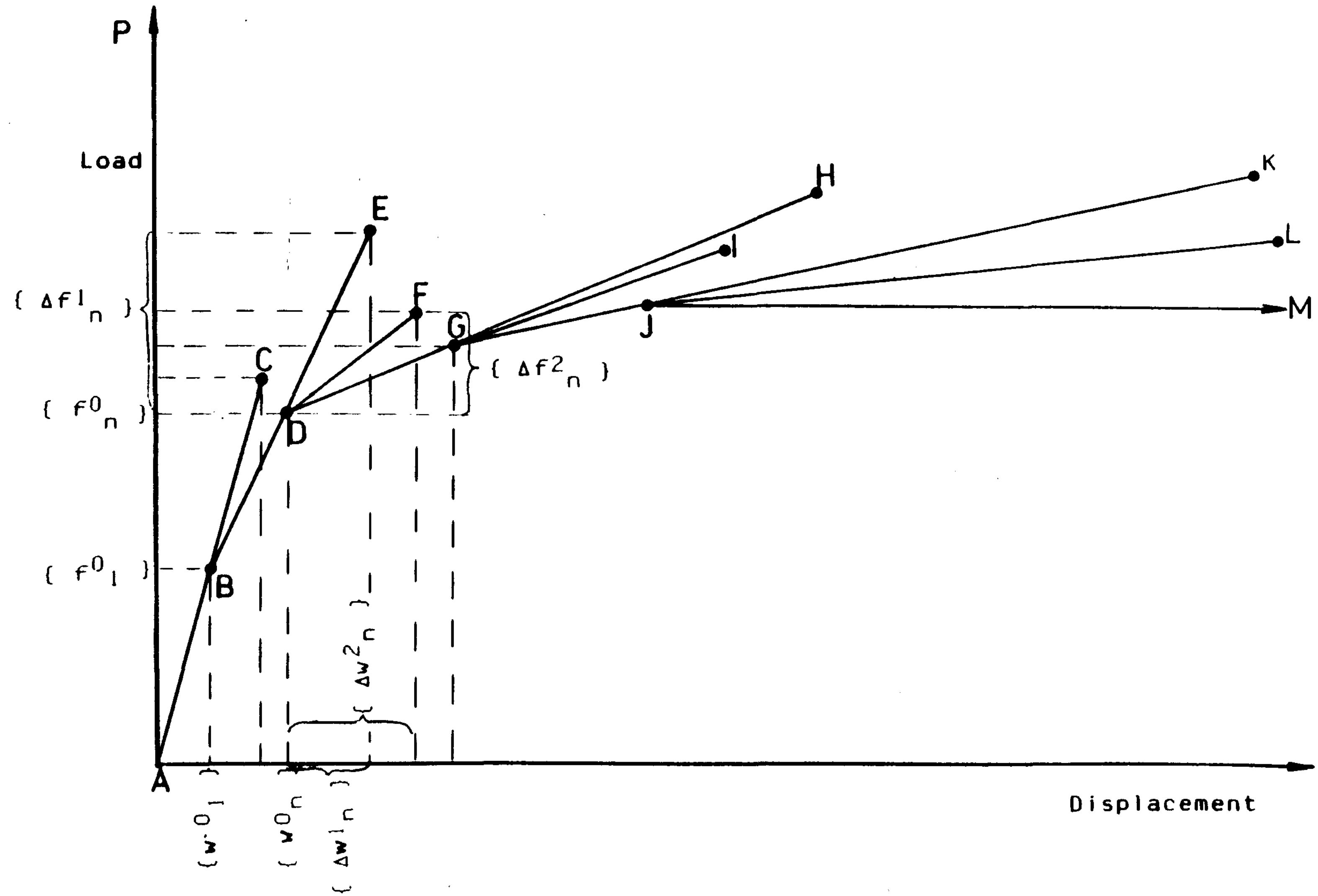

Fig.5.4 Incremental Solution Technique.

net residual load is (C_{n-1}). The displacement increment due to the first iteration of the n-th load increment can be calculated from:

$$[K^T(w_n^0, s_n^0)](\Delta w_n^m) = -(C_{n-1}) + (\Delta f_n^m) \tag{5.54}$$

where, (Δw_n^m) is the incremental displacement vector calculated in the m^{th} iteration.

4. The total displacement vector can then be updated:

$$(w_n^m) = (w_n^{m-1}) + (\Delta w_n^m) \tag{5.55}$$

where (w_n^m) is calculated in Eq.(5.54) or Eq.(5.69) if m 1. It can be represented by point E in Fig.5.4.

5. Then for each j-th triangular element:

a) The element nodal displacement vector $(w_{ne}^m)_j$ may be extracted from the global displacement vector (w_n^m).

b) The element nodal incremental displacement vector $(\Delta w_{ne}^m)_j$ may be extracted from (Δw_n^m).

c) Then the total strain matrix $[\overline{B}(w_{ne})_j]$ can be calculated.

d) The incremental strain vector can be calculated as:

$$(e_n^m)_j = [\overline{B}(w_{ne})_j](\Delta w_{ne})_j \tag{5.56}$$

e) So that the updated strains are:

$$(e_n^m)_j = (e_n^{m-1})_j + (\Delta e_n^m)_j \tag{5.57}$$

f) The incremental stress vector is:

$$(\Delta s_n^m)_j = [D]_j (\Delta e_m^n)_j \tag{5.58}$$

where, the elastic constitutive matrix $[\overline{D}]_j$ is defined in Section 5.3.2;

g) Then the updated stress would be :

$$(s_n^m)_j = (s_n^{m-1})_j + (\Delta s_n^m)_j \quad \text{and} \tag{5.59}$$

h) the internal element load vector can be calculated as:

$$(P_n^m) = \int_V [\overline{B}\ ((w_{ne}))]_j\ (s_n^m)_j\ dV \tag{5.60}$$

i) The updated, local stiffness matrix $[K(w_n^m, s_n^0)]_j$ can be calculated.

6. For each j-th mortar bond element the following steps are used:

a) The element nodal displacement vector, $(w_{ne}^m)_j^{BM}$, can be extracted from the total displacement vector (w_n^m);

b) From Section 5.3.3, the stresses, $(s_n^m)_{j0}^{BM}$, are calculated

c) The local element stiffness matrix, $[K(s_n)]_j^{BM}$ can be calculated.

d) The local internal load vector can be calculated from:

$$(P_n^m)_j^{BM} = [K(s_n^0)]_j^{BM} (w_{ne})_j^{BM} \tag{5.61}$$

7. For each j-th steel element the following steps are followed:

a) The incremental displacement vector $(\Delta w_{ne})_j^{ST}$ is extracted from the global incremental displacement vector (Δw_n);

b) Then the incremental strain and total strain are calculated:

$$\Delta e_{nj}^{mST} = \Delta l_{nj}^m / l_j \tag{5.62}$$

$$e_{nj}^{mST} = e_{nj}^{(m-1)ST} + e_{nj}^{mST} \tag{5.63}$$

where, Δl^{m}_{nj} = change in length of the j-th steel element after m-th iteration of the n-th load increment;

l_{j} = initial length of the j-th element;

c) This allows the incremental stress and total stress to be calculated:

$$\Delta s^{mST}_{nj} = E_{steel} \Delta e^{mST}_{nj} \tag{5.64}$$

$$s^{mST}_{nj} = s^{(m-1)ST}_{nj} + \Delta s^{mST}_{nj} \tag{5.65}$$

d) Hence the internal load vector may be calculated:

$$(P^{m}_{n})^{ST}_{j} = A (-s^{mST}_{nj} , s^{mST}_{nj})^{T} \tag{5.66}$$

8. For each j-th steel bond element (discussed in Section 5.3.5) the following sequence is followed:

a) The element local displacement vector $(w_{ne})^{BS}_{j}$ is extracted from the global displacement vector (w^{m}_{n});

b) Then the updated local stiffness matrix is $[K(w^{m}_{n})]^{BS}_{j}$; and

c) the local internal load vector $(P^{m}_{n})_{j}$ can be calculated.

9. The global tangential stiffness matrix $[K_{T} (w^{m}_{n} , s^{0}_{n})]$ is assembled.

10. The global internal load vector (P^{m}_{n}) is assembled.

11. Then the global residual load vector can be calculated:

$$(C^{m}_{n}) = (P^{m}_{n}) - (f^{1}_{n}) \tag{5.67}$$

where,

$$(f^{1}_{n}) = (f^{0}_{n}) + (\Delta f^{1}_{n}) \tag{5.68}$$

12. To obtain the incremental displacement vector, (Δw^{m+1}_{n}) the

following equation has to be solved:

$$[\, K_T (w_n^m , s_n^0)](\, \Delta w_n^{m+1}) = - (\, C_n^m) \tag{5.69}$$

13. Steps 4 to 13 have to be repeated, with m=m+1, until the incremental solution has converged, where the following convergence criterion is used:

$$q = \frac{\mathrm{Det}\,[\, K_T (w_n^m , s_n^0)] - \mathrm{Det}\,[\, K_T (w_n^{m-1} , s_n^0)]}{\mathrm{Det}\,[\, K_T (w_n^{m-1} , s_n^0)]}\ 100\% \tag{5.70}$$

If q is less than the prescribed value (usually 1%), then the next steps can be followed.

14. For each triangular element the stresses are checked to see if they satisfy the failure criterion described in Section 5.4.2.2.

a) If the condition is not satisfied ,then it means that there is an element which can fail. The load increment is decreased, as was described in Section 5.4.3.2:

$$(\, \Delta f_n^{m+1}) = t_1 \; (\, \Delta f_n^m) \tag{5.71}$$

The stiffnesses and the total stresses of this element are changed, according to the type of failure. Then the decreased load increment is applied in Step 2 and the modified global tangential stiffness matrix $[K_T (w_n^0 , s_n^m)]$ is used in Step 3. As the result of the next operations the point G and later the point H in Fig.5.4 can be reached.

For the element which failed, the elasticity matrix $[\overline{D}]_j$ in Step

5f is modified according to the type of failure as is described in Eqs (5.21) and (5.22). Similarly the total stresses calculated in Step 5 are modified in the manner discussed in Section 5.3.2.

b) If the condition is satisfied, which means that none of the triangular elements failed, the analysis proceeds to Step 15.

15. It is necessary to check if the tensile stresses satisfy the failure criterion described in Section 5.4.2.3 for each mortar bond element.

a) If the criterion is not satisfied then there is a bond element which has failed due to debonding. In this case it is necessary to decrease the load increment and change the stiffness of the joint element ,as discussed in Section 5.4.3.3. Then the procedure is repeated starting from Step 2.

b) If the criterion is satisfied , then none of the mortar joint elements failed and the analysis proceeds to Step 16.

16. At this point, for each steel bond element, the relative displacements are checked to see if they satisfy the failure criterion described in Section 5.4.2.4.

a) If there is a steel bond element for which the relative displacements are higher than a limiting value, then the stiffness of the element is modified.

b) If the slip in each element is lower than the maximum allowed slip, then the analysis proceeds to Step 17.

17. The next load increment ($\Delta f_{n+1}^{m=1}$) is applied and Steps 1 to 17 are repeated.

The failure load was assumed to be the maximum load reached in the incremental procedure. This means that it was the first load for which convergence of the analysis was not obtained due to the singularity of the global stiffness matrix. Extensive cracking or crushing causing change in stiffness of a wall proceeded the material mode of failure. The cases where large deformations caused the change in stiffness of a wall were identified as the instability mode of failure.

In some cases, it was found that a very large number of interations was required to reach the failure load. Therefore, limits on the number of iterations per load increment and on the maximum number of iterations for each case depending on size of analyzed wall and expected failure mode. Despite the fact that these limits were chosen arbitrarily, they were always large enough to secure reaching failure for analyzed case before running out of the limit of iterations. The usual limit of 10 iterations per load increment was believed to be enough to distribute the energy dissipated due to failure of one element without significant penalty. The total number of iterations per problem was 100 to 250, depending on the size of wall (The higher number was for analysis of 24 block high walls).

5.4.2 Local Failure Criteria

5.4.2.1 General

Separate failure criteria were applied to the local failures in the triangular elements which modeled the concrete part of a masonry wall and in the bond elements which modeled the bond between a block and a mortar and between the steel reinforcement and the grout. Yielding in the steel reinforcement was not considered since it was not expected that this level of stress could occur for the amount of steel used in the full scale walls described in Chapter 4. The stresses in steel never reached the yield stress in analyzed cases. Besides, in the CSA Standard S304-M84(31), it is required that at working loads the tensile stresses in reinforcement do not exceed 40% of the yield strength of the steel and are not greater than 165 MPa.

5.4.2.2 Failure Criterion for Concrete

The four parameter failure criterion, developed by Hsieh, Ting and Chen and reported by Chen[14], was used to check the stresses in an element for the possibility of cracking or crushing. The equation of the failure envelope is :

$$f(I_1, J_2, s_{max}) = 2.0108\, J_2 / f_c^2 + 0.9714 \sqrt{J_2/f_c} + 9.1412\, s_{max}/f_c$$

$$+ 0.2312\, I_1/f_c - 1.0 = 0 \qquad (5.72)$$

where, f_c = compressive strength of the material;

s_{max} = maximum (algebraically) principal stress;

s_1, s_2, s_3 = principal stresses

$$I_1 = s_1 + s_2 + s_3$$

$$J_2 = [(s_1 - s_2)^2 + (s_2 - s_3)^2 + (s_3 - s_1)^2]/6$$

As it was reported by Chen[14], the parameters of the failure envelope were determined to represent the following failure states exactly:

1. Uniaxial compressive strength equal to f_c

2. Uniaxial tensile strength equal to $f_t = 0.1\ f_c$
3. The stress state $(s_{OCT}/f_c, t_{OCT}/f_c) = (-1.95, 1.6)$ on the compressive meridian $(R = 60^\circ)$, which is the best fit for the test results by Mill and Zimmerman, as reported by Chen[14], where $s_{OCT} = I_1/3$ and $t_{OCT} = \sqrt{2J_2/3}$.
4. For equal biaxial stress a compressive strength of $f_{bc} = 1.15\ f_c$.

The comparison of the failure criterion with the results of the biaxial tests undertaken by Kupfer et al[49] indicated very good agreement.

It was assumed that an element failed if a point in 2 or 3 dimensional stress space was located outside the failure envelope. The stresses in the plane of the cross-section of the wall were taken into consideration to determine the type of failure. If both stresses were tensile, the element would crack in the direction perpendicular to the direction of the higher stress. If both stresses were compressive, the element was assumed to have crushed. Kupfer et al[49] stated that:

" Specimens subjected to combined tension and compression behaved similarly to the specimens loaded in biaxial compression as long as applied tensile stress was less than one fifteenth of the compressive stress.". Thus the limit of the ratio of stresses equal to -0.0667 was chosen to separate the two modes of material failure.

Since in the numerical procedure only one element can fail at a time, it was important to identify that element. It was assumed that this element would have the maximum positive value of the function describing the failure envelope $[\ f(I_1, J_2, s_{max})] = 0$.

5.4.2.3 Failure Criterion for Bond Between Block and Mortar

The uniaxial maximum tensile stress criterion was used to check stress in each mortar bond element for the possibility of debonding in the direction perpendicular to the mortar bed joint. The bond wrench test described in Section 3.4 was used to define the tensile bond strength for the particular blocks and mortar used in the experimental part of this study.

5.4.2.4 Failure Criterion for Bond Between Steel Bars and Grout

A slip criterion was used to check the relative longitudinal displacements in each steel bond element. It was assumed that the maximum allowable slip before debonding was equal to the average slip of the unloaded end of the bar in the pull-out test described in Section 3.5. Since the ends of bars embedded in the test walls were welded to steel end plates, complete debonding was impossible. Therefore, complete bond was introduced at the end of the steel bar by assuming a very high stiffness of the bond elements in that region.

5.4.3 Load Increment Reduction Coefficient

5.4.3.1 General

It was assumed that only one element could fail during each load increment. Therefore, it was necessary to establish a procedure to calculate the load increment at which only a single element would fail.

The load increment reduction coefficient is a scaling factor used to calculate that decreased increment. Only the failure in a triangular element or in a mortar bond element required calculation of the coefficient. The procedure was different for each type of elements, since different failure criteria were used.

5.4.3.2 Reduction Coefficient for Triangular Elements

In each constant stress triangular element, the state of stress was represented by three principal stresses. For a particular load level, (f^0_n), the stresses in the i-th element were s^0_{nki}, k=1,2,3. Applying a load increment (Δf^1_n), incremental displacements ,strains and stresses are obtained. The total stresses at the i-th element are: $s^1_{nki} = s^0_{nki} + \Delta s^1_{nki}$.

Calculation the value of the function describing the failure envelope for each element using Eq.(5.72), allowed the element for which that function reached the highest positive value to be identified. It was assumed that this element would fail first. Then the load increment was scaled down to the level where the stresses in the identified element were on the boundary of the failure envelope. Since it was assumed that stresses in the elements were proportional to the load, it was possible to use a parametric equation of the straight line in space to describe this relation:

$$s^*_{nki} = s0_{nki} + t\,\Delta s1_{nki} \qquad k=1,2,3$$

s^*_{nki} = principal stress in i=th element; t∊(0,1).

Therefore, the failure function $f(I_1, J_2, s_{max})$ from Eq.(5.72) can be transformed in the following way:

$$f(I_1, J_2, s_{max}) = g(\ s_1(t), s_1(t), s_3(t)) = g(\ t\ )$$

Then the equation $g(t)=0$ was solved using the method of halving of the interval. The solution for the equation was $t=t_1$, where $0 \leqslant t_1 \leqslant 1$.

Therefore, the reduced load increment was : $(\ f_2^n\ ) = t_1\ (\ f_1^n\ )$

This procedure was applied each time an element failed.

5.4.3.3 Reduction Coefficient for Mortar Bond Elements

A reduction coefficient had to be calculated when a bond element failed. A similar procedure as for triangular elements was used to identify an element which was going to fail, but, instead of using principal stresses, the normal stress in each mortar joint element was checked . The element for which the tensile stress was the highest and was higher than the bond tensile strength was assumed to fail first .

The reduction coefficient was then calculated in the following manner: The nodal displacement vector for that element was extracted from the global displacement vector and the nodal incremental displacement vector was extracted from the global incremental displacement vector. The relative displacements in the normal direction were calculated :

w_N^0 from $(\ w_{ne}^{BM}\ )$

w_N^1 from $(\ w_{ne}^{BM} + \Delta w_{ne}\ )$

Then the reduction coefficient was calculated using the following expression:

$$t_1 = (s^1_{Nj} - f_{bond})/(s^1_{Nj} - s^0_{Nj})$$

where, f_{bond} is the tensile bond strength of masonry in the direction perpendicular to the bed joint.

Using the relative displacements, it could be calculated as:

$$t_1 = (w^1_N - w_{cr}) / (w^1_N - w^0_N), \text{ since } w_N = s_{Ni} A_i / k_N$$

where, $w_{cr} = f_{bond} \times A / k_N$.

Therefore the modified load increment can be calculated as :

$$(\Delta f^n_2) = t_1 (\Delta f^n_1)$$

5.5 Verification of the Numerical Model

5.5.1 Small Deformation Analysis

The small deformation part of the model was checked for the theoretical case with the assumed constant isotropic properties in axial compression and in bending. For a symmetric grid of elements, loading and boundary conditions, a symmetric solution was obtained. The solution obtained for axial compression was equal to the exact solution. In bending, the numerical solution gave lower deflections than the classical exact solution. The accuracy of the solution improved with the refinement of the finite element grid. The use of elements with rotational degrees of freedom would improve the accuracy of the solution, but it would increase significantly the size of the problem.

5.5.2 Large Deformations Analysis

The large deformation part of the model was checked for the theoretical case where constant isotropic material properties were assumed. The solution obtained for the pure bending case was fairly close to the classical solution published by Wang et al[80]. Both results are compared in Fig.5.5. As was the case for the small deformation analysis, the refinement of the mesh improved the accuracy of the numerical solution in the large deformation analysis. Similarly the use of higher order elements, with rotational degrees of freedom, would improve the accuracy of the solution.

5.5.3 Sensitivity Analysis

Due to the substantial cost of running full scale problems and due to the large number of variables, it was decided to perform a sensitivity analysis for 2 block prisms. The following variables were investigated: grid size, number of load increments, type of analysis, material properties and geometry. The results are summarized in Table 5.1. where the identified standard set of data chosen for the analysis of prisms is the same as used for the analysis of the full scale walls. The results of the analysis of prisms are compared to the experimental results and to the numerical results for the standard set of data. Three different grids were compared. The cracking patterns obtained are shown in Fig.5.6. In all cases, failure modes were similar and failure loads were close. The numerical stress-strain relationships are compared to the experimental results in Fig.5.7. All numerical results were close to each other and modeled the initial part of the experimental curve well.

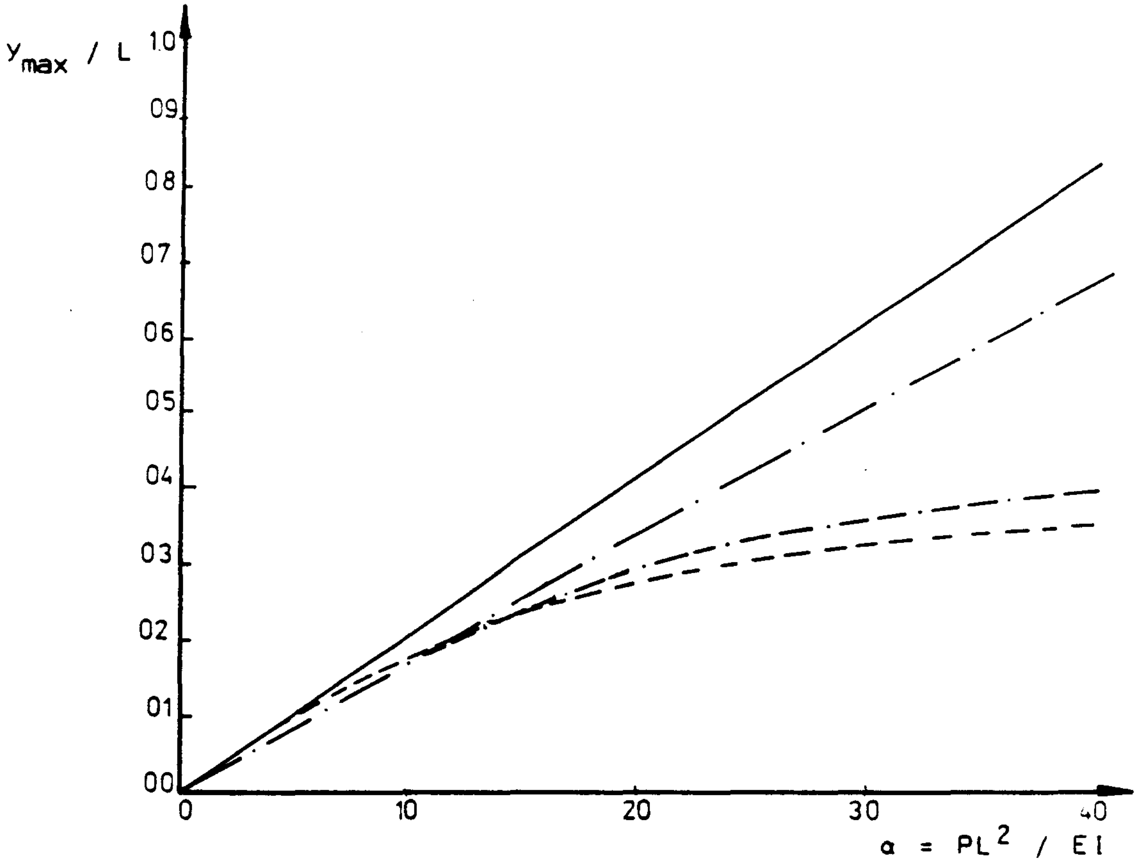

- small deformation theory classical solution $y_{max} = PL^3 / 48EI$

- small deformation theory, present numerical solution*

- large deformation theory, classical solution[80]

- large deformation theory, present numerical solution*

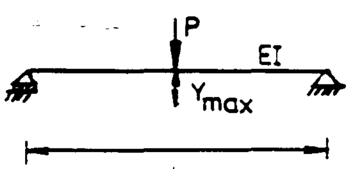

E = 20000 MPa

$I = 1 * 190^3 / 12$

L = 4000 mm

* - present numerical solution

- Finite Element Method, 41*8 constant stress triangular elements

Fig.5.5 Comparison of Analytical and Present Numerical Solutions.

Table 5.1 Comparison of the Predicted Capacities of 2 Block High Plain Prisms

Considered Cases *	Failure (kN)	Ratio Numerical/ Experimental	Ratio Numerical/ Standard **
2 block plain prism - experimental, 2-nd data set, Table 3.4	533 (COV=7.8%)		
Standard numerical solution **	518	0.97	1
6x6 grid for block (102 elements)	553	1.04	1.07
8x8 grid for block (168 elements)	514	0.96	0.99
5 load increments	554	1.04	1.07
20 load increments	538	1.01	1.04
small deflection	520	0.97	1.00
plane stress	534	1.00	1.03
fc concrete=19.2 MPa, fc mortar =16.8 MPa	451	0.84	0.87
E=1000 f'm , f'm=15.1	537	1.01	1.04
face shell thickness = 32 mm	440	0.82	0.85
face shell thickness = 38 mm	486	0.91	0.94
face shell thickness = 42 mm	586	1.10	1.13

*
E - modulus of elasticity;
fc, fm - compressive strength of concrete and masonry;
ft = 0.1 fc - tensile strength;
n - Poisson's ratio.

**
Standard numerical solution for:
4x4 grid for block (52 elements), 10 load increments,
large deflection, plane strain,
voids: E=10 MPa, n=0., fc=40.0 MPa, thickness 78 mm
webs: E=18220 MPa, n=0.19, fc=22.1 MPa, thickness=78 mm
mortar: E=16690 MPa, n=0.30, fc=20.8 MPa, thickness=390 mm
shells: E=18220 MPa, n= 0.19, fc=22.1 MPa, thickness=390 mm
tensile bond strength =0.33 MPa
face shell thickness = 40 mm

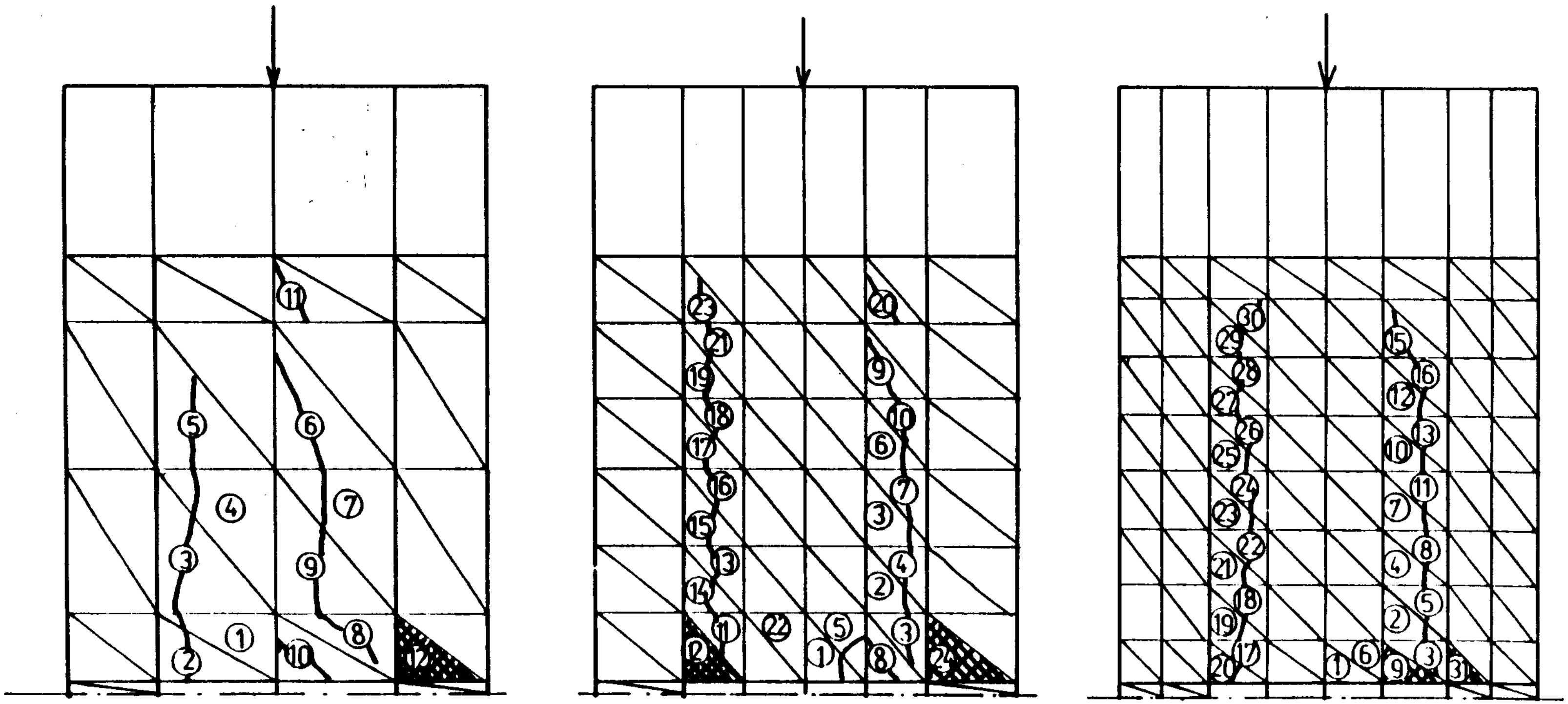

4*4 grid
first crack at 197 kN
crushed at 518 kN

6*6 grid
first crack at 144 kN
crushed at 553 kN

8*8 grid
first crack at 116 kN
crushed at 514 kN

Fig.5.6 Comparison of the Predicted Cracking and Crushing in a 2 Block High Plain Prism Using Different Finite Element Grids.

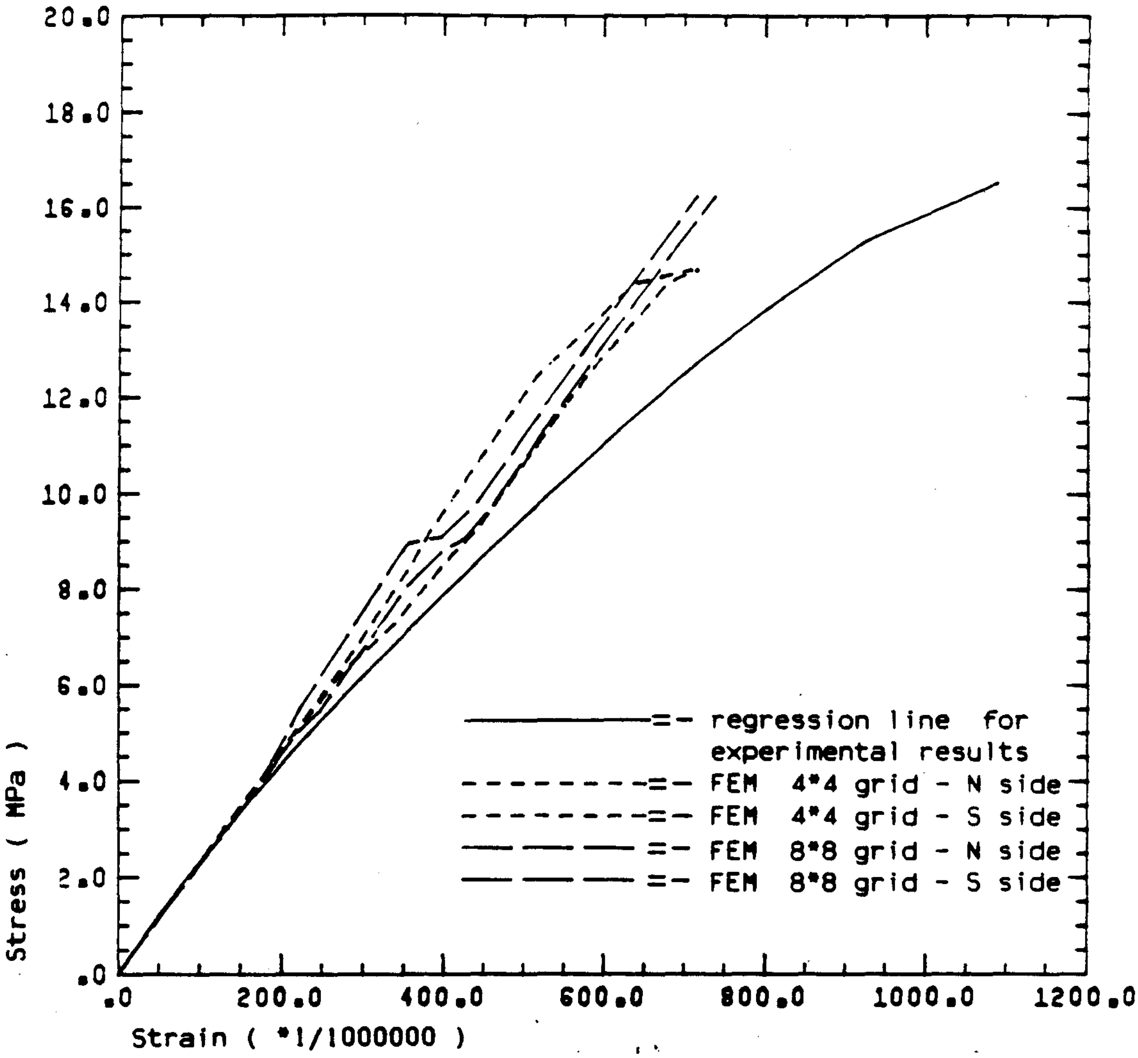

Fig.5.7 Comparison of Experimental and Numerical Stress-Strain Results for a 2 Block High Plain Prism.

Close to failure, where plastic deformations were significant, the elastic model could not predict behavior as accurately.

The influence of the size of load increment on the failure load was not significant for prisms since the special procedure previously described in Section 5.4.3 was used to scale down the load increment. However, for full scale walls, that influence was noticeable.

As could be expected for 2 block prisms, there was no influence of the large deformation analysis. Similarly there was no significant difference between plane stress and plane strain analysis.

The decreased strength of the materials resulted in significantly lower capacity. However, when standard masonry compressive strength and constant modulus of elasticity were used for both the mortar and tne concrete blocks, the capacity obtained was very close to the experimental result.

The influence of the assumed face shell thickness was significant. The results of the analysis suggested that the assumption of 40 mm thick face shells (as was explained in Section 3.3.3) for analyzing both the experimental and numerical results was a satisfactory approximation.

5.6 Summary

In this chapter, basic concepts of finite element modeling of masonry walls were described. In the beginning the previous application of the finite element method in modeling of masonry walls were reported. This was followed by a description of features of the current model. The method of modeling components of a masonry wall was described and derivations of some matrixes were included. Later the numerical procedure used to predict failure were explained. This included description of the failure criteria for triangular elements and for joint elements , as well as derivation of a coefficient used to control load increments. Finally, the numerical results obtained using the model were compared to some previously published results for isotropic beams.

CHAPTER 6

APPLICATION OF THE FINITE ELEMENT MODEL TO PREDICTION OF BEHAVIOR OF CONCRETE BLOCK WALLS

6.1 Introduction

In the previous chapter, the numerical model and results of the analysis of axially loaded 2 block high plain prism were presented . In this chapter analytical models representing the 4 block high prisms and the full scale concrete masonry walls subject to out-of-plane bending are investigated. Both plain and reinforced walls with different slendernesses and eccentricities of vertical loads are studied. The results of the full scale tests are compared with the numerical results obtained from the proposed finite element model and the justification of the geometry chosen for the numerical model is included.

The detailed analysis of the experimental and numerical results includes:

For prisms: failure loads, crack patterns, stress-strain relationships.

For each type of walls: failure load versus initial eccentricity results and load-moment interaction curves.

For each wall separately: failure loads, crack patterns, load-strain results, load-maximum moment results.

All of the experimental and numerical results are summarized in Table 6.1. All data concerning the specimens and the test results from the current experimental program were discussed in Chapters 3 and 4.

Table 6.1 Comparison of the Experimental* and Numerical Results.

Specimen Type	Initial Eccen-tricity	Failure Load	Experimental Maximum Bending Moment	Experimental Maximum Lateral Defl.	Ratio FEM/Experimental Failure Load	Ratio FEM/Experimental Maximum Bending Moment	Ratio FEM/Experimental Maximum Lateral Defl.
	mm	kN	kNm	mm	-	-	-
Prisms:							
2 bl. plain	0	533	---	---	0.97	---	---
4 bl. plain	0	550	---	---	0.99	---	---
4 bl.grouted	0	1007	---	---	1.10	---	---
Walls:							
16 bl. plain Wall P2	67	502	37.7	8.3	1.52	1.55	1.17
16 bl. plain Wall P3	32	1055	42.0	7.5	1.03	1.00	0.86
16 bl. plain Wall P5	13	1180	20.7	4.8	1.09	0.97	0.59
16 bl. plain Wall P6	63	750	57.3	13.7	1.04	0.98	0.66
16 bl. reinfor. Wall R1	61	594	44.0	13.3	1.53	1.46	0.74
16 bl. reinfor. Wall R2	102	216	32.2	46.9	0.87	0.67	0.29
16 bl. reinfor. Wall R3	65	521	43.2	18.0	1.32	1.23	0.67
16 bl. reinfor. Wall R4	96	231	33.7	50.1	0.90	0.67	0.26
16 bl. reinfor. Wall R5	34	1000	45.2	11.2	1.30	1.17	0.59
16 bl. reinfor. Wall R6	142	140	26.2	45.2	0.92	0.82	0.55
Beams:							
14 bl. reinfor. Wall S1	B	---	15.2	---	---	1.15	---
14 bl. reinfor. Wall S2	B	---	17.0	---	---	1.03	---

* These experimental results are from the experimental part of this investigation.

The results of the walls tested by Hatzinikolas et al [44, 45] are compared to the results of the finite element analysis in Tables 6.2 and 6.3. The failure loads, maximum moments and mid-height deflections are compared.

6.2 Comparison of the Numerical and Experimental Results for 4 Block High Prisms and Full Scale Walls

6.2.1 Four Block High Prisms

6.2.1.1 General

The geometry of the numerical models was defined in the same way as it will be described in Section 6.2.2.1 for full scale walls. The reasons for assuming an effective mortar bedded area based on 40 mm wide face shells were discussed previously in Section 3.3.3.

The predicted failure load was compared to the average failure load obtained during tests for each type of prism. Typical experimental cracking patterns were compared with those predicted and stress-strain relationships were obtained assuming the same equivalent mortar bedded areas of 2x40mmx390mm for plain prisms and 190mmx390mm for grouted prisms. The predicted curves were presented for the two sides of the specimens. Since the method of analysis allows only one element at a time to fail, this causes differences in results even for symmetrically loaded prisms. The results are compared to the regression curves and the actual results for the prisms.

6.2.1.2 Plain Prisms

The failure loads for plain prisms were predicted very well and predicted cracking patterns, shown in Figures 6.1 and 6.2, provided realistic representation of the actual failure modes. However, for the numerical analysis two vertical cracks were obtained in webs, whereas in the real prisms, single cracks occurred.

It is thought that this inconsistency was caused by a sharp change in the assumed stiffness between the face shell and web which caused a stress concentration resulting in cracking in that region . In the real prisms, there was a gradual change of the stiffness between the face shell and web. The weakest section was at the middle of the web where it had the minimum cross-section area. This double cracking did not seem to influence the capacity, since local instability and crushing of face shells were the cause of the final failure.

The predicted stress-strain relationships for the prisms, shown in Figs.6.3 and 6.4, were good estimates of the actual curves in the initial linear elastic stage. At higher loads, the linear model of materials overestimated the actual stiffness. The difference increases significantly near failure where non-linear behavior dominated. Thus it can be concluded that incorporation of material nonlinearity in the current model could improve results significantly.

6.2.1.3 Grouted Prisms

The equivalent cross sectional area of grout, based on actual dimensions of cores in blocks, was assumed. This assumption gave a 75% increase in the cross-section area of a grouted prism compared to a

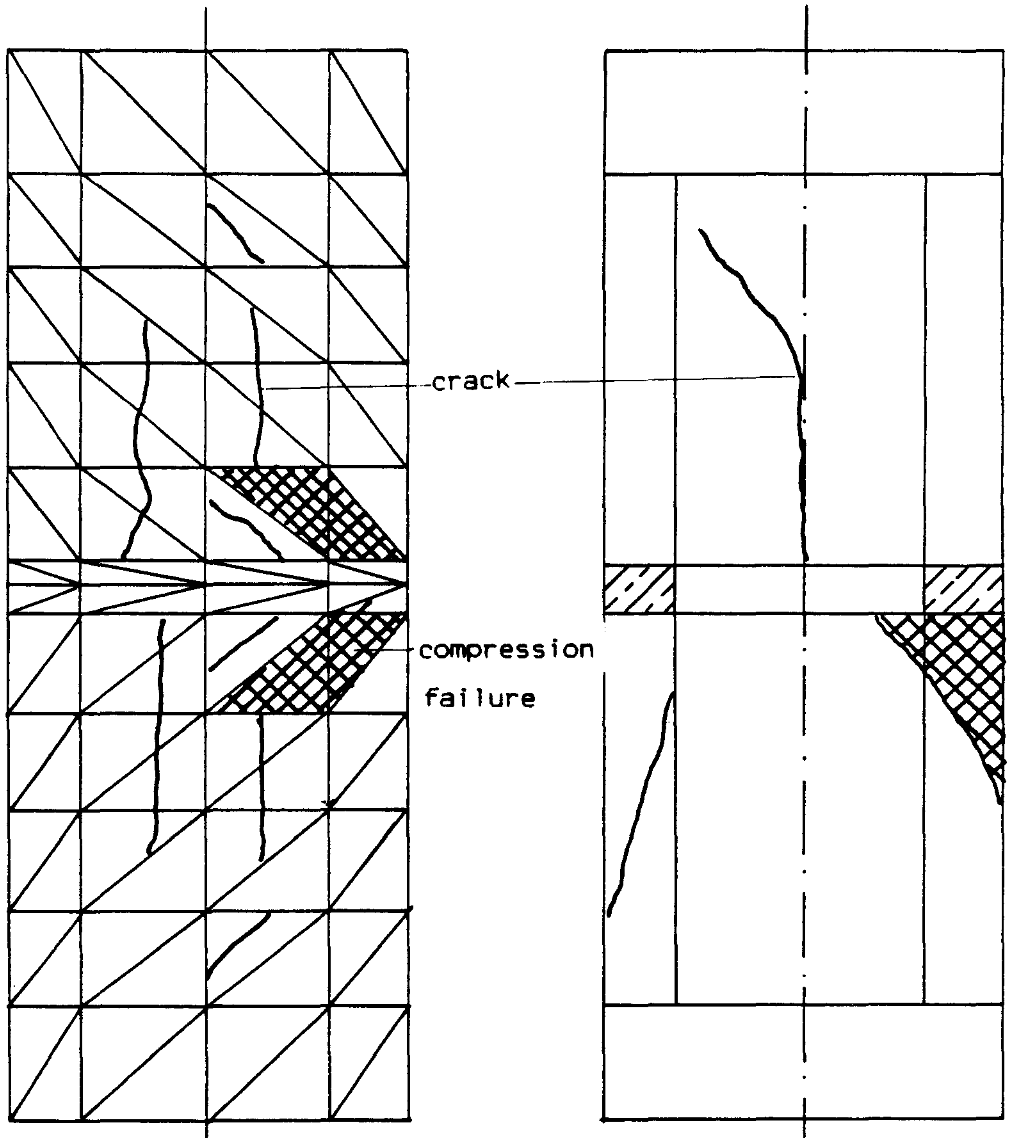

first crack -197 kN
failure - 519 kN

failure - 533 kN

a) Predicted Cracking Pattern

b) Experimental Cracking Pattern

Fig.6.1 Cracking Patterns for a 2 Block High Plain Prism.

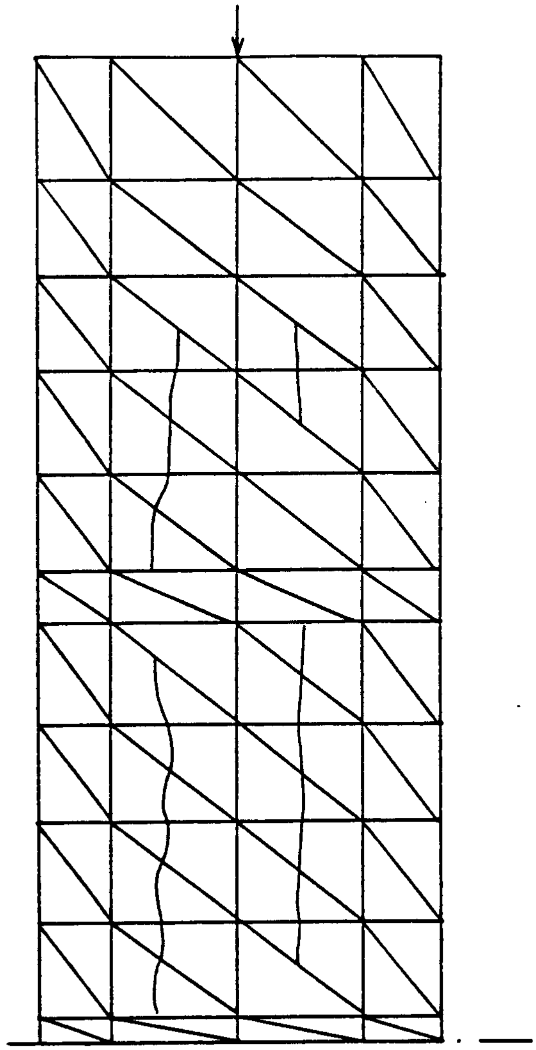

first crack -210 kN
failure - 546 kN

a) Predicted Cracking Pattern

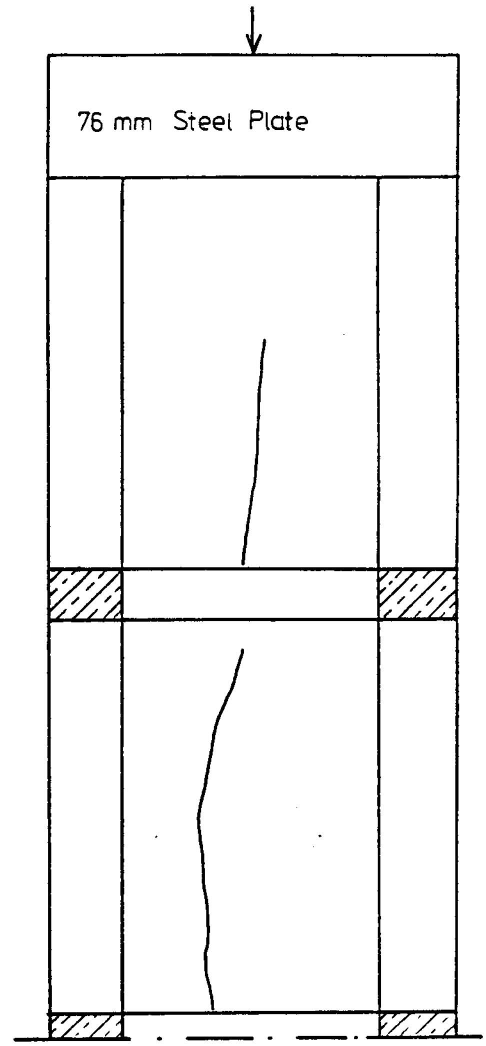

failure - 550 kN

b) Experimental Cracking Pattern

Fig.6.2 Cracking Patterns for a 4 Block High Plain Prism.

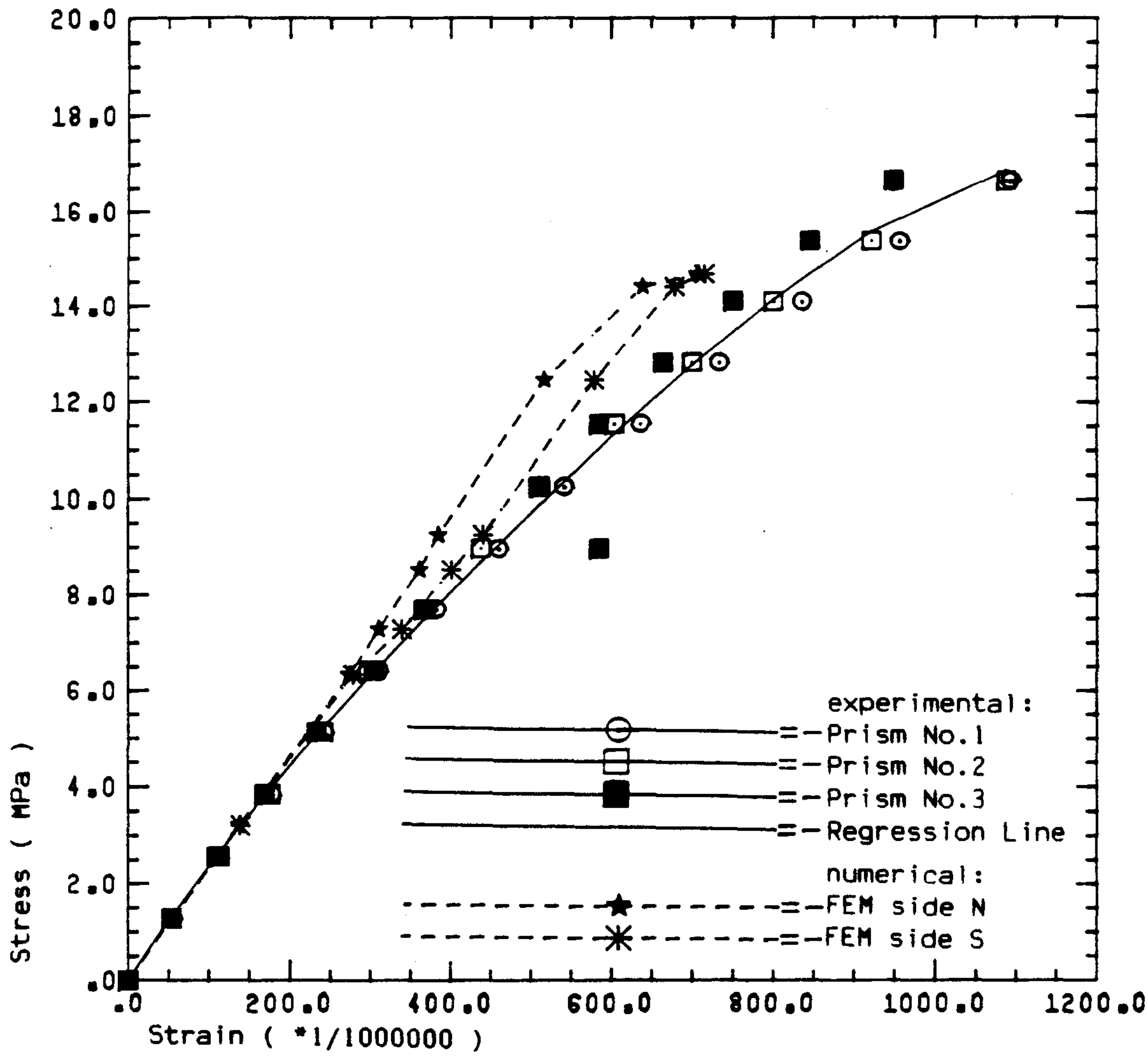

Fig.6.3 Experimental and Numerical Stress-Strain Relationships for 2 Block High Plain Prisms.

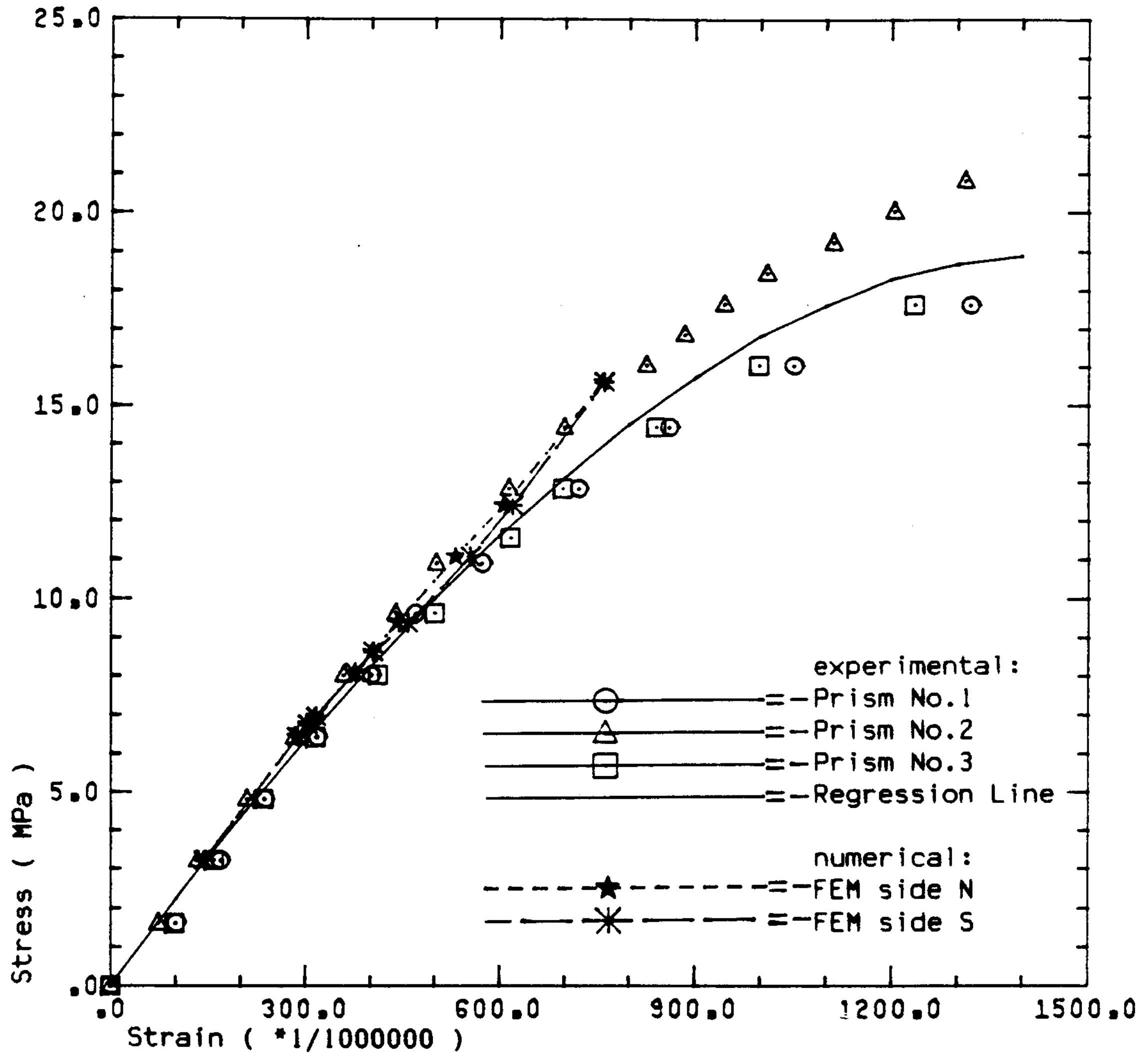

Fig.6.4 Experimental and Numerical Stress-Strain Relationships for 4 Block High Plain Prisms.

plain prism. Despite the fact, that the contributory area of grout was assumed to be only 63% of the minimum measured area of grout core, the predicted failure load for grouted prism was about 10% higher than the average failure load obtained during tests.

As was seen during tests of grouted prisms, failure occurred in the block due to vertical cracking of webs. Hamid and Drysdale[41] explained that, near failure, this cracking is attributed to the extensive lateral tension in block caused by the higher lateral expansion for the grout and mortar compared to the blocks. This phenomenon could not be modeled using an elastic two-dimensional model. In addition, the assumption of ideal bond between block and grout could increase the discrepancy between predicted and experimental results. The numerous experiments, conducted by Hamid and Drysdale[41], did not indicate any separation between block and grout. However Hegemier et al[46] suggested that such separation could occur.

Due to all the above mentioned reasons, the proposed model could not exactly predict behavior of the grouted masonry in axial compression near failure where the nonlinearity occurs. This influence is visible in the comparison of predicted and experimental cracking patterns shown in Fig.6.5. However, the failure mode, due to crushing of grout cores and face shells of blocks, was closely predicted.

The experimental and predicted stress-strain relationships based on the gross cross-section area of the prism (190x390 mm) are shown in Fig.6.6. As was the case for plain prism, the initial stiffnesses of the grouted prisms were closely predicted, but the numerical model

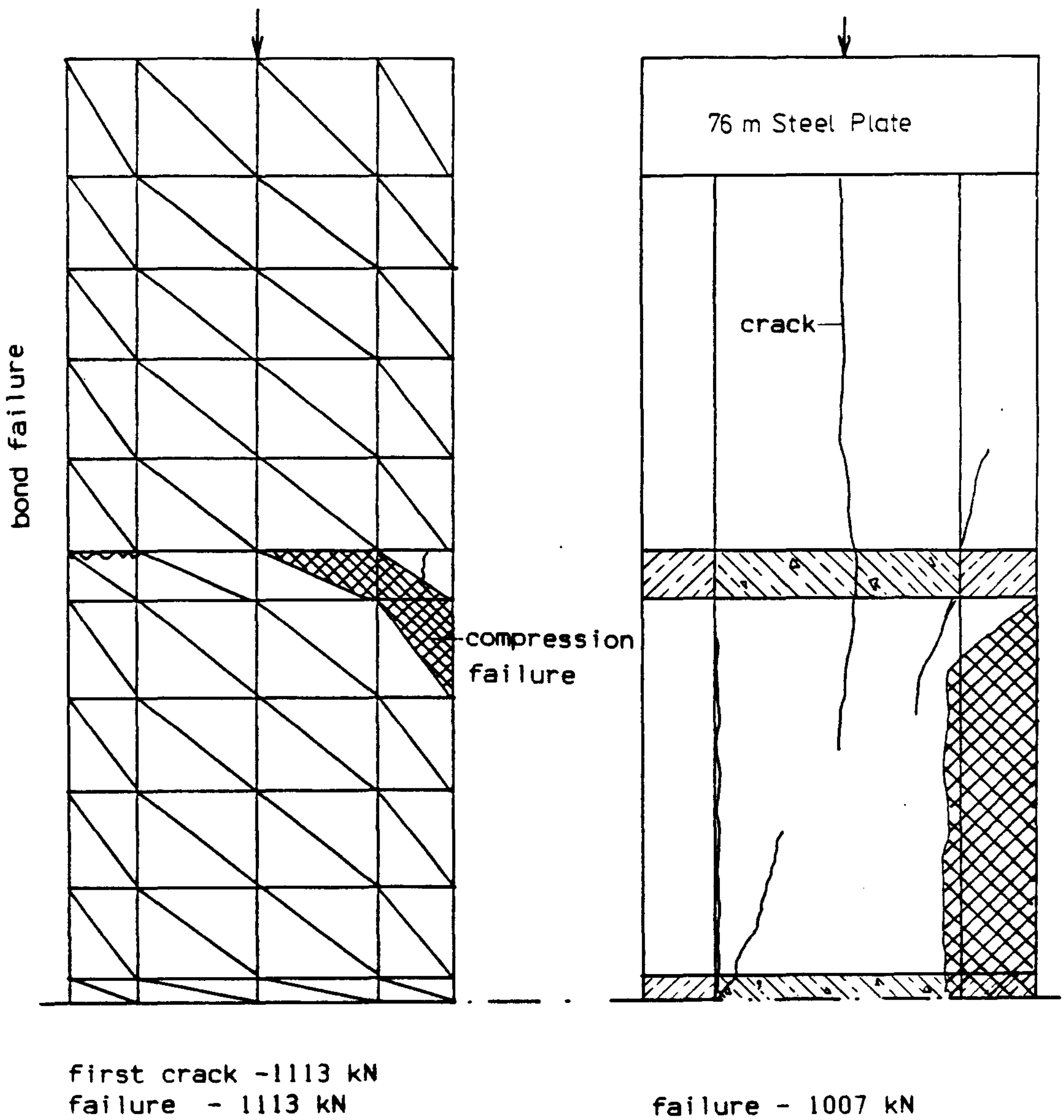

a) Predicted Cracking Pattern   b) Experimental Cracking Pattern

Fig.6.5 Cracking Patterns for a 4 Block High Grouted Prism.

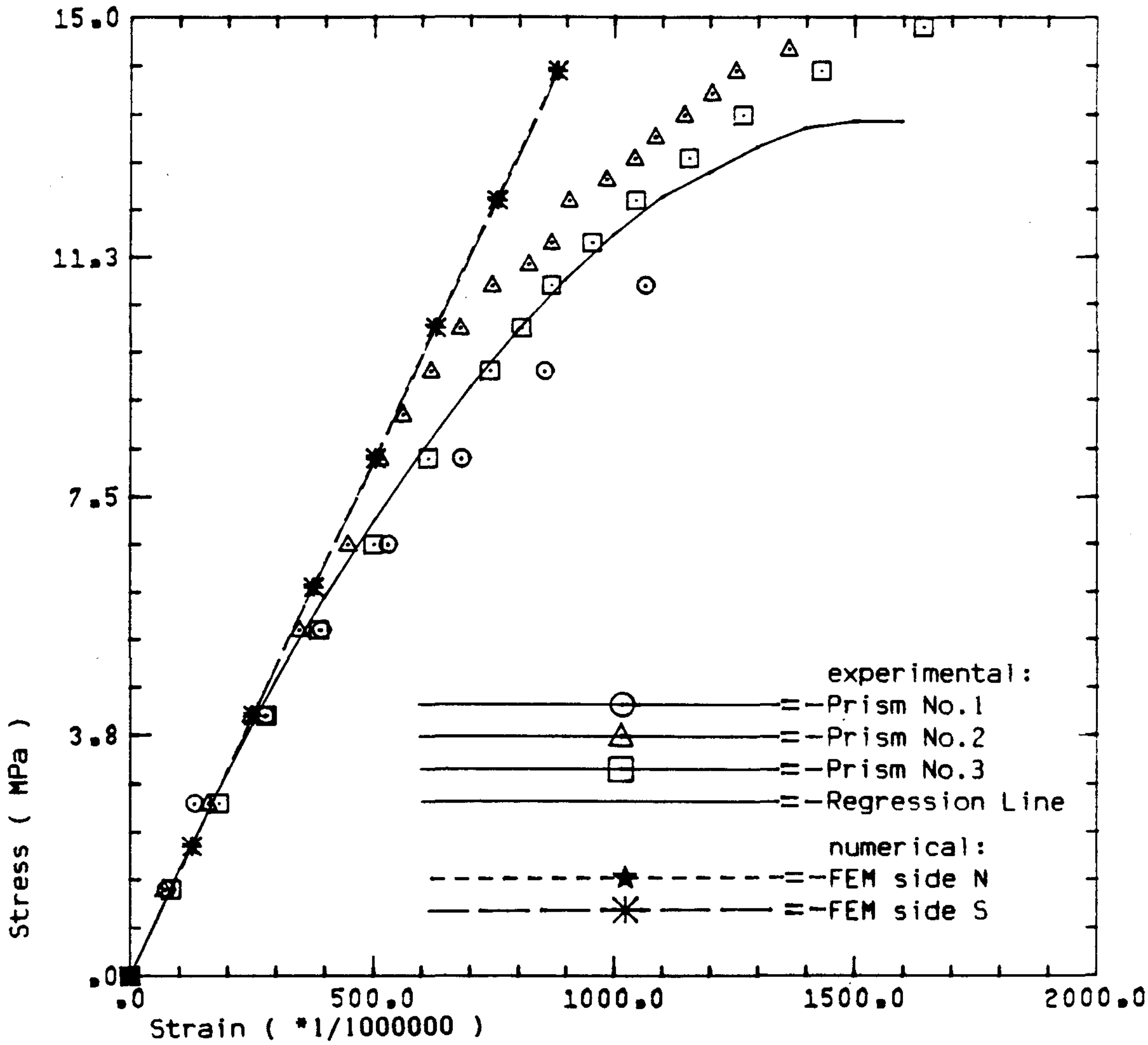

Fig.6.6 Experimental and Numerical Stress-Strain Relationships for 4 Block High Grouted Prisms.

failed to forecast the nonlinear part of the experimental curve. However, the effects of incompatibility of grout and blocks are lessened for the usual eccentric loading cases since the grouted part of a wall have lower strains due to eccentricity of applied load as was shown by Drysdale and Wong[32] during experiments on eccentrically loaded grouted prisms.

6.2.2 Plain Walls

6.2.2.1 General

The standard blocks used for the tests have a fairly complicated shape. Therefore it was necessary to find an equivalent more uniform cross section for use in the 2-dimensional numerical model. Sketches of the actual and chosen equivalent geometry are shown in Fig.6.7. It should be especially noted that a 40 mm thickness of face shells and width of mortar bed joints were assumed as was explained in Section 3.3.3. This assumption resulted in a mortar bedded area 25% larger than the minimum area based on the 32 mm minimum thickness of the face shells of these blocks. For the webs the equivalent thickness was assumed to be 8 times the 26mm minimum thickness of single web(2 full size units with 3 webs and half unit with 2 webs) . Thus the equivalent web thickness was 208 mm for full scale walls and 78 mm for prisms. All the numerical analyses for plain masonry summarized in Table 6.1 were carried out based on these assumed dimensions.

The failure loads versus the initial eccentricities for full scale plain walls are presented in Fig.6.8. All the experimental results were shown. However, as was mentioned in Section 4.3.3, it should be

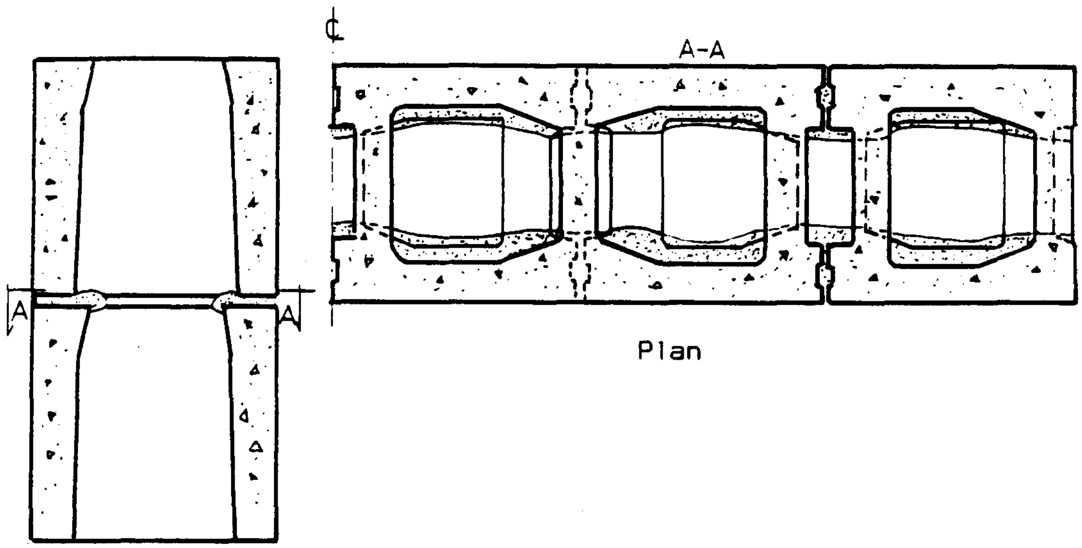

a) Actual Plain Concrete Block Wall

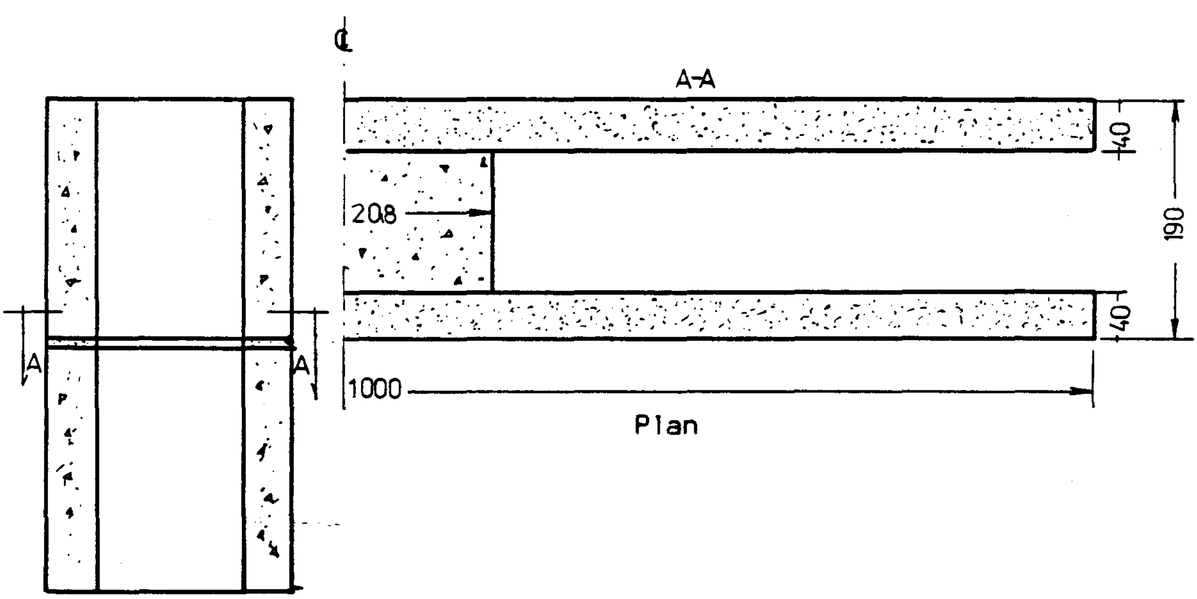

b) Equivalent Plain Concrete Block Wall

Fig.6.7 Actual and Equivalent Plain Wall Geometries.

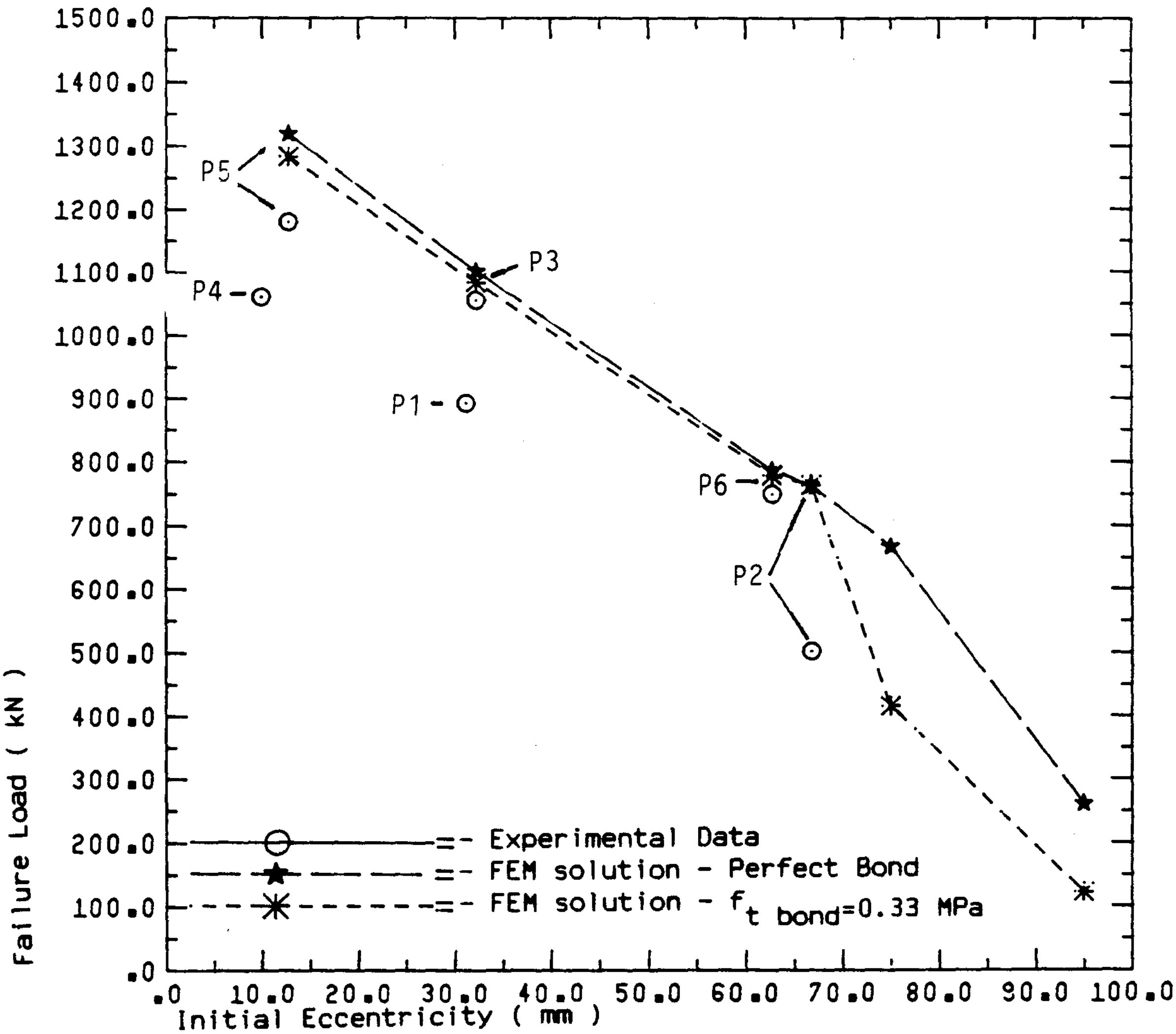

Fig.6.8 Experimental and Numerical Capacities of Plain Concrete Block Walls.

noted that in two cases, Walls P1 and P4, the failure may have been slightly premature due to problems with the loading apparatus. These walls tested under small eccentricities failed at lower loads than other walls loaded with similar eccentricities.

Experimental results were compared to two numerical results. In Fig.6.8, the higher results represent analyses with assumed ideal bond. The lower numerical results where obtained as results of analyses which included debonding between block and mortar for tensile stresses above 0.33 MPa. It can be seen that for small eccentricities up to the kern point, there is no significant difference between the two analyses. For eccentricities greater than the kern distance, debonding affected the capacities of walls. As can be seen for the eccentricity of t/2 (e=95 mm), the predicted value, assuming ideal bond, was twice as high as for the analysis incorporating the debonding effect. Both numerical models overestimated the capacities of the walls. This could be expected since the average strengths of materials were assumed in the numerical model, whereas in real walls the actual strength of materials in parts of wall which were cracked, crushed or displayed debonding controlled the capacity. Also the linear elastic analysis usually results in overestimation of capacity.

The numerical model gave good predictions for walls loaded with small eccentricities where material failure controlled the capacities. There were no experimental data for walls with high eccentricities, e t/2, to compare to numerical solutions.

Walls P2 and P6 were tested at eccentricities greater than the kern distance, which in this case was theoretically equal to 61 mm (for 40 mm strips of mortar). Wall P6, with an eccentricity of 63 mm, failed at 750 kN in the material failure mode. Wall P2, with a 4 mm larger eccentricity, failed at 33% lower load due to debonding along the mortar bed joint, which could be classified as an instability failure mode. These two results showed how sensitive the failure load is to slight changes in eccentricity in this region. In both cases, significant tensile stresses existed. However, in the case of Wall P6, total debonding between the mortar and blocks occurred. In the case of Wall P2, cracking was not so severe and high compressive stresses developed, which resulted in crushing of face shells of blocks on the compression side of the wall.

The numerical analysis did not predict the behavior for Walls P2 and P6 precisely. However, a similar significant drop in capacity was found for a slightly larger eccentricity. The inaccuracy could result from both imprecise evaluation of the actual material and geometrical characteristics of the wall and from the inadequacy of the numerical model which resulted in underestimation of deflections near failure. In Fig.6.8, the difference between the predicted and test results may be simply due to increased eccentricity caused by deflections of the walls.

The interaction diagram shown in Fig.6.9 provides a comparison of the predicted and experimental failure loads and corresponding bending moments considering the increase due to the lateral deflections. The comparison showed that the numerical model overestimated failure load for small eccentricities but overall the predicted strengths were quite close to the test results.

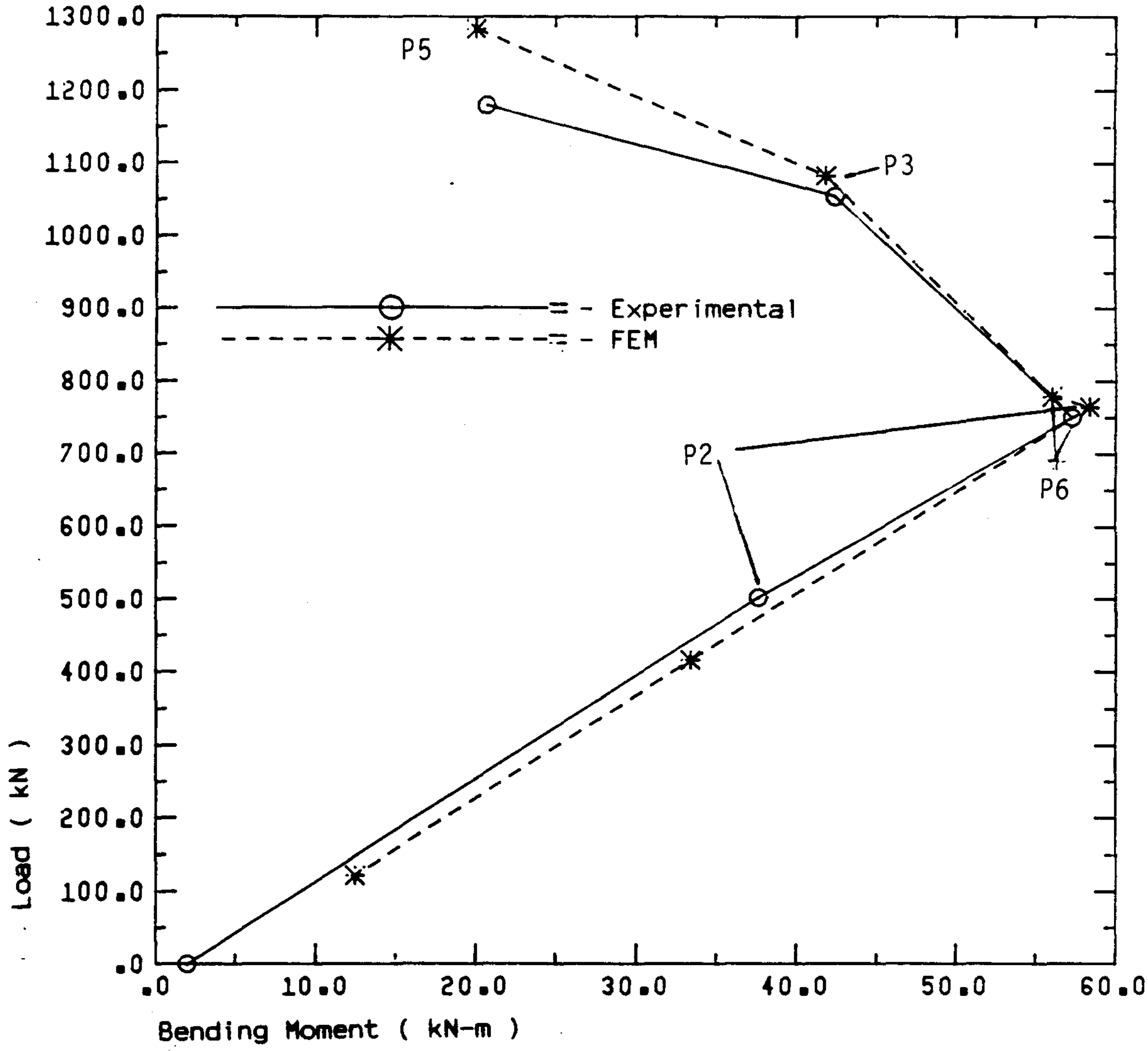

Fig.6.9 Interaction Diagram for Plain Walls.

6.2.2.2 Results for Walls P1 and P4

As was mentioned in Section 4.3.4 difficulties with the testing procedure have led to the conclusion that Walls P1 and P4 may have failed prematurely. Even so, these results do provide lower boundary values, and because they are not too different (less than 20%) from other similar tests, they have been included as added evidence of the adequacy of the analytical model. While no separate analyses were done for these walls, the discussion for Walls P3 and P5, respectively, apply to Walls P1 and P4.

6.2.2.3 Results for Wall P2 (e=67 mm)

The cracking pattern for Wall P2 is shown in Fig.6.10. The predicted cracking pattern was typical for the material mode of failure, whereas the actual wall failed due to debonding which resulted in an instability mode of failure.

The predicted failure load was 52% higher than the actual one. However, the predicted load-moment relationship, shown in Fig.6.11, closely resembles the experimental curve. The experimental and predicted load-strain relationships at the failure region are shown in Fig 6.12. The experimental results were obtained for the midheight region of the wall and the predicted relations are based on the deformations over the first bed joint above the midheight. The elastic part of the predicted strain curves provided good estimates of the experimental values. At about 475 kN, the experimental curves indicate significant increase in the tensile strains over the midheight bed joint. This led to debonding

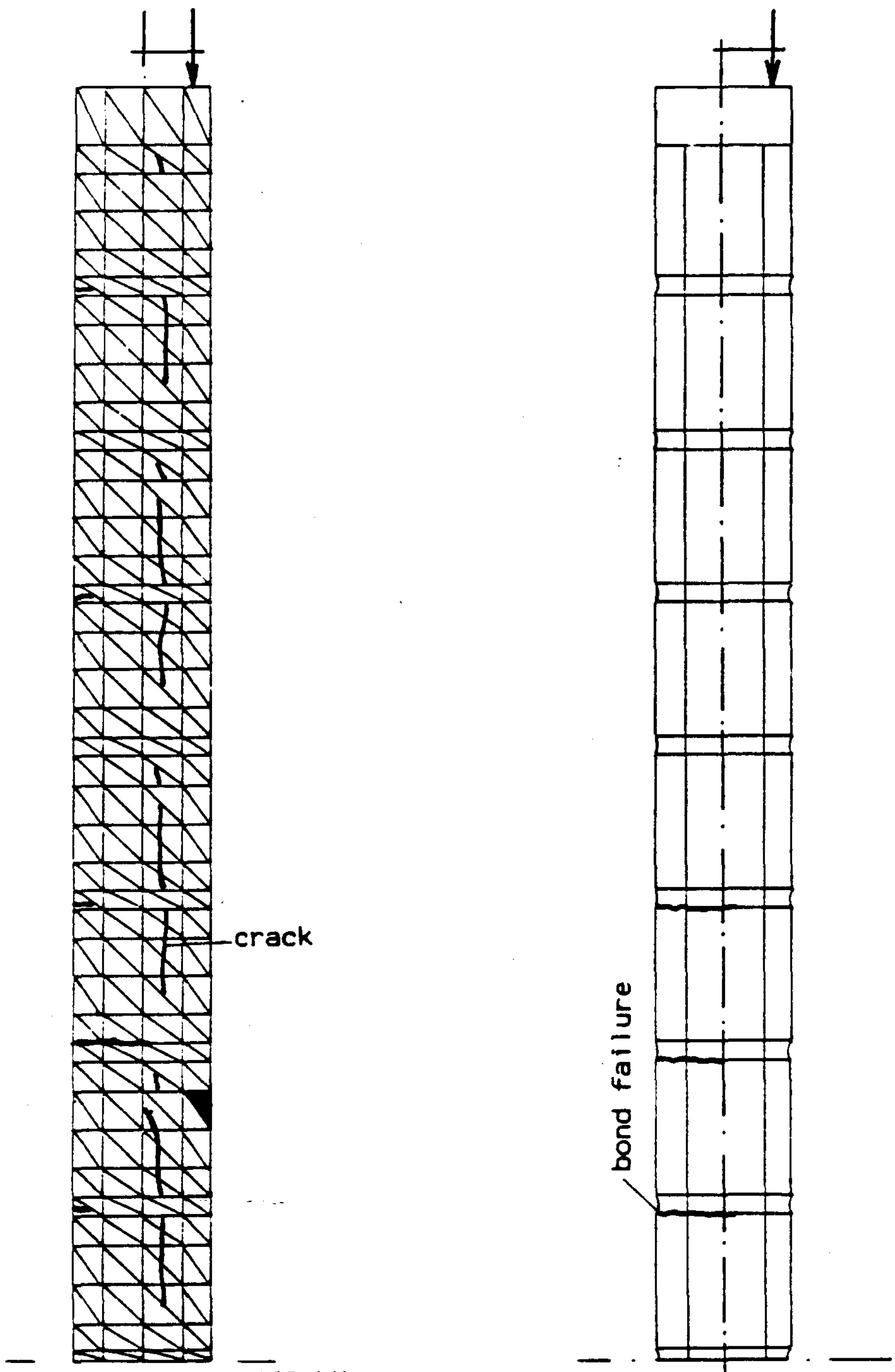

first crack -469 kN
failure - 764 kN

a) Predicted Cracking Pattern

failure - 502 kN

b) Experimental Cracking Pattern

Fig.6.10 Cracking Patterns for Wall P2.

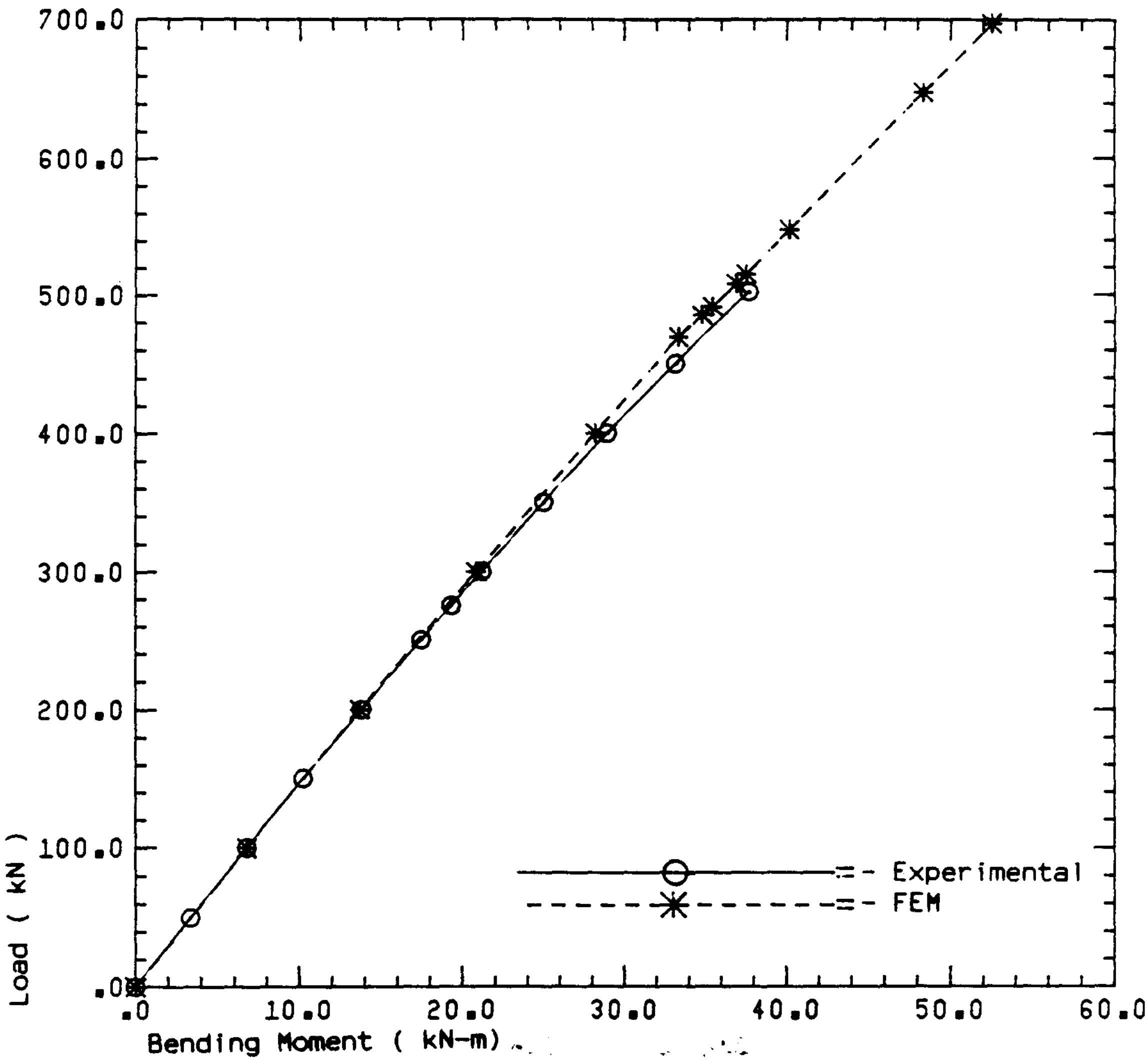

Fig.6.11 Experimental and Numerical Load-Moment Relationships for Wall P2.

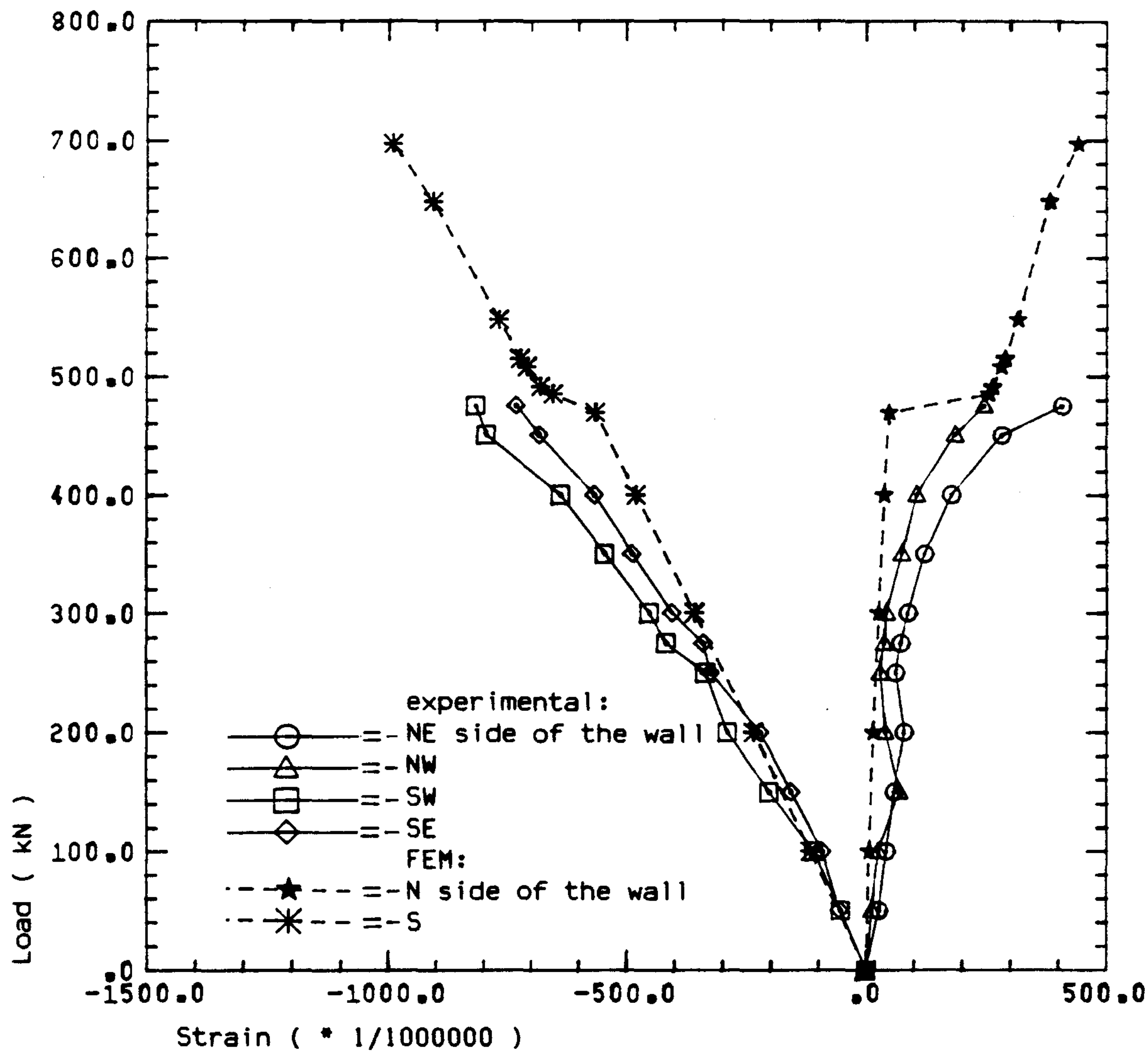

Fig.6.12 Experimental and Numerical Load-Strain Relationships for Wall P2.

and the final failure due to instability. The predicted behavior varied significantly. At 469.3 kN the first cracking occurred and among others a mortar element in the first joint above midheight was cracked. It caused a release of tensile strains at the midheight mortar bed joint, thus no cracks were developed there. Later cracks in webs leading to the material failure mode were predicted.

Aside from the inaccuracies associated with the elastic analysis and limited number of elements, it was pointed out in Section 6.2.2.1 that the capacity in this region of eccentricities is extremely sensitive to small changes in eccentricity. Therefore a few percent change in eccentricity can account for the difference between predicted and test results.

6.2.2.4 Results for Wall P3 (e=32 mm)

The comparisons of numerical and experimental results are shown in Figures 6.13 ,6.14 and 6.15 for Wall P3. The failure load and deformation behavior were very closely predicted. Both sides of the wall were in compression and splitting of webs was the cause of failure. It is important to notice that the numerical model predicted the first crack at the end of the wall as happened in the actual wall. This indicates that the stiffness of the end steel plates influenced the capacity of the wall.

6.2.2.5 Results for Wall P5 (e=13 mm)

The cracking patterns for Wall P5 are shown in Fig.6.16. The numerical analysis correctly predicted the cracking pattern and the web

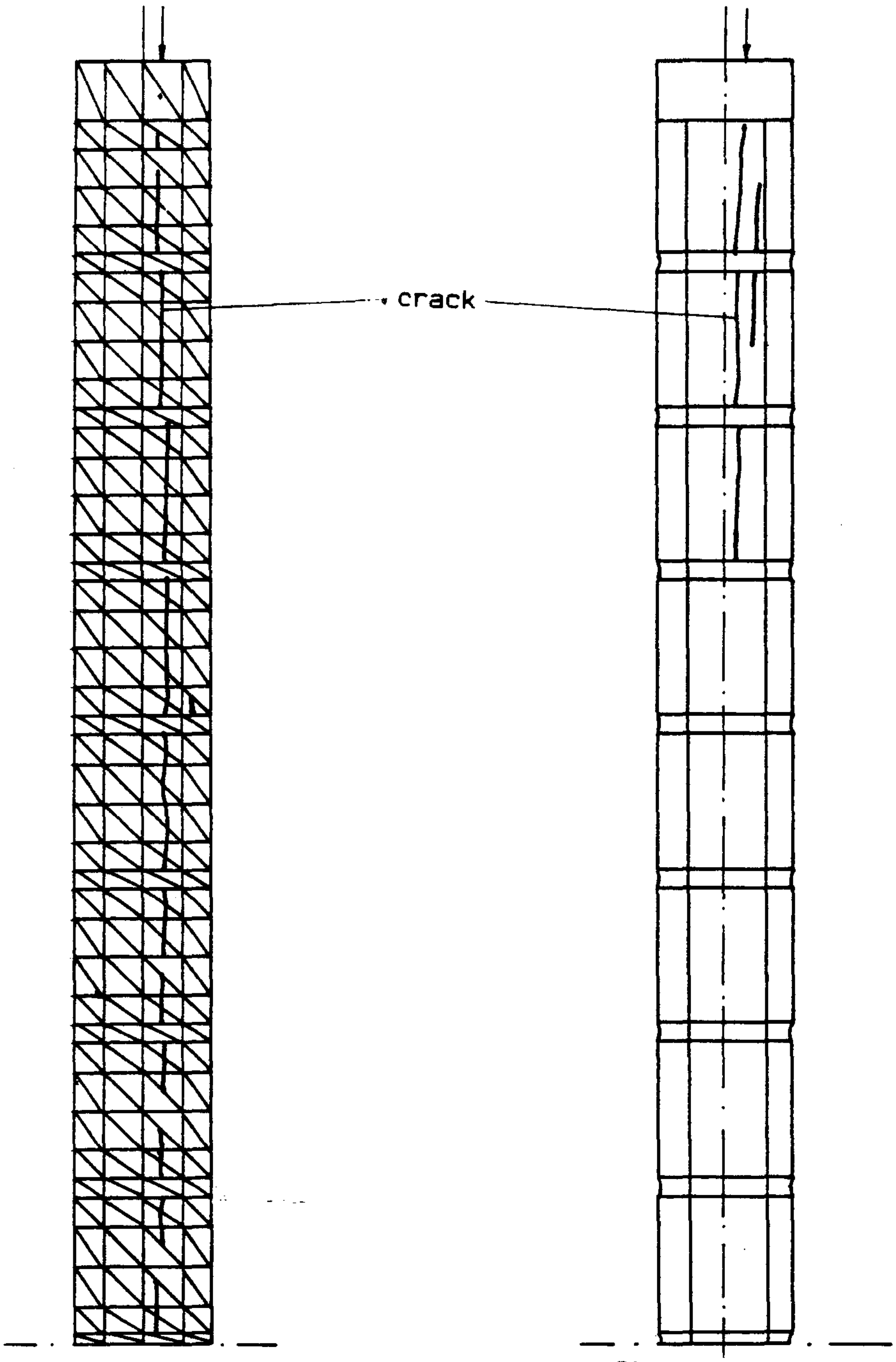

first crack -230 kN
failure - 1083 kN

a) Predicted Cracking Pattern

first crack - 200 kN
failure - 1055 kN

b) Experimental Cracking Pattern

Fig.6.13 Cracking Patterns for Wall P3.

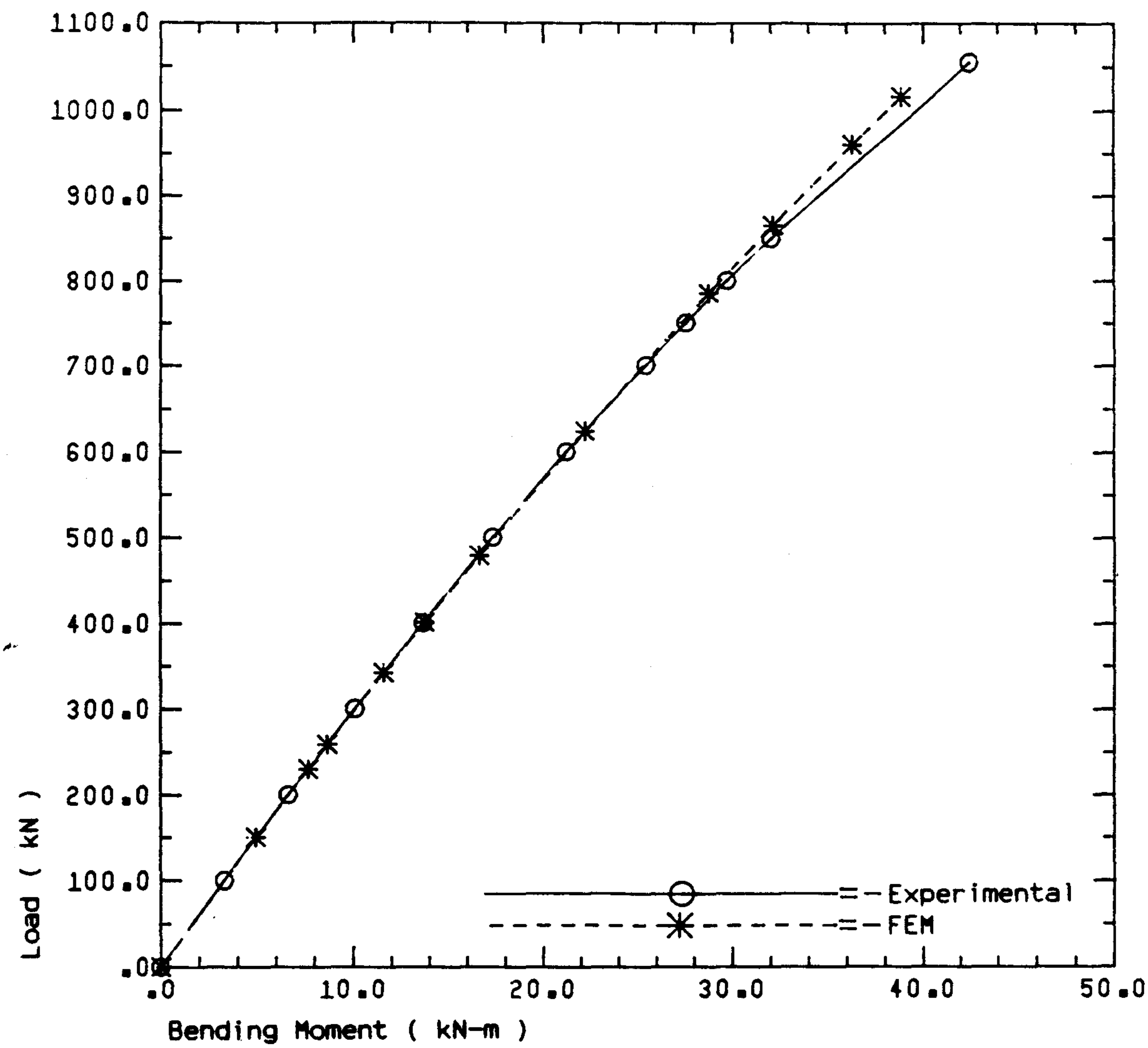

Fig.6.14 Experimental and Numerical Load-Moment Relationships for Wall P3.

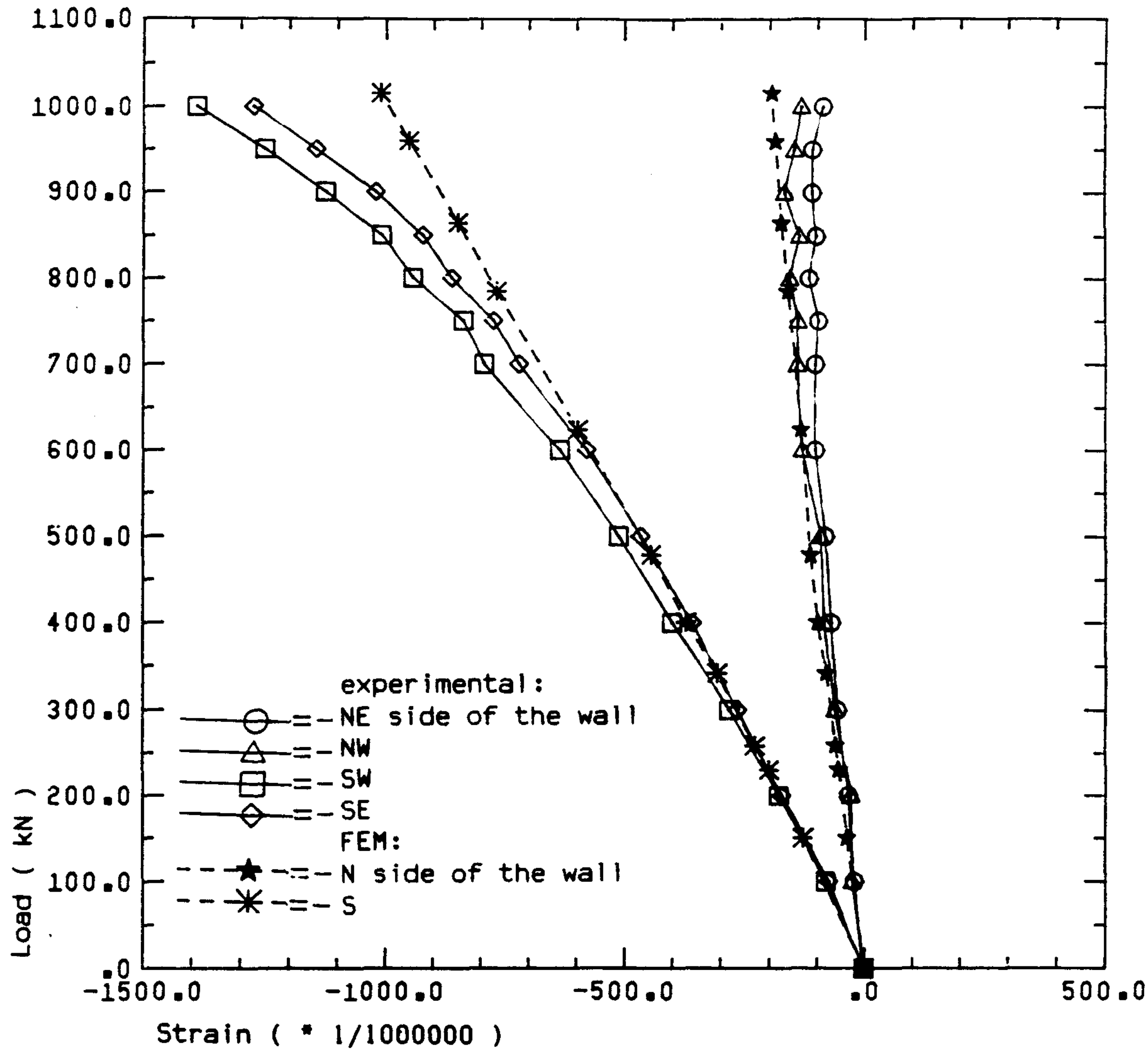

Fig.6.15 Experimental and Numerical Load-Strain Relationships for Wall P3.

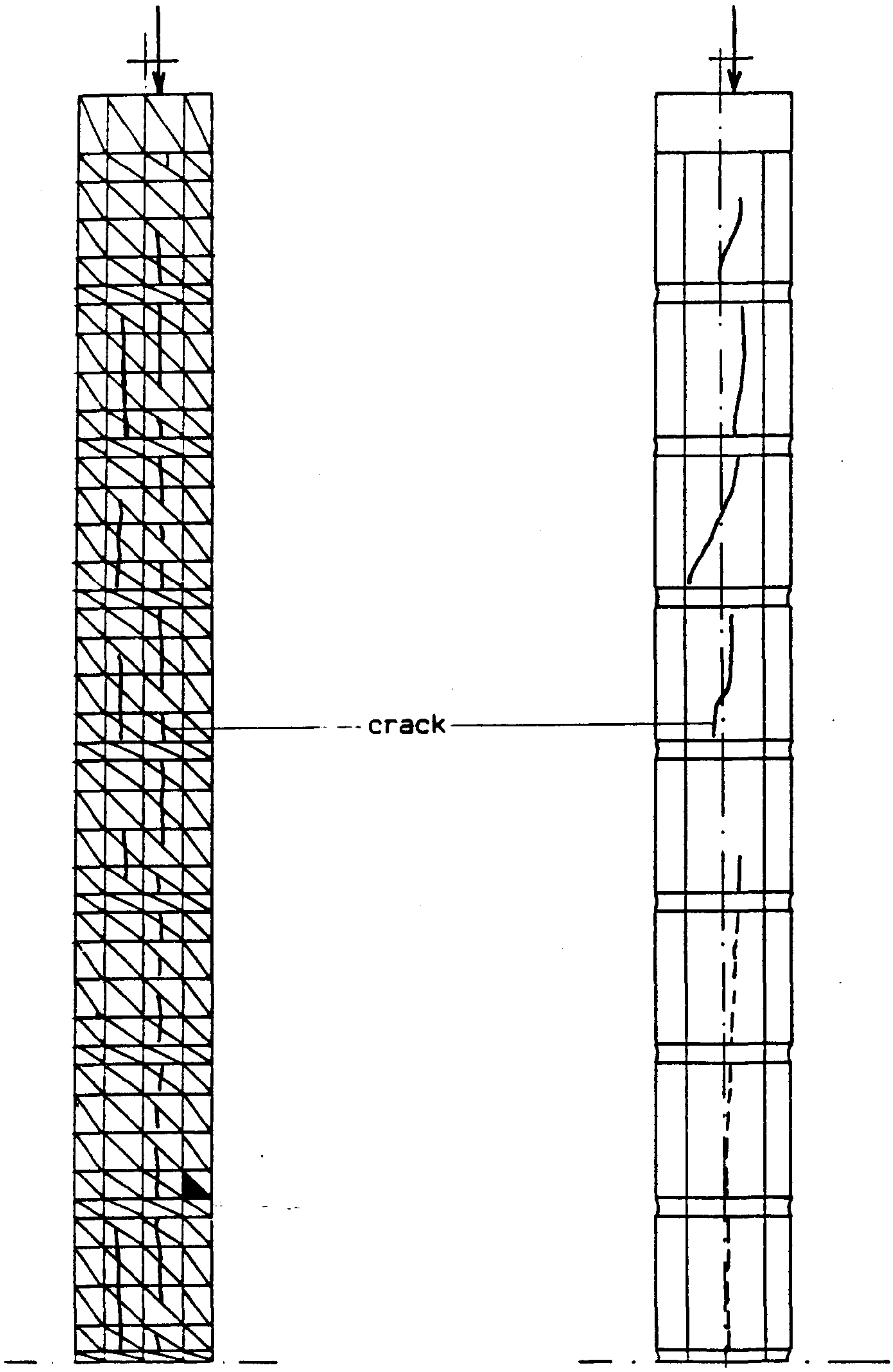

a) Predicted Cracking Pattern b) Experimental Cracking Pattern

Fig.6.16 Cracking Patterns for Wall P5.

cracking failure mode. Also, the load-moment relationship at midheight, shown in Fig.6.17, was predicted quite closely with the exception of the failure region where inelastic behavior is apparent. The predicted load-strain relationships shown in Fig.6.18 agree reasonably well with the test results for low loads. However for higher loads, the influence of the inelastic deformation is apparent. Also there was a significant difference in the experimental stiffnesses of the North sides of the wall. While the assumption of an ideal symmetric wall could cause the overestimation of failure load, the difference of approximately 9% is not very significant compared to normal experimental scatter. Besides, the tested wall would reach higher capacity if stiffer end plates were used. The stiffness of the end plates has a large influence on the capacity when failure is at the end of the wall. This finding was shown by the finite element analysis of block prisms performed by Chukwunenye and Hamid[15].

6.2.2.6 Results for Wall P6 (e=63 mm)

The predicted cracking pattern shown in Fig.6.19 closely represents the actual pattern. The failure due to cracking in webs and final crushing of the face shell was also predicted. The load-moment relationships shown in Fig.6.20 also indicate the very close agreement between the experimental and numerical analysis values. The load-strain relationships at the failure regions are shown in Fig.6.21. The failure occurred at midheight, whereas the predicted failure was in the first mortar joint above. The predicted relationships agree reasonably well with the pattern of the measured strains. Again, the difference in the

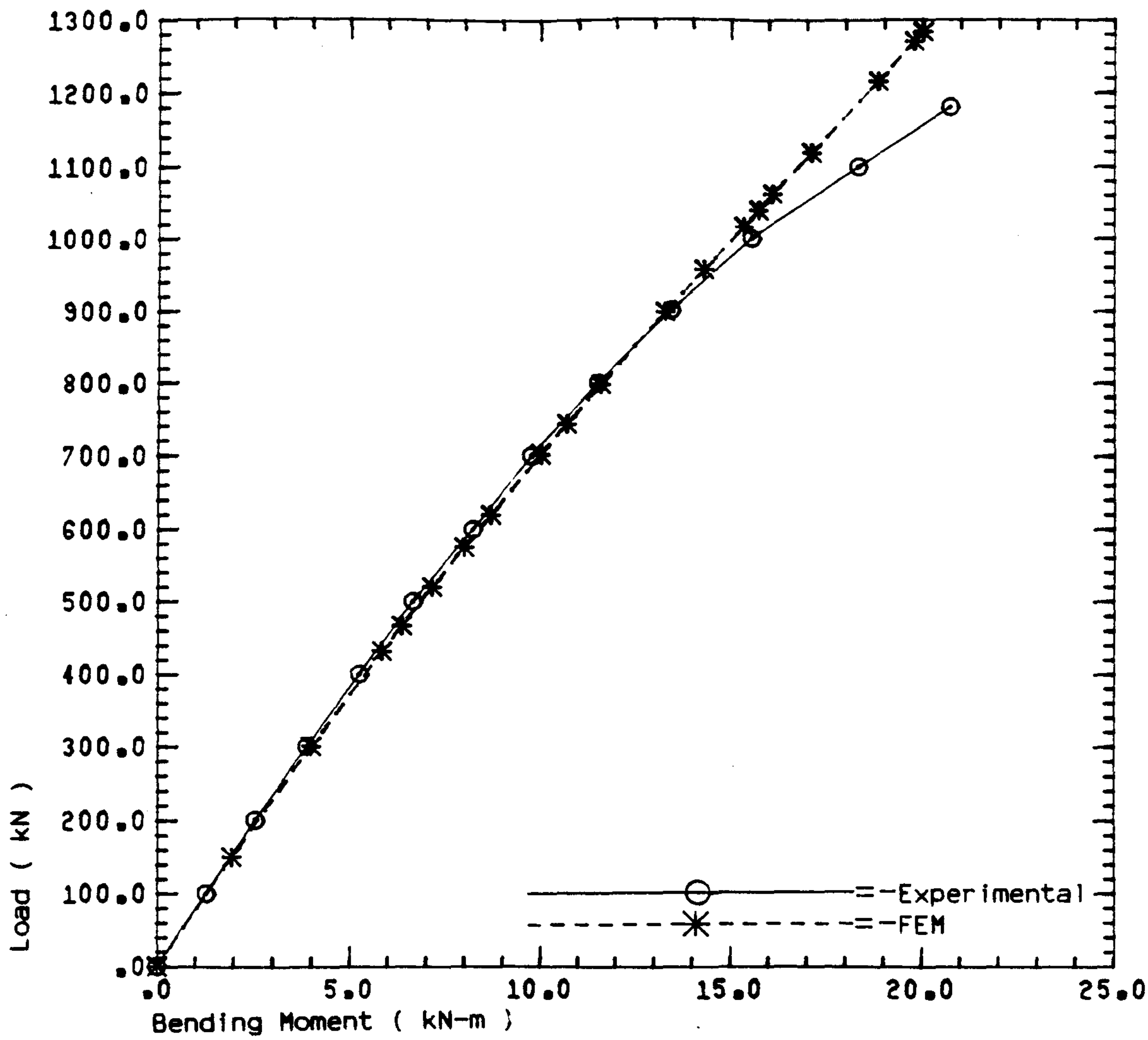

Fig.6.17 Experimental and Numerical Load-Moment Relationships for Wall P5.

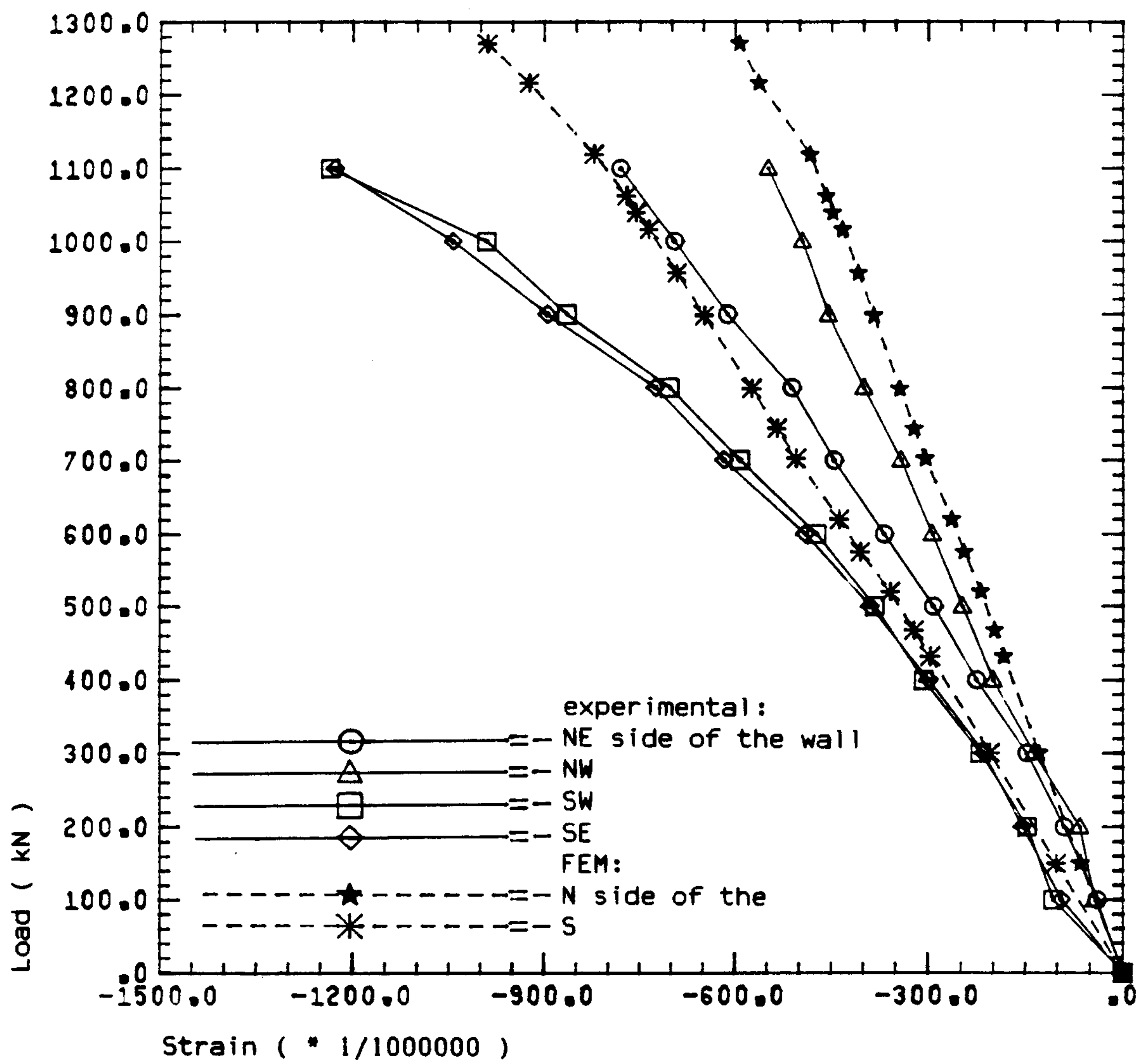

Fig.6.18 Experimental and Numerical Load-Strain Relationships for Wall P5.

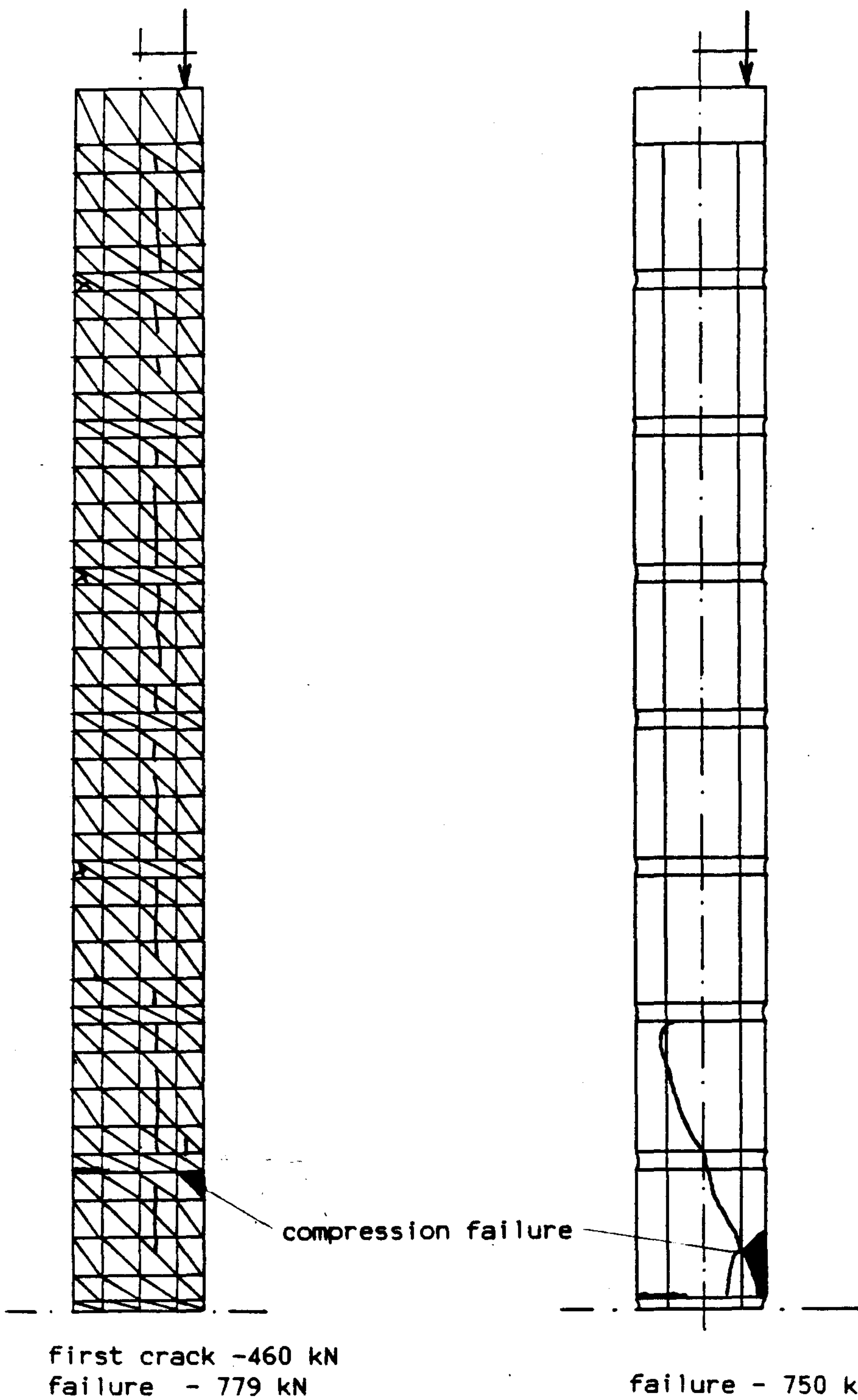

a) Predicted Cracking Pattern

b) Experimental Cracking Pattern

Fig.6.19 Cracking Patterns for Wall P6.

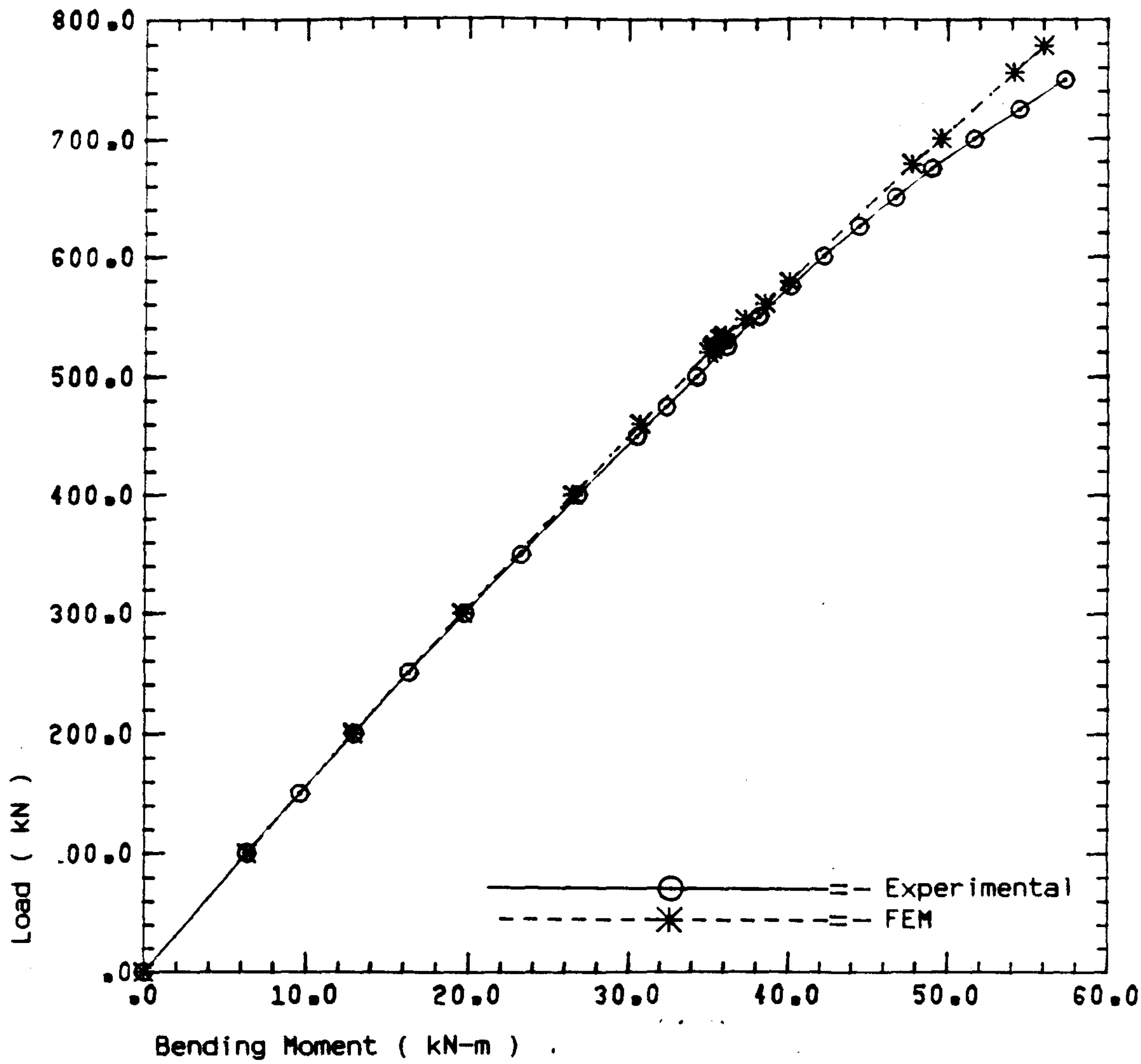

Fig.6.20 Experimental and Numerical Load-Moment Relationships for Wall P6.

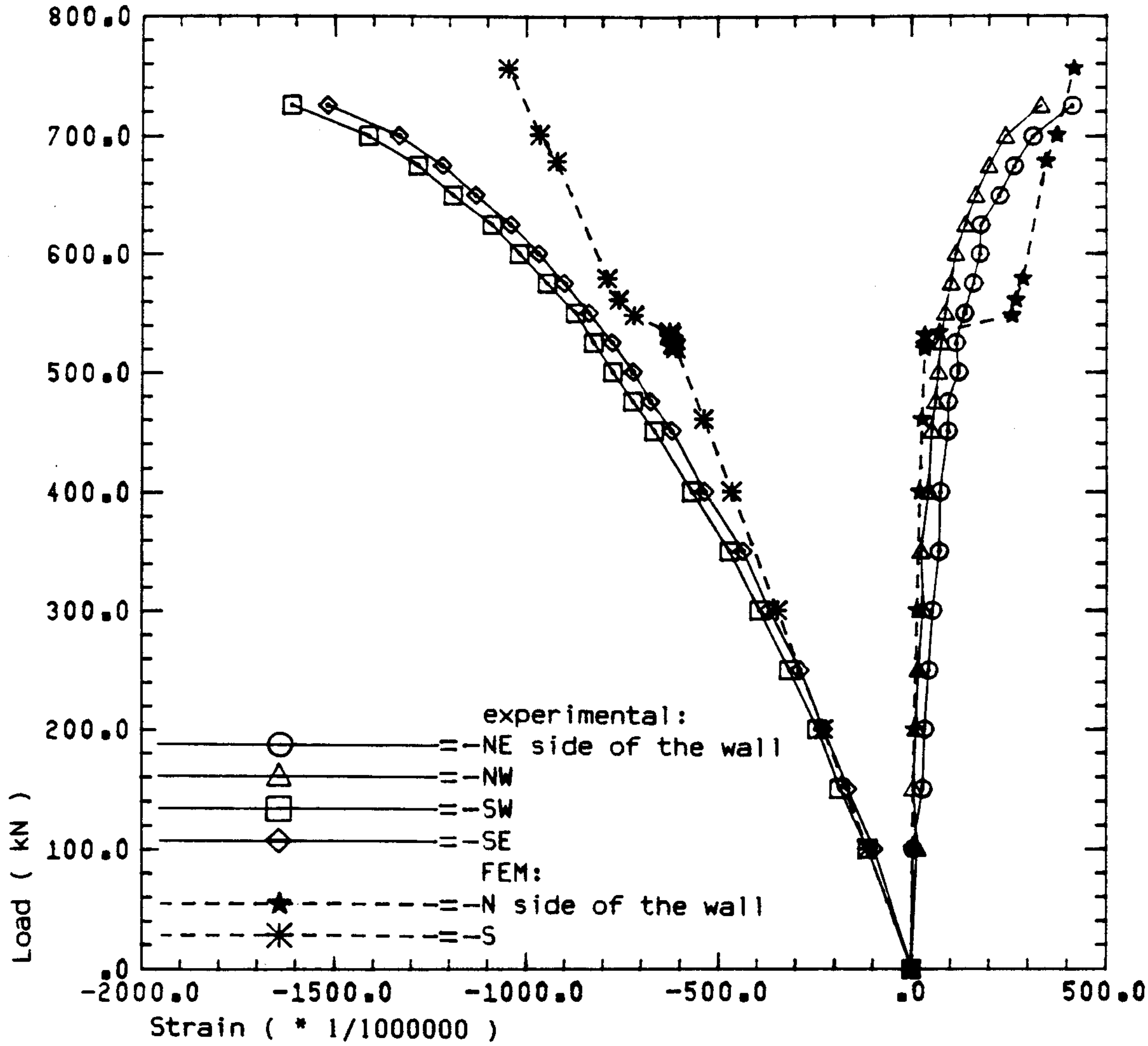

Fig.6.21 Experimental and Numerical Load-Strain Relationships for Wall P6.

maximum compressive strains can be attributed to the inelastic behavior of concrete at high strain levels.

6.2.2.7 Predicted Results for Walls with High Eccentricities (e=75 mm and e=95 mm)

No experimental results were available to compare to the numerical results for walls with high eccentricities. However, it was decided to include the numerical results to show a more complete pattern of behavior for eccentrically loaded plain walls. The predicted cracking patterns are shown in Fig.6.22. Both walls failed due to debonding which led to the subsequent instability mode of failure. For the 75 mm eccentricity some cracks in webs were predicted, while only one web element cracked and extensive debonding occurred in the case of the wall with the 95 mm eccentricity.

The results of the analyses for walls with very high eccentricities of load indicate the deficiency of the model concerning modeling the debonding along the mortar bed joints and its effect on capacities of walls. The limited number of elements used caused the tensile bond strength of the wall to be overestimated. Stresses were calculated in the center of each bond element which meant that, to cause debonding based on the calculated tensile stresses in the middle of the face shell, the stresses at the extreme fiber had to be larger than the assumed tensile bond strength. The increased number of elements along the thickness of wall would improve accuracy of analysis and probably would result in lower predicted wall capacity.

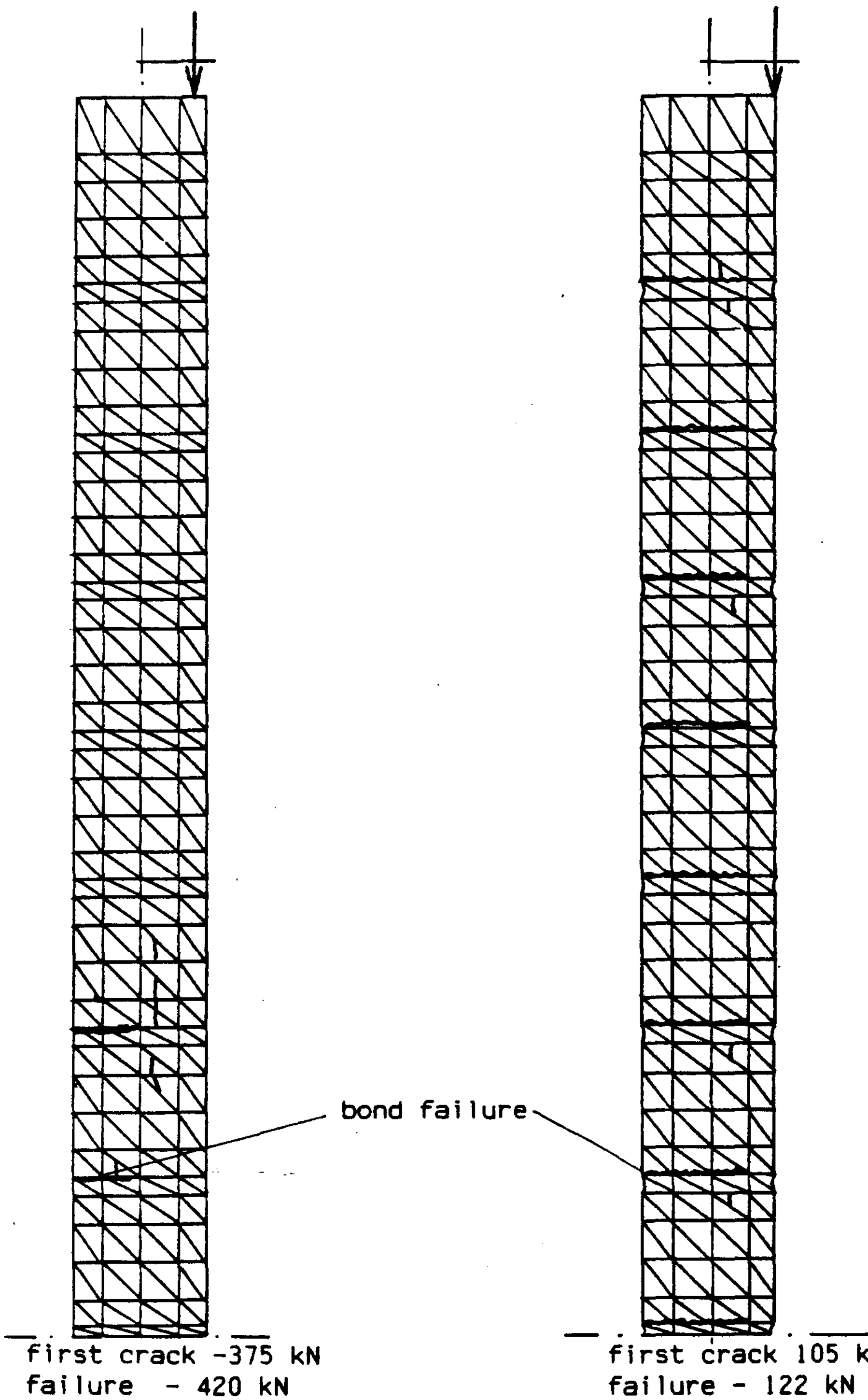

a) Predicted Cracking Pattern
e = 75 mm

b) Predicted Cracking Pattern
e = 95 mm

Fig.6.22 Predicted Cracking Patterns for Plain Walls Loaded with Initial Eccentricities of 75 mm and 95 mm.

6.2.2.8 Summary of the Results for Plain Walls

The numerical analysis was shown to be capable of close prediction of the behavior of walls with one dominating mode of failure. The following sequence of failure modes was established:

1) Low eccentricity ($0 \leq e \leq t/6$)- material failure, cracking of webs;

2) Middle eccentricity ($t/6 < e <$ kern distance) - material failure, crushing of face shells of blocks;

3) Large eccentricity ($e >$ kern distance) - instability failure, debonding of blocks and mortar.

The numerical analysis was not able to predict the exact eccentricity, where the instability failure mode started. An increased number of joint elements along the thickness of wall would improve the accuracy of the analysis.

The predicted load-moment and load-strain relationships were close to the experimental results in the elastic range. However, there was an increasing discrepancy between experimental and numerical results at high strain levels, where the inelastic deformations occurred. Deflections, with the exception of wall P2, were underestimated due to higher displacements in the actual walls resulting from lower actual stiffness then assumed in the model.

6.2.3 Reinforced Walls

6.2.3.1 General

Modeling of the reinforced concrete block walls is very complicated, since these walls are composed of four different materials:

concrete, grout, mortar and steel. In addition it is necessary to model the behavior in the planes of contact between the different materials. The details of the proposed numerical model were presented in Chapter 5.

The proper representation of the actual geometry of wall was the other important factor in modeling of its behavior. Sketches of the actual and the chosen equivalent geometry are shown in Fig.6.23. As in the case of plain walls, the 40 mm width of the mortar strips and block face shells was assumed. It was found that, in the plane of mortar bed joint, the cross section of the grout columns was significantly reduced compared to the maximum area of the cores in the blocks. Two factors are important:

1. Cores in blocks in successive courses were not aligned, as can be seen in Fig.6.23a;
2. Penetration of the mortar, which overlapped the blocks, additionally reduced the active cross section of grout.

The approximate minimum dimensions of one continuous grout core in the plane of the bed joint was assumed to be equal to 99.5x90 mm rectangle, based on the actual dimensions of elements of wall and taking in to account the factors mentioned above. Since the 110 mm thickness of grout cores used in the model resulted from the assumption of 40 mm mortar strips with the total wall thickness of 190mm , the width of grout had to be reduced to be equivalent to the actual stiffness of the grout cores. The criteria of equivalent axial stiffness or bending stiffness could be used. The equivalent moment of inertia was chosen since the behavior of the reinforced walls in out of plane bending is

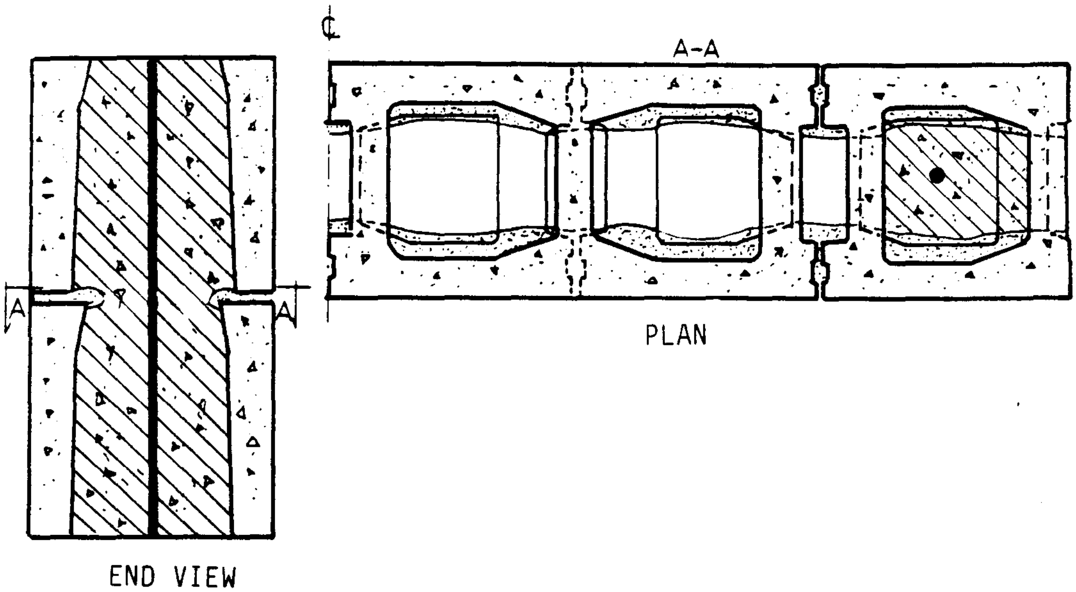

a) Actual Reinforced Concrete Block Wall

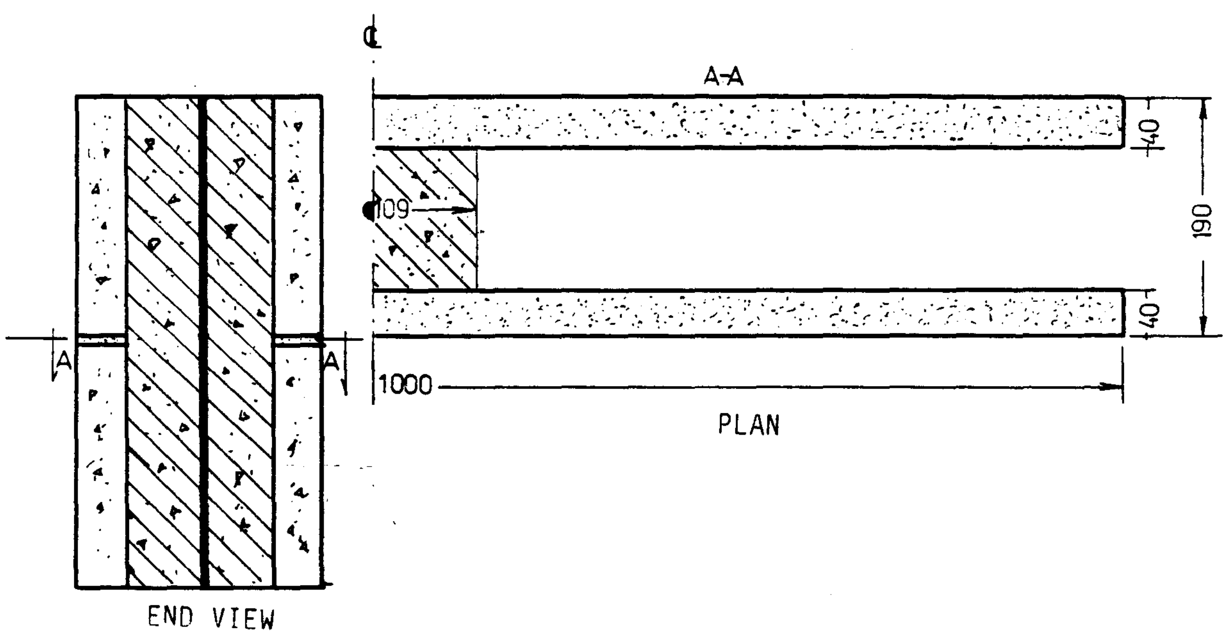

b) Equivalent Reinforced Concrete Block Wall

Fig.6.23 Actual and Equivalent Reinforced Wall Geometries.

the subject of the current analysis. For a specimen with two grouted cores, the thickness of a grout element was calculated from the following equation:

$$2x(\ 99.5 \times 90.^{3})/12 = (X \times 110^{3})/12$$

thus, X=109, as is shown in Fig.6.23b. This assumption was fairly conservative, but justified taking into account that this was the section where most probably the improper casting of grout and cracking due to shrinkage can occur. The area of grout displaced by the reinforcement was not excluded and the mortar on the webs was not taken into consideration since webs were not aligned.

The width of the elements representing block webs and grout cores was calculated as transformed area of the weaker material, in this case, concrete of the blocks. Thus, the calculated element thickness was:

$$8 \times \text{min. web thickness} + 2 \times \text{width of grout core} \times (E_{grout}/E_{block}) =$$
$$8 \times 26\ \text{mm} + 2 \times 114\ \text{mm} \times 17410/18216 = 426\ \text{mm}$$

The numerical results of the analyses of the walls with the assumed geometry discussed above and the corresponding experimental results are summarized in Table 6.1. The failure loads versus the initial eccentricity are presented in Fig.6.24 and the corresponding interaction diagram is shown in Fig.6.25. The predicted and experimental results, shown in Figs 6.24 and 6.25, are consistent with results of other experimental and analytical investigations. In the case of concentric compression, Hamid[(40)] found that the actual capacity of grouted concrete masonry was lower than that predicted from the elastic analysis, using transformed sections. Similar results were obtained from analyses using the current model. The experimental capacities of grouted

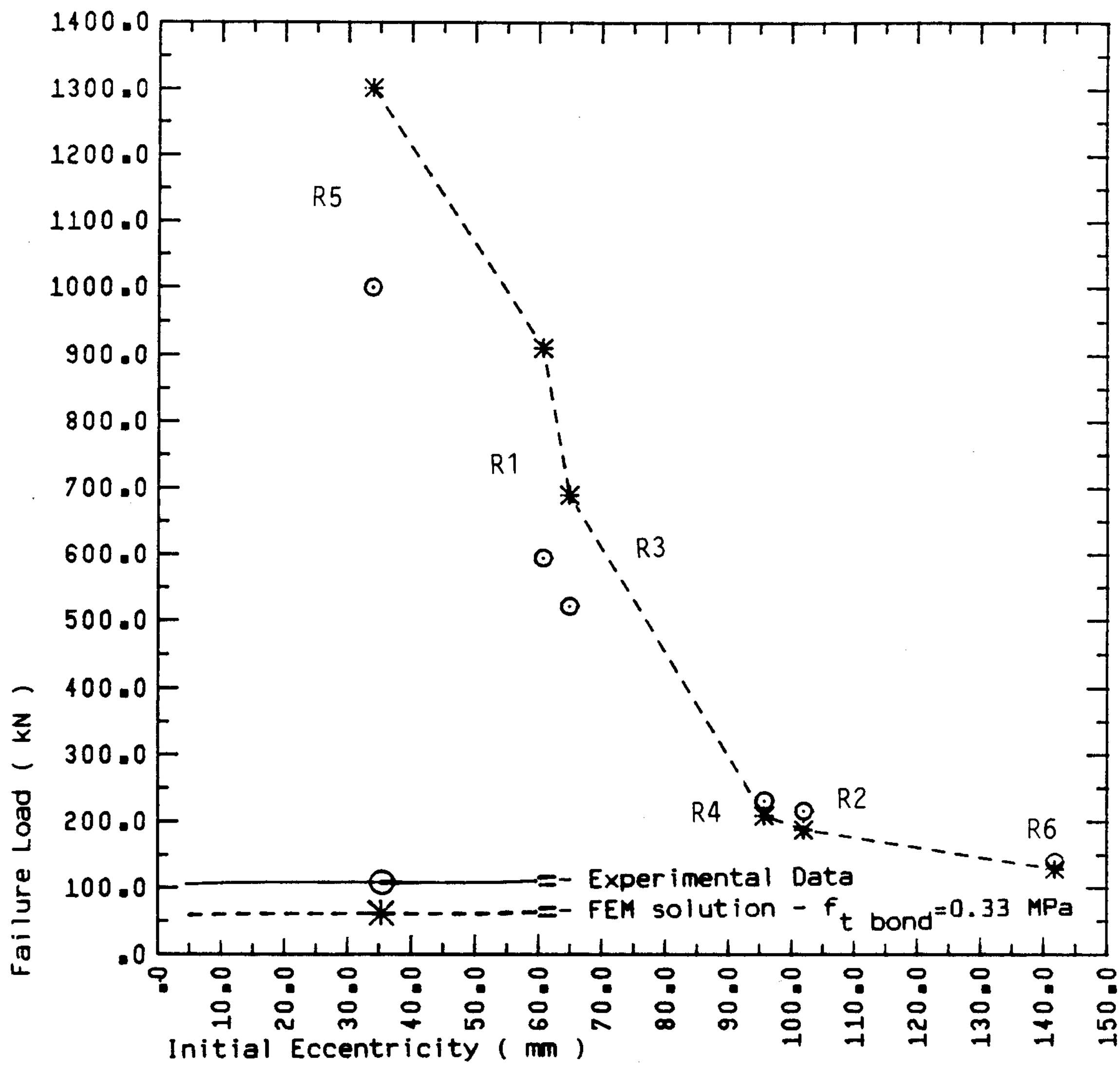

Fig.6.24 Experimental and Numerical Capacities of Reinforced Concrete Block Walls.

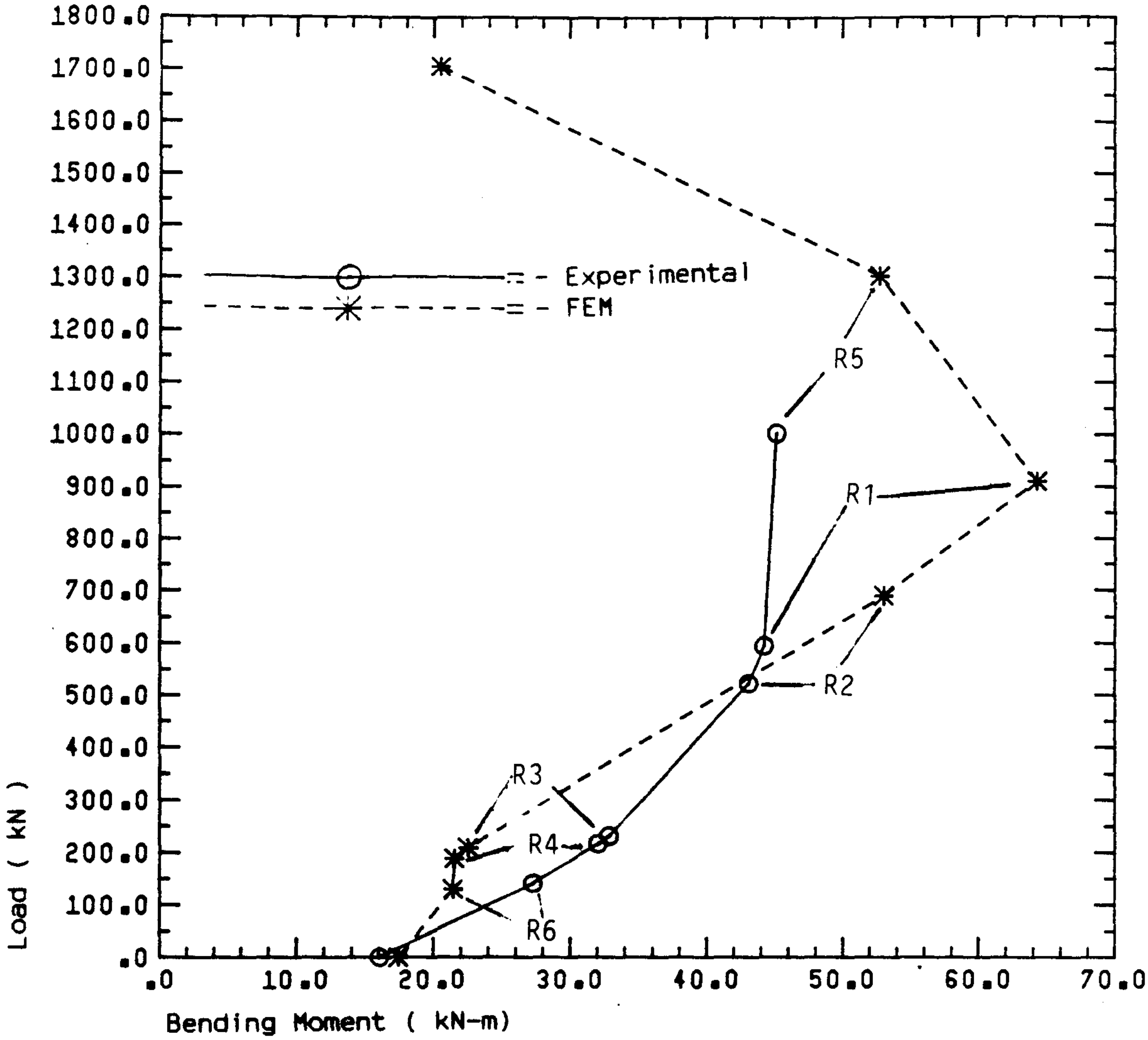

Fig.6.25 Interaction Diagram for Reinforced Walls.

prisms were lower than predicted despite a very conservative assumption concerning the contributory area of grout. In the case of eccentric loading Drysdale and Hamid[33] showed that the simple elastic analysis using transformed stiffness could not properly explain the significant increase in bending capacity of the grouted block walls compared to the ungrouted masonry. But difference between the experimental and the predicted results, obtained as a result of present analysis, could also result from the overly conservative assumption of the equivalent area of grout.

The assumption of ideal bond between the grout and the blocks seemed to be proper since no visible cracks or separation of grout cores took place during the tests. However, it was possible that microcracking or separation of grout cores took place. As was suggested by Nunn et al[58], the strength of the bond between the blocks and the grout could change the capacity of grouted masonry in bending up to 50%. This phenomenon seemed to have more effect on walls loaded with low eccentricities, where significant shear stresses could be developed on the compression side of wall. These shear stresses resulted mainly from the difference in vertical deformations of solid grout cores and blocks.

It is suggested that the higher stiffness of continuous grout columns, compared to blocks and mortar, meant that more load was carried by the grout cores. Then the higher lateral deformation of grout than of blocks, added to mortar causing significant lateral stresses in blocks, resulted in vertical cracking of block webs and decrease of capacity of grouted walls. These phenomena did not influence the behavior of walls loaded with high eccentricity, where the compressive stresses in the grout were relatively low. The predicted capacities of such walls were close to the experimental results.

Some reasons for discrepancies for the interaction diagram shown in Fig.6.25 were summarized above. There are certain factors concerning the behavior of walls loaded with high eccentricity which require explanation. It is suggested that the higher test values for the maximum bending moments than those predicted were caused by high inelastic deformations. This effect was illustrated in Fig.4.35 which showed the experimental load-deflection results for reinforced walls. Due to the higher stiffness of the model, the predicted maximum lateral displacements were 45 to 75 % lower than the corresponding experimental results near failure.

The moment capacity of the reinforced wall in pure bending was closely predicted. The slightly lower experimental value could result from the testing procedure, since the specimens used in these tests had been previously tested under eccentric loading. However it is believed that it should not have influenced the ultimate capacity of walls.

In the following sections the results for the individual walls are discussed. Discussion of Walls R1 and R2 were omitted since the experimental and numerical results are similar to the results for walls R3 and R4, respectively. All results are summarized in Table 6.1.

6.2.3.2 Results for Wall R3 (e=65 mm)

Wall R3 failed in the instability mode of failure due to debonding, whereas, the material mode of failure was predicted using the numerical model.

As was suggested in Section 6.2.2.2, concerning the results of the numerical analysis for plain wall loaded with an eccentricity similar to Wall R3, the limitations of the model resulted in lower tensile bond stress between blocks and mortar than actually occur. This inaccuracy of the analysis led to prediction of cracking in the webs of block and final failure due to crushing of block face shell. In the actual wall, the debonding between blocks and mortar occurred first. Therefore the tensile stresses in webs were released and the wall failed due to instability.

The predicted and experimental cracking patterns are shown in Fig.6.26. The difference in failure modes resulted in 32% overestimation of the predicted failure load. The load strain results for the failure region are shown in Fig.6.27. The experimental results represent strains measured over the midheight mortar bed joint. The predicted curvatures represent the relationships over the first joint above midheight, to include regions of high tensile and compressive stresses. The similarity of the experimental and numerical curves in the elastic range can be seen. Close to failure the discrepancy resulting from the higher stiffness of the model is apparent. The load-moment relationships, shown in Fig.6.28, follow the same pattern. Close to failure, where inelastic deformations are significant, large differences between numerical and experimental results can be seen.

6.2.3.3 Results for Wall R4 (e=96 mm)

The experimental and predicted cracking patterns at failure are

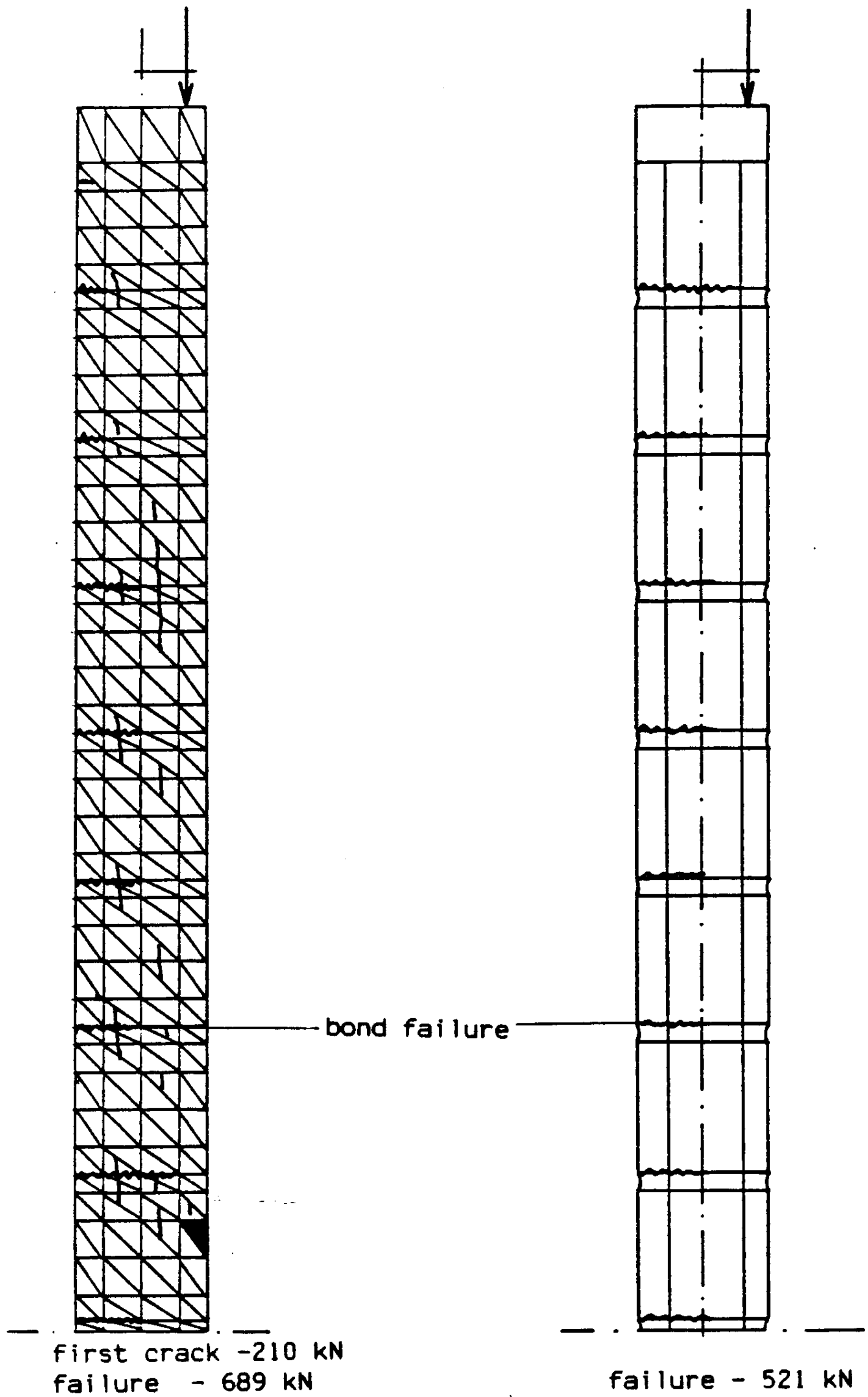

a) Predicted Cracking Pattern b) Experimental Cracking Pattern

Fig.6.26 Cracking Patterns for Wall R3.

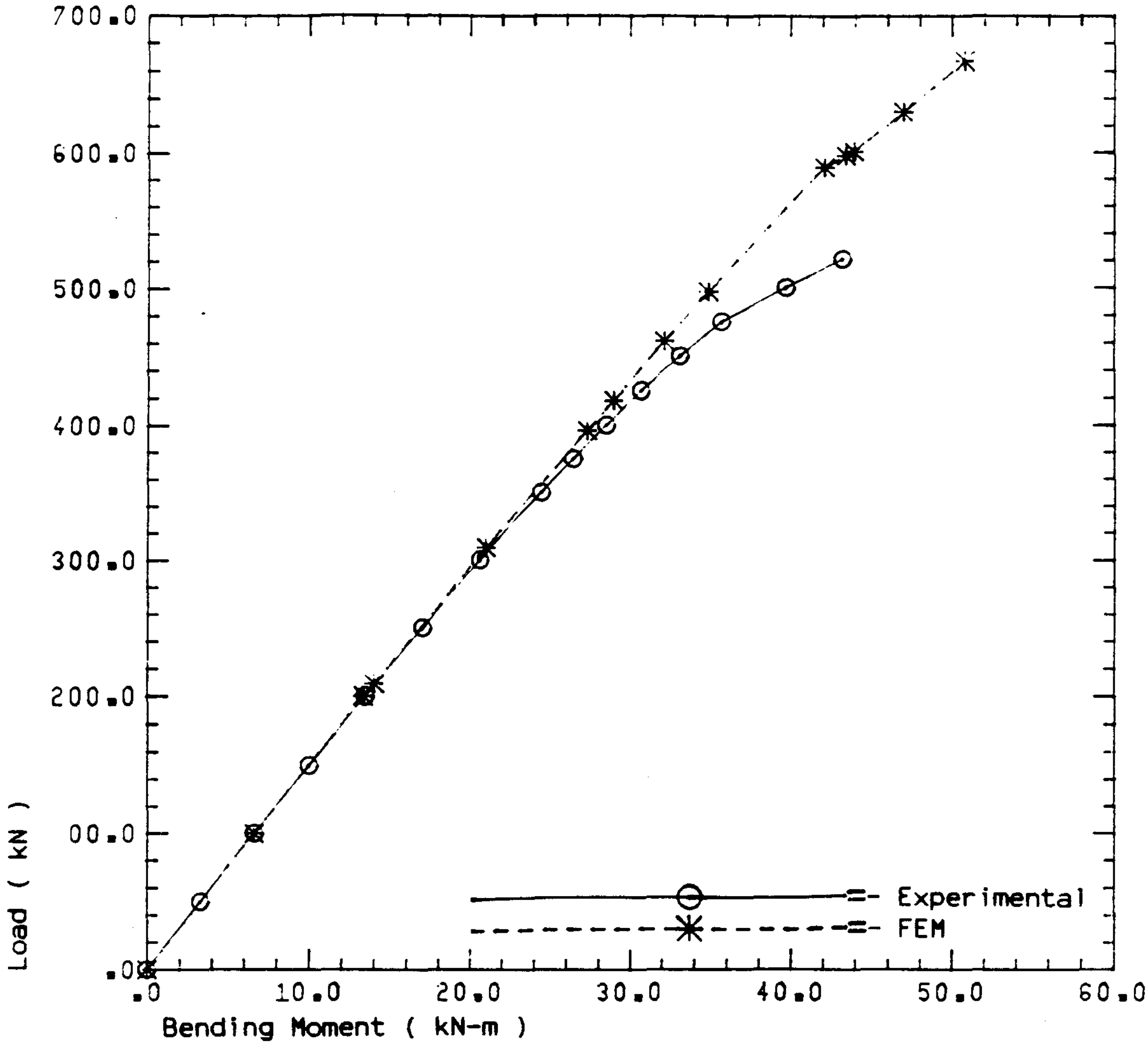

Fig.6.27 Experimental and Numerical Load-Moment Relationships for Wall R3.

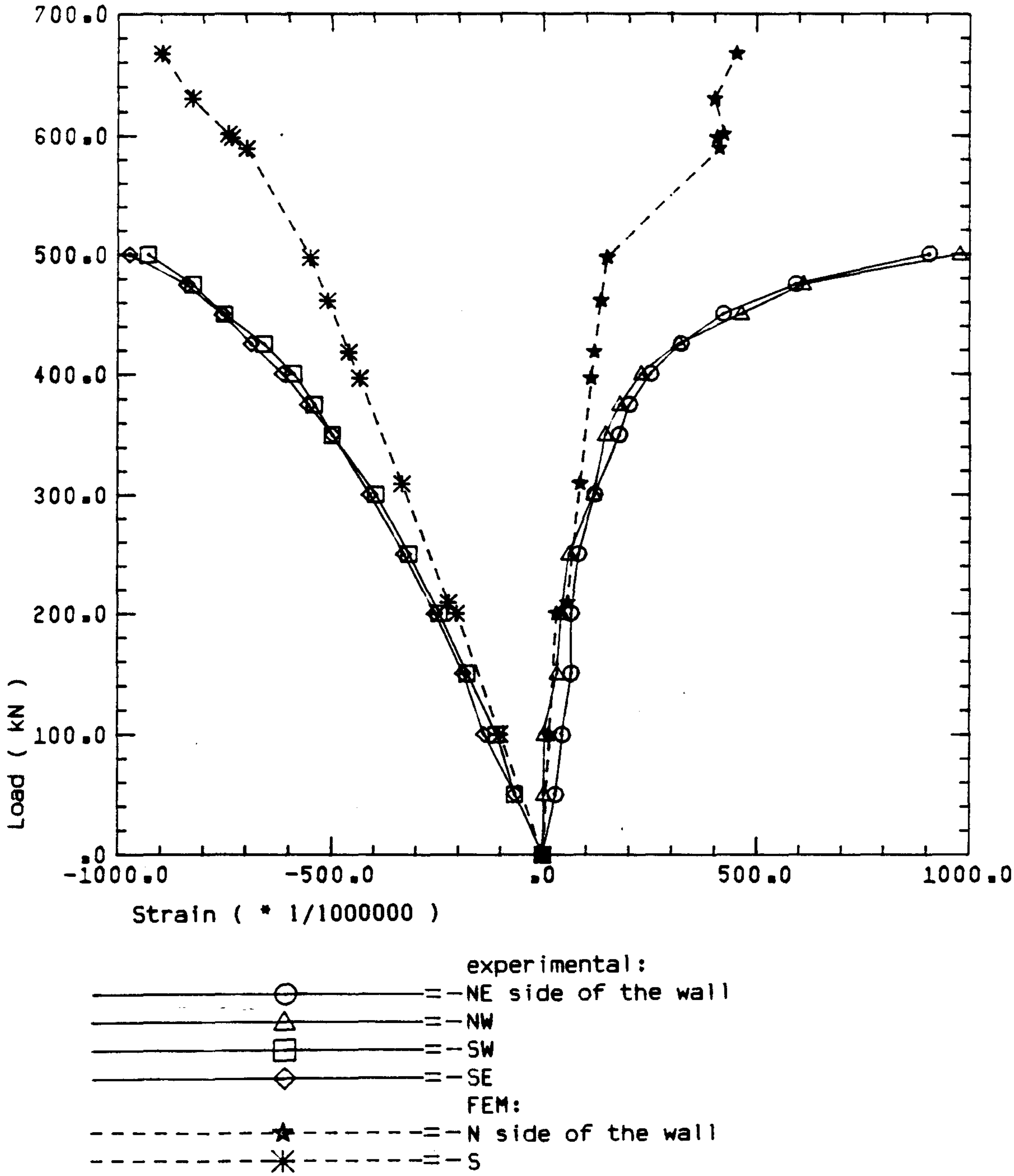

Fig.6.28 Experimental and Numerical Load-Strain Relationships for Wall R3.

shown in Fig.6.29. The instability mode of failure and failure load were closely predicted. The load-moment relationships, shown in Fig.6.30, are very close in the elastic range. The load-strain relationships are shown in Fig.6.31. Initial stiffness of the wall was accurately predicted but close to failure the inelastic deformation caused large differences between experimental and numerical curves.

6.2.3.4 Results for Wall R5 (e=34 mm)

Wall R5 failed in the material mode of failure due to crushing of grout and face shells of blocks . In addition, separation of grouted columns at the ends of the wall from the rest of wall occurred. The predicted failure load was 30% higher than the experimental capacity. However, higher capacity of the wall could be expected if the separation was prevented. The numerical analysis predicted material failure, as is shown in Fig.6.32. The crushing of face shells and grout reproduced the actual failure very accurately. The experimental and numerical load-moment results are shown in Fig.6.33. As was observed previously, the initial elastic part is predicted closely. At higher loads, the actual wall was more flexible than the model. Thus, the predicted moments at the midheight were lower than experimental values at the same load levels. The predicted strains, shown in Fig.6.34, are lower than the experimental values on the more loaded face and higher on the less loaded face of the wall. The discrepancy could be caused be the inelastic deformations and separation of the grouted ends of wall.

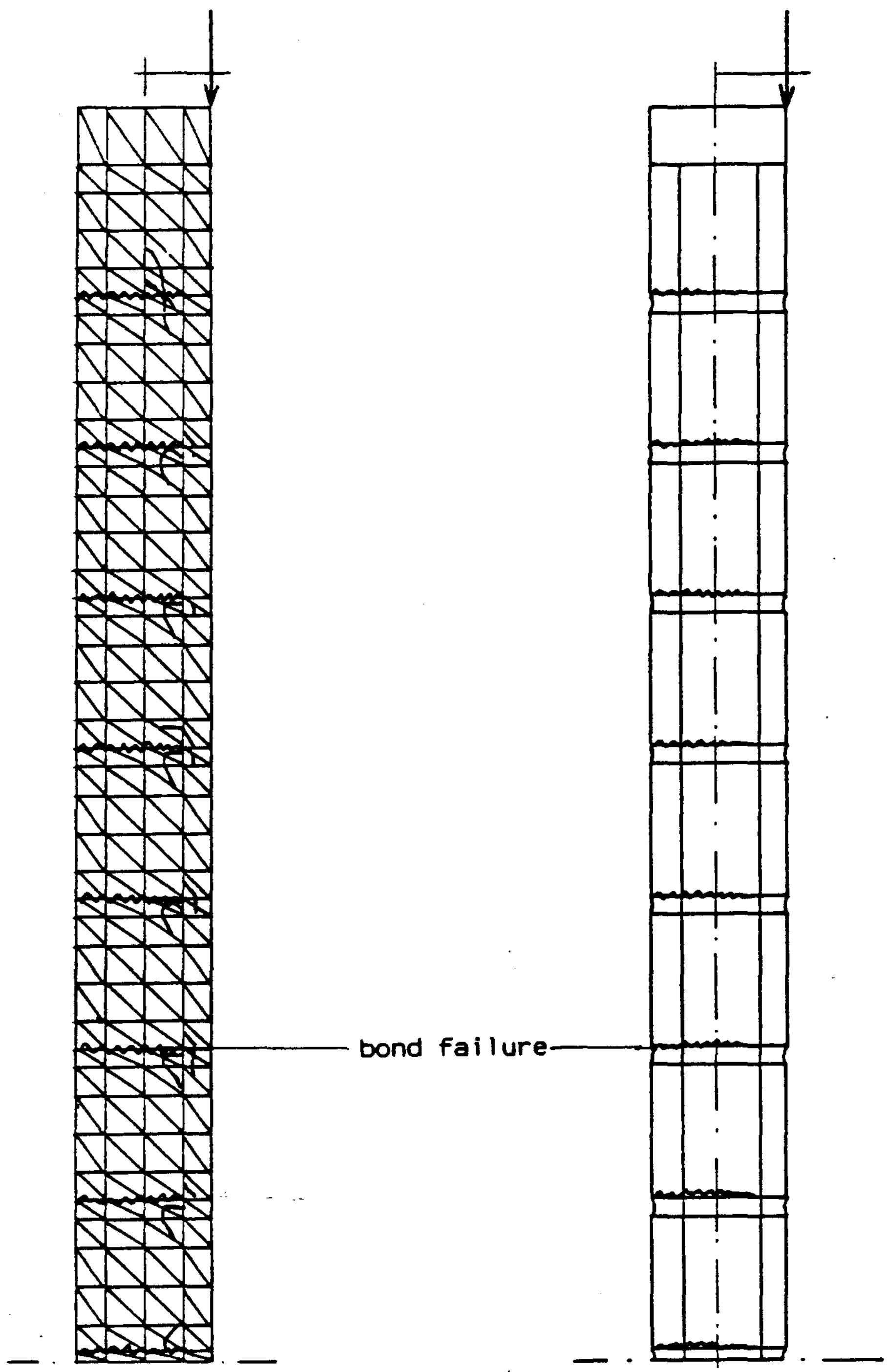

bond failure -53 kN
failure - 208 kN

failure - 231 kN

a) Predicted Cracking Pattern

b) Experimental Cracking Pattern

Fig.6.29 Cracking Patterns for Wall R4.

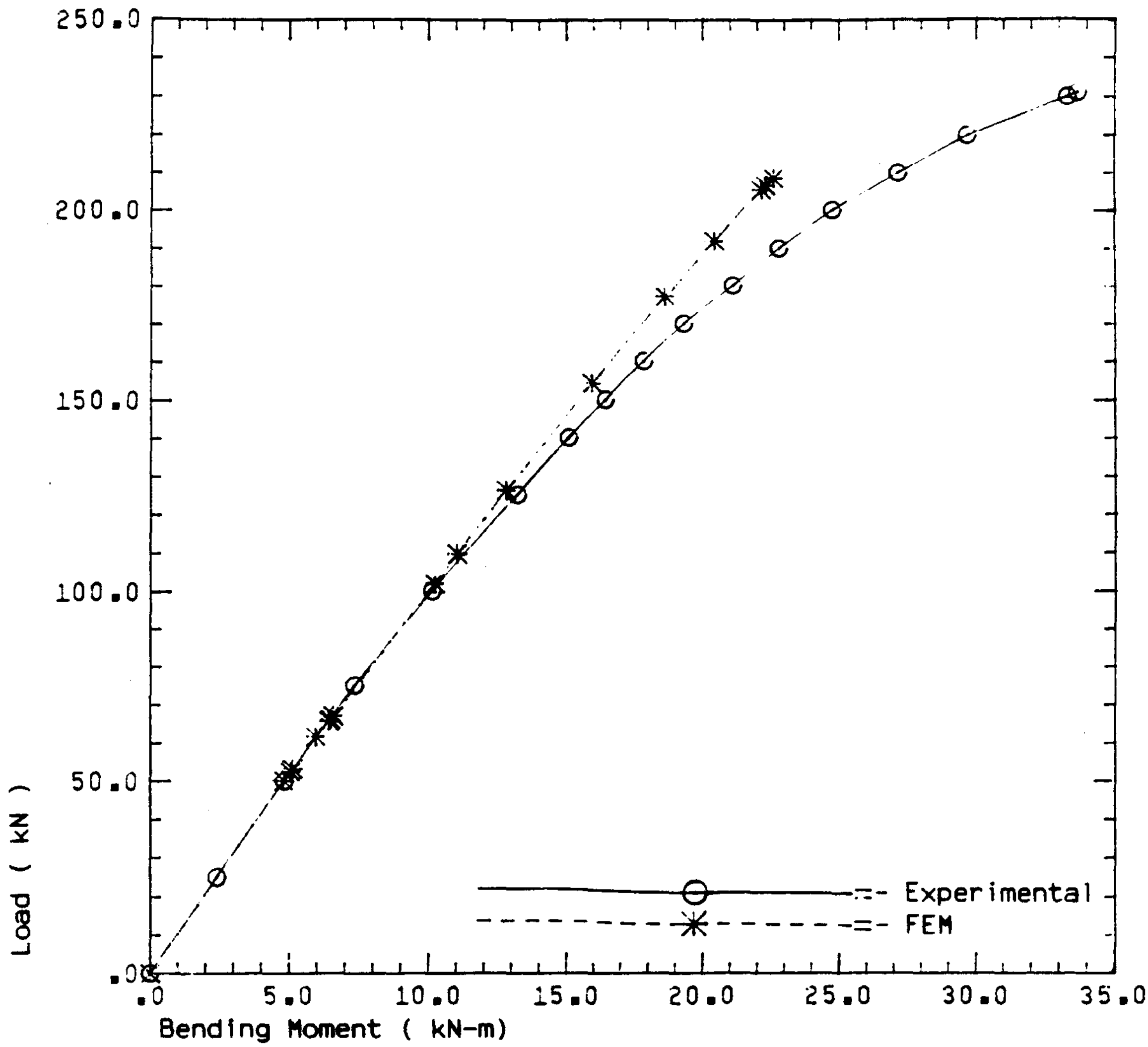

Fig.6.30 Experimental and Numerical Load-Moment Relationships for Wall R4.

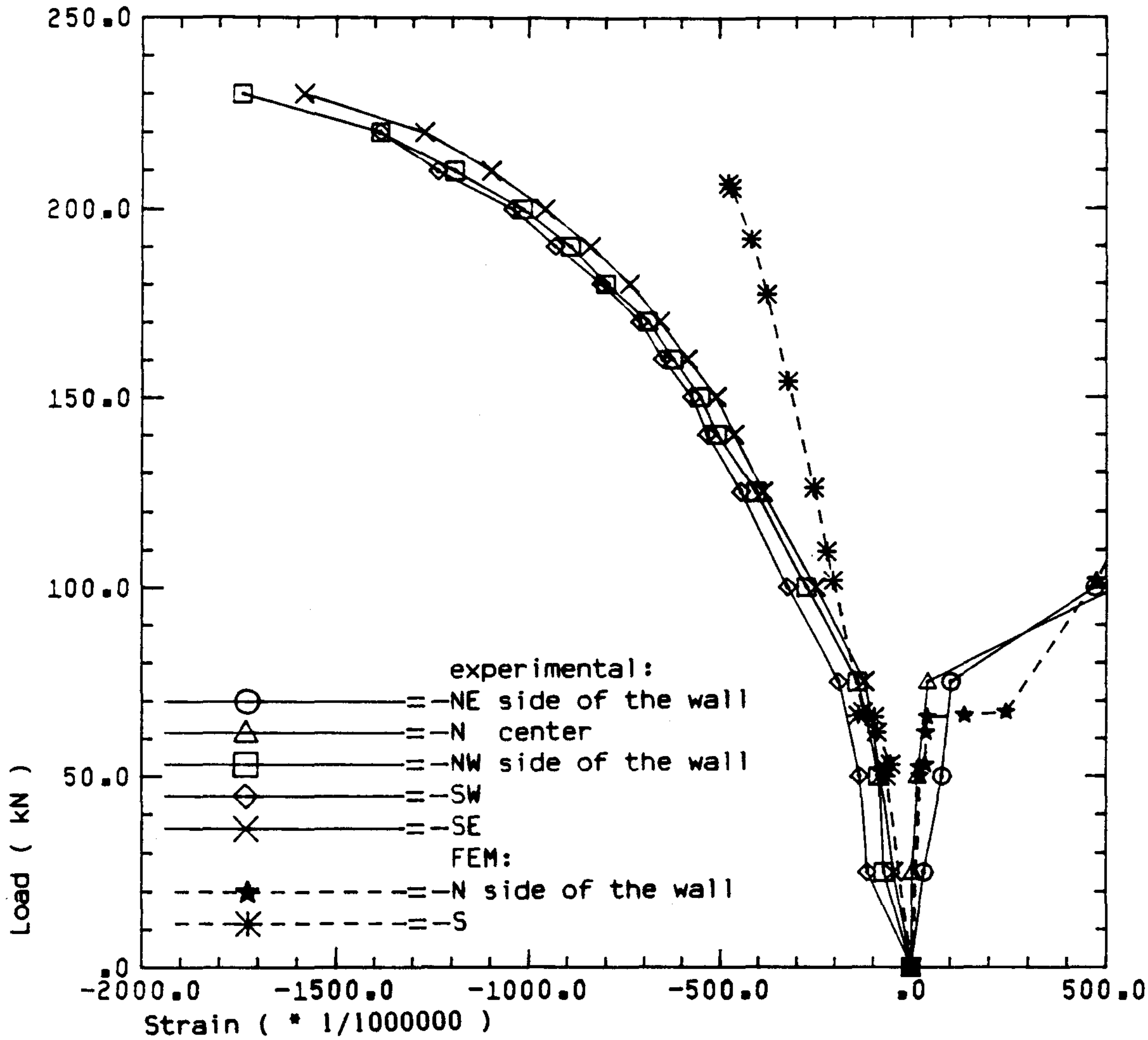

Fig.6.31 Experimental and Numerical Load-Strain Relationships for Wall R4.

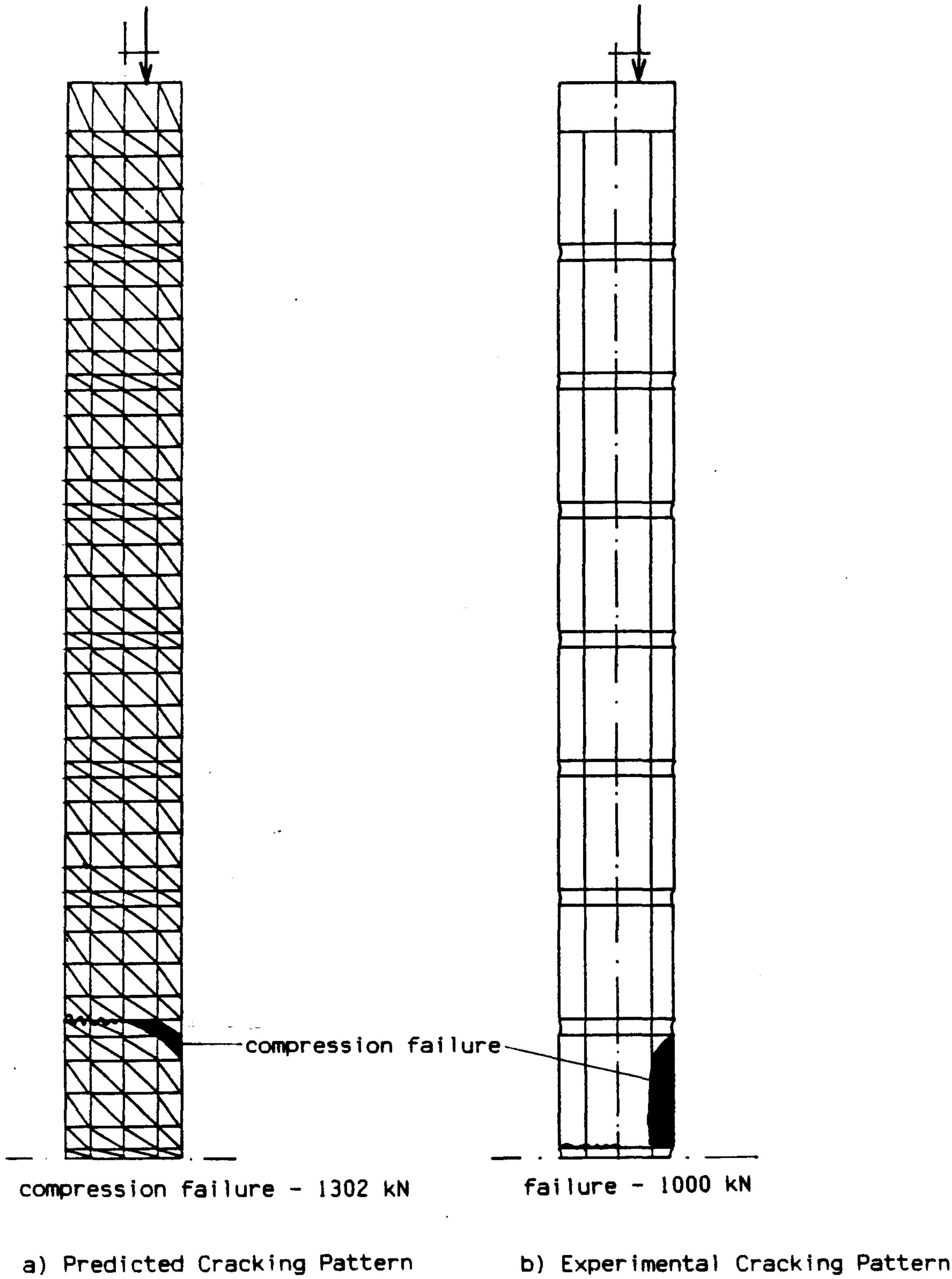

Fig.6.32 Cracking Patterns for Wall R5.

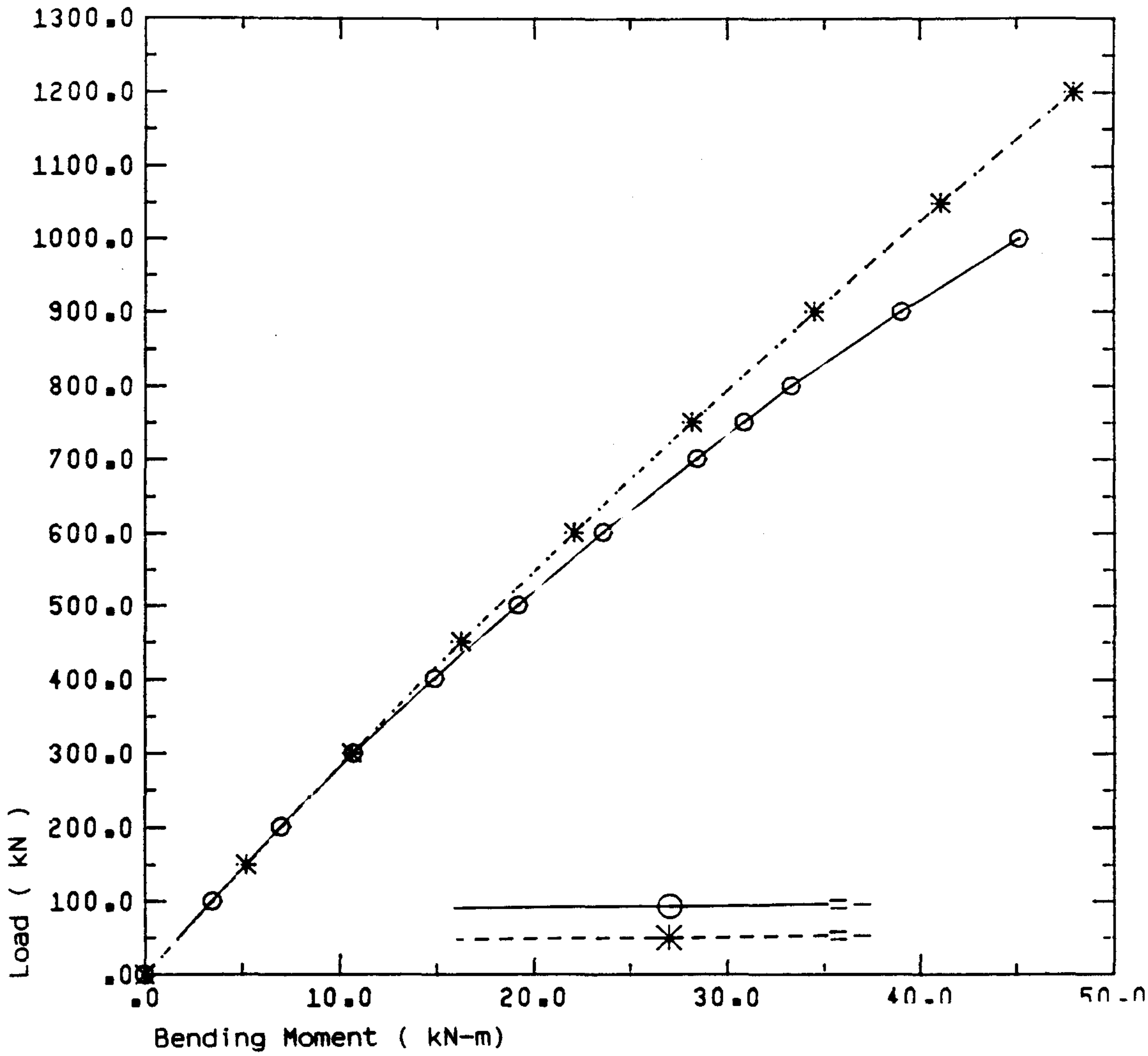

Fig.6.33 Experimental and Numerical Load-Moment Relationships for Wall R5.

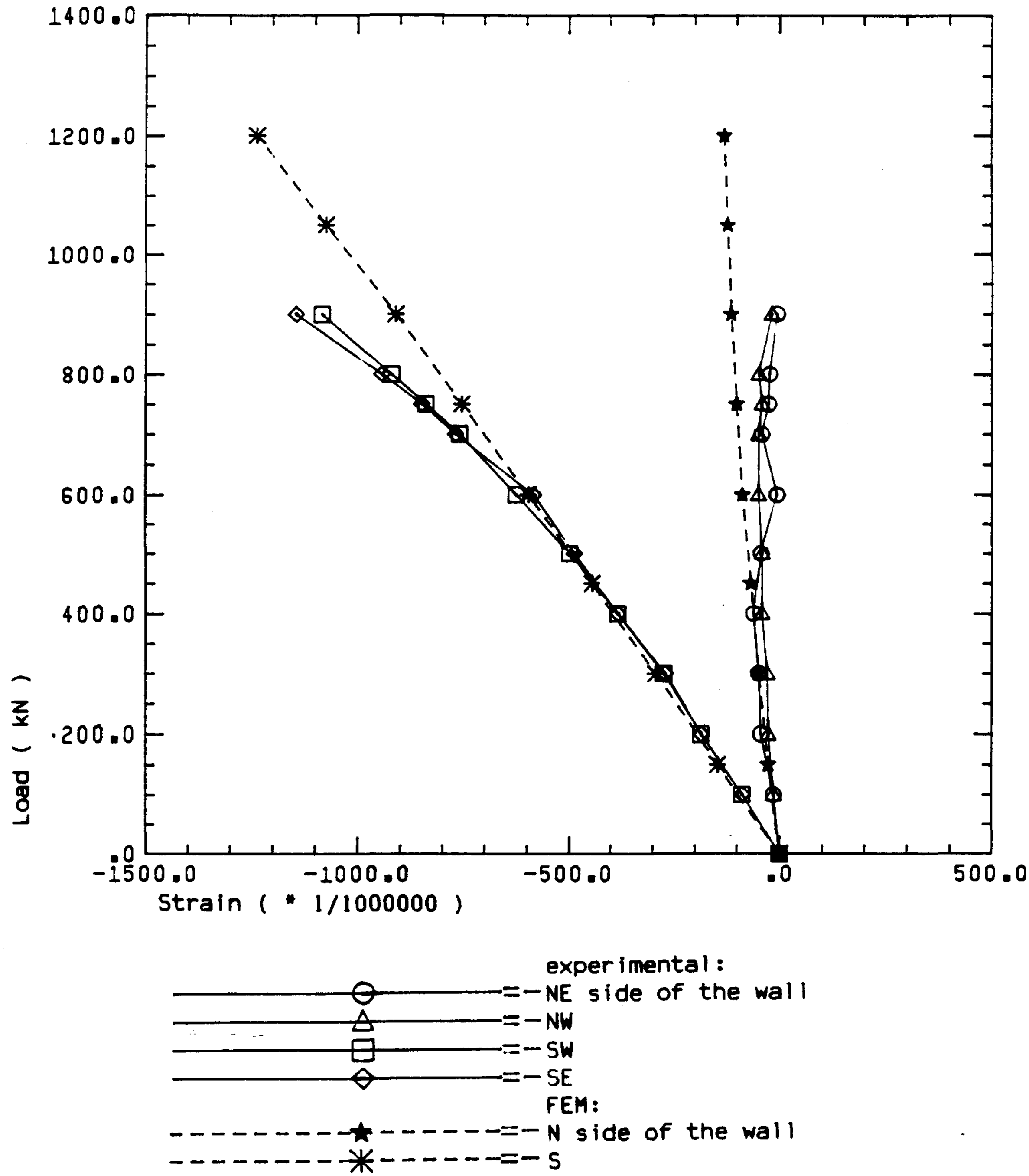

Fig.6.34 Experimental and Numerical Load-Strain Relationships for Wall R5.

6.2.3.5 Results for Wall R6 (e=142 mm)

The numerical analysis predicted the behavior of Wall R6 very accurately, as can be seen in Fig.6.35. Similarly, the experimental load-moment relationship, shown in Fig.6.37, was closely estimated by the model. The load-strain relationships are shown in Fig.6.36. Initial stiffness was closely predicted. However the malfunction of the load cell, used during the test, forced unloading of the wall at a load equal to 40 kN. Later the wall was loaded again to failure. This testing procedure likely caused some loss of stiffness of the wall since the first load had exceeded the elastic range, causing mortar debonding along bed joints (cracking) and the wall did not return to its initial shape. In spite of this, it is believed that the ultimate capacity was not affected.

6.2.3.6 Results for Wall S1 (e= B)

For the flexural test of Wall S1, only the cracking pattern is shown in Fig.6.38. Strains and deflections were not compared since the specimens had been tested previously as eccentrically loaded walls and had existing cracks along the mortar bed joints. However, this cracking should not have affected the ultimate moment capacity of the wall. The predicted crack pattern closely reproduced the actual failure mode. The moment capacity was closely predicted, as well.

6.2.3.7 Summary of the Results for Reinforced Walls

The numerical analysis provided fairly close predictions of the behavior of reinforced walls for the cases with large initial

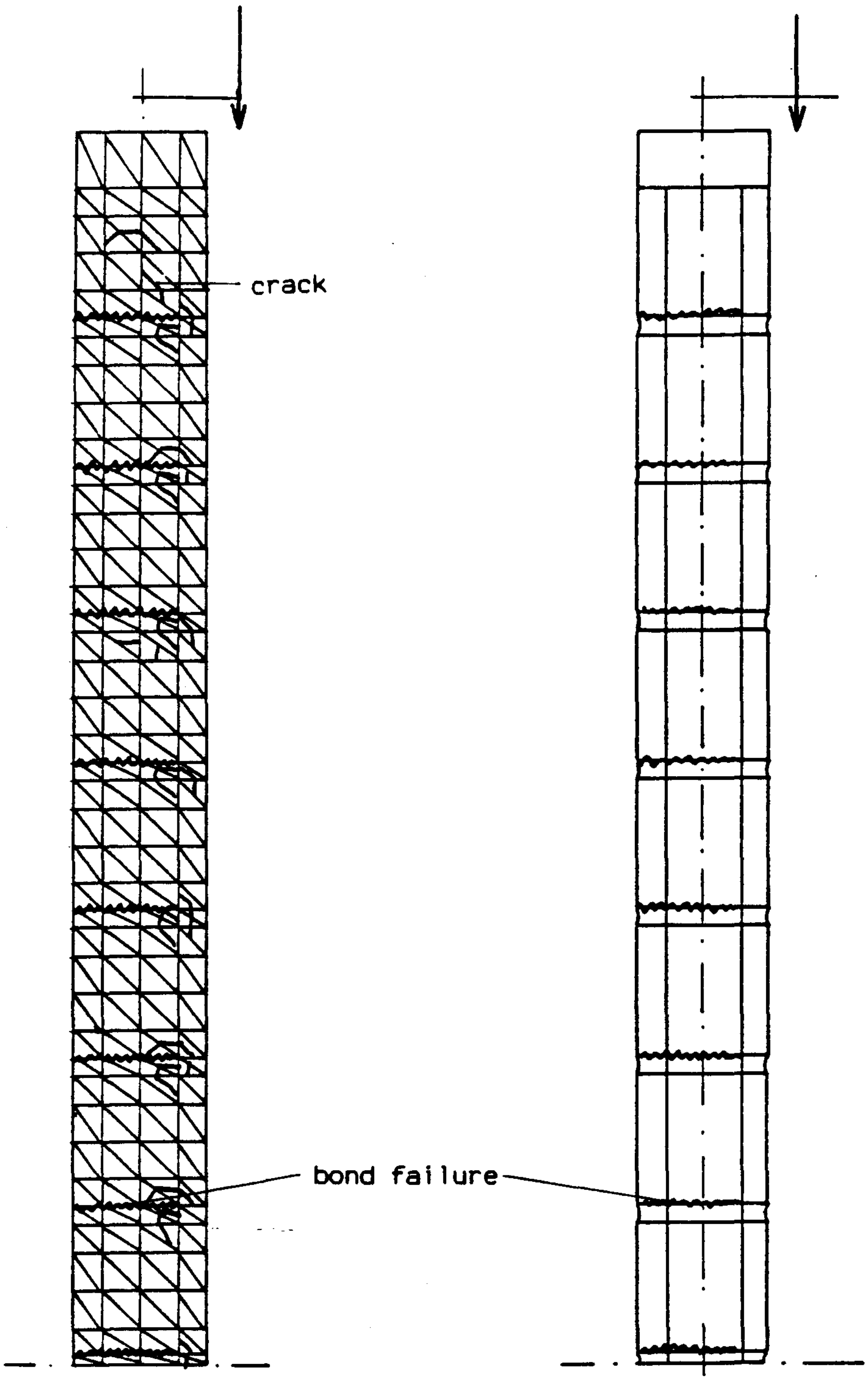

bond failure -25 kN
failure - 129 kN

failure - 140 kN

a) Predicted Cracking Pattern

b) Experimental Cracking Pattern

Fig.6.35 Cracking Patterns for Wall R6.

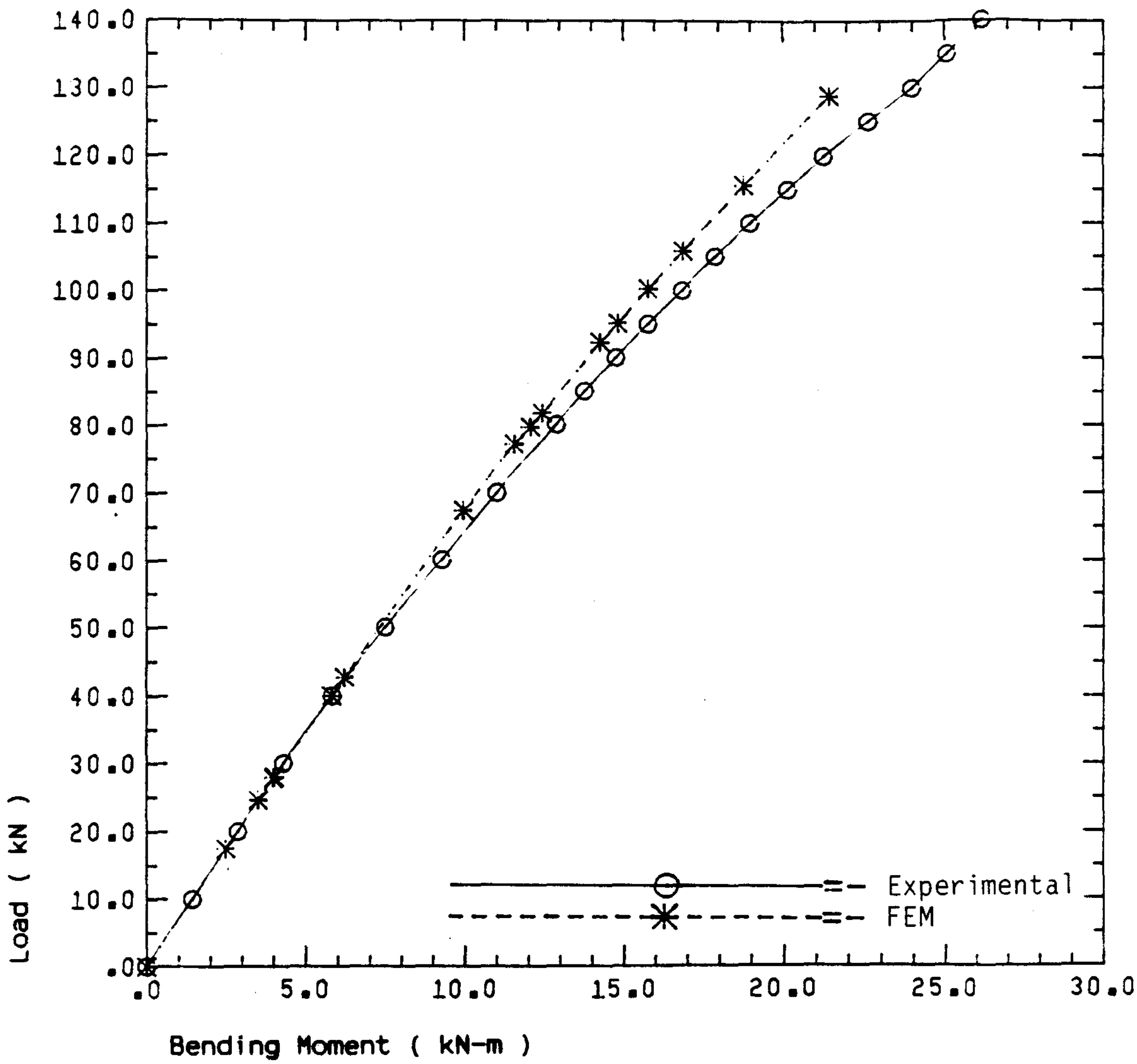

Fig.6.36 Experimental and Numerical Load-Moment Relationships for Wall R6.

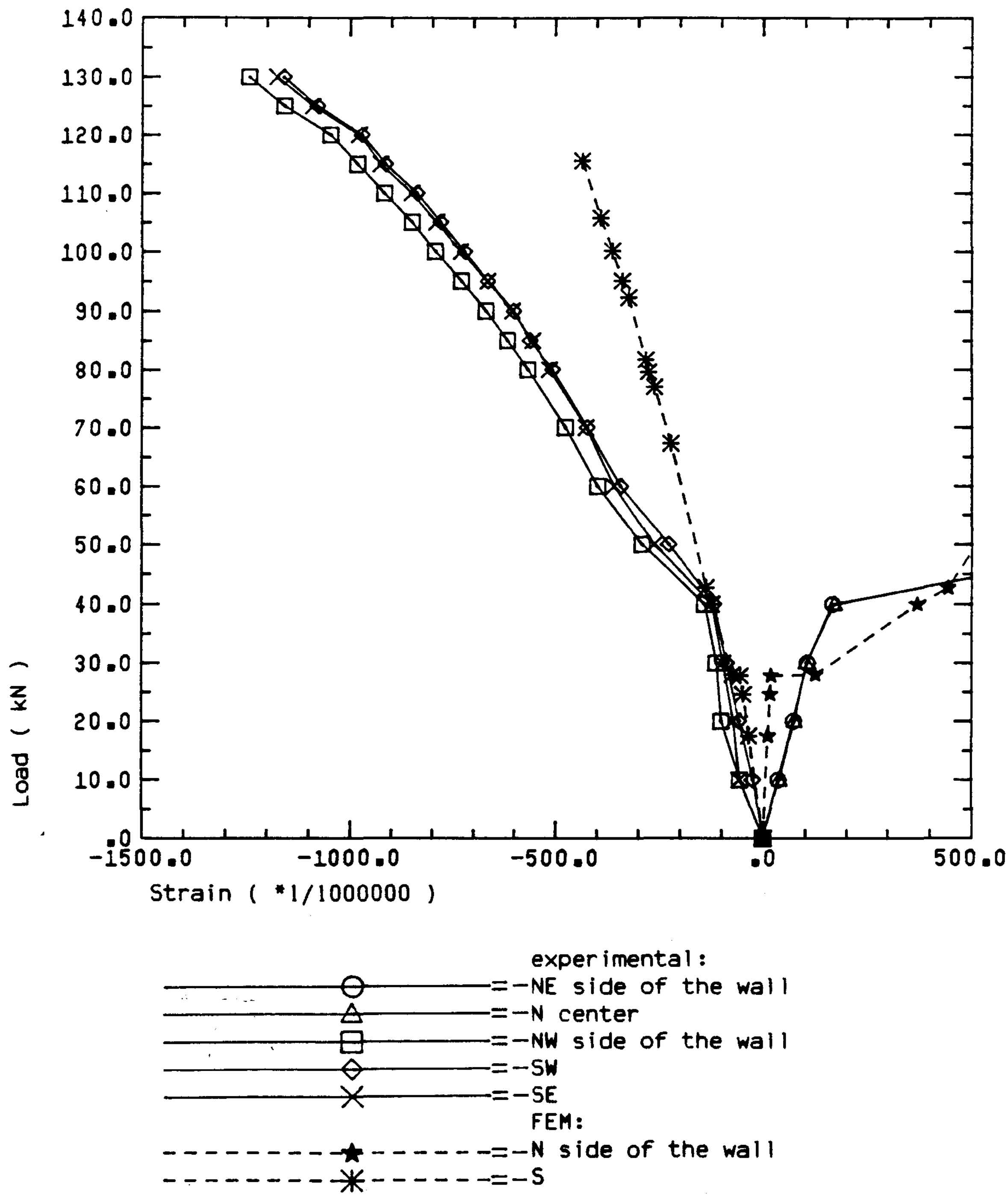

Fig.6.37 Experimental and Numerical Load-Strain Relationships for Wall R6.

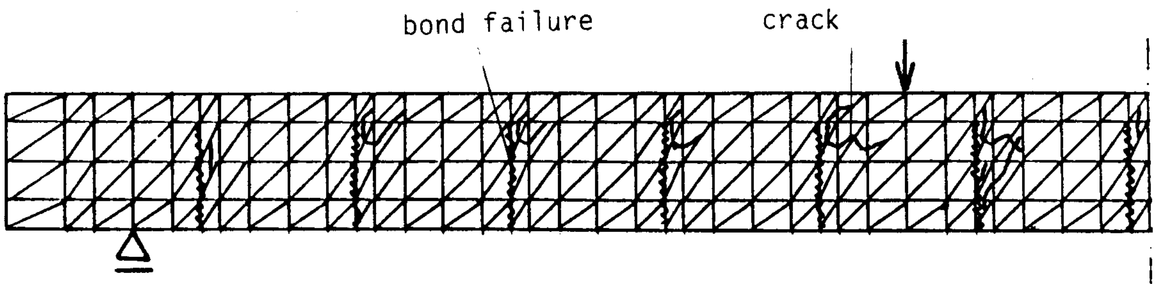

first crack - 2 kN-m
failure - 17.5 kN-m

a) Predicted Cracking Pattern

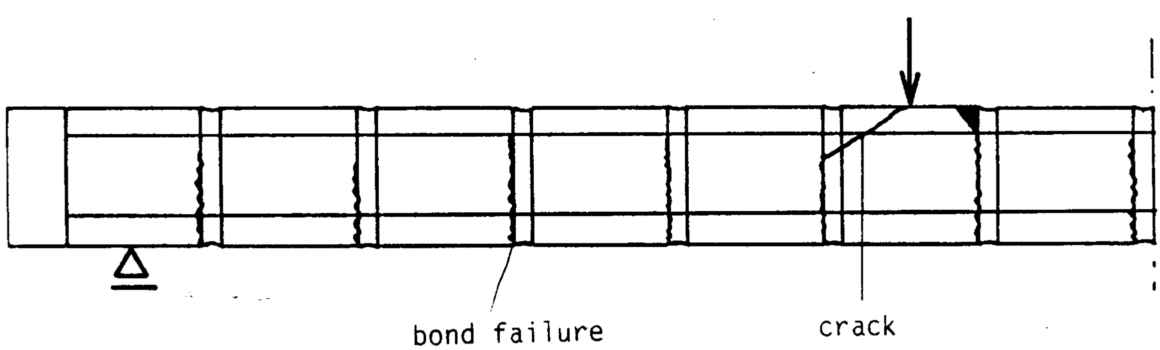

failure - 17 kN-m

b) Experimental Cracking Pattern

Fig.6.38 Cracking Patterns for Wall S1.

eccentricities. It was found that material failures dominated predicted failures for lower eccentricities. For higher eccentricities, $e = t/3$, the predicted stability failure mode was representative of the actual behavior of those walls. In the pure bending case, the predicted moment capacity, as well as the material failure were very close to experimental results.

The predicted capacities for eccentricities lower than half of the wall thickness were higher than the actual capacities. For higher eccentricities the predicted capacities were slightly lower than experimental values. Comparable displacements and strains were close in the elastic range. At higher load levels, where large inelastic deformations could be expected, there were increasing discrepancies between experimental and numerical results. Therefore, the maximum deflections from the numerical analyses were much smaller than those recorded during tests. Thus the predicted maximum moments were lower than the experimental values for the same load level. However, it should be noted that the failure modes were predicted accurately.

6.2.4 Discussion of Numerical Results

The experimental and numerical results for specimens tested as part of this study are summarized in Table 6.1. It was found that the average predicted failure load was 1.12 times the experimental failure load, with a coefficient of variation of 20%. The predicted maximum moments averaged 1.05 of the experimental moments, with a coefficient of variation of 29%. The predicted maximum lateral deflection at failure averaged 0.63 of the experimental deflection, with a coefficient of variation of 41%. This comparison indicates that the numerical model provided quite good prediction of capacity but tended to significantly underestimate deflections. The overestimation of failure loads resulted mainly from the lack of proper modeling of the inelastic behavior.

6.3 Comparison of the Numerical Results to the Experimental Results Reported by Hatzinikolas et al[44,45].

6.3.1 General

The results of the numerical analysis of 40 plain and grouted reinforced specimens are discussed in the following section. Only specimens loaded concentrically or in single curvature were considered. Also only cases of reinforced walls with vertical reinforcement were chosen for analysis, since the present model had no provisions for horizontal reinforcement. Since exact geometry and complete data concerning material properties were not available, the required information was assumed based on the data published by Hatzinikolas et al[44].

The concrete blocks used were 397x194x194 mm with two nearly rectangular cores. The minimum face shell thickness was 38 mm and the summed web thickness was 89 mm for 1 block and 241 mm for wall specimens. Since the mortar penetration was higher than the minimum face shell thickness, the authors assumed an additional 25% active penetration of mortar. This additional penetration of mortar would affect the effective area of grout columns in the cross section along the mortar bed joints. It was assumed that the area of one grout column was 98x141 mm. Therefore, as was discussed in Section 6.2.3.1, the area of grout element per grouted core was calculated as 82 mm by 118 mm thickness of grout column, based on the equivalent moment of inertia.

The bars used in the analyzed reinforced walls were:

3 - 9.5 mm diameter and 71 mm^2 area;

9 - 28.7 mm diameter and 645 mm^2 area.

The material properties were as follows:

mortar: E = 4800 MPa, n=0.3, f_c =17.5 MPa;

blocks: E = 9300 MPa, n=0.2, f_c =16.2 MPa;

grout: E = 9300 MPa, n=0.2, f_c = 16.4 MPa;

where, E = modulus of elasticity, n = Poisson's ratio, f_c = average compressive strength.

The values of modulus of elasticity for mortar and blocks and the strengths of material were published by Hatzinikolas et al [44]. The remaining data concerning mechanical properties of materials were assumed. The experimental tensile bond strength between the block and mortar in the direction perpendicular to the bed joints was 0.29 MPa.

6.3.2 Results for Plain Walls

Only 14 experimental results were reported for plain walls in single curvature bending. Those are listed along with the numerical results in Table 6.2. In general, the predicted results were close to

Table 6.2 Comparison of the Numerical Results with Experimental Results by Hatzinikolas et al[44].

Specimen Type	Initial Eccentricity	Failure Load*	Experimental Maximum Bending Moment	Experimental Maximum Lateral Defl.	Ratio FEM/Experimental Failure Load	Ratio FEM/Experimental Maximum Bending Moment	Ratio FEM/Experimental Maximum Lateral Defl.
	mm	kN	kNm	mm	kN	kNm	mm
2 bl. plain	fixed ends	350 (COV=18%)	---	---	1.27	---	---
5 bl. plain No.3,4	0	1033 (COV=10%)	---	---	0.99	---	---
5 bl. plain No.2,3	32	772 (COV=19%)	24.9**	---	0.88	0.88**	---
5 bl. plain No.4,5	64	618 (COV=20%)	39.8**	---	0.83	0.82**	---
5 bl. grout. 3 cores,No.6,7	0	1351 (COV=0)	---	---	0.90	---	---
5 bl. grout. 5 cores, No.3	0	1523	---	---	1.16	---	---
12 bl. plain Walls A1,A4	0	1114 (COV=7%)	---	---	0.81	---	---
12 bl. plain Wall A2	32	708	27.7	6.9	0.97	0.91	0.68
12 bl. plain Wall A3	64	357	29.6	18.6	1.41	1.35	0.78
12 bl plain Wall A5	76	116	9.9	9.3	3.68	3.63	0.85
16 bl plain Wall D1	0	971	---	---	1.00	---	---
22 bl. plain Wall M1	0	924	---	---	0.84	---	---
22 bl. plain Wall M2	32	534	33.4	30.3	1.23	1.26	1.06

* if more than one specimens, than an avarage failure load is given and COV - coefficient of variation;

** lateral deflections not considered in calculation of bending moment.

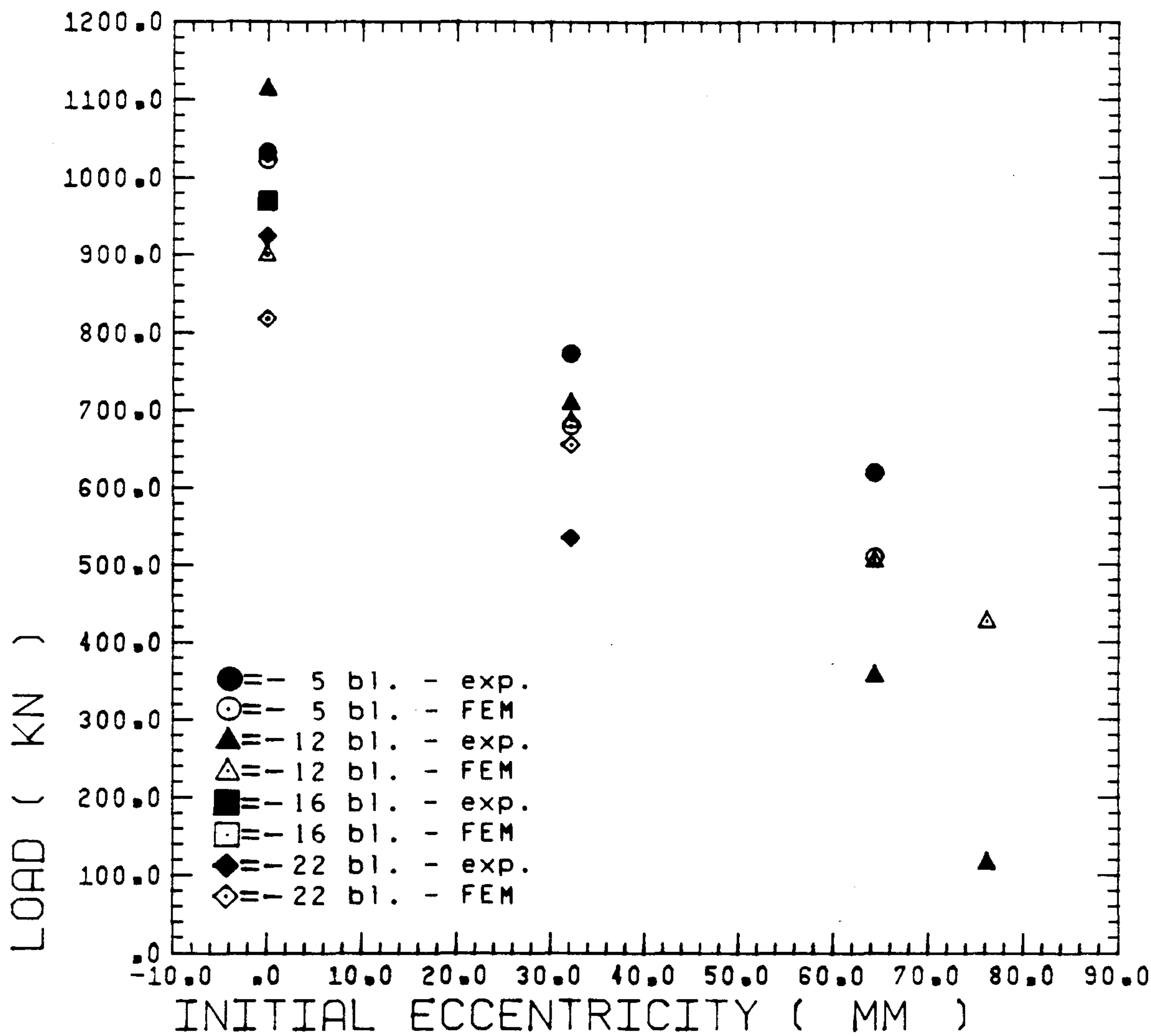

Fig.6.39 Experimental and Numerical Capacities of Plain Walls; Experimental Data Reported by Hatzinikolas et al [44].

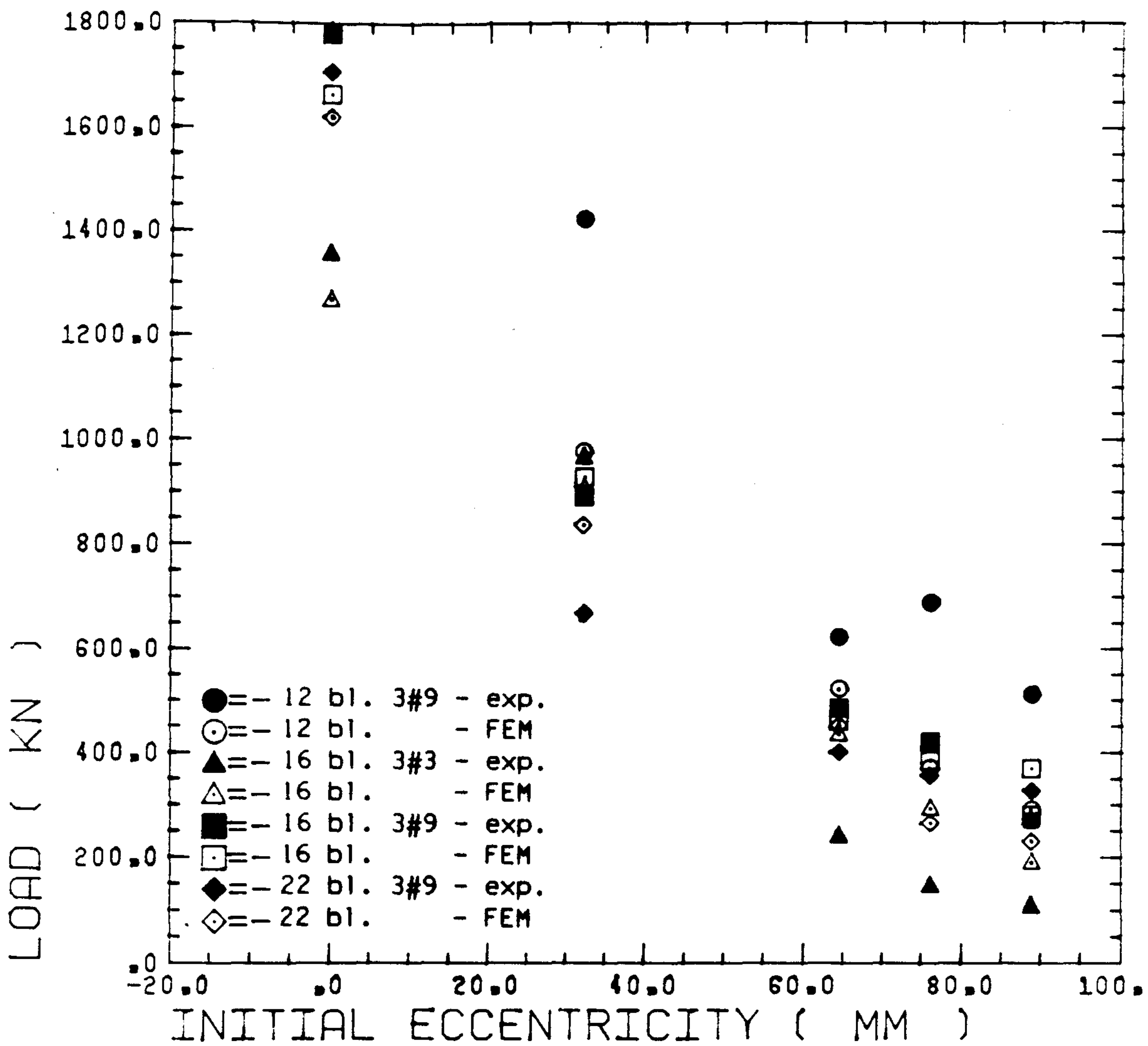

Fig.6.40 Experimental and Numerical Capacities of Reinforced Walls; Experimental Data Reported by Hatzinikolas et al [44].

the experimental results for walls loaded with eccentricities not greater than the kern distance (about 64 mm in this case). These correspond to cases where the material mode of failure occurred. The average predicted failure load was 1.02 times the experimental value, with a coefficient of variation of 21%. There was only one wall tested with a higher eccentricity and for it the predicted capacity was nearly 3.5 times higher than actual. The predicted and experimental capacities are shown in Fig.6.39.

The lack of a sufficient number of data points does not allow for firm conclusions. Only small eccentricities were tested for a few slendernesses and the predicted results were close to the experimental values for these case. However, even such a limited verification indicated the potential of the present model for predicting capacities of plain concrete block walls.

6.3.3 Results for Reinforced Walls

The predicted and the experimental failure loads are shown in Fig.6.40 as a function of the initial eccentricity for 12 block walls with 3#9 bars, 16 block walls with 3#3 bars, 16 block walls with 3#9 bars and 22 block walls with 3#9 bars.

The predicted failure loads were usually smaller than the actual results for concentric loading, nearly equal for e=t/6 and lower for the higher eccentricities. For the 16 block high walls with 3#3 bars(Fig.6.40) the predicted capacities for walls with high eccentricities were higher than the test results. However, information showing the reinforcement strains (Figs 2.95 and 2.96 in the report by Hatzinikolas et al[45]) indicates that, close to failure, complete or partial debonding may have occurred. At least, it seems to be the only reasonable explanation for the decreased strains when equilibrium of forces in the cross section of wall would suggest increases in stresses and increased strains in the reinforcement with an increase of applied bending moment.

Not all of the results reported by Hatzinikolas et al[44] were investigated. Representative cases were chosen. In general, the capacities of walls were closely predicted. Maximum moments calculated including the P-delta effects underestimated the actual maximum bending moments reached during the tests. As mentioned for McMaster tests, this resulted from the underestimation of the lateral deflections due to neglecting inelastic deformations. Since the final deflections were obtained from extrapolation of the last calculated deflection increments, there was the possibility of significant inaccuracy on the side of underestimation of deflections particularly if the load increment at failure was much higher than the last load increment for which the convergence occurred.

The predicted capacities for 16 block high walls, reinforced with 3#3 bars and loaded with high eccentricities were far off the experimental results. As was mentioned before, debonding of the bars was suspected and this would explain these low experimental results . The experimental and numerical results for reinforced walls are summarized in Table 6.3. As a general indication of agreement, the average predicted failure load was 0.90 of the experimental load, with a

Table 6.3 Comparison of the Numerical Results Experimental Results by Hatzinikolas et al(44) for Reinforced Specimens.

Specimen Type	Initial Eccen-tricity	Failure Load*	Experimental Maximum Bending Moment	Experimental Maximum Lateral Defl.	Ratio FEM/Experimental Failure Load	Ratio FEM/Experimental Maximum Bending Moment	Ratio FEM/Experimental Maximum Lateral Defl.
	mm	kN	kNm	mm	-	-	-
5 bl. reinfor. 3#3, No.12,13	0	1398 (COV=15%)	---	---	0.95	---	---
5 bl. reinfor. 3#9,No.8,9	0	1472 (COV=24%)	---	---	1.22	---	---
12 bl. reinfor. 3#9,Wall B2	32	1423	70.9	17.5	0.69	0.52	0.30
12 bl. reinfor. 3#9,Wall B3	65	623	74.7	55.4	0.84	0.55	0.27
12 bl reinfor. 3#9, Wall B4	76	689	63.1	15.4	0.54	0.54	1.03
12 bl. reinfor. 3#9, Wall B5	89	511	56.2	21.1	0.57	0.50	0.39
16 bl. reinfor. 3#3, Wall I1	0	1357	---	---	0.94	---	---
16 bl. reinfor. 3#3,Wall I2	32	965	54.1	23.8	0.94	0.84	0.76
16 bl. reinfor. 3#3, Wall I3	65	240	16.9	6.0	1.81	2.52	5.57
16 bl. reinfor. 3#3, Wall I4	76	146	11.9	5.1	2.00	2.29	3.27
16 bl. reinfor. 3#3, Wall I5	89	108	10.7	10.2	1.76	1.88	1.66
16 bl. reinfor. 3#9, Wall D2	0	1779	---	---	0.94	---	---
16 bl. reinfor. 3#9, Wall D3	32	890	48.1	21.8	1.04	0.80	0.42
16 bl. reinfor. 3#9, Wall D4	65	484	52.7	44.5	0.95	0.74	0.45
16 bl. reinfor 3#9, Wall D5	76	420	53.0	49.8	0.92	0.72	0.47
16 bl. reinfor 3#9, Wall D6	89	369	58.3	69.0	0.76	0.65	0.67
22 bl. reinfor. 3#9, Wall L1	0	1706	---	---	0.95	---	---
22 bl. reinfor. 3#9, Wall L2	32	667	36.2	22.0	1.25	1.15	0.80
22 bl. reinfor. 3#9, Wall L3	65	400	61.4	89.0	1.13	0.94	0.71
22 bl. reinfor. 3#9, Wall L4	76	356	57.9	86.4	0.74	0.52	0.42
22 bl. reinfor. 3#9, Wall L5	89	326	61.2	98.9	0.71	0.47	0.38

coefficient of variation of 22%. The average predicted maximum moment was 0.73 of the average experimental maximum moment, with a coefficient of variation of 29%. The predicted maximum deflection was equal to 0.55 of the average experimental deflection, with a coefficient of variation of 31%. These values were obtained for the cases investigated with the exception of the data for the 16 block high walls with 3#3 bars, where premature failure was suspected for the high eccentric loading.

6.4 Summary

In this chapter, the results obtained using the current numerical model were compared with experimental results. Predicted failure modes, capacities, load-strain and load-deflection results for prisms and walls were compared with the results obtained for specimens tested during the present study. In addition the numerical results were compared with some experimental results of tests carried out by Hatzinikolas et al[45]. The comparison of experimental and numerical results indicates that the numerical model is sufficiently accurate to investigate behavior of eccentrically loaded walls. Therefore an analysis using the developed model could be used to evaluate provisions of the current code as well as to extend data required for parametric analysis of capacities of concrete masonry walls. However before drawing any final conclusions the limitations of the current model resulting from assumptions such as ideal elastic behavior etc. should be remembered. Suggestions concerning improvements in model are included in Section 8.3.

CHAPTER 7

DEVELOPMENT OF DESIGN EQUATIONS FOR CONCRETE BLOCK WALLS AND COMPARISON TO CURRENT MASONRY CODE

7.1 Introduction

In this chapter the design of concrete block walls subject to axial load and out-of-plane bending moment is discussed. A parametric study was carried out to determine capacity as a function of slenderness ratio and eccentricity of applied load . Capacities of walls were determined using the finite element model described in Chapter 5. Results of this parametric study were used to evaluate the provisions of the current Canadian masonry code [23], as well as to develop original design equations.

This chapter is organized with the parametric study presented in Section 7.2, where the choice of the investigated parameters , their range and results of the analysis are discussed. In Section 7.3, the results of the parametric study are compared to the predicted values obtained using the provisions of the current Canadian masonry code, CSA Standard CAN3 S304-M84 [23]. The proposed design equations, obtained using the statistical analysis, are reported in Section 7.4. A description of these statistical methods is included. The predicted capacities, based on the developed equations, are compared to experimental results.

7.2 Parametric Study

In the design of a masonry structure, the calculation of the capacity is usually the main aim of analysis. The capacity of a concrete block wall can be influenced by factors such as slenderness ratio, eccentricity of applied load, and mechanical and geometrical properties of the materials. Since it is impossible to incorporate all of these effects, it is convenient to include only the more important factors through relationships describing the influence of these parameters. Less important factor may then be included as modifying coefficients. In the case of the present study, the slenderness ratio and the eccentricity of applied load were chosen as the most important parameters affecting the capacity of masonry walls subject to axial load and out-of-plane bending moment. The choice was justified by the experimental results and opinions of the numerous researchers,[27,36,44,70,77,82], as well as by the classical analysis of beam-columns. Besides these factors are traditionally included in design codes[9,23,24,42,55,74]. It is assumed that other factors can be incorporate through the characteristic compressive strength of masonry, obtain as a result of tests on prisms, and through the coefficients modifying that nominal strength.

The above assumption is valid if there are no interactions between slenderness ratio, eccentricity of load and the excluded factors. It is possible that some of them, such as the ratio of eccentricities, thickness of the face shells of blocks, thickness and width of mortar bed joints, or bond strength of masonry can show such effects. However, it would require a much more extensive numerical analysis to evaluate those relationships. They could be non-linear and therefore a multilevel analysis would be required to incorporate them properly over the range of application.

As mentioned before, only the influence of the slenderness ratio and the eccentricity of applied load were investigated. The assumed values of the other parameters were the same as obtained for the experimental investigation described in Chapters 3 and 4, and used to verify the numerical model in Chapter 6. The values of slenderness and eccentricity were chosen to cover the range of normal application of concrete block walls. It was intended to include in the analysis cases where the influence of slenderness was negligible. It is commonly assumed that capacity of a 4 block high prism is not influenced by the slenderness effect and at the same time the confining effect of end plates is not significant. Therefore, this slenderness was the minimum considered. The maximum slenderness ratio of 25 was chosen due to limits of available computer memory and significant cost of running large problems. In current Canadian masonry code[(23)], the maximum slenderness ratio allowed for single curvature symmetrical cases is equal to 20. However, results of a recent experimental study, published by Amrhein[(1)], indicated that this limit could be significantly increased. The increase in allowable slenderness ratio would allow for use of thinner walls in cases where thickness is controlled by slenderness requirements.

For the parametric study, the values of eccentricity of applied load were varied from one twentieth of wall thickness to the eccentricity where the resultant force was applied in the middle of the strip of mortar covering the face shells of the hollow blocks in the plain walls. For reinforced walls, the upper boundary of eccentricity considered was equal to the wall thickness. Values in between were chosen to represent the effects of different modes of failure.

In addition, for the reinforced wall, two amounts of vertical reinforcement were considered for eccentricities equal to one twentieth, one half and the wall thickness. For the remaining cases one amount of vertical reinforcement equal to 0.21% of the gross cross section area was used. This was slightly more than the 0.2% minimum amount of reinforcement recommended by the Canadian masonry code[(23)]. The choice of the second amount of reinforcement was dictated by choice of a realistic size of reinforcing bars based on requirements for proper casting of grout and effectiveness of reinforcement. It resulted in a cross section area of steel bars equal to 0.74% of the gross cross-sectional area of the wall. This was more than the balanced amount of steel of about 0.5%, calculated for wall loaded in pure bending assuming ultimate strengths of materials and a triangular shape of stress block.

The results of the parametric study are summarized in Table 7.1. These values represent ultimate capacities of concrete block walls. They were obtained as a result of the numerical analysis using the finite element model described in Chapter 5. These results led to the following conclusions:

1) For plain walls, it was found that the slenderness effect was not very significant for small eccentricities but was significant for large eccentricities.

Table 7.1 Summary of Numerical Analysis Results

		Ultimate Axial Loads (kN)											
		Plain Walls				Reinforced Walls							
						Reinforcement							
						2*15M Bars					2*30M Bars		
	e/t*	0.05	0.32	0.34	0.39	0.05	0.26	0.33	0.50	1.00	0.05	0.50	1.00
	h/t*												
4 bl.	4.2	1378	866	843	769	1726	1146	977	486	87	1989	586	205
12 bl.	12.6	1364	834	787	688	1706	1101	925	243	80	1973	359	110
16 bl.	16.8	1370	789	758	415	1705	1046	766	213	41	1939	298	102
20 bl.	21.	1368	753	728	352	1689	788	672	189	39	1889	243	96
24 bl.	25.2	1332	714	588	306	1678	962	478	151	29	1819	196	56

2) The effect of eccentricity on capacity was always noticeable and its significance increased with increased slenderness.

3) For reinforced walls similar relationships were observed. The influence of eccentricity on capacity was even more evident for the cases of very high eccentricities.

4) It was found that there was a significant influence of the amount of reinforcement on the capacity of a wall. This effect was more important for the higher eccentricities than for nearly concentric loading.

7.3 Evaluation of the Current Code

The current Canadian masonry code CSA Standard CAN3-S304-M84 [23] is based on the working stress design approach. However, it can be considered an interim provision before the introduction of a limit states design code, as well. In Clause 5.7, it contains the design methods for masonry walls loaded eccentrically in the minor axis direction. These are called a Load Deflection Method and a Coefficient Method.

As indicated in a draft of the limit states code [77], the Load Deflection Method could be a basis for design of eccentrically loaded walls in the future code. This method is based on consideration of deflections resulting from bending due to application of eccentric load to a masonry wall. Additional bending moment resulting from lateral deflection of the wall can be calculated directly by adding the axial load times deflection product to the initial moment in a Displacement Method. Alternately, through multiplication of the initial moment by a moment magnifier, nearly the same results are obtained in a Moment

Magnifier Method, where the same EI values are used in both cases.

In Table 7.2, predicted capacities of walls and ratios of numerically predicted capacities to design values, calculated based on the code[23] provisions, are shown. The shown values indicate that, using the Load-Deflection method, a more consistent safety of design is obtained for plain walls than for reinforced walls. As was indicated by Turkstra et al[76] the safety of design tended to decrease with increasing eccentricity for reinforced walls. A similar trend can be seen in Table 7.2. For eccentricities up to half of the wall thickness, ratios of numerically predicted capacities to design values for reinforced walls using the Load Deflection Method are between 6.5 and 2.6. These ratios decrease with increasing eccentricity.

Since there was no experimental data available for reinforced walls with eccentricities higher than half of the wall thickness when the code was developed, analysis of safety has been hampered for such cases. Two reinforced walls, tested during the present experimental program, were loaded with eccentricities equal to 0.54 and 0.75 of the wall thickness. The capacities predicted using the finite element model, described in Chapter 5, closely estimated the experimental failure loads. Therefore, it is believed that predicted capacities for block walls loaded with eccentricities equal to the wall thickness were fairly accurate. For this eccentricity, the ratio of the numerically predicted values and the design capacities using the Load Deflection Method was between 2.5 and 1.0, with safety of design decreasing with slenderness ratio. Some of the walls considered had slendernesses higher than the

Table 7.2 Comparison of Numerical and Design Capacities of Masonry Walls

Wall Type	h/t*	e/t*	FEM Failure Load (kN)	Ratio FEM to CSA(23) Methods: Coef-ficient Method	Displace-ment Method	Moment Magni-fier	FEM/ Design (Ult. Load)
		0.05	1378	4.6	5.5	5.5	1.0
		0.32	866	8.1	4.6	4.6	0.9
		0.34	843	9.4	9.2	9.2	0.9
	12.6	0.05	1364	6.5	5.5	5.5	1.0
		0.32	834	11.3	6.1	5.8	1.0
		0.34	787	12.5	9.6	9.4	1.0
	16.8	0.05	1370	8.6	5.6	5.6	1.0
Plain		0.32	789	14.0	6.6	6.3	1.0
		0.34	758	15.9	9.9	9.7	1.1
	21.0	0.05	1368	12.6	5.6	5.6	1.0
		0.32	753	19.6	7.3	6.9	1.0
		0.34	588	18.1	8.3	8.0	0.9
	25.2	0.05	1332	23.0	5.7	5.5	1.0
		0.32	714	34.9	8.7	7.8	1.0
		0.34	588	34.0	9.0	8.7	1.0
	4.2	0.05	1729	4.5	5.7	5.7	0.9
		0.33	977	7.7	6.2	6.2	1.4
		0.50	486	5.7	5.8	5.8	1.2
		1.00	87	2.5	2.5	2.5	0.8
	12.6	0.05	1706	6.4	5.6	5.6	0.9
		0.33	925	10.5	6.5	6.4	1.5
		0.50	244	4.1	3.3	3.3	0.8
		1.00	80	3.3	2.4	2.4	1.2
Rein-	16.8	0.05	1689	8.3	5.7	5.7	0.9
forced		0.33	672	10.0	5.4	5.4	1.2
		0.50	189	6.2	3.0	3.0	0.7
2 #15		1.00	41	2.2	1.3	1.3	0.8
	21.0	0.05	1689	12.2	5.7	5.7	0.9
		0.33	672	14.7	5.4	5.4	1.3
		0.55	189	6.2	3.0	3.0	0.8
		1.00	39	3.0	1.3	1.2	1.0
	25.2	0.05	1678	22.7	5.7	5.7	0.8
		0.33	478	19.6	4.2	4.2	1.0
		0.55	151	9.3	2.6	2.7	0.7
		1.00	29	4.2	1.0	1.0	1.0

*
t- wall thickness
h - wall height
e - eccentricity of load

maximum slenderness ratio of 20 allowed for single curvature symmetrical loading cases. However, even the design value for the 16 block high wall is not sufficiently safe, if it is remembered that the current code[23] is based on the working stress approach.

The design stresses are going to be increased substantially in the future limit sates code, if the reduction capacity factors proposed by Turkstra et al[77] are accepted. The subsequent increase in design capacities of reinforced walls loaded with high eccentricities will result in unsafe design. In this situation, there is an obvious need for checking the safety of design using the Load Deflection Method in the whole range of recommended applications. Until then, the code should limit the maximum allowable eccentricity to half of the wall thickness where slenderness is taken into account using the Load Deflection method.

The Coefficient Method can be used to design eccentrically loaded walls. The comparison of the numerically predicted capacities and design values indicates very inconsistent levels of safety, measured by the ratios of these two values. The ratios vary between 4.6 and 19.6 for plain walls and between 2.2 and 14.7 for reinforced walls, excluding the highest slenderness ratio which is beyond the allowable limit. This comparison indicates that the Coefficient Method, as described in the code[23], is a very inconsistent design method. However, because it is a much simpler design procedure than the Load Deflection Method it is likely to be preferred by designers.

The comparisons of the predicted design capacities of concrete block walls using the current Canadian masonry code[23] with the capacities obtained using the numerical analysis lead to the following evaluation:

1) The Load Deflection Method is adequate for plain and reinforced walls loaded with eccentricities not greater than half of the wall thickness.

2) The Load Deflection Method should not be used for design of walls with eccentricities higher than half of the wall thickness until proper experimental evidence proves the applicability of this method.

3) The Coefficient Method in its current form is very inaccurate and results in overly conservative design of walls for most cases.

7.4 Development of Design Equations

The prediction of the ultimate capacity of slender concrete block walls loaded with out-of-plane eccentricity was the main aim of the analysis. No attempt was made to consider other limit states or determine load and resistance factors resulting from variability of loading conditions and material properties. The finite element model, described in Chapter 5, allowed for fairly accurate prediction of behavior of eccentrically loaded walls. However in normal design practice the use of such complicated and expensive analysis is impractical.

The evaluation of the design methods from the current masonry code[23], carried out in the previous section, showed that the Coefficient Method was very inconsistent. Also, while the Load Deflection Method appeared to be more consistent in predicting capacities, it is debatable, whether the considerable extra design effort is warranted by the improved accuracy. Therefore, an attempt to develop an original design method was made, despite the limited range of factors investigated during the present analysis.

Various approaches to development of a method to account for slenderness were tried, including a moment magnifier method with a simplified method for calculation of stiffness, EI, and several forms of the coefficient method. Evaluation of these efforts led to the choice of a reduction coefficient method with a single reduction coefficient, combining both the influences of slenderness and eccentricity of applied load. It was decided to develop separate coefficients for plain and reinforced walls due to significant differences in behavior of these two types of walls. An ultimate strength approach was chosen to be consistent with future limit states codes.

The reduction coefficient was intended to be a factor to reduce the capacity of short concentrically loaded wall, as define from prism tests. The amount of reinforcement was included in the reduction factor for reinforced walls, since the results of the parametric study, discussed in Section 7.2, suggested that the influence of reinforcement on the capacity was modified by the eccentricity of the applied load. The influence of the ratio of eccentricities at the ends of walls was not considered. Other material factors were not included, since it was believed that they could be included through the characteristic strength of masonry, determined during prism tests or by factors modifying that value.

The reduction factors were developed using the parametric study results reported in Section 7.2. All variables were normalized instead of using them in direct form. In this way, the range of application was extended beyond the actual values of parameters used to generate the initial data. This situation could be avoided if a large number of experimental results covering the whole range of application of concrete block walls was available, or if a parametric study, including all variables in their usual range, was carried out.

To facilitate the development of the design method , it was decided to fix lower limits for some variables. Therefore, a minimum eccentricity equal to 1/20 of the wall thickness, a minimum slenderness ratio, h/t, equal to 4, and a minimum amount of reinforcement equal to 0.2% of the gross cross-sectional wall area were adopted.

As mentioned before, it was intended to develop reduction factors relating capacities of slender eccentrically loaded walls to the capacity of short concentrically loaded walls. Therefore, the capacities predicted by the numerical analysis were divided by the average strength of block prisms and by the mortared areas. These nondimensional dependent variable values were related to independent nondimensional variables like slenderness ratio, relative eccentricity and relative amount of reinforcement. The regression analysis, as described by Draper and Smith[26], was used to determine relationships between them.

For a better understanding of the results of statistical analysis, it can be useful to review some basic ideas behind this analysis. The regression analysis is used for fitting chosen types of mathematical functions to data consisting of points described by the values of dependent (response) variable , Y_i , and one or more independent variables, called predictor variables , X_{1i}, X_{2i}. The method of least squares can be used to examine data and to draw conclusions concerning relationships existing between variables. There are many possible mathematical models to express these relationships. Therefore, special procedures were established for selection of the best regression equation. It is necessary to chose the form of the proposed relationship and polynomial equations are the most common choice. In this case, a polynomial of the form shown below with 2 (or 3) predictors was chosen:

$$Y=b_0+b_1X_1+b_2X_2+b_3X_1X_2+b_4X_1^2+b_5X_2^2+\ldots$$

The square of the multiple correlation coefficient, R^2, is usually used to evaluate accuracy of fitting data by the proposed equation. R^2 is equal to the sum of squares due to regression divided by the sum of squares about the mean and usually is expressed in percent. It measures the proportion of the total variation about the mean response value, Y, explained by the regression. For perfect fit, R^2 equals 100%, which means that all variation in the data about the mean is explained. It is possible to obtained perfect fit if all predictor variables are different. Usually such perfect fit is not sought since it would require inclusions of too many terms in the regression equation. For example, 9 data points can be perfectly fit by an 8-degree polynomial.

Quite often it is not necessary to include high order terms or even all lower order terms in the regression equation to obtain a satisfactory fit. The stepwise regression analysis is one of the methods for selection of terms important for proper fitting of data. The terms are included one by one into the regression equation until proper fit is obtained. The order of insertion of terms is determined by the sequential F-test for significance of regression.

The value of F is a measure of the importance of each term for accuracy of fitting the data. The first included is the term with the highest value ,and then the remaining terms are added in order of declining value of F. The F-value is calculated as a mean square due to regression divided by a mean square about the regression. The mean square due to regression measures the deviation of predicted value from the mean response value and the mean square about regression measures the deviation of response value from predicted value. At adding each term, the regression equation is checked for improvement in the R^2 value. The partial F values are checked for all terms already included in the equation and compared to the appropriate F limits for significance. If the calculated value of F for a term is less than the limit, this term is excluded from the equation. This procedure is terminated when none of the terms excluded from the equation significantly improve the accuracy of fitting. A standard error of estimate, S, equal to the square root of the mean square about the regression, can be used as well to evaluate accuracy of fitting data by the regression equation. To provide an intuitive estimation of accuracy of fit, the standard error of estimate can be calculated as a percentage of the mean response.

In the analyses undertaken to develop the reduction factors, it was found that linear terms were not adequate for proper fitting of the data obtained from the parametric study. The regression analysis, using the Minitab[69] statistical package, showed that second degree polynomials were required for proper fitting of data. In addition, it was determined that certain terms in the full polynomials were not significant and could be dropped without significant decrease in accuracy of fitting.

The results of the analysis obtained for plain walls showed that inclusion of the eccentricity term, $(e/t-0.05)^2$, gave $R^2=89.4\%$. The standard error of estimate was equal to 13.4% of the mean response. When the mixed term, $(e/t-0.05)(h/t-4)$, was added the value of R^2 increased to 97.5 % and the standard error of estimate dropped to 6.7% of the mean response. The regression equation for plain walls was :

$$P=f_m A_n [0.9950-3.9958(e/t-0.05)^2-0.0395(e/t-0.05)(H/t-4)]$$

Other terms were excluded since they did not improve the accuracy of fitting. If the full second degree polynomial was used R^2 was equal to 97.6% and the standard error of estimate was 7.2% of the mean response, which meant worse fitting of data than the accepted equation.

It was found that the polynomial equation for the reduction coefficient for reinforced walls resulted in negative values for a range of eccentricities. Obviously negative wall capacities are not possible. Therefore, an exponential form of equation was adopted for the reduction coefficient for reinforced walls. The development required calculation of logarithmic values of the dependent variable. Then a stepwise regression analysis was applied to identify the statistically significant terms in the exponential quadratic polynomial equation in a similar way as was done for plain walls. The results for reinforced walls showed that the most important term was the eccentricity term, (e/t-0.05), for which R^2 equaled to 89.9% and the standard error of estimate was equal to 29.2% of the mean response. When the mixed term (e/t-0.05)(h/t-4) was included, the value of R^2 increased to 94.6% of the mean response. and the standard error of estimate decreased to 21.6%. The addition of the mixed term, $(e/t-0.05)(A_s/A_{s\,min}-1)$, increased the value of R^2 to 96.4% and standard error of estimate further decreased to 17.7% of the mean response. Finally, when the eccentricity quadratic term, $(e/t-0.05)^2$, was added, R^2 was equal to 96.9% and standard error of estimate was equal to 16.7% of the mean response. The regression equation for reinforced walls at this stage was:

$$P=f_m A_n \,EXP[0.1269-3.8396(e/t-0.05)-0.07069(e/t-0.05)(h/t-4)+0.2381(e/t-0.05)(A_s/A_{s\,min}-1)+0.8913(e/t-0.05)^2]$$

The remaining terms were excluded. The full second degree exponential polynomial with 3 variables yielded R^2 equal to 97.3% and standard error of estimate equal to 17% of mean response, which meant worse fitting than for the accepted equation.

The capacities predicted using the above equations were compared to some previously published experimental results [27,36,44] and to the experimental results from the current study. The results for the plain concrete block walls are summarized in Table 7.3. The experimental data for plain walls in single curvature bending published by Hatzinikolas et

Table 7.3 Comparison of Ultimate Capacities for Plain Block Walls

References	t*	h/t*	e/t*	Failure Load (kN) Experimental	FEM	Design	Ratio Design/Experimental
Current exper.	190	2.0	0.00	533	519	---	---
		4.0	0.00	550	546	---	---
		4.0**	0.00	1007	1113	---	---
		16.8	0.07	1180	1283	1348	1.14
		16.8	0.17	1055	1083	1204	1.14
		16.8	0.33	750	779	748	1.00
		16.8	0.35	502	764	667	1.33
Hatzinikolas et al.(44)	194	2.0	0.00	350	444	---	---
		5.0	0.00	1033	1023	1019	0.99
		5.0	0.17	772	678	959	1.24
		5.0	0.33	618	510	683	1.10
		5.0**	0.00	1351	1218	1693	1.25
		13.8	0.00	1114	900	1019	0.91
		13.8	0.17	708	685	922	1.30
		13.8	0.33	357	505	593	1.66
		13.8	0.39	116	427	415	3.58
		18.0	0.00	971	969	1019	1.05
		24.2	0.00	924	818	1019	1.10
		24.2	0.17	534	654	877	1.64
Drysdale et al.(27)	143	20.0	0.00	711	---	771	1.08
		20.0	0.17	465	---	677	1.44
		20.0	0.33	269	---	395	1.47
		20.0	0.33	204	---	395	1.94
Fattal & Cattaneo (36)	143	17.1	0.00	609	---	550	0.90
			0.00	570	---	550	0.97
			0.08	594	---	539	0.91
			0.08	531	---	539	1.02
			0.17	415	---	491	1.18
			0.17	254	---	491	1.94
			0.17	534	---	491	0.92
			0.25	440	---	411	0.93
			0.25	444	---	411	0.93
			0.33	267	---	302	1.13
			0.33	320	---	302	0.94

*t - wall thickness
h - wall height
e - eccentricity of load
** - grouted

al[44],[45] Drysdale et al[27], and Fattal and Cattaneo[36] were included. The general comparison indicates that an average ratio of predicted capacity to experimental capacity was 1.19, with a coefficient of variation equal to 26%. In general, predictions were better for lower eccentricities than for higher eccentricities.

The results for reinforced walls are summarized in Table 7.4. The experimental data were obtained from the current experimental program, from reports published by Hatzinikolas et al[44],[45] and Drysdale et al[27]. The general comparison showed that an average ratio of predicted capacity to experimental capacity was 1.15, with a coefficient of variation of 21%.

The overestimation of capacities, compared to experimental values, indicates the need for calibration of the proposed design equation to eliminate this bias. However, the limited range of walls and the very high discrepancy between the results for repetitions of identical tests indicate that this comparison is not conclusive. However, the verification of the finite element model, described in Chapter 6, indicated that inaccuracies of the model tended to result in overestimated capacities of walls. In particular, the fairly coarse finite element mesh results in underestimation of bond stress in the mortar joints. Also the underestimation of deflection, resulting from the assumption of linear elastic materials could cause underestimation of the influence of eccentricity on capacity. Also the assumed perfect shape of walls was not justified by experimental evidence obtained during the experimental study. The actual shape of walls could result in higher eccentricities. Similarly, it was noticed that very precise

Table 7.4 Comparison of Ultimate Capacities for Reinforced Block Walls

References	t* (mm)	As*	h/t*	e/t*	Failure Load (kN) Experimental	FEM	Design	Ratio Design/ Experimental
Current exper.	190	2*15M	16.8	0.18	1000	1302	1085	1.08
				0.32	594	911	583	0.98
				0.34	521	689	529	1.02
				0.50	231	209	277	1.20
				0.54	216	188	239	1.11
				0.75	140	129	110	0.79
Hatzinikolas, et al. (44)	194	3#9	5.0	0.00	1472	1799	1693	1.15
		3#3	5.0	0.00	1398	1323	1693	1.21
		3#9	13.8	0.17	1423	976	1129	0.79
				0.33	623	522	661	1.05
				0.39	689	371	551	0.80
				0.46	511	290	456	0.89
		3#3	18.0	0.00	1357	1268	1693	1.25
				0.17	965	906	965	1.00
				0.33	240	435	451	1.88
				0.39	146	293	346	2.42
				0.46	108	190	262	2.43
		3#6	18.0	0.00	1669	----	1693	1.01
				0.17	1154	----	1010	0.87
				0.33	384	----	504	1.31
				0.39	290	----	396	1.37
				0.46	249	----	308	1.24
		3#9	18.0	0.00	1779	1663	1693	0.95
				0.17	890	927	1091	1.23
				0.33	484	459	608	1.26
				0.39	420	385	499	1.18
				0.46	369	280	404	1.09
		3#9	24.0	0.00	1706	1620	1693	0.99
				0.17	667	835	1037	1.55
				0.33	400	451	537	1.34
				0.39	356	265	428	1.20
				0.46	326	230	337	1.03
Drysdale, et al. (27)	143	1#5	20.2	0.16	481	----	585	1.22
				0.33	200	----	272	1.36
				0.33	225	----	272	1.21
				0.50	83	----	131	1.58

*
t - wall thickness
h - wall height
e - eccentricity of load
A_s - amount of reinforcement

attachment of the loading devices to the wall ends was almost impossible. Therefore, the actual eccentricities varied slightly from the intended eccentricities.

When comparing predicted capacities with experimental results, it is important to recognize how sensitive capacity can be to small changes in eccentricity. Therefore, when judging the adequacy of design methods, it is worth considering the influence of varying the eccentricity by perhaps +5% of the wall thickness. For the same reason it may be a worthwhile practice to increase calculated design eccentricities by 5%.

7.5 Summary and Conclusions

The design of eccentrically loaded slender concrete masonry walls was discussed. The influence of slenderness and eccentricity of applied load on wall capacity was investigated through a parametric study. Results of this study were used to evaluate design provisions included in the current Canadian masonry code[23]. Furthermore, they were used to generate original design equations based on a reduction coefficient approach. Verification and discussion of the proposed design equation closed this chapter.

The following are the conclusions drawn from this investigation and discussion:

1) The capacity of a block wall is very dependent on the eccentricity of the applied load. The influence of slenderness is sensitive to the magnitude of eccentricity and for the considered range of slenderness ratios there is not much influence except for large eccentricities.

2) Current design methods[23] result in very inconsistent factors of safety. The Coefficient Method yields overly conservative design capacities. Whereas, the Load Deflection Method produces fairly even level of safety for case with eccentricity not greater than half of the wall thickness. However, for larger eccentricities this method results in unsafe design. In general, the current code[23] tends to underestimate the influence of eccentricity and overestimate the influence of slenderness on the capacity of concrete block walls.

3) The suggested design equations based on a reduction coefficient approach can satisfy the required accuracy for a design method. The simplicity of their use makes them attractive to designers. However, a much more extensive analysis will be required before it can be claimed that relationships similar to those presented here will retain simplicity of design and incorporate improved accuracy for all cases.

CHAPTER 8

SUMMARY, CONCLUSIONS AND RECOMMENDATIONS FOR FUTURE RESEARCH

8.1 Summary

Capacities of slender concrete block walls subjected to axial compression load with eccentricities resulting in out-of-plane bending moment, were investigated during the experimental and analytical studies. Suggestions concerning design methods were included.

An experimental investigation was undertaken to study behavior of slender wall subjected to eccentric vertical loading with symmetric single curvature. Tests of 12 full scale eccentrically loaded walls and 2 walls loaded in pure bending provided complete and dependable data. They were supplemented with experimental results from tests on materials and different types of assemblages. The experimental program was conducted mainly to provide all of the necessary data for development and verification of an analytical model. The finite element method was utilized to develop a 2-dimensional model. It included large deformation analysis together with material nonlinearity resulting from local failures due to cracking, crushing and debonding, and from the nonlinear bond-slip relationship representing the behavior at the interface between grout and steel reinforcing bars. Linear elastic-ideal brittle behavior was assumed for all materials except for steel where the assumed failure at the yield point was not a problem because this stress was never reached.

In the numerical representation, components of the concrete block walls were represented by triangular constant stress elements with properties varying according to the type and thickness of materials. Goodman Joint Elements were used to represent bond at interfaces between blocks and mortar, and between grout and reinforcement. The steel reinforcing bars were idealized by one-dimensional elements.

The smeared cracking approach was used to model cracking in masonry. The local failures in masonry were determined using a multiaxial stress failure criterion. The bond failures were determined using a uniaxial failure criteria.

The incremental iterative procedure was used.

The developed model was verified against the experimental results obtained during the present study. Material properties and geometry were obtained as part of experimental investigation. Detailed verification included comparison of failure modes and resulting ultimate capacities. Analyses of lateral deflections and deformations at midheight of the walls were included. In addition, the proposed model was verified against some experimental results published by Hatzinikolas, et al[(44),(45)].

A parametric study, based on the developed numerical model, was carried out to determine the influence of slenderness and eccentricity of applied load on the capacity of concrete block walls. The material and geometric properties, obtained during the present experimental program, were used in these analyses.

Numerically predicted capacities, obtained from the parametric study, were used to evaluate the design methods in the current Canadian masonry code[23]. The numerical results were also used to develop original design equations based on the reduction factor approach. Finally, the design capacities, yield by these equations, were compared to published experimental results.

8.2 Conclusions

Conclusions concerning each stage of the current study were presented in the respective chapters. However, some important general conclusions are presented here:

1) The capacity of a concrete block wall subjected to eccentric vertical loading is largely dependent on the magnitude of eccentricity of that load. For many cases the influence of the slenderness of the wall is secondary. For a nearly concentrically loaded wall the influence of slenderness was at most 8.5% for the considered range of slenderness ratio, h/t, between 4 and 25. The influence of slenderness becomes more significant with increase in eccentricity.

2) The finite element method provides for accurate modeling of masonry walls subjected to axial loading and out-of-plane bending moment. A two-dimensional linear elastic model with provisions for local failures due to cracking, crushing and debonding, and including large deformation analysis provided means for extending the available experimental data. Therefore, an analysis of the factors influencing the capacities of concrete masonry walls was possible. The developed model is not complete but it is believed to include the most important factors. The possible

modifications and improvements of the model are listed in the next section.

(3) The current Canadian masonry code[23] tends to overestimate the capacity reducing effect of slenderness for most of the allowable range of slenderness. Conversely, the influence of eccentricity of applied load tends to be underestimated, particularly for large eccentricities and slender walls. The Load Deflection Method, included in this code, is satisfactory for eccentricities up to half of the wall thickness but appears to be unsafe for higher eccentricities. Therefore, the limit of application should be established until proper experimental and analytical evidence is available to evaluate the applicability for the whole range of eccentricities. The Coefficient Method in its current form appears to be too conservative.

4) It appears that an adequate reduction coefficient design method can be effectively used for design of concrete block walls. It would be simpler to use than the current Load Deflection Method and can be comparatively accurate. The design equations, developed during the present study, proved to be fairly accurate, despite being based on a very limited source of analytical and experimental data. These equations should not be used in this current form for design purpose, but it has been shown that, the development of better documented equations, similar to ones described in the present study, is possible. However, a much more extensive parametric study , based on an improved model, will be required before it can be claimed with certainty that the design equations will give simple and accurate ways of designing eccentrically loaded concrete block walls.

5) The present experimental program provided complete and dependable data, required for development and verification of the finite element model, which were not available from any other sources.

8.3 Recommendations for Future Research

It is recommended that concrete block walls incorporating a wider range of variables be included in future studies. Much additional experimental and analytical research is needed before problems associated with behavior of eccentrically loaded walls are solved. In the course of the presented investigation, several areas of research, required for further advances, were identified. These are listed below:

For experimental research:

1) The reviewed experimental programs concentrated on the influence of slenderness, eccentricity , ratio of eccentricities, and amount of reinforcement. Quite often the influence of other factors such as initial shape of walls, actual eccentricity, bond strength of masonry and others were neglected. Actually, nothing has been done to identify all factors influencing the behavior of walls and their capacities In many cases existing experimental data cannot be used in statistical analyses or for verification of analytical models without arbitrary assumptions of properties. Therefore, it is necessary to identify all variables and establish methods of controlling and recording them. Besides, experimental results should cover the whole range of application of concrete block walls including different materials and loading conditions. In general, there is need for much more experimental

data including repetitions of identical tests to make any verification of analytical model or design equation statistically significant. Taking into consideration current design provisions[23], tests on reinforced block walls loaded with eccentricities higher than half of the wall thickness are urgently needed.

2) The phenomena of the bond between concrete blocks and mortar and between blocks and grout require further investigation. Methods of increasing the bond strength should be looked after since it appears to be the best way of improving effectiveness of block walls in out-of-plane bending.

For research in analytical modeling:

3) Significant improvement in predictions of maximum deflections and deformations at failure would be expected if nonlinear stress-strain relationships for materials were incorporated into the finite element model.

4) Modeling of the bond between the blocks and mortar requires improvements directed to limit the dependence of bond strength of wall on the size of joint elements.

5) A three-dimensional analysis or additional joint elements should be included to model the confining effect of concrete blocks on grout and mortar.

6) The influence of the deformed shape of reinforcing bars resulting from deflection of the wall should be included in analysis of forces existing in those bars and transformed through bond to the grout.

For development of design methods:

7) A much more extensive parametric study should be undertaken based on an improved numerical model. All variables should be included in such a study. Then a statistical analysis should be used to identify the variables influencing the capacities of walls. These predicted capacities should be experimentally verified to exclude the possibility of incorrect relationships which could result from improper model. However, if verification proves the existence of such relationships, they should be included in the design equations.

8) The research presented in this thesis indicates that a reduction coefficient method based of such parametric study would greatly improve the accuracy of design.

REFERENCES

(1) Amerheim, J.E "Reinforced Masonry Engineering Handbook", 3 rd edition, Masonry Institute of America, Los Angeles, California 1978, 445 pages.

(2) Amerheim, J.E. "Slender Walls Research by California Structural Engineers" The Masonry Society Journal, Vol.1, No.2, July - December 1981, pp. G 9 - G 16.

(3) Anand, S.C. and Young, D.T. "Finite Element Model for Composite Masonry ", Journal of Structural Division, Proceedings of the ASCE, Vol.108, No. ST 12, December 1982, pp.2637-2651.

(4) Araya, S.K. and Hegemier,G.A "On Nonlinear Response Predictions of Concrete Masonry Assemblages", Proceedings of the North American Masonry Conference, Boulder, Colorado, 1978, Paper No.19, 24 pages.

(5) Araya, S.K. and Hegemier, G.A "Finite Element Method for Interface Problems", Journal of the Structural Division, Proceedings of the ASCE, Vol.108, No. ST2, February 1982, pp.327-342.

(6) ASTM Standard C-67-81 "Brick and Structural Clay Tile, Sampling and Testing".

(7) ASTM Standard C-140-75 "Concrete Masonry Units, Sampling and Testing".

(8) ASTM Standard C-404-76 "Arrregates for Masonry Grout".

(9) British Standards Institution "Code of Practice for Structural Use of Masonry",

(10) Boult, B.F. "Concrete Masonry Prism Testing" American Concrete Institute Journal, April 1979, pp.513-535.

(11) Brooks, D.S, Payne, D.C.and Sved, G. "The Stiffness of Partially Cracked Brick Walls", 5-th International Brick Masonry Conference, Washington, October 1971.

(12) Chen,W.F. and Atsuta, T. "Strength of Eccentrically Loaded Walls", International Journal of Solids and Structures, 1973, pp.1283-1300.

(13) Chen, W.F and Atsuta, T. "Theory of Beam-Columns", Volume 1: In-Plane Behavior and Design", McGraw-Hill Inc., 1976, 513 pages.

(14) Chen, W.F. "Plasticity in Reinforced Concrete", McGraw-Hill Inc., New York,1981.

(15) Chukwunenye, A.O. and Hamid, A.A "Behavior of Concrete Block Prisms Under Concentric Loading: An Analytical Approach", Structural Masonry Laboratory, Report No MS 85/1, Department of Civil Engineering, Drexel University, Philadelphia, January 1985.

(16) Colville, J.and Hendry, A.W., " Test of a Load Bearing Masonry Structure" Proceedings of the British Ceramic Society, No.27, Dec. 1978, "Load - Bearing Brickwork (6)", pp. 77 - 84.

(17) Cranston, W.B. and Roberts, J.J "The Structural Behaviour of Concrete Masonry - Reinforced and Unreinforced" The Structural Engineer, Vol.54, No.11, November 1976, pp. 423 - 436.

(18) CSA Standard CAN3-A5-M83 "Portland Cement",Rexdale, Ont.,1983, 49 pages .

(19) CSA Standard A82.43-1950 "Hydrated Lime for Masonry Purposes", Rexdale, Ontario.

(20) CSA Standard A82.56M-1976 "Aggregate for Masonry Mortar", Rexdale, Ont., 1976, 6 pages.

(21) CSA Standard A179M-1976 "Mortar and Grout for Unit Masonry"

(22) CSA Standard CAN3-A369.1-M84 "Method of Test for Compressive Strength of Masonry Prisms", Rexdale, Ont., June 1984, 14 pages.

(23) CSA Standard CAN3-S304-M84 "Masonry Design for Buildings", Rexdale, Ont., 69 pages.

(24) Draft of Australian Code

(25) Draft of New Zealand Code

(26) Draper, N.R. and Smith, H. "Applied Regression Analysis", John Wiley and Sons, Inc., 1968.

(27) Drysdale, R.G., Sallam, S.E.A. and Karaluk, E. "Design of Masonry Walls and Column for Combined Axial Load and Bending Moment" I Canadian Masonry Conference, Calgary, June 1976, pp.394-408.

(28) Drysdale, R.G., Hamid, A.A. and Heidebrecht, A.C "Tensile Strength of Concrete Masonry", Journal of Structural Division, ASCE, Vol.105, ST7, July 1979, pp.1261-1276.

(29) Drysdale, R.G., Hamid, A.A. and Toneff, J.D. "Comments on Block Masonry Design Code Provisions For Allowable Stresses", 3rd Canadian Masonry Symposium, Edmonton, June 1983, 17 pages.

(30) Drysdale, R.G. and Hamid, A.A "Influence of the Characteristic of the Units on the Strength of Block Masonry" Proceedings of the Second North American Masonry Conference, Paper No.2,College Park, Maryland, August 1982, 13 pages.

(31) Drysdale, R.G. and Hamid, A.A. "Capacity of Block Masonry Under Eccentric Compression Loading", American Concrete Institute Journal, Vol. 80, No. 2, March-April 1983, pp.102-108.

(32) Drysdale, R.G. and Wong, H.E. "Interpretation of the Compressive Strength of Masonry Prisms", Proceedings of the 7th International Brick Masonry Conference, Paper No.114, Melbourne, Australia, February 1984, pp.617-625.

(33) Drysdale, R.G. and Hamid, A.A. "Effect of Grouting on the Flexural Tensile Strength of Concrete Block Masonry", McMaster University, Masonry Report No.37, February 1984, 20 pages.

(34) Essawy, A. "Strength of Concrete Masonry Walls Subjected to Lateral (Out-of-Plane) Wind Load", Phd Thesis, Department of Civil Engineering and Engineering Mechanics, McMaster University, Hamilton, Ont., draft March 1986.

(35) Fattal, S.G. and Caettano, L.E. "Evaluation of Structural Properties of Masonry in Existing Buildings" National Bureau of Standards, Washington, 1974.

(36) Fattal, S.G. and Caettano, L.E. "Structural Performance of Masonry Walls Under Compression and Flexure" National Bureau of Standards, Washington, 1976.

(37) Fenton, V.C. "Limit States Design Of Masonry - An Assessment of Proposed New Canadian Building Code Requirements", M.Eng. thesis, Carleton University, Ottawa 1983.

(38) Gazzola, E. "A Failure Criterion for Masonry in Biaxial Flexural Tension", M.Eng thesis, Department of Civil Engineering and Engineering Mechanics, McMaster University, Hamilton, Ont., April 1986.

(39) Goodman, R.E., Taylor, R.L. and Brekke, T.L. "A Model for the Mechanics of Jointed Rock", Journal of Mechanics and Foundations Division, Proceedings of the ASCE, Vol.94, No.SM3, May 1968, pp.637-658.

(40) Hamid, A.A "Behavior Characteristics of Concrete Masonry", Ph.D. thesis, McMaster University, September 1978.

(41) Hamid, A.A and Drysdale, R.G. "Suggested Failure Criteria for Grouted Masonry Under Axial Compression", ACI Journal, Oct. 1979, pp. 1047-1061.

(42) Haseltine, B.A. "Design of Masonry Structures", Building Research & Practice, Vol.12, No.4, July-August 1983.

(43) Hassan, S.S. and Hendry, A.W. "Effect of Slenderness and Eccentricity on the Compressive Strength of Walls" 4-th International Brick Masonry Conference, Brugge 1976.

(44) Hatzinikolas, M., Longworth, J.and Warwaruk, J."Concrete Masonry Walls", Report No.70, Edmonton, September 1978.

(45) Hatzinikolas, M., Longworth, J.and Warwaruk, J. "Experimental Data for Concrete Masonry Walls", Report No.71, Edmonton, September 1978.

(46) Hegemier, G.A., Krishuamoorthy, G., Nunn, R.O and Hoorthy, T.V. "Prism Tests for the Compressive Strength of Concrete Masonry" Proceedings of the North American Masonry Conference, Boulder, Colorado, August 1978, Paper No.18, 17 pages.

(47) Huges, D.M. and Zsembery, S. "A Method of Determining the Flexural Bond Strength of Brickwork at The Right Angles to the Bed Joint", Second Canadian Masonry Symposium, Ottawa, June 1980, pp.73-86.

(48) Isberner, A.W. "Grout for Reinforced Masonry", Masonry, Properties and Performance, ASTM STP 778, J.G. Borchelt, American Society for Testing and Materials, 1982, pp.38-56.

(49) Kuppfer, H., Hilsdorf, H. and Rush, H. "Behavior of Concrete Under Biaxial Stresses", American Concrete Institute Journal, August 1969.

(50) Maurenbrecher, A.H.P. "Use of the Prism Test to Determine Compressive Strength of Masonry", Proceedings of the North American Masonry Conference, Boulder, Colorado, August 1978, Paper No. 91, 13 pages.

(51) Maurenbrecher, A.H.P. "Effect of Test Procedures on Compressive Strength Of Masonry Prisms", Proceedings of the Second Canadian Masonry Symposium, Ottawa, June 1980, pp. 119-132.

(52) Maurenbrecher, A.H.P. "Compressive Strength of Eccentrically Loaded Masonry Prisms" Proceedings of the Third Canadian Masonry Symposium, Edmonton, June 1983, pp.10-13.

(53) Mirza F. "Derivation of Geometric Non-linear Stiffness Matrix (C.S.T.)"- private comunication.

(54) Mirza, S.M and Houde, J. "Study of Bond Stress-Slip Relationships in Reinforced Concrete", American Concrete Institute Journal, January 1979.

(55) National Building Code Of Canada, Supplement No 4, Part 1, "Plain and Reinforced Masonry", National Research Council of Canada, Ottawa, 1975.

(56) Ngo, D. and Scordelis, A.C "Finite Element Analysis of Reinforced Concrete Beams" ACI Journal, March 1967, pp.152-163.

(57) Nilson, A.H "Nonlinear Analysis of Reinforced Concrete by the Finite Element Method", ACI Journal, September 1968, pp.757-766.

(58) Nunn, R.O, Miller, M.E. and Hegemier, G. "Grout -Block Bond Strength in Concrete Masonry", Proceedings of the North American Masonry Conference, Paper No.3, Boulder, Colorado, August 1978, 9 pages.

(59) Ojinaga, J. "The Ultimate Strength of Load-Bearing Brick and Block Masonry Walls", M.Eng. thesis, Dept. of Civil Engineering, McGill University, Montreal, July 1976.

(60) Ojinaga, J. and Turkstra, C.J "the Design of Plain Masonry Walls", Canadian Journal of Civil Engineering, Vol.7, 1980, pp.233-242.

(61) Ojinaga, J. and Turkstra, C.J "Design of Reinforced Masonry Walls and Column for Gravity Loads", Canadian Journal of Civil Engineering, Vol.9, 1982, pp.-84-95.

(62) Page, A.W. "Finite Element Model for Masonry", Journal of the Structural Division, Proceedings of the ASCE, Vol. 104, No. ST2, February 1982, pp.327-342.

(63) Pristley, M.J.N. and Elder, D.M. "Stress-Strain Curves for Unconfined and Confined Concrete Masonry" American Concrete Institute Journal, May-June 1983.

(64) Read, J.B. and Clements, S.W. "The Strength of Concrete Block Walls", Phase I: "Construction and Proving of a Suitable Test Frame"

(65) Read, J.B. and Clements, S.W. "The Strength of Concrete Block Walls", Phase II: "Under Uniaxial Loading"

(66) Read, J.B. and Clements, S.W. "The Strength of Concrete Block Walls", Phase III: "Effects of Workmanship, Mortar Strength and Bond Pattern"

(67) Richart, F.E "The Structural Performance of Concrete Masonry Walls", Journal of the American Concrete Institute, Vol.3, No.6, February 1932, pp363-387.

(68) Risager, S. "The Buckling Load of Linear Elastic Wall Without Tensile Strength", Proceedings of the Second International Brick Masonry Conference, Stoke-on-Trent, England, April 1970, pp.133-136.

(69) Ryan, T.A., Joiner, B.L. and Ryan, B.F. "Minitab Reference Manual", The Pensylvania State University, University Park, Pa., March 1981.

(70) Sahlin, S., "Structural Masonry", Prentice-Hall, Inc., 1971,---- pages.

(71) Self, M.W. "Structural Properties of Load Bearing Concrete Masonry" Masonry: Past and Present, STP 58a, ASTM, Philadelphia, Pa, 1975.

(72) Smith, B.S and Rahman, K.M.K. "The Variations of Stress in Vertically Loaded Brickwork Walls", Proceedings of the Institution of Civil Engineers, Vol. 51, April 1972, pp.689-700.

(73) Stafford Smith,B.and Carter, C. "Distribution of Stresses in Masonry Walls Subjected to Vertical Loading", Proceedings of Second International Brick Masonry Conference, Stoke-on-Trent, England, 1970, pp.119-124.

(74) Structural Clay Products Institute "Recommended Practice for Engineered Brick Masonry", McLean, Virginia, November 1969.

(75) Turkstra, C. and Ojinaga, J. "Towards a Canadian Limit States Masonry Code ", Second Canadian Masonry Symposium, Ottawa, 1976.

(76) Turkstra, C.J., Ojinaga, J. and Shyu, C-T "Development of a Limit States Masonry Code", Proceedings 3rd Canadian Masonry Symposium, Paper No.2, Edmonton, June 1983, 13 pages.

(77) Turkstra,C. "Limit States Design in Masonry", Second Draft of CSA S304-1, 1985.

(78) Walker, J. "Long Term Deflections in Reinforced Concrete beams", M.Eng. thesis, Department of Civil Engineering and Engineering Mechanics, McMaster University, Hamilton, draft March 1986.

(79) Wang, C. and Salomon, C.G. "Reinforced Concrete Design" Thomas Y. Crowell, Harper & Row, Publishers, 1979, 918 pages.

(80) Wang, T.M., Lee, S.L. and Zienkiewicz, O.C. "A Numerical Analysis of Large Deflections of Beams", International Journal Mech. Sci., Pergamon Press Ltd., 1961, Vol.3, pp.219-228.

(81) Wong, H.E.and Drysdale, R.G. "Stress-Strain Characteristics of Concrete Block Masonry Prisms", ASTM Special Publication, Masonry: Research, Applications and Problems, Bal Harbour,Fla, December 1983, 17 pages.

(82) Yokel, F.Y. "Stability and Load Capacity of Members with no Tensile Strength", Journal of the Structural Division, Proceedings of the ASCE, Vol.97, No. ST7, July 1971, pp.1913-1926.

(83) Yokel, F.Y and Dikers, R.D. "Strength of the Load Bearing Masonry Walls", Journal of the Structural Division, Proceedings of the ASCE

(84) Zienkiewicz, O.C. "The Finite Element Method " Third Edition, McGraw-Hill Inc., London 1977.

(85) ---------- State-of-the-Art Report on " Finite Element Analysis of Reinforced Concrete", ASCE, New York.

APPENDIX A

LISTING OF THE FINITE ELEMENT PROGRAM

```
************************************************************************
************************************************************************
****************** PROGRAM MAIN ****************************************
************************************************************************
************************************************************************

C COMPUTER PROGRAM UTILZING THE FINITE ELEMENT METHOD, PREDICTS
C BEHAVIOUR OF MASONRY WALL UNDER AXIAL LOAD AND OUT-OF-PLANE BENDING.

C DATA:
C NPROB,IGR,ILIN,IT,MAXIT,JGR,ILO,CHECK,IPS,IKW,NDM      - 7I5,F10.0,3I2
C NB,NXB,NY,NVAR,NNODEL,NNSP,NNSEL,NBAR
C BDIA,ABOT
C EF(I),ANUF(I),FCF(I),FTF(I),GRF(I),TH(I)
C NLE
C NIN(I),FIN(I)
C WHERE:
C NPROB - PROBLEM NUMBER, IF NPROB= 20 THEN FULL LISLING,
C                         IF NPROB 20 THEN SHORT FORM
C IGR=0 - MANUALY DESCRIBED GRID, IGR=1 - GRID GENERATED AUTOMTICALLY
C ILIN=0 - SMALL DEFORMATION ANALYSIS, ILIN=1 - LARGE DEFORMATION ANA
C IT - NUMBER OF ITERATIONS PER LOAD INCREMENT
C MAXIT - MAXIMUM ALLOWED NUMBER OF ITREATIONS PER PROBLEM
C JGR=0 NO GRAVITY LOAD, JGR=1 GRAVITY LOAD CONSIDERED
C ILO - NOMINAL NUMBER OF LOAD INCREMENT
C CHECK - CONVERGENCE LIMIT
C IPS=0 - PLANE STRESS ANALYSIS, IPS=1 - PLANE STRAIN ANALYSIS
C IKW=0  - PLAIN WALL, IKW=1 - REINFORCED
C NDM - NUMBER OF DIFFERENT MATERIALS
C NB - NUMBER OF COURSES IN WALL
C NXB - NUMBER OF ELEMENTS PER HEIGHT OF 1 UNIT (4,5,6,...)
C NY - NUMBER OF ELEMENTS PER WIDTH OF 1 UNIT (4,6,8,...)
C NVAR=2 - NUMBER OF DOF PER NODE
C NNODEL=3 - NUMBER OF NODES PER 1 TRIANGULAR ELEMENT
C NNSP=4 - NUMBER OF NODES PER 1 JOINT ELEMENT
C NNSEL=2 - NUMBER OF NODES PER 1 BEAM ELEMENT
C NBAR - NUMBER OF REINFORCING BARS
C BDIA - DIAMETER OF THE REINFORCING BAR
C ABOT - TOTAL CROSS SECTIONAL AREA OF REINFORCING BARS
C EF(I) - MODULUS OF ELASTICITY FOR I-TH MATERIAL
C ANUF(I) - POISSON'S RATIO
C FCF(I) - COMPRESSIVE STRENGTH
C FTF(I)=.1*FCF(I) - TENSILE STRENGTH
C GRF(I) - DENSITY
C TH(I) - THICKNESS
C NLE - NUMBER OF LOADED DOF
C NIN(I) - NUMBER OF I-TH DOF
C FIN(I) - FORCE APPLIED IN DIRECTION OF I-TH DOF
```

```
      PROGRAM MAIN(DA,OUTPUT,PLOT,TAPE5=DA,TAPE6=OUTPUT,TAPE9=PLOT,
     *TAPE1,TAPE2,TAPE3,TAPE4,TAPE7,TAPE8)
      DIMENSION A(12500),B(900),BB(900),CC(900),DD(900),DU(900)
     1,XX(500),YY(500),JX(900),AREA(700),XLEN(100),IBF(2,100)
     2,U(8),V(8),AT(3),BT(3),BL(3,6),ICO(6),LJ(8),FL(8),S(8,8),Z(3,6)
     3,SIG(700,3),STR(700,3),EPS(700,3),AIN(700,3),ICR(700),ANG(700)
     4,ANUF(9),EF(9),E1F(9),E2F(9),E3F(9),FCF(9),FTF(9)
     5,TH(9),GRF(9),ICON(22),CON(22),PL(5,50),NP(4)
   10 CALL INP(XX,YY,ICO,AREA,NEL,JX,LJ,NNSP,NNSEL,NBAR,NNODEL,NVAR
     1,NNOD,NBSE,NVEL,NVELS,NVSEL,INEL,JNEL,KNEL,NMAT,NNET,IKW,IPS
     2,IGR,IT,MAXIT,XYZ,CHECK,XLEN,LBAND,NVA,JC,DDET,IIII,EF
     3,ANUF,FCF,FTF,GRF,TH,ES,CF,E1F,E2F,E3F,NCON,ICON,CON,TTT,XXX
     4,ABOT,BDIA,NPROB,NB3,ILIN,NP,SAREA,ILO,JGR)
      CALL PSET(ICR,700)
      IF(NPROB.GT.30) READ(5,*) (ICR(I),I=1,KNEL)
   11 IEXP=0
      KR=0
      KS=0
      COR=0.D0
      AL=0.D0
      BE=0.D0
      GA=0.D0
      DE=0.D0
      SSS=0.D0
      CALL PRESET(IBF,2,100)
      CALL PRESET(BL,3,6)
      CALL PRESET(Z,3,6)
      CALL PRESET(SIG,700,3)
      CALL PRESET(EPS,700,3)
      CALL PRESET(STR,700,3)
      CALL PRESET(AIN,700,3)
      CALL PSET(BB,900)
      CALL PSET(DU,900)
      CALL PSET(CC,900)
      CALL PSET(DD,900)
      CALL PSET(ANG,700)
      IF(JNEL.GT.700) STOP
      IF(NPROB.EQ.0) GO TO 130
      REWIND 9
   20 REWIND 1
      REWIND 2
      REWIND 3
      REWIND 4
      REWIND 7
      REWIND 8
      IIII=IIII+1
      IF(IIII.GT.MAXIT) GO TO 110
      CALL PSET(B,900)
      CALL PSET(FL,8)
      CALL PSET(A,12500)
      CALL PRESET(S,8,8)
```

```
      CALL STLOC(NEL,A,S,B,FL,ICO,JX,LJ,AT,BT,BL,AREA,XX,YY
     1,NNODEL,NVEL,NVAR,LBAND,TH,GRF,E1F,E2F,E3F,ANUF,EF,JC
     2,IGR,U,CC,SIG,ANG,ICR,AL,BE,GA,DE,KR,ILIN)
      CALL PSET(FL,8)
      CALL PRESET(S,8,8)
      CALL STLOM(INEL,NEL,A,S,B,FL,ICO,JX,LJ,U,CC,LBAND
     1,NVAR,NVSEL,NNSP,JC,TH,EF,ANUF,FTF,YY,ICR)
      IF(IKW.EQ.0) GO TO 60
      CALL PSET(FL,8)
      CALL PRESET(S,8,8)
      CALL STLOS(JNEL,INEL,A,S,B,FL,ICO,JX,LJ,XLEN,SIG
     1,ABOT,ES,CF,NVELS,JC,NNSEL,NVAR,LBAND)
      CALL PSET(FL,8)
      CALL PRESET(S,8,8)
      CALL STLOB(KNEL,JNEL,A,S,B,FL,ICO,JX,LJ,U,CC,XLEN
     1,BDIA,NBAR,NBSE,LBAND,NVAR,NVSEL,NNSP,CF,JC,IBF)
   60 CONTINUE
      CALL NLOAD(B,JC,PMAX)
      CALL LOADIN(B,BB,DD,NNET,XXX,JC)
      IF(NCON.EQ.0) GO TO 70
      CALL PLACEZ(B,A,CON,ICON,NCON,NNET,LBAND)
   70 DET=1.E-8
      CALL BAND(A,B,NNET,NB3,1,DET)
      IF(DET.LE.0.DO) GO TO 110
      CALL CONV(CC,B,NNET,DET,DDET,RATIO,CHECK,IPR,JC,ILO,III,IIII)
      REWIND 1
      REWIND 2
      REWIND 3
      REWIND 8
      CALL CHSIG(BL,AT,BT,LJ,B,V,CC,Z,IBF,IPS,IKW,NEL
     1,INEL,JNEL,KNEL,NVEL,SIG,STR,EPS,AIN,ANG,ES,FCF,FTF,ANUF
     2,XLEN,KR,KS,ICR,COR,IPR,RATIO,CHECK,NPROB,JC,DU)
      IF(RATIO.GT.CHECK) GO TO 90
      CALL SIGCON(JNEL,INEL,ICR,SIG,STR,EPS,AIN,ANG)
      CALL BACK(XXX,TTT,SSS,COR,KS,KR,NNET,DU,CC,XYZ,IPR,XXXL,III)
   90 IF(IPR.EQ.0) GO TO 100
      IEXP=IEXP+1
      CALL EXPAND(DD,NMAT,CC,JX,NNOD,NVAR,NPROB)
      CALL PLOT(DD,NP,XXX,PL,IEXP,PMAX,SAREA,NPROB)
  100 CALL ITER(XXX,XYZ,RATIO,CHECK,JC,IT,DDET,DET,KS,KR
     1,SSS,TTT,IJI)
      IF(IJI.EQ.1) GO TO 110
      GO TO 20
  110 WRITE(6,101)
      CALL DAPLOT(IEXP,PL,NP,SAREA,NPROB)
      IF(NPROB.LT.10) GO TO 120
      CALL LARGE(JNEL,INEL,NEL,STR,AIN,XXXL,DD,NMAT,CC,JX,NNOD,NVAR)
  120 GO TO 10
  130 STOP
  101 FORMAT(//,10X,"********************** END **********************")
      END
```

```
************************************************************************
****************** SUBROUTINE BACK *************************************
************************************************************************

C CALCULATES CURENT LOAD INCREMENT AND DISPLACEMNT VECTOR

      SUBROUTINE BACK(XXX,TTT,SSS,COR,KS,KR,NNET,DU,CC,XYZ,IPR,XXXL,III)
      DIMENSION DU(900),CC(900)
      IF(COR.LT.0.0) COR=0.DO
      IF(KS.NE.1.AND.KR.NE.1) GO TO 20
      III=0
      DO 10 I=1,NNET
      CC(I)=DU(I)
   10 CONTINUE
      TTT=TTT-COR*(TTT-SSS)
      XXX=TTT/XYZ
   20 WRITE(6,101) XXX
      III=III+1
      DO 30 I=1,NNET
   30 DU(I)=CC(I)
      IF(IPR.EQ.1) XXXL=XXX
      RETURN
  101 FORMAT(/,5X,"SOLUTION FOR ",F8.4,3X,"OF TOTAL LOAD",/)
      END

************************************************************************
****************** SUBROUTINE BAND *************************************
************************************************************************

C SOLVES SYSTEM OF LINEAR EQUATIONS

      SUBROUTINE BAND(A,B,N,M,LT,DET)
      DIMENSION A(12500),B(900)
      MM=M-1
      NM=N*M
      NM1=NM-MM
      IF (LT.NE.1) GO TO 55
      MP=M+1
      KK=2
      FAC=DET
      A(1)=1./SQRT(A(1))
      BIGL=A(1)
      SML=A(1)
      A(2)=A(2)*A(1)
      A(MP)=1./SQRT(A(MP)-A(2)*A(2))
      IF(A(MP).GT.BIGL)BIGL=A(MP)
      IF(A(MP).LT.SML)SML=A(MP)
      MP=MP+M
      DO 62 J=MP,NM1,M
      JP=J-MM
```

```
      MZC=0
      IF(KK.GE.M) GO TO 1
      KK=KK+1
      II=1
      JC=1
      GO TO 2
1     KK=KK+M
      II=KK-MM
      JC=KK-MM
2     DO 65 I=KK,JP,MM
      IF(A(I).EQ.0.)GO TO 64
      GO TO 66
64    JC=JC+M
65    MZC=MZC+1
      ASUM1=0.
      GO TO 61
66    MMZC=MM*MZC
      II=II+MZC
      KM=KK+MMZC
      A(KM)=A(KM)*A(JC)
      IF(KM.GE.JP)GO TO 6
      KJ=KM+MM
      DO 5 I=KJ,JP,MM
      ASUM2=0.
      IM=I-MM
      II=II+1
      KI=II+MMZC
      DO 7 K=KM,IM,MM
      ASUM2=ASUM2+A(KI)*A(K)
7     KI=KI+MM
5     A(I)=(A(I)-ASUM2)*A(KI)
6     CONTINUE
      ASUM1=0.
      DO 4 K=KM,JP,MM
4     ASUM1=ASUM1+A(K)*A(K)
61    S=A(J)-ASUM1
      IF(S.LT.0.)DET=S
      IF(S.EQ.0.)DET=0.
      IF(S.GT.0.)GO TO 63
      NROW=(J+MM)/M
      WRITE(6,99) NROW
99    FORMAT(35HOERROR CONDITION ENCOUNTERED IN ROW,I6)
      RETURN
63    A(J)=1./SQRT(S)
      IF(A(J).GT.BIGL)BIGL=A(J)
      IF(A(J).LT.SML)SML=A(J)
62    CONTINUE
      IF(SML.LE.FAC*BIGL)GO TO 54
      GO TO 53
54    DET=0.
      RETURN
```

```
53    DET=SML/BIGL
55    B(1)=B(1)*A(1)
      KK=1
      K1=1
      J=1
      DO 8 L=2,N
      BSUM1=0.
      LM=L-1
      J=J+M
      IF(KK.GE.M)GO TO 12
      KK=KK+1
      GO TO 13
12    KK=KK+M
      K1=K1+1
13    JK=KK
      DO 9 K=K1,LM
      BSUM1=BSUM1+A(JK)*B(K)
      JK=JK+MM
9     CONTINUE
8     B(L)=(B(L)-BSUM1)*A(J)
      B(N)=B(N)*A(NM1)
      NMM=NM1
      NN=N-1
      ND=N
      DO 10 L=1,NN
      BSUM2=0.
      NL=N-L
      NL1=N-L+1
      NMM=NMM-M
      NJ1=NMM
      IF(L.GE.M)ND=ND-1
      DO 11 K=NL1,ND
      NJ1=NJ1+1
      BSUM2=BSUM2+A(NJ1)*B(K)
11    CONTINUE
10    B(NL)=(B(NL)-BSUM2)*A(NMM)
      RETURN
      END
```

```
************************************************************************
****************** SUBROUTINE BANDWH ***********************************
************************************************************************

C COMPUTES HALF BAND WIDTH LBAND

      SUBROUTINE BANDWH(ICO,JX,LJ,NE,NVAR,LBAND,NNOD)
      DIMENSION ICO(6),JX(900),LJ(8)
      LBAND=0
      NV2=2*NVAR
      DO 3 I=1,NE
      READ(4) (ICO(M),M=1,NNOD)
```

```
      DO 4 J=1,NVAR
      DO 4 K=1,NNOD
      K1=(K-1)*NVAR
      LJ(J+K1)=JX(NVAR*ICO(K)-NVAR+J)
    4 CONTINUE
      MAX=0
      MIN=1000
      NV3=NVAR*NNOD
      DO 8 J=1,NV3
      IF(LJ(J).EQ.0) GO TO 8
      IF(LJ(J)-MAX) 6,6,5
    5 MAX=LJ(J)
    6 IF(LJ(J)-MIN) 7,8,8
    7 MIN=LJ(J)
    8 CONTINUE
      NB1=MAX-MIN
      IF(NB1.GT.LBAND) LBAND=NB1
    3 CONTINUE
      RETURN
      END

************************************************************************
******************* SUBROUTINE BLMAT ***********************************
************************************************************************

C CALCULATES THE STRAIN SHAPE MATRIX

      SUBROUTINE BLMAT(BL,A,B,U,AL,BE,GA,DE,JC,ILIN)
      DIMENSION BL(3,6),A(3),B(3),U(8)
      IF(ILIN.EQ.0) GO TO 1
      AL=B(1)*U(1)+B(2)*U(3)+B(3)*U(5)
      BE=B(1)*U(2)+B(2)*U(4)+B(3)*U(6)
      GA=A(1)*U(1)+A(2)*U(3)+A(3)*U(5)
      DE=A(1)*U(2)+A(2)*U(4)+A(3)*U(6)
      IF(JC) 1,2,1
    2 AL=AL/2.DO
      BE=BE/2.DO
      GA=GA/2.DO
      DE=DE/2.DO
    1 BL(1,1)=AL*B(1)+B(1)
      BL(1,2)=BE*B(1)
      BL(1,3)=AL*B(2)+B(2)
      BL(1,4)=BE*B(2)
      BL(1,5)=AL*B(3)+B(3)
      BL(1,6)=BE*B(3)
      BL(2,1)=GA*A(1)
      BL(2,2)=DE*A(1)+A(1)
      BL(2,3)=GA*A(2)
      BL(2,4)=DE*A(2)+A(2)
      BL(2,5)=GA*A(3)
      BL(2,6)=DE*A(3)+A(3)
```

```
      BL(3,1)=GA*B(1)+AL*A(1)+A(1)
      BL(3,3)=GA*B(2)+AL*A(2)+A(2)
      BL(3,5)=GA*B(3)+AL*A(3)+A(3)
      BL(3,2)=DE*B(1)+BE*A(1)+B(1)
      BL(3,4)=DE*B(2)+BE*A(2)+B(2)
      BL(3,6)=DE*B(3)+BE*A(3)+B(3)
      RETURN
      END

************************************************************************
******************* SUBROUTINE BONDARY *********************************
************************************************************************

C CALCULATES LOCAL LOAD VECTOR FOR TRIANGULAR ELEMENTS

      SUBROUTINE BONDARY(X,Y,FL,AR,GR,H,IB,IGR,IS,NVEL)
      DIMENSION X(3),Y(3),FL(8),PX(3),PY(3)
      IF(IS.EQ.0) GO TO 1000
      DO 1 I=1,NVEL
    1 FL(I)=0.D0
      IF(IGR.EQ.0) GO TO 11
      GRAV=AR*H*GR/3.D0
      FL(1)=GRAV
      FL(3)=GRAV
      FL(5)=GRAV
   11 IF(IB.EQ.0) GO TO 1000
      XL=SQRT(((X(2)-X(1))**2)+((Y(2)-Y(1))**2))
      XL=XL*H
      READ(5,5) PX(1),PY(1),PX(2),PY(2),PX(3),PY(3)
      IF(IB.EQ.2) GO TO 12
      FL(1)= FL(1)+XL*(2.D0*PX(2)+PX(1))/6.D0
      FL(2)= FL(2)+XL*(2.D0*PY(2)+PY(1))/6.D0
      FL(3)= FL(3)+XL*(2.D0*PX(2)+PX(3))/6.D0
      FL(4)= FL(4)+XL*(2.D0*PY(2)+PY(3))/6.D0
      GO TO 1000
   12 CONTINUE
 1000 RETURN
    5 FORMAT(6F10.0)
      END

************************************************************************
******************* SUBROUTINE BONDEL **********************************
************************************************************************

C CALCULATES LOCAL STIFNESS MATRIX AND LOAD VECTOR FOR STEEL JOINT ELEM.

      SUBROUTINE BONDEL(S,U,XLEN,DIA,NBAR,IEL,FL,JC,IBF,NBSE,CF)
      DIMENSION S(8,8),FL(8),U(8),XLEN(100),R(3),Q(3),IBF(2,100)
      CALL PRESET(S,8,8)
      R(1)=-.774597
      R(2)=0.
```

```
      R(3)=.774597
      Q(1)=.555556
      Q(2)=.888889
      Q(3)=.555556
      S11=0.
      S31=0.
      S33=0.
      T1=0.
      T2=0.
      IF(IEL.EQ.1) Q(1)=1E3
      IF(IEL.EQ.NBSE) Q(3)=1E3
      PD=ASIN(1.0)*DIA*NBAR*XLEN(IEL)
      U1=U(7)-U(1)
      U2=U(5)-U(3)
      U13=U(1)-U(3)
      DO 10 I=1,3
      IF(U13.GE.0.) Q(I)=1E3
      B1=.5*(1-R(I))
      B2=.5*(R(I)+1)
      UREL=ABS(B1*U1+B2*U2)
      VREL=B1*U1+B2*U2
      IF(UREL.GT..144 ) VREL=VREL/UREL*.144
      IF(UREL.GT..144 ) UREL=.144
      SK=PD*(205.-2419.*UREL+11184.*UREL*UREL-74039.*UREL**4)
      S11=S11+Q(I)*B1*B1*SK
      S31=S31+Q(I)*B1*B2*SK
      S33=S33+Q(I)*B2*B2*SK
      IF(JC.EQ.-1) GO TO 10
      IF(UREL.EQ.0.) GO TO 10
      TS=VREL/UREL*(205.*UREL-1209.5*UREL**2+3728.*UREL**3-
     $18510.*UREL**5)
      T1=T1+Q(I)*B1*TS
      T2=T2*Q(I)*B2*TS
   10 CONTINUE
      S(1,1)=S11
      S(3,1)=S31
      S(5,1)=-S31
      S(7,1)=-S11
      S(3,3)=S33
      S(5,3)=-S33
      S(7,3)=-S31
      S(5,5)=S33
      S(7,5)=S31
      S(7,7)=S11
      IF(JC.EQ.-1) GO TO 15
      FL(7)=T1*PD
      FL(5)=T2*PD
      FL(3)=-FL(5)
      FL(1)=-FL(7)
   15 DO 20 I=1,7,2
      DO 20 J=I,7,2
```

```
      S(I,J)=S(J,I)
   20 CONTINUE
      RETURN
      END
```

```
**************************************************************************
****************** SUBROUTINE BONDMO ***********************************
**************************************************************************

C CALCUTATES LOCAL STIFFNESS MATRIX AND LOAD VECTOR FOR MORTAR BOND ELEM

      SUBROUTINE BONDMO(S,U,FL,FB,BOAR,SN,SK,JC,ICR,IEL)
      DIMENSION S(8,8),FL(8),U(8),ICR(700)
      CALL PSET(FL,8)
      IF(ICR(IEL).NE.2) GO TO 10
      SN=0.D0
      SK=0.D0
   10 A=BOAR*SN/6.D0
      B=BOAR*SK/6.D0
      S(1,1)=2.*A
      S(1,3)=A
      S(1,5)=-A
      S(1,7)=-2.*A
      S(2,2)=2*B
      S(2,4)=B
      S(2,6)=-B
      S(2,8)=-2.*B
      S(3,3)=2.*A
      S(3,5)=-2.*A
      S(3,7)=-A
      S(4,4)=2.*B
      S(4,6)=-2.*B
      S(4,8)=-B
      S(5,5)=2.*A
      S(5,7)=A
      S(6,6)=2.*B
      S(6,8)=B
      S(7,7)=2.*A
      S(8,8)=2.*B
      DO 20 I=1,8
      DO 20 J=I,8
   20 S(J,I)=S(I,J)
      DO 30 I=1,8
      DO 30 J=1,8
   30 FL(I)=FL(I)+S(I,J)*U(J)
      RETURN
      END
```

```
************************************************************************
****************** SUBROUTINE CHSIG ************************************
************************************************************************

C CALCULATES TOTAL DEFLECTION, STRAIN, STRESS VECTORS;
C CHECKS FAILURE CRITERIA FOR ALL ELEMENTS

      SUBROUTINE CHSIG(BL,AT,BT,LJ,DD,V,CC,Z,IBF,IPS,IKW,NEL
     6,INEL,JNEL,KNEL,NVEL,SIG,STR,EPS,AIN,ANG,ES,FCF,FTF,ANUF
     2,XLEN,KR,KS,ICR,COR,IPR,RATIO,CHECK,NPROB,JC,DU)
      DIMENSION BL(3,6),AT(3),BT(3),LJ(8),IBF(2,100),ICR(700),Z(3,6)
     *,DD(900),V(8),CC(900),SIG(700,3),STR(700,3),EPS(700,3),AIN(700,3)
     2,ANG(700),XLEN(100),ANUF(9),FCF(9),FTF(9),DU(900),U(8)
      DIMENSION ZSIG(700),DSIG(3),DEPS(3)
      CALL PSET(DSIG,3)
      CALL PSET(DEPS,3)
      CALL PSET(ZSIG,700)
      IANG=0
      IBNG=0
      URELM=0.D0
      IFAIL=0
      FC=0.D0
      FAIL=0.D0
      SIG1=0.D0
      SIG2=0.D0
      SIG3=0.D0
      UREL1=0.D0
      IF(KR.EQ.1.AND.RATIO.LT.CHECK) KR=2
      IF(KS.EQ.1.AND.RATIO.LT.CHECK) KS=2
      COR=0.D0
      CALL SIGEPS(NEL,BL,AT,BT,LJ,V,ICR,NVEL,Z,ANG,DD
     1,SIG,DSIG,STR,EPS,DEPS,AIN,IPS,FCF,FC,FAIL,SIG1,SIG2,SIG3
     2,PSG1,PSG2,PSG3,IFAIL,A1,RATIO,CHECK,ZSIG)
      KKK=NEL+1
      MFAIL=0
      RATM=1.0
C ICR()=-1 -FOR ELEMENT IN COMP,THAT FAILED PREVIIOUSLY
C      =0  -FOR ELEMENT IN COMP (PERFECT BOND)
C      =1  -FOR ELEMENT IN TENS
C      =2  -BOND FAILURE
      DO 1 IEL=KKK,INEL
      READ(3) (LJ(J),J=1,8)
      ID=0
      READ(8) SN,SK,BOAR,FB,ID
      DO 2 I=1,8
      IKK=LJ(I)
      IF(IKK) 4,3,4
    3 V(I)=0.D0
      U(I)=0.D0
      GO TO 2
    4 V(I)=CC(IKK)
```

```
      U(I)=DU(IKK)
    2 CONTINUE
      SIG(IEL,3)=0.D0
      SIG(IEL,1)=0.D0
      VBOND=(-V(1)-V(3)+V(5)+V(7))/2
      UBOND=(-U(1)-U(3)+U(5)+U(7))/2
      VSHER=(-V(2)-V(4)+V(6
      SIG(IEL,1)=0.D0
      VBOND=(-V(1)-V(3)+V(5)+V(7))/2
      UBOND=(-U(1)-U(3)+U(5)+U(7))/2
      VSHER=(-V(2)-V(4)+V(6)+V(8))/2
      IF(RATIO.GT.CHECK) GO TO 5
      IF(ICR(IEL).EQ.2.AND.VBOND.LT.0.0) PRINT*," BOND ELEMENT ",IEL,
     *"CLOSED"
      IF(ICR(IEL).EQ.2.AND.VBOND.LT.0.0) KR=1
      IF(ICR(IEL).EQ.2.AND.VBOND.LT.0.0) ICR(IEL)=-1
      IF(ICR(IEL).EQ.2) GO TO 1
      VCR=FB/SN
      RAT=VBOND/VCR
      IF(VBOND.GT.0.0) ICR(IEL)=1
      IF(VBOND.LE.0.0.AND.ICR(IEL).EQ.1) ICR(IEL)=0
      IF(RATM.GT.RAT) GO TO 5
      RATM=RAT
      MFAIL=IEL
      COR=(VBOND-VCR)/(VBOND-UBOND)
    5 SIG(IEL,1)=SN*VBOND
      SIG(IEL,3)=SK*VSHER
    1 CONTINUE
      IF(KR.EQ.1.OR.MFAIL.EQ.0) GO TO 6
      ICR(MFAIL)=2
      SIG(MFAIL,1)=0.D0
      SIG(MFAIL,3)=0.D0
      KR=1
      IPR=0
      PRINT*,"FAILURE IN MORTAR BOND ELEMENT ",MFAIL
      GO TO 170
    6 IF(KR.EQ.1) IPR=0
      IF(KR.EQ.1) GO TO 170
      IF(IKW.EQ.0) GO TO 60
      KKK=INEL+1
      DO 50 IEL=KKK,JNEL
      READ(3) (LJ(J),J=1,4)
      DO 40 I=1,4
      IKK=LJ(I)
      IF(IKK) 30,20,30
   20 V(I)=0.D0
      GO TO 40
   30 V(I)=DD(IKK)
   40 CONTINUE
      UREL=V(3)-V(1)
      DEPS(1)=UREL/XLEN(IEL-INEL)
```

```
      DSIG(1)=ES*DEPS(1)
      SIG(IEL,1)=SIG(IEL,1)+DSIG(1)
      EPS(IEL,1)=EPS(IEL,1)+DEPS(1)
   50 CONTINUE
   60 IF(RATIO.GT.CHECK) GO TO 170
C       TRIAXIAL 4 PRAMETERS FAILURE CRITERION
      IF(FAIL.LE.0.0) GO TO 100
      CALL KOF(SIG1,SIG2,IANG,IBNG,IFAIL)
      IF(IANG.NE.0) GO TO 70
      IF(IBNG.NE.0) GO TO 90
      GO TO 100
   70 IF(ICR(IANG).EQ.1) ICR(IANG)=2
      IF(ICR(IANG).EQ.0) ICR(IANG)=1
      ANG(IANG)=.5D0*ATAN(2*SIG(IANG,3)/(SIG(IANG,1)-SIG(IANG,2)))
      AN=2*ANG(IANG)
      SX=.5*(SIG(IANG,1)+SIG(IANG,2))+.5*(SIG(IANG,1)-SIG(IANG,2))
     $*COS(AN)+SIG(IANG,3)*SIN(AN)
      IF(SIG1.GT.(SX-.1).AND.SIG1.LT.(SX+.1)) GO TO 80
      ANG(IANG)=ANG(IANG)-ASIN(1.0)
   80 AII=90.0*ANG(IANG)/ASIN(1.0)+90.0
      FT=0.1*FC
      WRITE(6,101) IANG,AII,FT
      IF(ICR(IANG).EQ.2) WRITE(6,106)
      CALL COREL(COR,SIG1,SIG2,SIG3,A1,FC,PSG1,PSG2,PSG3)
      IF(COR.GT.1.0) COR=1.D0
      IF(KR.EQ.2) COR=0.D0
      IF(COR.LT.0.0) COR=0.D0
      KR=1
      IPR=0
      GO TO 170
   90 ICR(IBNG)=-1
      WRITE(6,104) IBNG,FC
      CALL COREL(COR,SIG1,SIG2,SIG3,A1,FC,PSG1,PSG2,PSG3)
      IF(COR.GT.1.0) COR=1.D0
      IF(KS.EQ.2) COR=0.D0
      IF(COR.LT.0.0) COR=0.D0
      KS=1
      IPR=0
      GO TO 170
  100 IF(IKW.EQ.0) GO TO 170
      KKK=JNEL+1
      DO 150 IEL=KKK,KNEL
      READ(3) (LJ(J),J=1,8)
      DO 130 I=1,8
      IKK=LJ(I)
      IF(IKK) 120,110,120
  110 V(I)=0.D0
      GO TO 130
  120 V(I)=CC(IKK)
  130 CONTINUE
      IF(IEL.NE.KKK) GO TO 140
```

```
      IF(IBF(1,1).EQ.1) GO TO 140
      UREL=ABS(V(7)-V(1))
      IF(UREL.GT..03048) UREL1=UREL
  140 IF(IBF(2,IEL-JNEL).EQ.1) GO TO 150
      UREL=ABS(V(5)-V(3))
      IF(UREL.LT.URELM) GO TO 150
      URELM=UREL
      MAX=IEL-JNEL
  150 CONTINUE
      IF(UREL1.LE.URELM) GO TO 160
      IBF(1,1)=1
      KR=1
      IPR=0
      GO TO 170
  160 IF(URELM.LE..03048) GO TO 170
      IBF(1,MAX+1)=1
      IBF(2,MAX)=1
      KR=1
      IPR=0
      PRINT*," FAILURE IN ELEMENT ",MAX
  170 IF(RATIO.GT.CHECK) GO TO 220
      DO 210 IEL=1,JNEL
      MM=3
      IF(IEL.GT.INEL) MM=1
      IF(KR.NE.1.AND.KS.NE.1) GO TO 200
      DO 180 I=1,MM
      SIG(IEL,I)=STR(IEL,I)
      EPS(IEL,I)=AIN(IEL,I)
  180 CONTINUE
  200 IF(IPR.EQ.0.OR.NPROB.GE.10) GO TO 210
      IF(IEL.EQ.1) WRITE(6,105)
      IF(IPS.EQ.0)WRITE(6,102) IEL,(SIG(IEL,J),J=1,MM),ZSIG(IEL)
      IF(IPS.EQ.1)WRITE(6,102) IEL,(SIG(IEL,J),J=1,MM)
      WRITE(6,103) (EPS(IEL,J),J=1,MM)
  210 CONTINUE
  220 CONTINUE
  101 FORMAT(/," ELEMENT ",I4," IS CRACKED AT AN ANGLE ",F10.4,
     *5X,"F'T=",F10.2)
  102 FORMAT(2X,I5,10E12.3)
  103 FORMAT(7X,9E12.3)
  104 FORMAT(/,5X,"ELEMENT",I4," IS CRUSHED",5X," F'C=",F10.2)
  105 FORMAT(//,2X,"ELEM.",7X,"TXX",9X,"TYY",9X,"TXY",9X,"TZZ",
     1/,14X,"EXX",9X,"EYY",9X,"EXY",8X,"EZZ",//)
  106 FORMAT(/,5X,"ELEMENT IS CRACKED IN TWO DIRECTIONS")
      RETURN
      END
```

```
***********************************************************************
****************** SUBROUTINE CONV ************************************
***********************************************************************

C CHECKS CONVERGENCE

      SUBROUTINE CONV(CC,B,NNET,DET,DDET,RATIO,CHECK,IPR,JC,ILO,III,IT)
      DIMENSION CC(900),B(900)
      DO 10 I=1,NNET
      CC(I)=CC(I)+B(I)
   10 CONTINUE
      RATIO=100.DO*ABS(DDET-DET)/DDET
      IF(JC.LT.0) RATIO=100.DO
      WRITE(6,102) JC,RATIO,IT
      WRITE(6,101) DET
      IPR=0
      IF(III.EQ.ILO) IPR=1
      IF(RATIO.GT.CHECK) IPR=0
      IF(RATIO.LT.CHECK) IPR=1
      IF(IPR.EQ.0) GO TO 20
      IF(JC.LT.0) WRITE(6,103)
   20 RETURN
  101 FORMAT(/,5X,"DETERMINANT IS ",E20.8)
  102 FORMAT(//,5X,"SOLUTION AFTER THE NO. OF ITERATIONS = ",I2,2X,"AND
     1RATIO = ",F12.5,2X,"TOTAL NO. OF ITRERATIONS = ",I3)
  103 FORMAT(//,5X,"**** LINEAR ELASTICITY SOLUTION ****",//)
      END

***********************************************************************
****************** SUBROUTINE COREL ***********************************
***********************************************************************

C CALCULATES REDUCTION FACTOR FOR LOAD INCREMENT

      SUBROUTINE COREL(COR,SIG1,SIG2,SIG3,A1,FC,PSG1,PSG2,PSG3)
      EPS=0.0001
      XL=0.
      XR=1.
   10 YL=ENV(XL,SIG1,SIG2,SIG3,PSG1,PSG2,PSG3,FC)
      YR=ENV(XR,SIG1,SIG2,SIG3,PSG1,PSG2,PSG3,FC)
      S=YL*YR
      IF(S.LT.0.0) GO TO 20
      XR=XL
      XL=TEMP
      XL=(XL+XR)/2.
      GO TO 10
   20 DELT=(XR-XL)/2.
      IF(DELT.LT.EPS) GO TO 30
      TEMP=XL
      XL=(XL+XR)/2.
      GO TO 10
```

```
   30 ROOT=(XL+XR)/2.
      COR=1.-ROOT
      RETURN
      END

************************************************************************
****************** SUBROUTINE DAPLOT **********************************
************************************************************************

C WRITES DATA FOR PLOTS OF STRAINS VERSUS LOADS OR STRESSES

      SUBROUTINE DAPLOT(IEXP,PL,NP,SAREA,NPROB)
      DIMENSION PL(5,50),NP(4)
      IF(NPROB.LT.20) WRITE(6,103) SAREA
      IF(NPROB.LT.20) WRITE(6,104) (NP(I),I=1,4)
      IF(NPROB.GE.20) WRITE(6,106) (NP(I),I=1,4)
      WRITE(6,105)( (PL(I,J),I=1,5),J=1,IEXP)
      WRITE(9,101) (PL(2,I),PL(1,I),I=1,IEXP)
      WRITE(9,102)
      WRITE(9,101) (PL(3,I),PL(1,I),I=1,IEXP)
      WRITE(9,102)
      WRITE(9,107)
      WRITE(9,101) (PL(4,I),PL(1,I),I=1,IEXP)
      WRITE(9,102)
      WRITE(9,101) (PL(5,I),PL(1,I),I=1,IEXP)
      WRITE(9,102)
      RETURN
  101 FORMAT(F12.2,1X,F9.3)
  102 FORMAT("99999. 99999.")
  103 FORMAT(1X,"ASSUMED MIN. CROSSECTION =",F10.1," SQ. MM",/)
  104 FORMAT(1X,"STRESS (MPA)",2X,"STRAIN (1.E-6) FOR DOF ",I3,2X,
     *"STRAIN (1.E-6) FOR DOF ",I3,2X,"VERTICAL DISPL. FOR DOF ",
     *I3,2X"LATERAL DISPL. FOR DOF ",I3,/)
  105 FORMAT(3X,F10.3,6X,F10.1,18X,F10.1,12X,F10.2,20X,F10.2)
  106 FORMAT(1X,"LOAD (KN)",2X,"STRAIN (1.E-6) FOR DOF ",I3,2X,
     *"STRAIN (1.E-6) FOR DOF ",I3,2X,"VERTICAL DISPL. FOR DOF ",
     *I3,2X"LATERAL DISPL. FOR DOF ",I3,/)
  107 FORMAT(1X," VERT. & LAT. DISPL.")
      END

************************************************************************
****************** SUBROUTINE DLOAD ***********************************
************************************************************************

C CALCULATES THE LOCAL LOAD VECTOR FOR CRACKED ELEMENTS

      SUBROUTINE DLOAD(BL,FL,SIG,AR,H,IEL,ICR,ANG)
      DIMENSION BL(3,6),FL(8),SIG(700,3),ICR(700),ANG(700)
      EE=AR*H
      DO 1 I=1,6
      XX=0.D0
```

```
      YY=0.D0
      DO 2 J=1,3
      YY=YY+BL(J,I)*SIG(IEL,J)
    2 CONTINUE
      FL(I)=EE*(YY-XX)
    1 CONTINUE
      IF(ICR(IEL).LE.0) GO TO 40
      DO 50 J=1,5,2
      A=FL(J)*COS(ANG(IEL))-FL(J+1)*SIN(ANG(IEL))
      B=FL(J)*SIN(ANG(IEL))+FL(J+1)*COS(ANG(IEL))
      FL(J)=A
   50 FL(J+1)=B
   40 RETURN
      END

************************************************************************
******************* FUNCTION ENV **************************************
************************************************************************

C CALCULATES FAILURE ENVELOPE FOR 4 PRAMETRIC FAILURE CRITERION

      FUNCTION ENV(T,X2,Y2,Z2,X1,Y1,Z1,FC)
      A1=X2-X1
      A2=Y2-Y1
      A3=Z2-Z1
      A=X1-Y1
      B=A1-A2
      C=Y1-Z1
      D=A2-A3
      E=Z1-X1
      F=A3-A1
      XI1=X1+Y1+Z1+(A1+A2+A3)*T
      XJ2=(A*A+C*C+E*E)/6.+T*(A*B+C*D+E*F)/3.+T*T*(B*B+D*D+F*F)/6.
      XMAX=0.D0
      X=X1+A1*T
      Y=Y1+A2*T
      Z=Z1+A3*T
      IF(X.GT.XMAX) XMAX=X
      IF(Y.GT.XMAX) XMAX=Y
      IF(Z.GT.XMAX) XMAX=Z
      ENV=2.0108*XJ2/(FC*FC)+0.9714*SQRT(XJ2)/FC+9.1412*XMAX/FC+0.2312*
     *XI1/FC-1.
      RETURN
      END
```

```
*************************************************************************
****************** SUBROUTINE EXPAND ************************************
*************************************************************************

C WRITES DISPLACEMENTS OF NODES

      SUBROUTINE EXPAND(AMODE,NAM,VV,JX,NDS,NVAR,NPROB)
      DIMENSION VV(900),AMODE(900),JX(900)
      DO 5 I=1,NAM
      AMODE(I)=0.0
      IF(JX(I).EQ.0) GO TO 5
      AMODE(I)=VV(JX(I))
    5 CONTINUE
      IF(NPROB.GE.10) GO TO 15
      WRITE(6,40)
      DO 10 I=1,NDS
      I2=NVAR*I
      I1=I2-NVAR+1
      WRITE(6,41) I,(AMODE(J),J=I1,I2)
   10 CONTINUE
      GO TO 20
   15 WRITE(6,42)
   40 FORMAT(///,5X,"NODE",9X,"U-DISPL.",9X,"V-DISPL.",/)
   41 FORMAT(I7,8X,E12.6,5X,E12.6)
   42 FORMAT(/," PROGRAM CONVERGED      ",/)
   43 FORMAT(2X,10(E8.2,2X))
   20 RETURN
      END

*************************************************************************
****************** SUBROUTINE GRID **************************************
*************************************************************************

C GENERATES COORDINATES OF NODES

      SUBROUTINE GRID(X,Y,IX,XB,YB,NB,NXB,X1,XM,YM,XC,YZ,NX,NY,
     *NN,NVAR,IKW)
      DIMENSION X(500),Y(500),IX(900)
      NNY=NY+IKW
      NS=(NY+1)/2
      IL=1
      IF(NY.GT.7) IL=2
      NW=NS-IL-1
      YW1=(YB/2.-YM-YZ)/NW
      YW2=(YB/2.+YZ-YM)/NW
      DO 30 I=1,NX
      K=NNY*(I-1)
      Y(K+IL)=YB/2.-YM/2.
      Y(K+1)=YB/2.
      DO 10 J=1,NW
   10 Y(K+IL+J)=YB/2.-YM-(J-1)*YW1
```

```
      Y(K+1+NNY-IL)=-YB/2.+YM/2.
      Y(K+NNY)=-Y(K+1)
      DO 20 J=1,NW
   20 Y(K+NNY+1-IL-J)=-YB/2.+YM+(J-1)*YW2
      Y(K+NS)=YZ
      Y(K+NS+IKW)=YZ
   30 CONTINUE
      DO 35 J=1,NNY
   35 X(J)=0.DO
      DO 70 K=1,NB
      XX=XC+(K-1)*(XB+XM)
      N=NNY+(K-1)*NNY*NXB
      DO 40 I=1,NNY
      X(I+N)=XX
   40 X(I+NNY+N)=XX+X1
      X2=(XB-2.*X1)/(NXB-4)
      L=NXB-2
      DO 50 I=2,L
      DO 50 J=1,NNY
   50 X(J+NNY*I+N)=XX+X1+(I-1)*X2
      L=NNY*(NXB-2)+N
      DO 60 I=1,NNY
      X(I+L+NNY)=XX+XB
   60 X(I+L)=XX+XB
   70 CONTINUE
      L=(NX-1)*NNY
      DO 80 I=1,NNY
C  80 X(I+L)=XX+XM+XB
   80 X(I+L)=XX+XM/2+XB
      NNN=NN*NVAR
      DO 90 I=1,NNN
   90 IX(I)=1
      IF(IKW.EQ.0) GO TO 110
      DO 100 I=1,NX
      L=2*I*NNY-NNY+2
  100 IX(L)=0
  110 CONTINUE
      RETURN
      END

************************************************************************
****************** SUBROUTINE ICOGR ***********************************
************************************************************************
C GENERATES ICO MATRIX

      SUBROUTINE ICOGR(IKW,NX,NY,NB,NXB,NE,INE,JNE,KNE)
      DIMENSION IO(700,4)
      NNY=NY+IKW
      IL=2
      IF(NY.GT.7) IL=4
      J1=IL+1
```

```
      J2=2*NY-2-IL
      L=NNY-2
      NB1=NB+1
      DO 30 MN=1,NB1
      III=NXB-1
      DO 30 J=1,III
      K=0
      II=2*(NNY-1)-1
      IF(IKW.EQ.1) II=L-1
      DO 10 I=1,II,2
      M=I+(J-1)*2*(NY-1)+(MN-1)*2*(NY-1)*(NXB-1)
      N=NNY*(J-1)+K+1+(MN-1)*NNY*NXB
      IO(M,1)=N
      IO(M,2)=N+1
      IO(M,3)=N+NNY
      IO(M+1,1)=N+NNY+1
      IO(M+1,2)=N+NNY
      IO(M+1,3)=N+1
   10 K=K+1
      IF(IKW.EQ.0) GO TO 30
      K=NNY/2
      JJ=L+1
      JJJ=2*L-1
      DO 20 I=JJ,JJJ,2
      M=I+(J-1)*2*(NNY-2)+(MN-1)*2*(NY-1)*(NXB-1)
      N=NNY*(J-1)+K+1+(MN-1)*NNY*NXB
      KK=0
      IF(I.EQ.L+1) KK=-1
      IO(M,1)=N+KK
      IO(M,2)=N+1
      IO(M,3)=N+NNY+KK
      IO(M+1,1)=N+NNY+1
      IO(M+1,2)=N+NNY+KK
      IO(M+1,3)=N+1
   20 K=K+1
   30 CONTINUE
      KK=2*(NNY-1-IKW)
      DO 35 I=1,KK
   35 IO(I,4)=5
      DO 80 I=1,NB
      LL=NXB-2
      DO 50 J=1,LL
      JJ=KK+(J-1)*KK+(I-1)*KK*(NXB-1)
      DO 40 IJ=1,IL
      IO(JJ+IJ,4)=4
   40 IO(JJ+2*NY-1-IJ,4)=4
      DO 50 L=J1,J2
   50 IO(JJ+L,4)=2+IKW
      II=JJ+KK
      DO 60 IJ=1,IL
      IO(II+IJ,4)=3-2*IKW
```

```
   60 IO(II+2*NY-1-IJ,4)=3-2*IKW
      DO 70 L=J1,J2
   70 IO(II+L,4)=1+IKW
   80 CONTINUE
      LL=NE-KK
      DO 90 I=1,NE
   90 WRITE(1) (IO(I,J),J=1,3),1,0,IO(I,4)
      M=NE+1
      DO 95 I=1,NB
      NBO=NY-1
      NBA=(NBO/2)+1
      I1=0
      I2=0
      DO 95 J=1,NBO
      K=NE+(I-1)*(NY-1)+J
      L=NXB*NNY*I-NNY+J
      IF(J.EQ.NBA.AND.IKW.EQ.1) I1=1
      IF(J.GT.NBA.AND.IKW.EQ.1) I2=1
      IO(K,1)=L+I2
      IO(K,2)=L+1+I1+I2
      IO(K,3)=L+NNY+1+I1+I2
      IO(K,4)=L+NNY+I2
      I1=0
      IOI=7
      IF(J.EQ.1.OR.J.EQ.NBO) IOI=6
      IF(NY.GT.7.AND.J.EQ.(NBO-1)) IOI=6
      IF(NY.GT.7.AND.J.EQ.2) IOI=6
      WRITE(9) (IO(K,L),L=1,4),IOI,0
   95 CONTINUE
      IF(IKW.EQ.0) GO TO 120
      M=INE+1
      L=NNY/2+1
      DO 100 I=M,JNE
      IO(I,1)=L
      IO(I,2)=L+NNY
      IO(I,3)=1
      IO(I,4)=0
      L=L+NNY
  100 WRITE(1) (IO(I,J),J=1,4)
      M=JNE+1
      L=NNY/2+1
      DO 110 I=M,KNE
      IO(I,1)=L
      IO(I,2)=L+NNY
      IO(I,3)=IO(I,2)-1
      IO(I,4)=IO(I,1)-1
      L=L+NNY
  110 WRITE(2) (IO(I,J),J=1,4),1,0
  120 CONTINUE
      RETURN
      END
```

```
************************************************************************
****************** SUBROUTINE INP *************************************
************************************************************************

C READS ALL INPUT DATA

      SUBROUTINE INP(XX,YY,ICO,AREA,NEL,JX,LJ,NNSP,NNSEL,NBAR,NNODEL
     1,NVAR,NNOD,NBSE,NVEL,NVELS,NVSEL,INEL,JNEL,KNEL,NMAT,NNET
     2,IKW,IPS,IGR,IT,MAXIT,XYZ,CHECK,XLEN,LBAND,NVA,JC,DDET,IIII,EF
     3,ANUF,FCF,FTF,GRF,TH,ES,CF,E1F,E2F,E3F,NCON,ICON,CON,TTT,XXX
     4,ABOT,BDIA,NPROB,NB3,ILIN,NP,SAREA,ILO,JGR)
      DIMENSION XX(500),YY(500),ICO(6),AREA(700),JX(900),LJ(8)
     *,EF(9),EAF(9),ANUF(9),FCF(9),FTF(9),GRF(9),TH(9),E1F(9),E2F(9)
     2,E3F(9),CON(22),ICON(22),NP(4),XLEN(100)
      DIMENSION IX(900)
      READ(5,103) NPROB,IGR,ILIN,IT,MAXIT,JGR,ILO,CHECK,IPS,IKW,NDM
      READ(5,124) (NP(I),I=1,4),SAREA
      IF(NPROB.EQ.0) GO TO 50
      WRITE(6,102)
      WRITE(6,101) NPROB,IKW
      IF(NPT.EQ.0) NPT=1
      IF(ILIN.EQ.0) WRITE(6,120)
      IF(ILIN.EQ.1) WRITE(6,119)
      IF(IPS.EQ.0) WRITE(6,122)
      IF(IPS.GT.0) WRITE(6,121)
      WRITE(6,123)
      WRITE(6,118) IT,MAXIT,IGR,IPS,ILO,CHECK
      READ(5,108) NB,NXB,NY,NVAR,NNODEL,NNSP,NNSEL,NBAR
      PRINT*,"NB NXB NY NVAR NNODEL NNSP NNSEL NBAR"
      PRINT*,NB,NXB,NY,NVAR,NNODEL,NNSP,NNSEL,NBAR
      NX=NXB*NB+2
      NEL=(NX-NB-1)*(NY-1)*2
      NNOD=NX*(NY+IKW)
      NBSE=0
      IF(IKW.EQ.1) NBSE=NX-1
      READ(5,109) BDIA,ABOT
      PRINT*," BDIA=",BDIA," ABOT=",ABOT
      NVEL=NVAR*NNODEL
      NVELS=NVAR*NNSEL
      NVSEL=NVAR*NNSP
      INEL=NEL+NB*(NY-1)
      JNEL=INEL+NBSE
      KNEL=JNEL+NBSE
      REWIND 1
      REWIND 2
      REWIND 4
      REWIND 8
      REWIND 9
      IF(JGR.EQ.0) READ(5,199) JNEL,KNEL,NB3,LBAND,NVA
      CALL LAYOUT(XX,YY,ICO,IX,JX,AREA,NEL,NNOD,NVAR,NMAT,NNET,NNODEL,
```

```
     *NNSEL,XLEN,NNSP,INEL,JNEL,KNEL,JGR,NB,NXB,NX,NY,IKW)
      REWIND 4
      IF(JGR.EQ.0) GO TO 1
      CALL BANDWH(ICO,JX,LJ,NEL,NVAR,LBAND,NNODEL)
      LBAND=LBAND+1+IKW
      NB3=LBAND+1
      NVA=NB3*NNET
    1 WRITE(6,104) NPROB,NNET,LBAND,NVA
      DDET=1.DO
      IIII=0
      ND2=NDM+2
      DO 10 I=1,ND2
      READ(5,105) EF(I),ANUF(I),FCF(I),FTF(I),GRF(I),TH(I)
      WRITE(6,113) I
      IF(I.LE.NDM) WRITE(6,114) EF(I),ANUF(I),FCF(I),FTF(I)
      IF(I.GT.NDM) WRITE(6,125) EF(I),ANUF(I),FTF(I)
   10 IF(I.LE.NDM) WRITE(6,112) GRF(I),TH(I)
      ES=EF(NDM)
      READ(5,108) NCON
      CF=SQRT(FCF(3)/34.4735)*0.97835
      WRITE(6,111) NCON
      DO 30 I=1,NDM
      IF(IPS.EQ.1) GO TO 20
      EAF(I)=EF(I)/((1.DO+ANUF(I))*(1.DO-2.DO*ANUF(I)))
      E1F(I)=EAF(I)*(1.DO-ANUF(I))
      E2F(I)=ANUF(I)/(1.DO-ANUF(I))
      E3F(I)=(1.DO-2.DO*ANUF(I))/(2.DO*(1.DO-ANUF(I)))
      GO TO 30
   20 E1F(I)=EF(I)/(1.DO-(ANUF(I)**2))
      EAF(I)=E1F(I)
      E2F(I)=ANUF(I)
      E3F(I)=(1.DO-ANUF(I))/2.DO
   30 CONTINUE
      IF(NCON.EQ.0) GO TO 40
      READ(5,106) (ICON(I),I=1,NCON)
      WRITE(6,107) (ICON(I),I=1,NCON)
      READ(5,115) (CON(I),I=1,NCON)
      WRITE(6,116)
      WRITE(6,117) (CON(I),I=1,NCON)
   40 CONTINUE
      JC=-1
      TTT=1.DO
      XXX=1.DO
      XYZ=FLOAT(ILO)
      XXX=TTT/XYZ
   50 RETURN
  101 FORMAT(5X,"PROBLEM NO ",I2,5X,"TYPE OF WALL ",I2,/)
  102 FORMAT("1",10X," **************** 2-DIMENSIONAL FINITE ELEMENT ANA
     1LYSIS **************** ",//)
  103 FORMAT(7I5,F10.0,3I2)
  104 FORMAT(/,5X,"PROB. NO.",I5,3X,"TOTAL UNKNOWNS",I5,3X,"BANDWIDTH",I
```

```
    15,3X,"MATRIX SIZE",I8)
 105 FORMAT(6F10.0)
 106 FORMAT(25I3)
 107 FORMAT(/,"     CONSTRAINTS ON",22I5)
 108 FORMAT(8I5)
 109 FORMAT(2F10.0)
 111 FORMAT(/,5X,"NO OF CONSTRAINTS = ",I6,/)
 112 FORMAT(5X,"DENSITY =",F8.4,2X,"THICKNESS =",F8.1,/)
 113 FORMAT(2X,"MATERIAL NO",I2)
 114 FORMAT(2X,"MODULUS OF ELASIICITY =",F12.1,2X,"POISSONS RATIO =
    1 ",F6.4,2X,"COMPRESSIVE STRENGTH =",F10.2,2X,"TENSILE STRENGTH ="
    2,F8.2)
 115 FORMAT(22F5.0)
 116 FORMAT(//,5X,"BOUNDARY CONSTRAINED VALUES ARE",/)
 117 FORMAT(5X,22F5.1)
 118 FORMAT(//,5X,"IT = ",I3,5X,"MAXIT = ",I3,5X,"IGR = ",I2,5X,"IPS= ",
    1I2,//,5X,"ILO =",I3,5X,"CHECK =",F7.3,//)
 119 FORMAT(10X,"**************** LARGE DEFLECTION ELASTIC ************
    1****",//)
 120 FORMAT(10X,"**************** SMALL DEFLECTION ELASTIC *********
    1*",//)
 121 FORMAT(10X,"**************** PLANE STRESS ANALYSIS ***************
    1*",//)
 122 FORMAT(10X,"************PLANE STRAIN ANALYSIS ***********")
 123 FORMAT(//,15X,"********************* GOOD LUCK *****************
    1****",////)
 124 FORMAT(4I5,F10.0)
 125 FORMAT(2X,"KN = ",F12.1,2X,"KS = ",F12.1,2X,"BOND STRENGTH = "
    1,F6.2)
 199 FORMAT(5I5)
     END

***********************************************************************
******************* SUBROUTINE ITER ***********************************
***********************************************************************

C CALCUTATES WHAT PART OF LOAD IS APPLIED  IN TERMS OF TOTAL LOAD

      SUBROUTINE ITER(XXX,XYZ,RATIO,CHECK,JC,IT,DDET,DET,KS
     1,KR,SSS,TTT,IJI)
      IJI=0
      IF(KR.EQ.2) KR=0
      IF(KS.EQ.2) KS=0
      IF(XXX.GT.2.) IJI=1
      IF(RATIO.GT.CHECK) GO TO 10
      GO TO 20
   10 IF(JC.GT.IT) WRITE(6,101) JC,IT
      IF(JC.GT.IT) IJI=1
      DDET=DET
      JC=JC+1
      GO TO 30
```

```
   20 JC=1
      IF(KS.EQ.1.OR.KR.EQ.1) GO TO 30
      IF(ABS(TTT-XYZ).LT.1E-6) IJI=1
      SSS=TTT
      TTT=TTT+1.DO
      IF(TTT.GT.XYZ) TTT=XYZ
      XXX=TTT/XYZ
   30 RETURN
  101 FORMAT(//,5X,"TOTAL ITERATIONS= ",I5,3X,"IS EQUAL TO THE TOTAL ALL
     1OWED NO. OF ITERATIONS = ",I5,//)
      END

************************************************************************
****************** SUBROUTINE KOF **************************************
************************************************************************

C INDICATES TYPE OF FAILURE ( CRACKING OR CRUSHING )

      SUBROUTINE KOF(S1,S2,IA,IB,IX)
      IF(S2.EQ.0.0.AND.S1.GT.0.0) GO TO 2
      IF(S2.EQ.0.0.AND.S1.LE.0.0) GO TO 3
      ALFA=S1/S2
      IF(ALFA.GE.0.0) GO TO 1
      IF(ALFA.GE.-0.06667) GO TO 3
C  CRACKING
    2 IA=IX
      GO TO 4
    1 IF(S1.GT.0.0) GO TO 2
C  CRUSHING
    3 IB=IX
    4 RETURN
      END

************************************************************************
****************** SUBROUTINE LARGE ************************************
************************************************************************

C WRITE OUTPUT DISPLACEMENTS OF NODES, STRAINS AND STRESSES

      SUBROUTINE LARGE(JNEL,INEL,NEL,STR,AIN,XXXL,AMODE,NAM,VV,JX,NDS,
     *NVAR)
      DIMENSION STR(700,3),AIN(700,3),VV(900),AMODE(900),JX(900)
      WRITE(6,101) XXXL
      DO 5 I=1,NAM
      AMODE(I)=0.0
      IF(JX(I).EQ.0) GO TO 5
      AMODE(I)=VV(JX(I))
    5 CONTINUE
      WRITE(6,40)
      DO 6 I=1,NDS
      I2=NVAR*I
```

```
      I1=I2-NVAR+1
      WRITE(6,41) I,(AMODE(J),J=I1,I2)
    6 CONTINUE
   40 FORMAT(///,5X,"NODE",9X,"U-DISPL.",9X,"V-DISPL.",/)
   41 FORMAT(I7,8X,F12.6,5X,F12.6)
      WRITE(6,102)
      DO 10 IEL=1,JNEL
      MM=3
      IF(IEL.GT.INEL) MM=1
      IF(IEL.EQ.(NEL+1)) WRITE(6,105)
      IF(IEL.EQ.(INEL+1)) WRITE(6,106)
      WRITE(6,103) IEL,(STR(IEL,J),J=1,MM)
   10 IF(IEL.LE.NEL.OR.IEL.GT.INEL) WRITE(6,104) (AIN(IEL,J),J=1,MM)
  101 FORMAT(//,5X,"SOLUTION FOR ",F8.4,3X,"OF TOTAL LOAD",//)
  102 FORMAT(//,2X,"ELEM.",7X,"TXX",9X,"TYY",9X,"TXY",9X,"TZZ",
     1/,14X,"EXX",9X,"EYY",9X,"EXY",8X,"EZZ",//)
  103 FORMAT(2X,I5,10F12.5)
  104 FORMAT(7X,9E12.3)
  105 FORMAT(/,2X,"ELEM.",7X,"TN",21X,"TT",/)
  106 FORMAT(/,2X,"ELEM.",7X," TSTEEL",/,14X,"ESTEEL",/)
      RETURN
      END

************************************************************************
****************** SUBROUTINE LAYOUT ***********************************
************************************************************************

C COMPUTES NODAL COORDINATES, ICO AND JX MATRIXES

      SUBROUTINE LAYOUT(X,Y,ICO,IX,JX,AREA,NE,NN,NVAR,NMAT,NDEG,NNODEL,
     *NNSEL,XLEN,NNSP,INEL,JNEL,KNEL,JGR,NB,NXB,NX,NY,IKW)
      DIMENSION X(500),Y(500),ICO(6),IX(900),JX(900),AREA(700),XLEN(100)
      NNN=NNODEL+3
      NNS=NNSEL+2
      NNP=NNSP+2
      IF(JGR.EQ.1) READ(5,103) XB,YB,XX1,XM,YM,XC,YZ
      PRINT*,"XB   YB   XX1   XM   YM  XC  YZ"
      PRINT*,XB,YB,XX1,XM,YM,XC,YZ
      IF(JGR.EQ.1) CALL GRID(X,Y,IX,XB,YB,NB,NXB,XX1,XM,YM,XC,YZ,NX,
     *NY,NN,NVAR,IKW)
      DO 10 I=1,NN
      I2=NVAR*I
      I1=I2-NVAR+1
      IF(JGR.EQ.0) READ(5,101) X(I),Y(I),(IX(J),J=I1,I2)
C     WRITE(6,101) X(I),Y(I),(IX(J),J=I1,I2)
   10 CONTINUE
      IF(JGR.EQ.1) CALL ICOGR(IKW,NX,NY,NB,NXB,NE,INEL,JNEL,KNEL)
      REWIND 1
      REWIND 2
      REWIND 9
      DO 20 I=1,NE
```

```
      IF(JGR.EQ.0) READ(5,102) (ICO(J),J=1,NNN)
      IF(JGR.EQ.1) READ(1) (ICO(J),J=1,NNN)
      WRITE(4) (ICO(J),J=1,NNN)
C     WRITE(6,102) (ICO(J),J=1,NNN)
      N1=ICO(1)
      N2=ICO(2)
      N3=ICO(3)
      X1=X(N1)
      X2=X(N2)
      X3=X(N3)
      Y1=Y(N1)
      Y2=Y(N2)
      Y3=Y(N3)
      AREA(I)=(X1*Y2+X2*Y3+X3*Y1-Y1*X2-Y2*X3-Y3*X1)/2.D0
   20 CONTINUE
      KKK=NE+1
      DO 25 I=KKK,INEL
      IF(JGR.EQ.0) READ(5,102) (ICO(J),J=1,NNP)
      IF(JGR.EQ.1) READ(9) (ICO(J),J=1,NNP)
C     WRITE(6,102) (ICO(J),J=1,NNP)
   25 WRITE(4) (ICO(J),J=1,NNP)
      IF(IKW.EQ.0) GO TO 40
      KKK=INEL+1
      CALL SGEOM(KKK,JNEL,ICO,NNS,XLEN,X,INEL,JGR)
      KKK=JNEL+1
      DO 30 JJ=KKK,KNEL
      IF(JGR.EQ.0) READ(5,102) (ICO(J),J=1,NNP)
      IF(JGR.EQ.1) READ(2) (ICO(J),J=1,NNP)
C     WRITE(6,102) (ICO(J),J=1,NNP)
      WRITE(4) (ICO(J),J=1,NNP)
   30 CONTINUE
   40 NMAT=NVAR*NN
      NDEG=0
      DO 110 I=1,NMAT
      IF(IX(I)) 90,100,50
   50 IF(IX(I)-1) 70,70,60
   60 NDEG=NDEG+IX(I)
      GO TO 80
   70 NDEG=NDEG+1
   80 JX(I)=NDEG
      GO TO 110
   90 NDEG=NDEG+IX(I)+1
      JX(I)=NDEG
      GO TO 110
  100 JX(I)=0
  110 CONTINUE
  101 FORMAT(2F10.1,6I3)
  102 FORMAT(16I3)
  103 FORMAT(10F10.0)
      RETURN
      END
```

```
************************************************************************
****************** SUBROUTINE LJMAT ***********************************
************************************************************************

C COMPUTES LJ MATRIX

      SUBROUTINE LJMAT(LJ,NNODEL,NVAR,ICO,JX)
      DIMENSION LJ(8),ICO(6),JX(900)
      DO 72 J=1,NNODEL
      J1=(J-1)*NVAR
      J2=NVAR*(ICO(J)-1)
      DO 72 I=1,NVAR
   72 LJ(I+J1)=JX(J2+I)
      RETURN
      END

************************************************************************
****************** SUBROUTINE LOADIN **********************************
************************************************************************

C CALCULATES CURENT LOAD VECTOR

      SUBROUTINE LOADIN(B,BB,DD,NNET,XXX,JC)
      DIMENSION B(900),BB(900),DD(900)
      IF(JC.GT.-1) GO TO 20
      DO 10 I=1,NNET
      BB(I)=B(I)
   10 B(I)=XXX*BB(I)
      WRITE(3) (BB(I),I=1,NNET)
      GO TO 40
   20 READ(3) (BB(I),I=1,NNET)
      DO 30 I=1,NNET
      B(I)=XXX*BB(I)-B(I)
   30 DD(I)=B(I)
      GO TO 50
   40 WRITE(6,101)
   50 RETURN
  101 FORMAT(//,5X,"GLOBAL LOAD VECTOR IS.",/)
      END

************************************************************************
****************** SUBROUTINE NLOAD ***********************************
************************************************************************

C READS LOADS APPLIED IN NODES

      SUBROUTINE NLOAD(B,JC,PMAX)
      DIMENSION B(900),NIN(12),FIN(12)
      IF(JC.NE.-1) GO TO 20
      PMAX=0.DO
```

```
      READ(5,101) NLE
      DO 10 I=1,NLE
      READ(5,102) NIN(I),FIN(I)
      WRITE(6,103) NIN(I),FIN(I)
      PMAX=PMAX+FIN(I)
      N=NIN(I)
      B(N)=FIN(I)
   10 CONTINUE
   20 RETURN
  101 FORMAT(I5)
  102 FORMAT(I5,F10.0)
  103 FORMAT(/,"FORCE IN NODE NO.",I5,"=",F15.3,/)
      END

************************************************************************
****************** SUBROUTINE NONLIN **********************************
************************************************************************

C CALCULATES LOCAL STIFFNESS MATRIX AND LOAD VECTOR FOR TRIANGULAR ELEM.

      SUBROUTINE NONLIN(S,SIG,A,B,E1,E2,E3,AR,H,AL,BE,GA,DE,IS,NEL,
     *IEL,ICRL,ILIN)
      DIMENSION S(8,8),SIG(700,3),A(3),B(3)
      IF(IS.EQ.0) GO TO 1000
      P1=(((AL+1.DO)**2)+E3*(GA**2))*E1
      P2=(E2+E3)*GA*(AL+1.DO)*E1
      P3=(E3*((AL+1.DO)**2)+(GA**2))*E1
      P4=(BE*(AL+1.DO)+E3*GA*(DE+1.DO))*E1
      P5=(E2*(AL+1.DO)*(DE+1.DO)+E3*BE*GA)*E1
      P6=(E3*(AL+1.DO)*(DE+1.DO)+E2*BE*GA)*E1
      P7=(E3*BE*(AL+1.DO)+GA*(DE+1.DO))*E1
      P8=((BE**2)+E3*((DE+1.DO)**2))*E1
      P9=(E2+E3)*BE*(DE+1.DO)*E1
      P10=(E3*(BE**2)+((DE+1.DO)**2))*E1
      EE=H*AR
      IF(ICRL.EQ.-1) EE=EE/1000000.
      IF(ILIN.EQ.1) GO TO 4
      XX=0.DO
      YY=0.DO
      XY=0.DO
      GO TO 3
    4 XX=SIG(IEL,1)
      YY=SIG(IEL,2)
      XY=SIG(IEL,3)
    3 DO 1 I=1,5,2
      K=I+1
      KK=K/2
      DO 2 J=I,5,2
      L=J+1
      LL=L/2
      Z1=B(KK)*B(LL)
```

```
      Z2=B(KK)*A(LL)
      Z3=B(LL)*A(KK)
      Z4=A(KK)*A(LL)
      S(I,J)=EE*(Z1*(P1+XX)+(P2+XY)*(Z2+Z3)+Z4*(P3+YY))
      S(I,L)=EE*(Z1*P4+Z2*P5+Z3*P6+Z4*P7)
      S(K,L)=EE*(Z1*(P8+XX)+(Z2+Z3)*(P9+XY)+Z4*(P10+YY))
      S(K,J)=EE*(Z1*P4+Z2*P6+Z3*P5+Z4*P7)
      S(J,I)=S(I,J)
      S(L,I)=S(I,L)
      S(L,K)=S(K,L)
    2 S(J,K)=S(K,J)
    1 CONTINUE
 1000 RETURN
      END

************************************************************************
******************* SUBROUTINE NONLINC *********************************
************************************************************************

C CALCULATES LOCAL  STIFFNESS MATRIX AND LOAD VECTOR FOR CRACKED
C OR CRUSHED TRIANGULAR ELEMENT

      SUBROUTINE NONLINC(S,SIG,A,E,AR,H,IS,IEL,BL,ANG,ICRL,ILIN)
      DIMENSION S(8,8),SIG(700,3),A(3),BL(3,6),ANG(700),T(6,6)
      IF(IS.EQ.0) GO TO 100
      EE=H*AR
      IF(ICRL.EQ.2) EE=EE/1000000.
      DO 2 J=1,6
      DO 2 I=J,6
      T(I,J)=E*BL(2,J)*BL(2,I)
      T(J,I)=T(I,J)
    2 CONTINUE
      IF(ILIN.EQ.0) GO TO 4
      DO 3 I=1,5,2
      DO 3 J=I,5,2
      II=.5D0*(I+1)
      JJ=.5D0*(J+1)
      AK=A(II)*A(JJ)*SIG(IEL,2)/(4.D0*AR)
      T(J,I)=T(J,I)+AK
      T(J+1,I+1)=T(J+1,I+1)+AK
      T(I,J)=T(J,I)
      T(I+1,J+1)=T(J+1,I+1)
    3 CONTINUE
    4 CO=COS(2*ANG(IEL))
      SI=SIN(2*ANG(IEL))
      DO 5 J=1,5,2
      DO 5 I=J,5,2
      S(I,J)=(.5D0*(T(I,J)+T(I+1,J+1))+.5D0*(T(I,J)-T(I+1,J+1))*CO
     $-.5D0*(T(I,J+1)+T(I+1,J))*SI)*EE
      S(I+1,J)=(.5D0*(T(I+1,J)-T(I,J+1))+.5D0*(T(I+1,J)+T(I,J+1))*CO
     $+.5D0*(T(I,J)-T(I+1,J+1))*SI)*EE
```

```
      S(I+1,J+1)=(.5D0*(T(I+1,J+1)+T(I,J))+.5D0*(T(I+1,J+1)-T(I,J))*CO
     $+.5D0*(T(I,J+1)+T(I+1,J))*SI)*EE
      S(I,J+1)=(.5D0*(T(I,J+1)-T(I+1,J))+.5D0*(T(I,J+1)+T(I+1,J))*CO
     $+.5D0*(T(I,J)-T(I+1,J+1))*SI)*EE
      S(J,I)=S(I,J)
      S(J,I+1)=S(I+1,J)
      S(J+1,I+1)=S(I+1,J+1)
    5 S(J+1,I)=S(I,J+1)
  100 RETURN
      END

************************************************************************
******************* SUBROUTINE PLACEZ *********************************
************************************************************************

C INCLUDES BOUNDARY CONDITIONS

      SUBROUTINE PLACEZ(PP,C,CON,ICON,NCON,NN,LBAND)
      DIMENSION C(12500),CON(22),PP(900),ICON(22)
      DO 18 I=1,NCON
      I1=ICON(I)
      I2=LBAND*(I1-1)+I1
      LC1=I1-LBAND
      IF(LC1.LE.0) LC1=1
      LC2=I1+LBAND
      IF(LC2.GT.NN) LC2=NN
      DO 17 J=LC1,LC2
      IF(I1-J) 9,10,10
   10 IJ=LBAND*(J-1)+I1
      GO TO 16
    9 IJ=LBAND*(I1-1)+J
   16 PP(J)=PP(J)-C(IJ)*CON(I)
   17 C(IJ)=0.D0
   18 CONTINUE
      DO 25 I=1,NCON
      I1=ICON(I)
      I2=LBAND*(I1-1)+I1
      C(I2)=1.E08
      PP(I1)=1.E08*CON(I)
   25 CONTINUE
      RETURN
      END
```

```
**********************************************************************
****************** SUBROUTINE PRESET *********************************
**********************************************************************

C PRESETS MATRIX A(M,N)

      SUBROUTINE PRESET(A,M,N)
      DIMENSION A(M,N)
      DO 1 I=1,M
      DO 2 J=1,N
    2 A(I,J)=0.DO
    1 CONTINUE
      RETURN
      END

**********************************************************************
****************** SUBROUTINE PLOT ***********************************
**********************************************************************

C GENERATES PLOT DATA
C     PL(1,*)-STRESSES (MPA) OR LOADS (KN)
C     PL(2,*),PL(3,*)-STRAINS (MICROSTRAINS)
C     PL(4,*)-VERTICAL DISPLACEMENT (MM);MULTIPLIED BY 2 SINCE DIRECT SOL'N
C         CONCERNS ONLY HALF OF WALL
C     PL(5,*)-LATERAL DISPLACEMENT (MM)

      SUBROUTINE PLOT(DD,NP,XXX,PL,IEXP,PMAX,SAREA,NPROB)
      DIMENSION DD(900),PL(5,50),NP(4)
      NPS=NP(1)
      NPN=NP(2)
      NPT=NP(3)
      NPL=NP(4)
      PL(1,IEXP)=XXX*PMAX/SAREA
      PL(2,IEXP)=1.E+4*DD(NPS)
      PL(3,IEXP)=1.E+4*DD(NPN)
      PL(4,IEXP)=2.*DD(NPT)
      PL(5,IEXP)=DD(NPL)
      IF(NPROB.GE.20) PL(1,IEXP)=XXX*PMAX/1000.
      RETURN
      END

**********************************************************************
****************** SUBROUTINE PRISIG *********************************
**********************************************************************

C CALCULATES PRINCIPAL STRESSES FOR TRIANGULAR ELEMENT

      SUBROUTINE PRISIG(SIGX,SIGY,SIGXY,SMAX,SMIN,SZ,ANU,IPS)
      SMAX=.5DO*(SIGX+SIGY)+SQRT((.5*(SIGX
     $-SIGY))**2+SIGXY**2)
      SMIN=.5DO*(SIGX+SIGY)-SQRT((.5*(SIGX
```

```
     $-SIGY))**2+SIGXY**2)
      SZ=0.DO
      IF(IPS.EQ.0) SZ=ANU*(SMAX+SMIN)
      RETURN
      END

************************************************************************
****************** SUBROUTINE PSET ***********************************
************************************************************************

C PRESETS VECTOR A(M)

      SUBROUTINE PSET(A,M)
      DIMENSION A(M)
      DO 1 I=1,M
    1 A(I)=0.DO
      RETURN
      END

************************************************************************
****************** SUBROUTINE SETUP **********************************
************************************************************************

C SETS UP GLOBAL STIFFNESS MATRIX AND LOAD VECTOR

      SUBROUTINE SETUP(A,B,S,FL,NVEL,LJ,LBAND)
      DIMENSION A(12500),B(900),S(8,8),FL(8),LJ(8)
      DO 12 I=1,NVEL
      LJR=LJ(I)
      IF(LJR.EQ.0) GO TO 12
      B(LJR)=B(LJR)+FL(I)
      DO 11 J=I,NVEL
      LJC=LJ(J)
      IF(LJC.EQ.0)  GO TO 11
      IF(LJR-LJC) 9,10,10
   10 K=(LJC-1)*LBAND+LJR
      GO TO 13
    9 K=(LJR-1)*LBAND+LJC
   13 A(K)=A(K)+S(I,J)
   11 CONTINUE
   12 CONTINUE
      RETURN
      END

************************************************************************
****************** SUBROUTINE SGEOM **********************************
************************************************************************

C CALCULATES LENGTH OF STEEL BEAM ELEMENTS

      SUBROUTINE SGEOM(M,N,IIO,NNS,XLEN,X,NE,JGR)
```

```
      DIMENSION IIO(6),XLEN(100),X(500)
      DO 10 II=M,N
      JJ=II-NE
      IF(JGR.EQ.0) READ(5,101) (IIO(J),J=1,NNS)
      IF(JGR.EQ.1) READ(1) (IIO(J),J=1,NNS)
      WRITE(4) (IIO(J),J=1,NNS)
C     WRITE(6,101) (IIO(J),J=1,NNS)
      XLEN(JJ)=ABS(X(IIO(2))-X(IIO(1)))
      IF(XLEN(JJ).EQ.0.D0) XLEN(JJ)=1.E-6
   10 CONTINUE
  101 FORMAT(4I3,F20.6)
      RETURN
      END

*************************************************************************
****************** SUBROUTINE SIGCON ************************************
*************************************************************************

C CALCULATES STRESSES IN DIRECTION OF LOCAL COORDINATES

      SUBROUTINE SIGCON(INEL,NEL,ICR,SIG,STR,EPS,AIN,ANG)
      DIMENSION ICR(700),ANG(700),SIG(700,3),STR(700,3),EPS(700,3)
     3,AIN(700,3)
      DO 20 IEL=1,INEL
      JJ=3
      IF(IEL.GT.NEL) JJ=1
      IF(ICR(IEL).LT.1) GO TO 10
      CO=COS(2*ANG(IEL))
      SI=SIN(2*ANG(IEL))
      SIG(IEL,2)=.5D0*(SIG(IEL,1)+SIG(IEL,2))-SIG(IEL,3)*SI
     $-.5D0*(SIG(IEL,1)-SIG(IEL,2))*CO
      SIG(IEL,1)=0.D0
      SIG(IEL,3)=0.D0
      EXP=.5D0*(EPS(IEL,1)+EPS(IEL,2))+.5D0*(EPS(IEL,1)-EPS(IEL,2))
     $*CO+.5D0*EPS(IEL,3)*SI
      EYP=.5D0*(EPS(IEL,1)+EPS(IEL,2))-.5D0*(EPS(IEL,1)-EPS(IEL,2))
     $*CO-.5D0*EPS(IEL,3)*SI
      EXYP=-(EPS(IEL,1)-EPS(IEL,2))*SI+EPS(IEL,3)*CO
      EPS(IEL,1)=EXP
      EPS(IEL,2)=EYP
      EPS(IEL,3)=EXYP
   10 DO 20 I=1,JJ
      IF(ICR(IEL).EQ.-1) SIG(IEL,I)=0.D0
      STR(IEL,I)=SIG(IEL,I)
      AIN(IEL,I)=EPS(IEL,I)
   20 CONTINUE
      RETURN
      END
```

```
*********************************************************************
****************** SUBROUTINE SIGEPS ********************************
*********************************************************************

C CALCULATES INCREMENTAL AND TOTAL STRAIN AND STRESSES MATRIXES;
C INDICATES THE MOST CRITICAL ELEMENTS DUE TO MATERIAL FAILURE

      SUBROUTINE SIGEPS(NEL,BL,AT,BT,LJ,V,ICR,NVEL,Z,ANG,DD
     1,SIG,DSIG,STR,EPS,DEPS,AIN,IPS,FCF,FC,FAIL,SIG1,SIG2,SIG3
     2,PSG1,PSG2,PSG3,IFAIL,A1,RATIO,CHECK,ZSIG)
      DIMENSION BL(3,6),AT(3),BT(3),LJ(8),DD(900),V(8),ICR(700)
     *,Z(3,6),FCF(5),SIG(700,3),ZSIG(700),DSIG(3),STR(700,3),ANG(700)
     2,EPS(700,3),DEPS(3),AIN(700,3)
      DO 120 IEL=1,NEL
      SIGM=0.D0
      SIGN=0.D0
      SIGZ=0.D0
      PSGM=0.D0
      PSGN=0.D0
      PSGZ=0.D0
      READ(8) E1,E2,E3,ANU,E,ID,THICK
       READ(1)  ((BL(I,J),J=1,6),I=1,3)
      READ(2) (AT(I),I=1,3),(BT(I),I=1,3)
      READ(3) (LJ(I),I=1,6)
      DO 30 J=1,6
      IKK=LJ(J)
      IF(IKK) 20,10,20
   10 V(J)=0.D0
      GO TO 30
   20 V(J)=DD(IKK)
   30 CONTINUE
      IF(ICR(IEL).EQ.-1) GO TO 80
      IF(ICR(IEL).EQ.0) GO TO 60
      DO 40 I=1,NVEL,2
      V1=V(I)*COS(ANG(IEL))+V(I+1)*SIN(ANG(IEL))
      V2=V(I+1)*COS(ANG(IEL))-V(I)*SIN(ANG(IEL))
      V(I)=V1
   40 V(I+1)=V2
      DO 50 J=1,6
      Z(1,J)=0.D0
      Z(2,J)=E*BL(2,J)
   50 Z(3,J)=0.D0
      GO TO 80
   60 XA=E1*E2
      XB=E1*E3
      DO 70 J=1,6
      Z(1,J)=E1*BL(1,J)+XA*BL(2,J)
      Z(2,J)=E1*BL(2,J)+XA*BL(1,J)
   70 Z(3,J)=XB*BL(3,J)
   80 DO 100 I=1,3
      ZZ=0.D0
```

```
      XX=0.D0
      DO 90 J=1,6
      ZZ=ZZ+BL(I,J)*V(J)
   90 XX=XX+Z(I,J)*V(J)
      DSIG(I)=XX
      SIG(IEL,I)=SIG(IEL,I)+DSIG(I)
      IF(ICR(IEL).EQ.-1.OR.ICR(IEL).EQ.2) SIG(IEL,I)=0.D0
      DEPS(I)=ZZ
  100 EPS(IEL,I)=EPS(IEL,I)+DEPS(I)
      IF(RATIO.GT.CHECK) GO TO 120
      IF(ICR(IEL).EQ.-1.OR.ICR(IEL).EQ.2) GO TO 120
      CALL PRISIG(SIG(IEL,1),SIG(IEL,2),SIG(IEL,3),SIGM,SIGN,SIGZ,ANU
     *,IPS)
      ZSIG(IEL)=SIGZ
      A1=0.D0
      IF(SIGZ.GT.A1) A1=SIGZ
      IF(SIGM.GT.A1) A1=SIGM
      IF(SIGN.GT.A1) A1=SIGN
      AI1=SIGM+SIGN+SIGZ
      AJ2=((SIGM-SIGN)**2+(SIGN-SIGZ)**2+(SIGZ-SIGM)**2)/6.
      CRIT=(2.0108*AJ2/FCF(ID)**2)+(0.9714*SQRT(AJ2)/FCF(ID))+(9.1412
     **A1/FCF(ID))+(0.2312*AI1/FCF(ID))-1.
      IF(CRIT.LT.FAIL) GO TO 110
      CALL PRISIG(STR(IEL,1),STR(IEL,2),STR(IEL,3),PSGM,PSGN,PSGZ,ANU
     *,IPS)
      FAIL=CRIT
      SIG1=SIGM
      SIG2=SIGN
      SIG3=SIGZ
      PSG1=PSGM
      PSG2=PSGN
      PSG3=PSGZ
      IFAIL=IEL
      FC=FCF(ID)
  110 IF(ICR(IEL).EQ.0) GO TO 120
      CO=COS(2*ANG(IEL))
      SI=SIN(2*ANG(IEL))
      SYY=SIG(IEL,2)
      SIG(IEL,1)=.5D0*SYY-.5D0*SYY*CO
      SIG(IEL,2)=.5D0*SYY+.5D0*SYY*CO
      SIG(IEL,3)=-.5D0*SYY*SI
      EPX=EPS(IEL,1)
      EPY=EPS(IEL,2)
      EPXY=EPS(IEL,3)
       EPS(IEL,1)=.5D0*(EPX+EPY)+.5D0*(EPX-EPY)*CO-.5D0*EPXY*SI
      EPS(IEL,2)=.5D0*(EPX+EPY)-.5D0*(EPX-EPY)*CO+.5D0*EPXY*SI
      EPS(IEL,3)=(EPX-EPY)*SI+EPXY*CO
  120 CONTINUE
      RETURN
      END
```

```
************************************************************************
****************** SUBROUTINE STIFF ***********************************
************************************************************************
C CALCULATES LOCAL STIFFNESS MATRIX FOR STEEL BEAM ELEMENT

      SUBROUTINE STIFF(S,ST,OR)
      DIMENSION S(8,8)
      CALL PRESET(S,8,8)
      CO=COS(OR)*COS(OR)*ST
      SI=SIN(OR)*SIN(OR)*ST
      S(1,1)=CO
      S(3,1)=-CO
      S(1,3)=-CO
      S(2,2)=SI
      S(2,4)=-SI
      S(4,2)=-SI
      S(3,3)=CO
      S(4,4)=SI
      RETURN
      END

************************************************************************
****************** SUBROUTINE STLOB ***********************************
************************************************************************

C CALCULATES GLOBAL STIFFNESS MATRIX AND LOAD VECTOR FOR STEEL BOND ELEM

      SUBROUTINE STLOB(JNEL,INEL,A,S,B,FL,ICO,JX,LJ,U,CC,XLEN
     1,BDIA,NBAR,NBSE,LBAND,NVAR,NVSEL,NNSP,CF,JC,IBF)
      DIMENSION A(12500),B(900),S(8,8),FL(8),ICO(6),JX(900),LJ(8)
     *,U(8),CC(900),XLEN(100),IBF(2,100)
      KKK=INEL+1
      DO 60 IEL=KKK,JNEL
      IF(JC.GT.-1) GO TO 10
      READ(4) (ICO(J),J=1,6)
      CALL LJMAT(LJ,NNSP,NVAR,ICO,JX)
      WRITE(3) (LJ(I),I=1,8)
      GO TO 20
   10 READ(3) (LJ(J),J=1,8)
   20 DO 50 I=1,8
      IKK=LJ(I)
      IF(IKK) 40,30,40
   30 U(I)=0.D0
      GO TO  50
   40 U(I)=CC(IKK)
   50 CONTINUE
      KEL=IEL-INEL
      CALL BONDEL(S,U,XLEN,BDIA,NBAR,KEL,FL,JC,IBF,NBSE,CF)
   60 CALL SETUP(A,B,S,FL,NVSEL,LJ,LBAND)
      RETURN
      END
```

```
***********************************************************************
****************** SUBROUTINE STLOC ***********************************
***********************************************************************
C CALCULATES GLOBAL STIFFNESS MATRIX AND LOAD VECTOR FOR TRIANGULAR ELEM

      SUBROUTINE STLOC(NEL,A,S,B,FL,ICO,JX,LJ,AT,BT,BL,AREA,XX,YY
     1,NNODEL,NVEL,NVAR,LBAND,TH,GRF,E1F,E2F,E3F,ANUF,EF,JC
     2,IGR,U,CC,SIG,ANG,ICR,AL,BE,GA,DE,KR,ILIN)
      DIMENSION A(12500),B(900),S(8,8),FL(8),ICO(6),JX(900),LJ(8)
     *,AT(3),BT(3),BL(3,6),AREA(700),XX(500),YY(500),TH(9),GRF(9),E1F(9)
     2,E2F(9),E3F(9),ANUF(9),EF(9),U(8),CC(900),SIG(700,3),ANG(700)
     3,ICR(700)
      DIMENSION X(3),Y(3)
      DO 140 IEL=1,NEL
      AR=AREA(IEL)
      IF(JC.GT.-1.AND.KR.NE.1) GO TO 30
      ARR=2.DO*AR
      READ(4) (ICO(J),J=1,6)
      DO 10 I=1,NNODEL
      ICOO=ICO(I)
      COT=COS(ANG(IEL))
      SIT=SIN(ANG(IEL))
      X(I)=XX(ICOO)*COT+YY(ICOO)*SIT
      Y(I)=YY(ICOO)*COT-XX(ICOO)*SIT
   10 CONTINUE
      IS=ICO(NNODEL+1)
      IB=ICO(NNODEL+2)
      ID=ICO(NNODEL+3)
      THICK=TH(ID)
      GR=GRF(ID)
      AT(1)=(X(3)-X(2))/ARR
      AT(2)=(X(1)-X(3))/ARR
      AT(3)=(X(2)-X(1))/ARR
      BT(1)=(Y(2)-Y(3))/ARR
      BT(2)=(Y(3)-Y(1))/ARR
      BT(3)=(Y(1)-Y(2))/ARR
      IF(JC.GT.-1) GO TO 20
      CALL BONDARY(X,Y,FL,AR,GR,THICK,IB,IGR,IS,NVEL)
      CALL LJMAT(LJ,NNODEL,NVAR,ICO,JX)
      WRITE(3) (LJ(I),I=1,6)
C     PRINT*,IEL,(LJ(I),I=1,6)
   20 WRITE(2) (AT(I),I=1,3),(BT(I),I=1,3)
      GO TO 40
   30 READ(2) (AT(I),I=1,3),(BT(I),I=1,3)
   40 IF(JC.GE.0) READ(3) (LJ(I),I=1,6)
      DO 70 I=1,NVEL
      IKK=LJ(I)
      IF(IKK) 60,50,60
   50 U(I)=0.DO
      GO TO 70
   60 U(I)=CC(IKK)
```

```
   70 CONTINUE
      IF(ICR(IEL).LE.0) GO TO 90
      DO 80 I=1,NVEL,2
      U1=U(I)*COT+U(I+1)*SIT
      U2=U(I+1)*COT-U(I)*SIT
      U(I)=U1
   80 U(I+1)=U2
   90 CALL BLMAT(BL,AT,BT,U,AL,BE,GA,DE,JC,ILIN)
      IF(JC.GT.-1) GO TO 100
      E1=E1F(ID)
      E2=E2F(ID)
      E3=E3F(ID)
      ANU=ANUF(ID)
      E=EF(ID)
      WRITE(8) E1,E2,E3,ANU,E,ID,THICK
      IF(JC.LT.0) GO TO 110
  100 READ(8) E1,E2,E3,ANU,E,ID,THICK
      CALL DLOAD(BL,FL,SIG,AR,THICK,IEL,ICR,ANG)
  110 IF(JC.GT.-1) IS=1
      ICRL=ICR(IEL)
      IF(ICRL.LE.0) GO TO 120
      CALL NONLINC(S,SIG,AT,E,AR,THICK,IS,IEL,BL,ANG,ICRL,ILIN)
      GO TO 130
  120 CALL NONLIN(S,SIG,AT,BT,E1,E2,E3,AR,THICK,AL,BE,GA,DE,IS,NEL,
     *IEL,ICRL,ILIN)
  130 CALL SETUP(A,B,S,FL,NVEL,LJ,LBAND)
       WRITE(1) ((BL(I,J),J=1,6),I=1,3)
  140 CONTINUE
      RETURN
      END

************************************************************************
****************** SUBROUTINE STLOM ***********************************
************************************************************************
C CALCULATES GLOBAL STIFFNESS MATRIX AND LOAD VECTOR FOR MORTAR BOND ELE

      SUBROUTINE STLOM(INEL,NEL,A,S,B,FL,ICO,JX,LJ,U,CC,LBAND
     1,NVAR,NVSEL,NNSP,JC,TH,EF,ANUF,FTF,YY,ICR)
      DIMENSION A(12500),B(900),S(8,8),FL(8),ICO(6),JX(900),LJ(8)
     2,ICR(700),YY(500),CC(900),U(8),TH(9),EF(9),ANUF(9),FTF(9)
      KKK=NEL+1
      DO 60 IEL=KKK,INEL
      IF(JC.GT.-1) GO TO 10
      READ(4) (ICO(J),J=1,6)
      N1=ICO(1)
      N2=ICO(2)
      ID=ICO(5)
      THICK=TH(ID)
      SN=EF(ID)
      SK=ANUF(ID)
      FB=FTF(ID)
```

```
      BOAR=ABS(YY(N1)-YY(N2))*THICK
      WRITE(8) SN,SK,BOAR,FB,ID
      CALL LJMAT(LJ,NNSP,NVAR,ICO,JX)
C     PRINT*,IEL,(LJ(J),J=1,8)
      WRITE(3) (LJ(J),J=1,8)
      GO TO 20
   10 READ(3) (LJ(J),J=1,8)
      READ(8) SN,SK,BOAR,FB,ID
   20 DO 50 I=1,8
      IKK=LJ(I)
      IF(IKK) 40,30,40
   30 U(I)=0.D0
      GO TO 50
   40 U(I)=CC(IKK)
   50 CONTINUE
      CALL BONDMO(S,U,FL,FB,BOAR,SN,SK,JC,ICR,IEL)
   60 CALL SETUP(A,B,S,FL,NVSEL,LJ,LBAND)
      RETURN
      END

************************************************************************
****************** SUBROUTINE STLOS ***********************************
************************************************************************
C CALCULATES GLOBAL STIFFNESS MATRIX AND LOAD VECTOR FOR STEEL BEAM ELEM

      SUBROUTINE STLOS(INEL,NEL,A,S,B,FL,ICO,JX,LJ,XLEN,SIG
     1,ABOT,ES,CF,NVELS,JC,NNSEL,NVAR,LBAND)
       DIMENSION A(12500),S(8,8),B(900),FL(8),ICO(6),JX(900),LJ(8)
     *,XLEN(100),SIG(700,3)
      ARST=ABOT
      KKK=NEL+1
      DO 50 IEL=KKK,INEL
      IF(JC.GT.-1) GO TO 20
      READ(4) (ICO(J),J=1,4)
      CALL LJMAT(LJ,NNSEL,NVAR,ICO,JX)
      WRITE(3) (LJ(I),I=1,4)
      ST=ES*ARST/XLEN(IEL-NEL)
      CALL STIFF(S,ST,0.0)
      DO 10 I=1,8
   10 WRITE(7) (S(I,J),J=1,8)
      GO TO 40
   20 READ(3) (LJ(I),I=1,4)
      DO 30 I=1,8
   30 READ(7) (S(I,J),J=1,8)
   40 IF(JC.LT.0) GO TO 50
      FL(1)=-ARST*SIG(IEL,1)
      FL(3)=-FL(1)
   50 CALL SETUP(A,B,S,FL,NVELS,LJ,LBAND)
      RETURN
      END
*********************** END ****************************************
```